

Fall 2010

# The instrumentation, testing, and structural modeling of a steel girder bridge for long-term structural health monitoring

Paul J. Lefebvre

*University of New Hampshire, Durham*

Follow this and additional works at: <https://scholars.unh.edu/thesis>

---

## Recommended Citation

Lefebvre, Paul J., "The instrumentation, testing, and structural modeling of a steel girder bridge for long-term structural health monitoring" (2010). *Master's Theses and Capstones*. 584.  
<https://scholars.unh.edu/thesis/584>

This Thesis is brought to you for free and open access by the Student Scholarship at University of New Hampshire Scholars' Repository. It has been accepted for inclusion in Master's Theses and Capstones by an authorized administrator of University of New Hampshire Scholars' Repository. For more information, please contact [nicole.hentz@unh.edu](mailto:nicole.hentz@unh.edu).

**THE INSTRUMENTATION, TESTING, AND STRUCTURAL MODELING OF A STEEL  
GIRDER BRIDGE FOR LONG-TERM STRUCTURAL HEALTH MONITORING**

**BY**

**PAUL J. LEFEBVRE  
BS, University of New Hampshire, 2002**

**THESIS**

**Submitted to the University of New Hampshire  
in Partial Fulfillment of  
the Requirements for the Degree of**

**Master of Science  
In  
Civil Engineering**

**September, 2010**

UMI Number: 1486999

All rights reserved

**INFORMATION TO ALL USERS**

The quality of this reproduction is dependent upon the quality of the copy submitted.

In the unlikely event that the author did not send a complete manuscript and there are missing pages, these will be noted. Also, if material had to be removed, a note will indicate the deletion.



UMI 1486999

Copyright 2010 by ProQuest LLC.

All rights reserved. This edition of the work is protected against unauthorized copying under Title 17, United States Code.



ProQuest LLC  
789 East Eisenhower Parkway  
P.O. Box 1346  
Ann Arbor, MI 48106-1346

This thesis has been examined and approved.



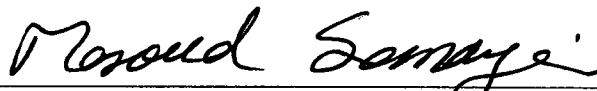
---

Thesis Director Erin Bell, Ph.D., P.E. Civil Engineering



---

Ricardo Medina, Ph.D. Civil Engineering



---

Masoud Sanayei, Ph.D. Civil Engineering, Tufts University

August 10, 2010  
Date



## ACKNOWLEDGEMENTS

This thesis is a result of 2 years of research that could not have been accomplished without help. The funding for this project was partially provided by a grant from the National Science Foundation's Partnership for Innovation (NSF-PFI) program (Grant# 0650258). The NSF-PFI project was a joint venture with partners from academia, industry, and government. These partners played a critical role in the success of every step of this research and for that I thank them.

First I'd like to thank my advisor Dr. Erin Bell for her daily guidance and support at every step of my research and education; Dr. Masoud Sanayei of Tufts University and Brian Brenner of Fay, Spofford and Thorndike, INC helped guide the research activities for the entire project, keeping me on track toward my goals. Jesse Sipple and John Phelps from Tufts University, and Jason Peddle and Phil Brogan from UNH for their help at every stage; High Steel Structures, FST, ET&L, Atlantic Bridge & Engineering, and MassDOT for access to the construction site, to their equipment, and to lab test data; and Geocomp, Inc. for their professional assistance with instrumentation, data acquisition, and post processing.

In addition to the members of the research group, many others played a vital role. Corey Clark, Josh Clayton, Heather Newton, and Antonio Garcia-Palencia were all there when I needed to talk through a problem. My parents and brothers provided support, reminding me there is life outside of graduate school. Finally, I'd like to thank my fiancée Tanya for her support and patience when things weren't going so well and for her enthusiasm when I made a break through. I couldn't have done it without you.

## TABLE OF CONTENTS

ACKNOWLEDGEMENTS.....	iii
TABLE OF CONTENTS .....	iv
LIST OF TABLES .....	x
LIST OF FIGURES.....	xii
ABSTRACT .....	xviii
1. INTRODUCTION.....	1
1.1 State of the US Highway System .....	3
1.2 Current Bridge Design Practice.....	6
1.3 Current Bridge Inspection Practice.....	8
1.4 Examples of Structural Health Monitoring .....	9
1.5 Baseline Modeling and Structural Health Monitoring .....	12
1.5.1 Element Type Selection.....	13
1.5.2 Redefining Baseline.....	15
1.6 Instrumentation and Structural Health Monitoring.....	15
1.6.1 State of the Art of Bridge Instrumentation .....	16
1.7 Research Goals and Activities .....	16
2. CASE STUDY: THE VERNON AVENUE BRIDGE .....	20
2.1 History.....	22

2.2 Site Layout.....	24
2.3 Summary .....	29
3. INSTRUMENTATION.....	30
3.1 Preliminary Modeling.....	30
3.2 Instrumentation Plan by Sensor Type .....	34
3.2.1 Strain Gauges.....	34
3.1.2 Temperature Gauges.....	36
3.1.3 Tiltmeters.....	37
3.2.4 Accelerometers.....	38
3.2.5 Pressure Cells .....	38
3.2.6 Datalogging .....	42
3.3 Installation.....	44
3.3.1 Installation Prior to Steel Erection.....	44
3.3.2 Installation Prior to Concrete Formwork.....	47
3.3.3 Installation Prior to Concrete Pour .....	50
3.3.4 Installation Prior to Load Test .....	51
3.5 Logistical Considerations .....	53
3.5.1 Legal Concerns .....	53
3.5.2 Power and Internet .....	54
3.6 Instrumentation Summary .....	56
4. FIELD DATA COLLECTION .....	59

4.1 Data Collection During Construction .....	60
4.1.1 Data Collection Prior to Concrete Pour .....	60
4.1.2 Data Collection During Concrete Pour .....	63
4.1.3 Data Collection After Concrete Pour .....	64
4.2 Controlled Load Test.....	65
4.2.1 Test Truck Specifications.....	65
4.2.2 Load Test Plan .....	67
4.2.3 Data Acquisition.....	71
4.2.4 Load Test Summary .....	73
4.3 Field Data Post Processing .....	73
5. FIELD DATA QUALITY ASSURANCE AND QUALITY CONTROL.....	75
5.1 Functionality of Strain Gauges .....	75
5.2 Symmetry of Sensor Placement.....	77
5.3 Measurement Sign, Magnitude, and Time of Occurrence.....	79
5.4 Additional Quality Assurance and Quality Control Measures.....	81
5.4.1 Extraction of Strain Values for Model Comparison.....	82
5.4.2 Extraction of Composite Section Neutral Axis for Model Strain Calculation and Design Verification .....	86
5.5 Summary of QA/QC Efforts.....	97
6. STRUCTURAL MODELING.....	99
6.1 Modeling Program Selection .....	99

6.2	Initial Baseline EDM Creation.....	102
6.2.1	Variation of Deck Section .....	104
6.2.2	Bridge Deck Mesh .....	107
6.2.3	Insertion Points of Girders .....	109
6.3	Load Application .....	111
6.4	Post Processing of Model Output.....	116
6.4.1	Output of Composite Section Forces .....	116
6.4.2	Calculation of Strain from Model Forces .....	118
6.5	Model Updating.....	122
6.5.1	Updating of Concrete Deck Material Properties .....	123
6.5.2	Addition of Safety Curb.....	125
6.5.3	Updating of Boundary Conditions .....	126
6.5.4	Addition of Deck Reinforcement .....	130
6.6	Baseline Model Evaluation.....	133
6.6.1	J-Value Metric.....	139
6.6.2	Percent Passing Metric.....	141
6.6.3	Average Residual Metric.....	143
6.6.4	Deflection Comparison .....	145
6.6.5	Summary of Baseline Model Evaluation.....	148
7.	BASELINE MODELING FOR BRIDGE MANAGEMENT.....	150
7.1	Bridge Inspection .....	150

7.2 Load Rating .....	153
7.2.1 Inventory Load Rating Using LRFR Method.....	154
7.2.2 Load Rating Using Baseline EDM.....	159
7.2.3 Load Rating Comparison Considering Girder Section Loss .....	163
7.3 Results of Baseline EDM usage for Bridge Management .....	166
8. CONCLUSIONS .....	168
8.1 Development and Deployment of Instrumentation Plan.....	169
8.2 Design Verification .....	171
8.3 Baseline Structural Modeling.....	171
8.4 Modeling for Bridge Management .....	173
8.5 Facilitation of Industry Partnerships .....	174
8.6 Recommendations for Future Work.....	174
8.6.1 Instrumentation and Data Acquisition .....	175
8.6.2 Modeling.....	178
8.1 Summary .....	181
REFERENCES.....	182
APPENDICES .....	185
APPENDIX A: CALCULATION OF STRAIN IN STRAIN GAUGE CALIBRATION.....	186
APPENDIX B: CALCULATION OF VAB COMPOSITE SECTION PROPERTIES.....	187
APPENDIX C: CALCULATION OF AS-BUILT CONCRETE MATERIAL PROPERTIES .....	190

APPENDIX D: CALCULATION OF STIFFNESS COEFFICIENTS FOR MODEL BOUNDARY CONDITIONS.....	193
APPENDIX E: KEY FOR MASSDOT INSPECTION REPORT.....	198
APPENDIX F: CALCULATION OF LOAD RATING FACTORS.....	199
APPENDIX G: INSTRUMENTATION LITERATURE.....	216
APPENDIX H: INSTRUMENTATION PLAN.....	CD-ROM
APPENDIX I: BRIDGE DESIGN PLANS.....	CD-ROM
APPENDIX J: FULL MODEL-TO-DATA COMPARISON.....	CD-ROM

## LIST OF TABLES

Table 1. Instrumentation breakdown by type .....	56
Table 2. Distribution of sensors w.r.t. girder # for stations 1 to 6.....	57
Table 3. Distribution of sensors w.r.t. girder # for stations 7 to 12.....	58
Table 4. Data Collection Summary.....	59
Table 5. Test Truck Wheel Size and Axle Spacing Dimensions.....	66
Table 6. Average test truck wheel weights.....	67
Table 7. Location of Faulty Gauges from Sept 3 Load Test.....	76
Table 8. Analysis of Measured Neutral Axes for Strain Stations on all Six Girders.....	92
Table 9. Measured Distance versus Design Distance to Neutral Axis from Bottom Flange of Steel .....	93
Table 10. Transformed section properties of composite section for model strain calculation..	119
Table 11. Description and basis for manual model updates in order of confidence.....	123
Table 12. Comparison Original and Updated Concrete Material Properties.....	125
Table 13. Comparison of bulk moduli, K, for changing values of Poisson’s ratio .....	128
Table 14. Updated model boundary condition stiffness coefficients for SAP2000® model.....	129
Table 15. LRFD load factors and plastic moment capacities of interior and exterior girders used in the calculation of all Inventory rating factors.....	155
Table 16. Live load distribution factors for moment for interior and exterior girders (AASHTO, 2008-B).....	156
Table 17. Summary of live loads applied to LRFR calculations and EDM for rating factor calculation .....	157
Table 18. Moments at the midpoint of the center span due to DL and patterned LL.....	158
Table 19. Comparison of Total moments at midpoint of center span using both rating methods .....	161



Table 20. EDM moments and rating factors for each girder .....	162
Table 21. Changes in capacity and LRFR load rating due to 10 mm loss thickness of bottom flange at the midspan .....	164
Table 22. Changes in EDM load rating due to 10 mm loss of thickness in bottom flange of a girder at the midpoint of the center span .....	165

## LIST OF FIGURES

Figure 1. Vehicle traffic trends nationally since 1985 (FHWA, 2010), .....	5
Figure 2. Traffic Management Center at the NHDOT .....	9
Figure 3: New Rollins Road Bridge, opened in 2000.....	10
Figure 4. Boston's Tobin Memorial Bridge is instrumented for SHM and proactive maintenance .....	11
Figure 5. The Vernon Avenue Bridge in Barre, MA.....	17
Figure 6. Interaction of partnerships involved in the NSF-PFI project (Brenner, Sanayei, Santini-Bell, & Abriola, 2007) .....	18
Figure 7. Location of the VAB in Barre, MA .....	21
Figure 8. Underside of VAB prior to 2008 demolition. ....	23
Figure 9. Steel plates installed on bridge deck to protect degrading concrete deck. ....	23
Figure 10. The new VAB, opened in September 2009. ....	24
Figure 11. Plan and elevation views of the VAB (FST, 2007).....	25
Figure 12. Framing Plan of the VAB ((FST, 2007) .....	26
Figure 13. Water main crossing the bridge between girders 4 and 5.....	27
Figure 14. Elastomeric bearing pad cross sections from shop drawings(DS Brown, 2008).....	28
Figure 15. Sole plates on top of the elastomeric bearing pads at the south abutment prior to steel erection.....	28
Figure 16. Preliminary modeling and analysis for the planning of instrumentation .....	31
Figure 17. Annotated framing plan with instrumentation station numbers marked along the top of figure .....	32
Figure 18. Sample girder elevation showing instrumentation of the north section of girder 2...	33
Figure 19. Typical strain gauge locations on top and bottom girder flanges (depiction is of an interior girder).....	35

Figure 20. Illustration of neutral axis of a composite section.....	36
Figure 21. Location of thermistors on longitudinal reinforcing steel .....	37
Figure 22. Plan view of pressure cell installation location.....	40
Figure 23. Cross Section of Vernon Ave Approach with pressure cell installed locations.....	41
Figure 24. iSite Central Internet-based remote monitoring system.....	43
Figure 25. Schematic describing data collection process .....	44
Figure 26. Three of the steel girders at the steel fabrication plant in Lancaster, PA. ....	45
Figure 27. Strain gauge installed on prepared surface .....	46
Figure 28. Strain gauge and steel-mounted thermistor installation with environmental protection and labeling .....	47
Figure 29. Water pipe between girders 4 and 5. Researchers can be seen in the background splicing the DAQ cabling over the steel field splice. ....	48
Figure 30. Installed iSite boxes with completed cabling, angle mounting, and c-clamp installation .....	49
Figure 31. Cabling grouped across girders to accommodate iSite placement .....	49
Figure 32. Book-keeping for 200 gauges during iSite installation .....	50
Figure 33. Installation of concrete thermistor on deck rebar.....	51
Figure 34. Accelerometer adhered to girder with epoxy putty.....	51
Figure 35. Tiltmeter adhered to girder with epoxy putty, prior to application of environmental protection.....	52
Figure 36. Pressure Cell Layout prior to Installation.....	53
Figure 37. Pressure cells installed in subgrade prior to paving .....	53
Figure 38. Meter box just before power hook-up .....	55
Figure 39. iSite-HS boxes distributed across all six girders .....	55
Figure 40. Permanent cabling attached to abutment wall .....	55
Figure 41. Temporary concrete formwork on exterior girder for deck overhang. ....	60
Figure 42. A researcher measures strain using the P3500 for calibration to iSite strain readings .....	62

Figure 43. To the left is a sample of collected strain data from concrete pour of deck. To the right is a photo of the construction crew conducting the pour.....	64
Figure 44. Test Truck for Sept. 3 Load Test.....	65
Figure 45. Researcher recording wheel weights.....	67
Figure 46. Load test lane and stop location layout.....	69
Figure 47. Truck approaching “dummy scales” during impact test.....	71
Figure 48. Center span digital image correlation test setup.....	73
Figure 49. Repeatability of strain measurements for 3 repetitions of the lane #2 truck runs, for strain in the bottom flange of girder 2 at the midspan (SG22).....	74
Figure 50. Comparison of Clean and Noisy Collected data.....	77
Figure 51. Comparison of parallel sensors on Girder 3 Stations 8 and 10 during a west lane test. ....	78
Figure 52. Comparison of Magnitude and Sign of Measured Strain for Locations in Positive Flexure.....	80
Figure 53. Truck Stops Numbered for Identification of Strain Plateaus .....	81
Figure 54. Typical plot of filtered strain data from a load test with truck stop "plateau" and sampling window .....	83
Figure 55. Plot of standard deviations of 100 strain readings with respect to each of the 135 truck stops.....	83
Figure 56. Plot of Pooled Standard Deviations of collected strain with respect to load case. ....	85
Figure 57. Plot of variation of Pooled Standard Deviation of Collected Strain with respect to Amplitude.....	86
Figure 58. Calculation of Neutral Axis from Strain in Top and Bottom Flange .....	88
Figure 59. Original Plot of Neutral Axis Location for Girder 2 during a Lane 1 Test.....	89
Figure 60. Filtered Plot of Neutral Axis Location for Girder 2 Stations during a Lane 1 Test. The black line at the top represents the neutral axis for a fully composite bridge. The black line at the bottom represents the centerline of the girder and the neutral axis of a fully non-composite girder. ....	90
Figure 61. Illustration of local loading effects on top flange axial strain.....	91
Figure 62. Measured and Calculated Neutral Axes for each Girder at Station 2.....	95

Figure 63. Measured and Calculated Neutral Axes for each Girder at Station 4.....	95
Figure 64. Measured and Calculated Neutral Axes for each Girder at Station 6.....	95
Figure 65. Measured and Calculated Neutral Axes for each Girder at Station 8.....	96
Figure 66. Measured and Calculated Neutral Axes for each Girder at Station 10.....	96
Figure 67. SAP Bridge Modeler Wizard User Interface (SAP2000® v14.1).....	101
Figure 68 SAP BrIM Bridge Cross Section Definition (SAP2000® v14.1) .....	103
Figure 69. SAP BrIM Bridge Object Data Definition (SAP2000® v14.1).....	104
Figure 70. Varying deck section as given by design framing plan (FST, 2007).....	106
Figure 71. Display of section variation definition form for deck width variation (SAP2000® v14.1).....	107
Figure 72. Three links are used to create the connectivity between girder, bearing, and foundation.....	109
Figure 73. BrIM bearing definition form. A “roller” bearing type is defined here (SAP2000® v14.1).....	111
Figure 74. SAP BrIM Truck Load and Dimension Definition (SAP2000® v14.1) .....	113
Figure 75. SAP BrIM Lane Definition (SAP2000® v14.1).....	114
Figure 76. Load Pattern Definition Form (SAP2000® v14.1).....	115
Figure 77. Modeled Load Truck at Stop #6 of Lane 1 (SAP2000® v14.1) .....	116
Figure 78. Section cut concept illustrated with red elements and respective nodes (SAP2000® v14.1).....	117
Figure 79. BrIM Object Response displaying the moment diagram for the full bridge section for Truck Stop #9 in Lane 2 (SAP2000® v14.1).....	118
Figure 80. Example of Model Improvement by Model Post-Processing Update.....	121
Figure 81. The safety curb reinforcement was integral with main deck .....	126
Figure 82. Elastomeric bearing pad supporting one of the girders. This location is at a pier, characterized by the anchor bolts.....	127
Figure 83. Boundary condition stiffness definition form (SAP2000® v14.1).....	130
Figure 84. Modeling of steel reinforcement using SAP2000 layered shell element (Sipple, 2008). .....	131

Figure 85. SAP BrIM Layered Shell Definition .....	132
Figure 86. The center span station of girder 1 shows updated model closer to collected measurement in top flange (SG5) and farther from collected measurement in bottom flange (SG6).....	134
Figure 87. Measurements on the bottom flange of girder 3 just to the north of the south pier illustrate the effects of local loading on bending moment strain. Truck stop 7 is located directly above SG35 and SG36. ....	134
Figure 88. Varying strain magnitude with lane is illustrated by south pier strain gauges on the bottom flange of girder 2 (SG17 and SG18). The largest amplitudes are found when the truck is directly overhead (lane 1), and the smallest amplitudes when truck is on the opposite side of the bridge (lane 3). The original model better predicts the measured response in the lane 1 test and the updated in the lane 3 test.....	135
Figure 89. Mixed results are shown in the comparison of modeled to collected strains in SG25 and SG26, which are strain gauges on the bottom flange of girder 2 at the north pier. Also depicted here are the small strains for southern truck stops for a measurement on the north pier. ....	136
Figure 90. Strain on the bottom flange of girder 5 at the south pier. The modeled data is much closer to measurements on the left side of the web (SG73) than the right side (SG74)....	137
Figure 91. J-value of all measurements .....	140
Figure 92. Algorithm for percent passing metric.....	142
Figure 93. Residuals with less than 10% error from measured for varying minimum measurements .....	143
Figure 94. Algorithm for average residual metric.....	144
Figure 95. Average Residual for varying minimum measurements.....	145
Figure 96. South Span Camera Setup Location .....	146
Figure 97. Comparison of Vertical Deflections near midspan of west exterior girder for truck in west lane .....	147
Figure 98. Comparison of Vertical Deflections in south span of west exterior girder for truck in west lane .....	147
Figure 99. Comparison of Vertical Deflections near midspan of west exterior girder for truck in center lane .....	148
Figure 100. Comparison of Vertical Deflections in south span of west exterior girder for truck in center lane .....	148

Figure 101. Photo from VAB inspection reporting section loss in beam lower flange(MHD, 2007). .....	151
Figure 102. Sample page from MassHighway routine inspection of the former VAB.....	152
Figure 103. Design Truck (AASHTO, 2008-B).....	157
Figure 104. Influence Line for moment at the midpoint of the center span.....	158
Figure 105. Depiction of truck location for worst-case loading condition at the midpoint of the center span.....	160
Figure 106. Location for lane loading for maximum force effects according to LRFD design specifications are shaded in black. The EDM lane loading conservatively included the area between the lanes.....	161
Figure 107. Comparison of LRFR and EDM Inventory rating factors for girders 1 to 6.....	163
Figure 108. Comparison of EDM and LRFR Inventory ratings for a damaged EXTERIOR Girder (Girder 1).....	166
Figure 109. Comparison of EDM and LRFR Inventory Ratings for a damaged INTERIOR Girder (Girder 3).....	166
Figure 110. Strain in the bottom flange of Girder 2 at the midspan (SG21) from 4/12/2010 to 4/13/2010 showing large changes in amplitude from the ambient pattern suggesting possible heavy truck loads. ....	176
Figure 111. SAP has an option of nonlinear material behavior definition for concrete (SAP2000® v14.1).....	180
Figure 112. Concrete Cylinder Break Strengths, Deck Pour values highlighted .....	191
Figure 113. Mix design, Aggregate Industries Lunenburg,MA Plant.....	192
Figure 114. Elastomeric bearing pad lab test results (1 of 2) .....	196
Figure 115. Elastomeric bearing pad lab test results (2 of 2) .....	197

## ABSTRACT

### THE INSTRUMENTATION, TESTING, AND STRUCTURAL MODELING OF A STEEL GIRDER BRIDGE FOR LONG-TERM STRUCTURAL HEALTH MONITORING

by

Paul Lefebvre

University of New Hampshire, September, 2010

The currently accepted bridge design practice is individual element design through approximate “worst-case” loading scenarios and distribution with appropriate safety factors. The resulting design is not necessarily representative of the true behavior of a bridge. Computer structural modeling advancements have made it practical to improve the design process by capturing the design intelligence in the bridge model for use in bridge management and condition assessment. Nearly 1/3 of U.S. bridges are nearing the end of their design life and the design of the next generation of highway bridges has begun. The time is optimum to consider advancements in bridge design protocol for inclusion of baseline modeling.

A baseline structural model is created and verified using collected field data during construction. This model is then integrated with instrumentation and field testing as part of a long-term structural health monitoring program. The model can be used and updated for the purpose of design verification, condition assessment, load rating and proactive maintenance.



## CHAPTER 1

### INTRODUCTION

The development of infrastructure management protocols in the United States is at a critical juncture. Many bridges are nearing the end of their original design life and a country-wide rehabilitation, replacement and retrofit phase is underway. The tragedy of the collapse of the I-35W Bridge in Minneapolis in 2007 has sensitized the public to the potential safety impact of aging infrastructure. In the three years since the collapse, both the American Society of Civil Engineering (ASCE) and American Association of State Highway and Transportation Officials (AASHTO) have released publications urging for increased federal funding into roads and bridges (ASCE, 2009),(AASHTO, 2008-A). In 2009, the American Reinvestment and Recovery Act (ARRA) allocated \$26.6 billion to state DOT's for highway repair (FHWA, 2010). With this funding, a new fleet of highway bridges will be designed and constructed.

Recognizing the creation of a new generation of bridges, the Federal Highway Administration (FHWA) began a 20-year study in 2007 entitled the Long term Bridge Performance (LTBP) Program to study how bridge performance changes over time using instrumentation, structural modeling and advanced data management techniques (Ghasemi, 2009). This effort is focused on the "work horse" highway bridge, i.e. the short to mid-sized span overpass, as opposed to a signature bridge for which these

studies were normally reserved such as Boston's Maurice J. Tobin Bridge or Delaware's Commodore Barry Bridge. One of the purposes of LTBP program was to improve inspection standards and condition assessment through non-destructive testing and structural health monitoring (SHM) (Ghasemi, 2009).

The International Society for Structural Health Monitoring of Intelligent Infrastructure (ISHMII) defines SHM as "a type of system that provides information on demand about any significant change or damage occurring in the structure" (ISHMII, 2010). SHM typically includes data collection through sensor based instrumentation, post-processing the collected responses with respect to predicted responses from both hand calculations and structural modeling and then monitoring of any changes to the structure. This process can be effectively integrated with a structural model of the instrumented bridge for the purpose of objective condition assessment, parameter estimation, design verification and bridge management.

The research reported herein focuses on the structural health monitoring of a highway bridge in Massachusetts. The bridge was instrumented during construction for long-term SHM. A baseline structural model was created and calibrated using non-destructive test (NDT) data collected prior to bridge commission. The calibrated model was used in conjunction with the long-term SHM system for bridge management in terms of inspection load rating protocol.

The layout of this document is as follows. First there is an introduction of the current state of the national highway system, bridge design protocol, and bridge inspection protocol. This is followed by an investigation of past research in instrumentation, modeling, and SHM, as well as a summary of research goals and activities to be discussed in the chapters that follow. Chapter 2 introduces the case study bridge in terms of the history, geography, site layout, construction sequence, bridge materials, and bridge geometry. Chapter 3 discusses the design and installation

of an instrumentation plan, including sensor choice, sensor layout, and installation procedures. Chapter 4 reports on the field data collection protocol in terms of point of time during construction, purpose, and design and implementation of a controlled NDT for baseline model calibration. Chapter 5 examines field data quality assurance and quality control protocol and design verification of bridge neutral axis using NDT data. Chapter 6 discusses the creation and calibration of a baseline structural model, post processing of model output for comparison with NDT data, and an evaluation of the original and calibrated models with respect to NDT data. Chapter 7 outlines a procedure for using the calibrated model in terms of bridge inspection load rating calculation. Finally, Chapter 8 summarizes the findings and conclusions of this research and reports recommendations for future work.

### **1.1 State of the US Highway System**

As of December 2009, there were over 600,000 bridges in the U.S. Many of these bridges were built in the years following World War II, when the US launched a massive highway infrastructure project capped by the Interstate Highway Program (IHP). The vision of the IHP recognized a nation's highway system as crucial to the function of its economy and defense. With nearly 200,000 bridges past the typical design life of 50 years, the U.S. highway system is in a fragile state (Federal Highway Administration, 2009).

In addition to age, the FHWA tracks bridges in need of service and classifies them as either structurally deficient or functionally obsolete. AASHTO recommends that a bridge structure be categorized as structurally deficient when "Significant load-carrying elements are found to be in poor condition due to deterioration", and functionally obsolete when the structure does "not having adequate lane widths, shoulder widths, or

vertical clearances to serve current traffic demand" (AASHTO, 2008-A). Over 10% of the bridges in the U.S. are structurally deficient and over 13% are functionally obsolete (Federal Highway Administration, 2009).

Concurrent with the aging and deterioration of the nation's bridges is the increased use and dependence on them. America, like most industrialized nations, has a highly mobile population and annually the FHWA compiles statistics on vehicle distance traveled per year on the nation's roads. Figure 1 displays the trend since 1985, showing an increase of about 50 billion miles per year from 1985 to 2008. According to AASHTO, more than 3 trillion vehicle miles occur annually on bridges, with 223 billion miles from trucks. This number has doubled in the past 20 years, and is continuing to do so. Additionally, tonnage carried by trucks is also expected to double in the next 20 years (AASHTO, 2008-A). Research into increased truck weights has been found to expedite the deterioration and decrease the remaining useful service years of highways bridges (Fu, Feng, & Dekelbab, 2008). Given that 74% of goods transported within the U.S. are done so with trucks on the interstate highways system, it is essential that investment into the maintenance of US highway bridges continue (TRIP, 2010).

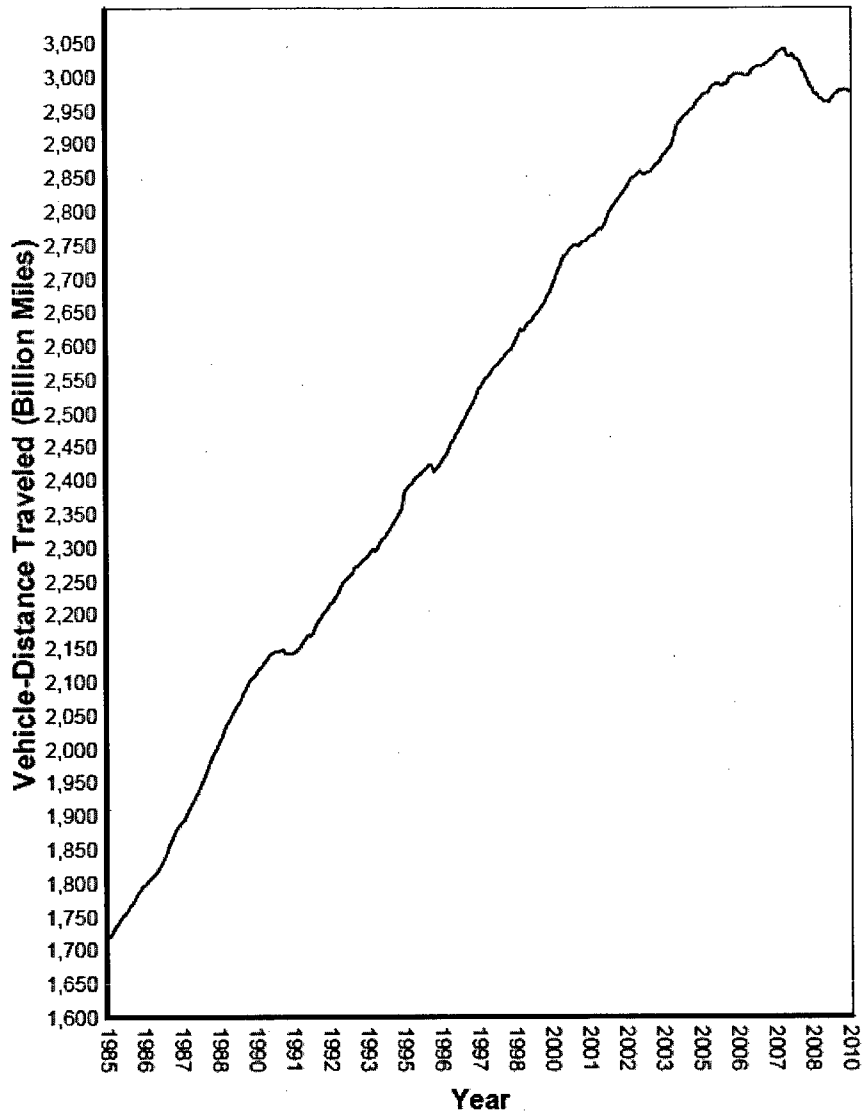


Figure 1. Vehicle traffic trends nationally since 1985 (FHWA, 2010).

The juxtaposition of age, increased volume, and increased weight on the nation's bridges suggests that it is increasingly important to adequately monitor the bridges for structural health, but the vast majority of the US bridge fleet is not monitored beyond the standard visual inspection requirements. Some state DOT's such as NH have included provisions for instrumentation on new bridge when a SHM system plan is submitted during design, such as the Rollins Rd Bridge in Rollinsford NH, but there is no

national specification or standard requiring a SHM system for new bridges (Sipple, 2008).

## **1.2 Current Bridge Design Practice**

The current AASHTO bridge design practice is an elemental approach. Conservatively factored traffic loads are applied to main load carrying members using distribution factors and tributary deck widths, and each member is designed individually. The elemental design process continues to the design of the bridge bearings, the abutments, and the piers.(Baker, 2003). The interaction and system performance of the bridge elements is not considered beyond the calculation of moment and shear distribution factors and the design of composite behavior between the deck and the girders. Distribution factors describe the percentage of a traffic load applied to the bridge that a girder is expected to experience. Composite behavior is accomplished through the use of shear studs welded to the steel girders and encased in the concrete deck.

There are many additional components of a bridge that must be designed beyond the main load-carrying members of the girders and deck. For most highway bridges, haunches between the girders and the bridge deck and diaphragms connecting the girders are included for the purpose of bracing and constructability. For local overpasses pedestrian sidewalks, safety curbs, and parapets are commonly integrated into the deck. For bridges in the northeastern US, an asphalt wearing surface is often applied to the deck. The design process does not account for the contribution of any of these components to the overall stiffness or strength of the bridge. These elements are considered non-structural and even though that may be tied to the bridge structure, they can be removed and replaced with smaller elements at any time throughout the life of the bridge. For example, a concrete parapet may add significant stiffness to the bridge

deck but this element may be replaced with a light-weight metal tube guardrail. Both are installed for safety purposes, but the parapet may have a significant impact on bridge performance. For example, a 2008 study of a concrete girder bridge with carbon fiber-reinforced polymer deck in Rollinsford NH showed the concrete parapets had a significant impact on the stiffness of the bridge superstructure (Sipple, 2008).

The current design process ends on opening day. The bridge designer plays an integral role in the construction of the bridge, providing information on design intention when needed, and oversight to ensure a quality product is delivered to the public upon its completion. But once opening day arrives, the design intelligence is filed away and the designer turns over management responsibilities to the owner. In many cases the bridge owner is a local municipality that played no role in the design or construction of the bridge. The result is an owner that has limited understanding of the design intelligence and structural functionality of each element of the bridge, but who is charged with its management.

A SHM system installed during construction can verify that design intent was successfully realized and quantify as-built performance compared to designed performance using measurements of force and deflection. For example, an appropriately designed instrumentation system can verify that shear studs are properly delivering composite action by transferring forces from the deck to the girders. The system could also verify the distribution of those forces to each individual girder is as expected.

If the system is installed prior to construction and a model is created during design, SHM could verify that girders do not become overstressed during transport, shake out, steel erection and during placement of the deck. It could provide information to quantify how much stress is locked into the girders prior to obtaining composite

strength. This information could be used to verify design assumptions and a structural model of the bridge as well.

### **1.3 Current Bridge Inspection Practice**

In 1967, the Silver Bridge over the Ohio River in Point Pleasant, WV collapsed, killing 46 people (Phares, Rolander, Graybeal, & Washer, 2000). The result was an increase in public awareness of bridge safety standards similar to the recent collapse of the I35-W Bridge in 2007. In partial response to the Silver Bridge tragedy, FHWA put in place the National Bridge Inspection Standards (NBIS) in 1971 to ensure that state DOT's were properly and systematically evaluating the condition of bridges within their inventory by conducting a bi-annual inspection where bridge components are visually examined for damage and deterioration. Despite the best attempts at a comprehensive set of standards, the current bridge inspection process is still an extremely subjective one (Phares, Rolander, Graybeal, & Washer, 2001). Some state DOT's such as New York State have realized the possible consequences of this, and taken the initiative to study ways to improve their own inspection program, independent of NBIS standards (NYSDOT, 2007).

The level of deterioration or damage is accounted for in terms of member section loss, and strength calculations similar to those during the design process are conducted to determine the traffic load that the damaged member can safely withstand. With the updated strength calculations, a decision can be made of whether the bridge needs repair or replacement, or if it is sufficient to post a weight limit on the bridge (AASHTO, 2003).

The inspection process is necessary to ensure the safety of the public. In a world that is becoming increasingly automated, this process has for the most part remained manual, time consuming, and expensive. The traffic management center



(TMC) at the New Hampshire DOT in Concord, shown in Figure 2, is an example of how facilities already exist that could serve to network and monitor bridge that are instrumented for SHM. The TMC monitors traffic, road closures and accidents for alternate route management.

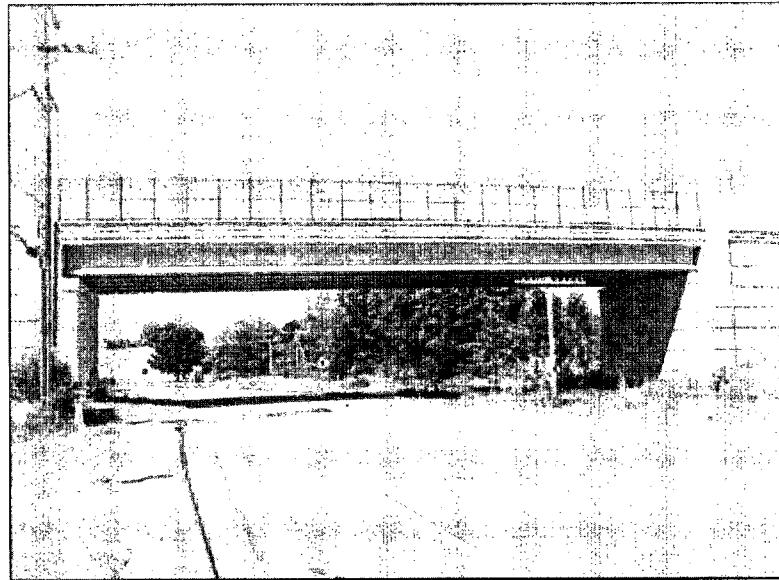


Figure 2. Traffic Management Center at the NHDOT

#### **1.4 Examples of Structural Health Monitoring**

Over the life of the bridge, SHM through instrumentation and baseline modeling can provide objective information to verify inspection reports, provide supplemental information between routine inspections, or trigger a special inspection to address a change in the response of the bridge. This idea is often employed when new and innovative materials or shapes are used, as SHM can provide a means to verify that a structure behaves as intended. Such is the case with the Arsta Railway Bridge in Stockholm Sweden, which is a particularly sleek and slender bridge, and was

instrumented during construction to verify design, monitor cracking in the most slender sections, and evaluate dynamic properties such as fundamental period, mode shapes, and damping ratios (Wiberg, 2006). The Rollins Road Bridge in Rollinsford NH used SHM in the form of embedded fiber optic strain gauges to monitor the performance of carbon fiber reinforced polymers in the deck and high performance concrete in the girders (Sipple, 2008).



**Figure 3: New Rollins Road Bridge, opened in 2000**

Some bridges have known problems that need to be monitored continuously. The Kishwaukee River Bridge in Rockford, IL was instrumented for long-term SHM. The bridge is a post-tensioned concrete segmental box girder bridge that developed cracking across the shear key of the box girder web segments shortly after construction. The cracking was due to an epoxy resin between the segments that did not harden. To address cracking, engineers installed steel pins across the webs in place of the failed epoxy. The pins were found to be a successful retrofit in the short term, but SHM using linear variable displacement transducers (LVDTs) was used to monitor any propagation of the crack over the life of the bridge (Wang, 2008).

Traditional visual inspection can be used in conjunction with SHM for a more objective evaluation of condition assessment. The University of Delaware has developed multiple generations of in-service bridge monitoring systems (ISBMS) that collected strain data using a battery operated data acquisition system, transmitted data using the cellular network and communicated with the user through a web interface. The researchers envisioned the system to be rapidly deployable for use alongside traditional load rating procedures, or with battery life for multiple weeks to investigate fatigue (Howell & Shenton, 2006).

Some bridge owners seek structural modeling to supplement bridge management for proactive maintenance. Boston's Tobin Memorial Bridge, shown in Figure 4, is a long span truss bridge and one of the main arteries out of a congested downtown. Given its importance to traffic flow in Boston and limited funds for maintenance, the Tobin makes an ideal case for SHM for the purpose of proactive maintenance and future condition assessment (Brenner, Bell, Sanayei, Pheifer, & Durack, 2010).



Figure 4. Boston's Tobin Memorial Bridge is instrumented for SHM and proactive maintenance

Some DOT's have realized that research into monitoring techniques of their critical infrastructure can save time and money. The Connecticut DOT and the

University of Connecticut have been studying different methods of SHM for more than 20 years, comparing different methodologies on different types of bridges for different purposes. The research began with short-term SHM of few bridges and has developed into long-term continuous monitoring of 6 bridges in the state. Each bridge is a different type, from a concrete box girder bridge to a twin steel box girder to a multiple steel girder bridge with composite concrete deck. The bridges were monitored using a combination of dynamic and static measurements. Strain gauges were used to get information on traffic loading and studied the use of bridge structures as a potential weigh-in-motion station. Accelerations were used to determine frequency spectra; temperature gauges and inclinometers were used to determine the impacts on the structure from changing ambient conditions. The study is a long term one with the goal of developing techniques for objective condition assessment (Liu, Olund, Cardini, D'Attilio, Feldblum, & DeWolf, 2008).

As academia researches the importance of SHM, NDT, condition assessment, and the best ways to employ these ideas, some companies are already specialized in this field at a commercial level. Some state DOT's employ these teams to perform NDT and monitor specific structures within their fleet. Bridge Diagnostics Inc. (BDI), from Boulder CO used NDT on a selection of bridges owned by the Rhode Island DOT for condition assessment and load rating. On these bridges, typical inspection procedures were not applicable due to access or potential damage. For example, one bridge was a concrete-encased steel girder bridge and the condition of the steel was not inspectable.

### **1.5 Baseline Modeling and Structural Health Monitoring**

Structural modeling can be combined with SHM for many purposes, including instrumentation placement, data quality assessment, design verification, bridge assessment and management, and parameter estimation. Some analytical models are

as simple as a set of design calculations used to verify the quality and reliability of collected data. Other models are more complicated structural and FE models. With structural modeling, more complex and comprehensive structural assessments can be made based on the measured response of the bridge. Once a structural model is grossly calibrated, it can be updated using model updating and parameter estimation algorithms to create a baseline model and set of predicted responses (Schlune, Plos, & Gylltoft, 2009). This can result in a structural model that accurately reflects the local and global behavior of the bridge and can be used for long-term SHM. This structural baseline model can also be used as a signature to capture changes in the bridge structural performance.

### **1.5.1 Element Type Selection**

Different levels of modeling can be used depending on the level of calibration desired. Frame elements are the typical structural modeling element used for both static and modal structural analysis. Frame elements are one-dimensional with a specified length. Users must input section properties such as cross-sectional area and inertial properties, as well as material properties. Shell or area elements are two-dimensional elements where the user draws the surface area of the element and assigns a thickness as a section property. Solid elements are three-dimensional elements where geometric properties are drawn or modeling, including length, width and thickness and only the material properties, such as modulus of elasticity and density are assigned. In this document, a structural model refers to a model consisting mainly of frame elements and a FE model refers to one consisting of mainly shell and solid elements.

The benefits of using frame elements in a baseline model are that the verification of computer output is reasonable using matrix structural analysis, however much of the true behavior of a frame element is lost in the geometric generalizations and assumptions of behavior. With increased complexity of the shell and solid elements

comes increased reliability in the distribution of forces across the element, but verification of computer output by hand is tedious and time consuming, and is not practical for complicated models. Solid elements are the most complicated mathematically, and have only been utilized in complex models recently, as computer speed and graphical interfaces have improved to levels that allow the models to be created in a timely manner.

Many researchers choose to use frame elements to simplify model construction and output verification. A comparative study was done of two three-span continuous precast post-tensioned concrete box girder bridges in Irvine, CA. In this study, frame elements were used to model the superstructure and substructure of both models for the purpose of baseline model verification using vibration testing (Feng, Doo, Jin-Hak, & Yangbo, 2004). By using simple 3D frame elements for the superstructure and piers, the authors were able to concentrate on the boundary conditions of a preliminary model to reasonably match field-measured dynamic characteristics such as natural frequency.

The Cross-County Bridge in Cincinnati OH was instrumented and modeled for SHM and condition assessment. This bridge is a three-span continuous steel girder bridge with non-composite concrete deck. In this study, two different types of models were created. The first was a 3 dimensional model using shell elements for the concrete deck, frame elements for the steel girders and cross-bracing, and rigid links for connectivity between them. The second model consisted entirely of frame elements, with the concrete deck represented as part of the girder below it, using the design principle of effective width (Zhang & Aktan, 1997). The authors recognized the complexity of the three-dimensional model to create, use, manipulate, and understand for an amateur modeler, a category in which most bridge engineers are included. Consequently, this type of modeling can be expensive undertaking. On the other hand, the two-dimensional model makes many more assumptions, not limited to the splitting of

the deck to individual girders, and output is limited to element forces as opposed to stresses within the cross section of the element. The authors recommended that continuing the research using the two-dimensional model for reasons relating mostly to the computational efforts required in working with the three-dimensional model.

A three-span concrete-encased steel girder with composite concrete deck bridge in Wilmington, DE was modeled for determination of a load rating based on collected data. The bridge was nearly 50 years old at the time of the study. The model of this bridge consisted of frame elements for the concrete-encased steel girders, and shell elements for the deck (Chajes, Mertz, & Commander, 1997). As in the above study, the author noted the importance of the cost-to-benefit ratio regarding model simplicity.

### **1.5.2 Redefining Baseline**

In previous work, a baseline model is a model that is used for parameter estimation and model updating for calibration to collected data. The model is updated based on the condition of the bridge at the time of data collection (Liu, DeWolf, & Kim, 2009), (Ren, Peng, & Lin, 2005). In other words, the calibrated baseline model represents the condition of the bridge at some snapshot in time. In this study, baseline model additionally refers to the fact that the model represents the bridge at its birth, before traffic, environment, or time has had a chance to impact its behavior. This way, the model can be calibrated to the original condition of the bridge, and condition assessment can be conducted with respect to its original behavior.

## **1.6 Instrumentation and Structural Health Monitoring**

The type and location of instrumentation used for SHM is dependent of the geometry of the bridge, the type of monitoring, and the goal of that monitoring. Global behavior is best captured from dynamic measurements using accelerometers. Local behavior is best captured from static measurements of deflection, strain, temperature,

and rotation. Deflection can be captured from linear-varying displacement transducers, slide-wire potentiometers, and dial gauges. Strain is captured from foil strain gauges or strain transducers. Temperature can be collected from typical thermometers or from current-measuring thermistors. Rotation can be collected using tiltmeters or inclinometers. There are also several emerging non-contact techniques for measurement such as digital image correlation (DIC), described below.

### **1.6.1 State of the Art of Bridge Instrumentation**

There are several new monitoring techniques available for instrumentation of large civil engineering structures such as bridges. One area of particular interest to SHM is the idea of digital image correlation, where highly sensitive cameras use pixel size in digital images along with triangulation of multiple cameras to determine deflections. The technology is used mostly in indoor controlled environments because the sensitivity of the cameras to changes in lighting conditions. DIC is typically used in situations where the cameras can be placed within a few feet of the item to be analyzed, such as with the traditional tensile test of materials engineering in place of a strain transducer (Brogan, 2010).

Traditional inclinometers used an electrolytic-type (EL) sensing device with the bubble-level principle of typical carpenter's levels, where newer models use a Micro-Electro-Mechanical Sensor (MEMS) that has been shown to have less signal degradation over long cable lengths. Recently, a fiber-optic type inclinometer was created and tested for potential use as part of a SHM system (Kim, 2008).

### **1.7 Research Goals and Activities**

The Vernon Ave Bridge (VAB), shown in Figure 5, is a three span continuous steel girder bridge with composite reinforced concrete deck located in central Massachusetts. The VAB is the target bridge for a project funded by the National



Science Foundation-Partnership for Innovation program (NSF-PFI), which focuses on the integration of academia, industry, and government into research efforts, as illustrated in Figure 6. Interaction of partnerships involved in the NSF-PFI project . This NSF-funded project entitled “Whatever happened to long-term bridge design”, is focused on the evaluation and improvement of bridge design process to account for the long-term behavior of bridges. The team consists of researchers from Tufts University and the University of New Hampshire, the industry partners of instrumentation and testing specialists from Bridge Diagnostics Inc and Geocomp Inc, bridge designers from Fay, Spofford, and Thorndike, bridge construction specialists from ET&L Corp and Atlantic Bridge and Engineering, and government representatives from MassHighway and the town of Barre, MA.



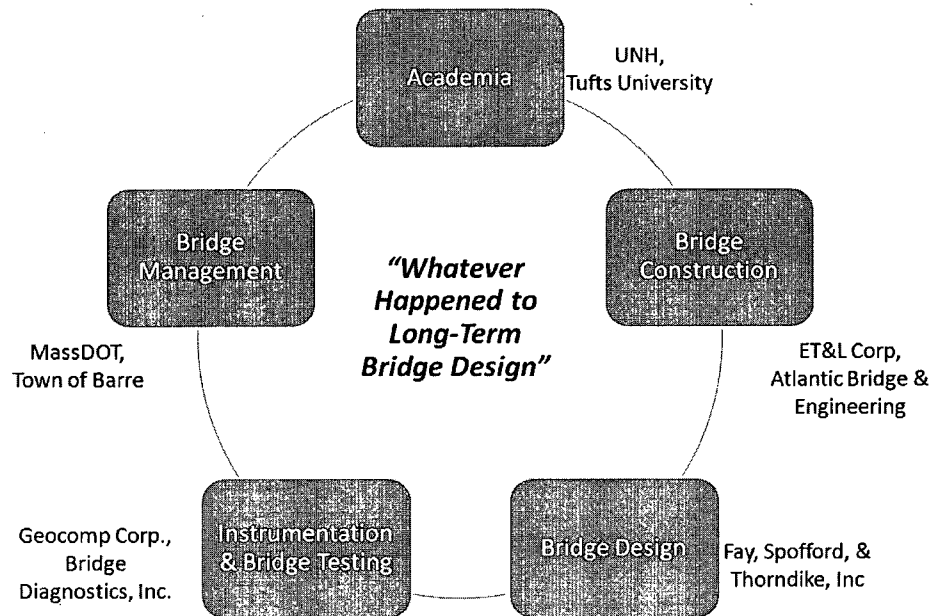
Figure 5. The Vernon Avenue Bridge in Barre, MA

The goals of the research project are extensive, but certain goals relate directly to the research included to this thesis. These goals are the following:

- *Design of Instrumentation for a long-term SHM system working with the highway bridge design team.*

- *Design verification of a highway bridge during construction to improve design techniques for future projects.*
- *Dissemination of benchmark non-destructive test data from an in-situ structure that may be used for parameter estimation and model updating research.*(Brenner, Sanayei, Santini-Bell, & Abriola, 2007)

The research activities covered in this thesis incorporate the goals of the research project while taking into account past research in SHM, instrumentation, data acquisition (DAQ), and structural modeling. An instrumentation plan for the VAB was developed prior to construction and instrumentation installed during construction for the purpose of long term SHM and design verification. Concurrently, a three-dimensional structural model was created in SAP2000®, a FE software program, using design drawings, as-built drawings, and field measurements.



3

Figure 6. Interaction of partnerships involved in the NSF-PFI project (Brenner, Sanayei, Santini-Bell, & Abriola, 2007)

With the installed instrumentation, bridge behavior was observed from data collected during construction. Data was collected after the erection of steel, after installation of stay-in-place formwork, and during the pouring of the concrete deck in order to observe the behavior of the bridge as a non-composite system, calibrate boundary conditions, and witness the change of behavior of the system from non-composite to composite. After construction and before opening day, high speed data was collected through static and dynamic load tests for design verification of the bridge, calibration of the baseline structural model, and long-term SHM. Finally, the calibrated baseline model was used to calculate load ratings for comparison with typical rating techniques.

## CHAPTER 2

### CASE STUDY: THE VERNON AVENUE BRIDGE

This research project focuses on a bridge in Barre, Massachusetts, which is a small town of approximately 1100 people located about 20 miles northwest of Worcester and 15 miles southwest of Gardner, MA. The Vernon Ave Bridge (VAB), MassDOT Bridge # B-02-012 connects Worcester Rd, also known as MA state route 122, with the Barre Depot Rd.

Worcester Rd and Barre Depot Rd run on opposite banks of the Ware River, as shown in Figure 7, and the VAB serves as a convenient crossing of the river. Vernon Ave also serves as a bypass of downtown Barre and a direct connection to the Barre state forest and the Barre-Martone regional landfill and recycling facility for points to the north of the Ware River. In 2001, the VAB had a design annual average daily traffic count of 2000 vehicles per day (Vpd), nearly double the population of the town, and the bridge is expected to see nearly 2500 Vpd by 2015 (FST, 2007).

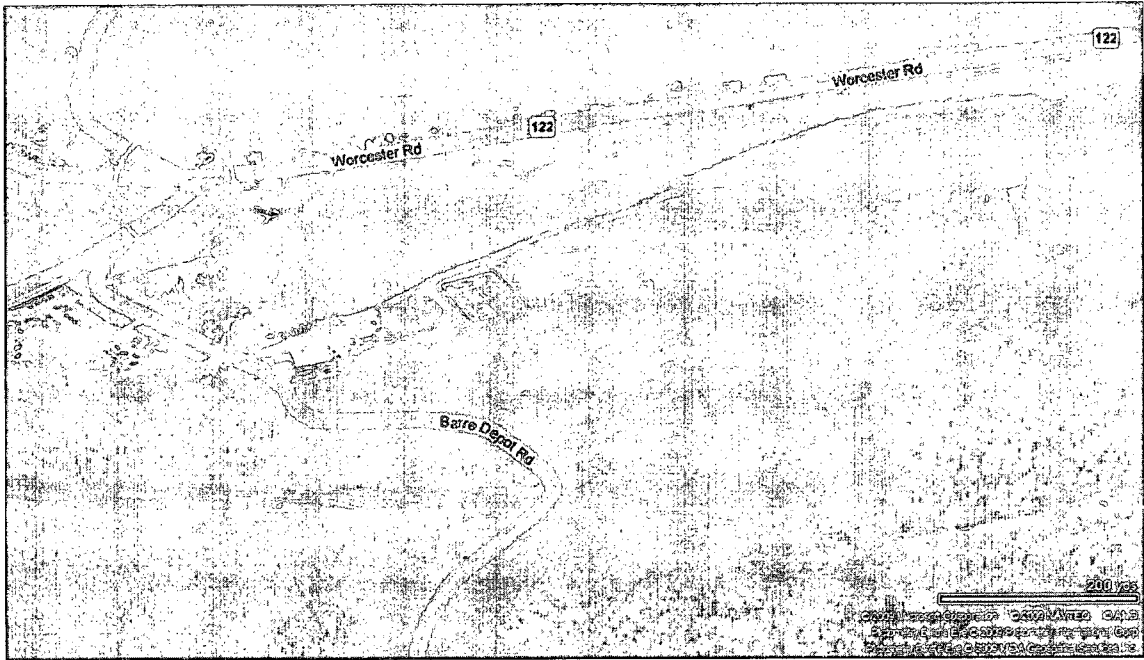


Figure 7. Location of the VAB in Barre, MA

The original research plan was for a single span bridge in Manchester, NH. Preliminary planning had begun and a working relationship with the bridge owner had been developed in previous years. Early on in this thesis work, it became apparent that the bridge was not going to be constructed in the timeline that had been planned. Therefore, the case study was shifted to Barre MA and the VAB. The complexity of the bridge was increased due to the fact it was a 3-span bridge and because the cross-section of the bridge changed over its length. However, most bridges are not single span, simply supported, “textbook” bridge, and it seemed appropriate to research a bridge that balanced simple characteristics with some that were more complex. For example, the bridge has no skew or curvature to it although there is a considerable grade of 3.5% to the roadway, which may have an effect on the shear and axial force distributions.

## **2.1 History**

The VAB site has a long history. To local residents it is known as the Powder Mill Bridge, referring to a gun powder mill that existed at a small dam immediately upstream to the west. According to the Barre Historical Society, the mill was the largest supplier of gun powder to the Union forces during the Civil War. In 1938, the rains from a hurricane flooded much of Barre Plains and South Barre, two communities of Barre. The dam was overrun by the river and many of the bridges were washed out, including the Powder Mill Bridge. The bridge was wooden, like many others of that era.

The events of the 1938 hurricane were not unique, as the Ware River has a long history of massive floods. In the 1950's, the Army Core of Engineers built the Barre Falls Dam, a massive earth dam to control the flooding that resulted in the destruction of many structures such as the Powder Mill Bridge. The original bridge's replacement, a steel girder bridge with a reinforced concrete deck stood until June of 2008, when severe deterioration necessitated its demolition. The final inspection report by MassHighway reported full-depth section loss of the concrete deck in several bays across the bridge. The underside of the bridge deck prior to demolition is shown in Figure 8. The holes in the deck had been temporarily covered up by seven 8' x 20' x 1" steel plates to prevent local failure, shown in Figure 9 (MHD, 2007).



Figure 8. Underside of VAB prior to 2008 demolition.

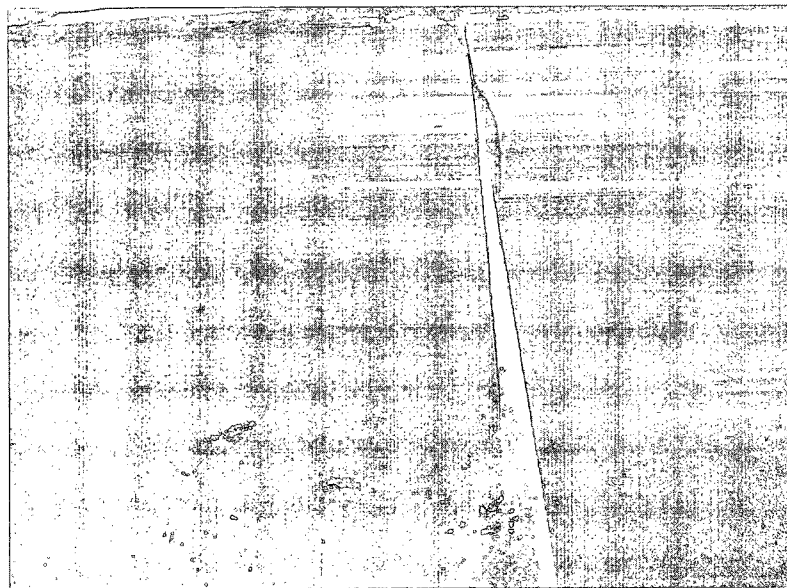


Figure 9. Steel plates installed on bridge deck to protect degrading concrete deck.

Although the bridge lasted for nearly 70 years, its condition was undoubtedly affected by its proximity to the Barre-Martone Landfill and the resulting truck traffic. The replacement bridge, another steel girder bridge with composite concrete deck, opened in September 2009, complete with instrumentation for long-term SHM. The replacement bridge is the target bridge for this research, and is shown in Figure 10.

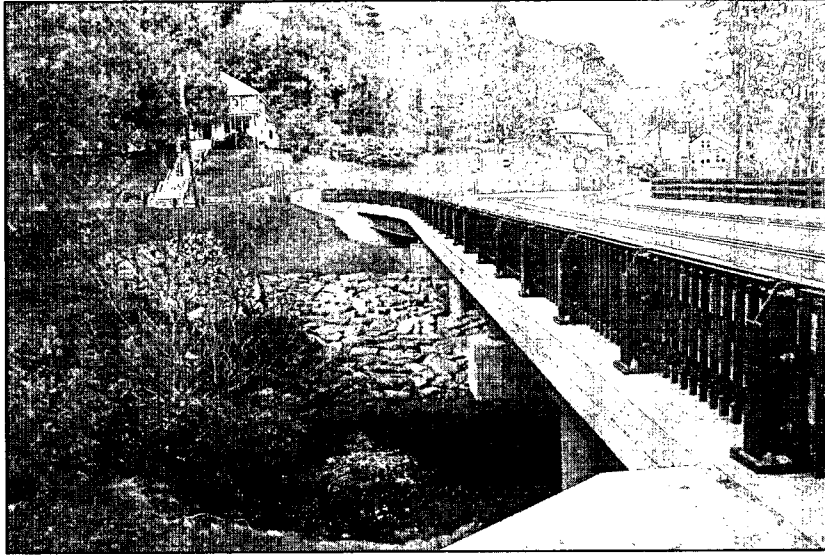


Figure 10. The new VAB, opened in September 2009.

## **2.2 Site Layout**

The VAB is a 3-span continuous steel girder bridge with a composite reinforced concrete deck. The bridge is 47m (154 ft) long with a 23.5m (77 ft) center span and two 11.75m (38.5 ft) outer spans. The bridge is 12.7m (41.7 ft) wide in the south and center spans and widens to about 19m (62.3 ft) at the north abutment to accommodate the intersection with state highway MA122. There is a 3.47% grade in the roadway from south to north and a 2% crown with respect to the roadway baseline, as seen by the design plan and elevation views shown in Figure 11.



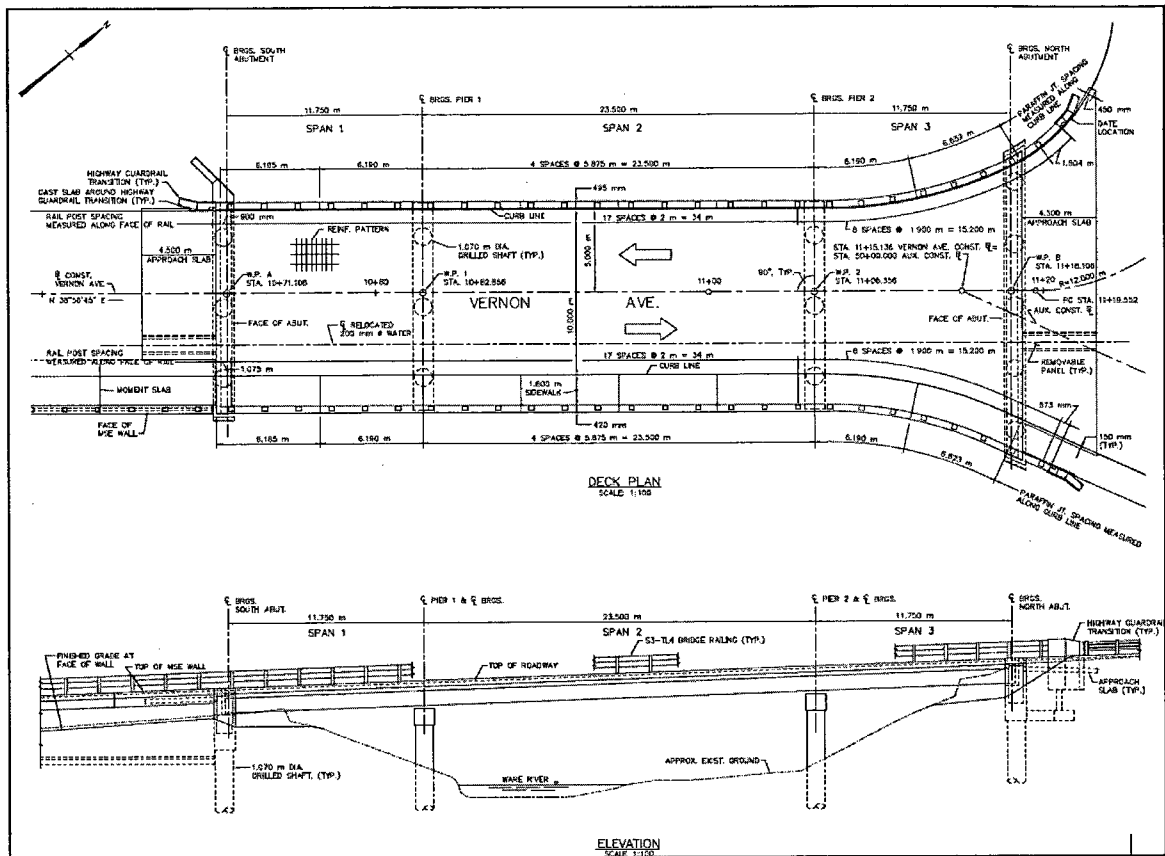


Figure 11. Plan and elevation views of the VAB (FST, 2007)

The concrete deck is a 200mm thick deck and is made of high performance concrete with a nominal design strength of 30MPa (4 ksi). On the west edge is a safety curb and on the east edge is a 1.8m (71 in) wide x 200mm (7.9 in) thick sidewalk. Both the safety curb and sidewalk were poured separate from the deck, but contain steel reinforcement that is integral with the deck. On both edges of the bridge is a steel guardrail. Above the concrete, there is a waterproof membrane topped by a 40mm (1.6 in) thick hot-mix asphalt dense binder course topped by another 40mm of hot-mix asphalt top course as the wearing surface. The deck was designed and constructed to be fully composite using 19mm (3/4 in) steel shear studs which are welded to the top flange of the girders. Stainless steel stay-in-place formwork was used in the interior

bays to hold the concrete in place during pouring and temporary wood formwork was used to support the deck overhang.

There are 6 main girders that run the length of the bridge, evenly spaced at 2.25m (7.4 ft), giving a deck overhang of 732.5mm (28.8 in), as seen in the framing plan in Figure 12. The girders are continuous by design, but with one field splice made up during construction that is located 4.4 m (14.4 ft) south of the north abutment. At the  $\frac{1}{4}$  point of the north span, two new girders are joined to the exterior girders with a web-to-web connection and linearly fan out at a  $10^\circ$  angle to the edge of the bridge in order to accommodate the widening deck. At the north abutment, the fascia girders are spaced about 2.4m (7.9 ft) from the exterior girders. Throughout this document, the main girders shall be referred to by number with girder 1 being the westernmost girder, and girder 6 being the easternmost, as in Figure 12.

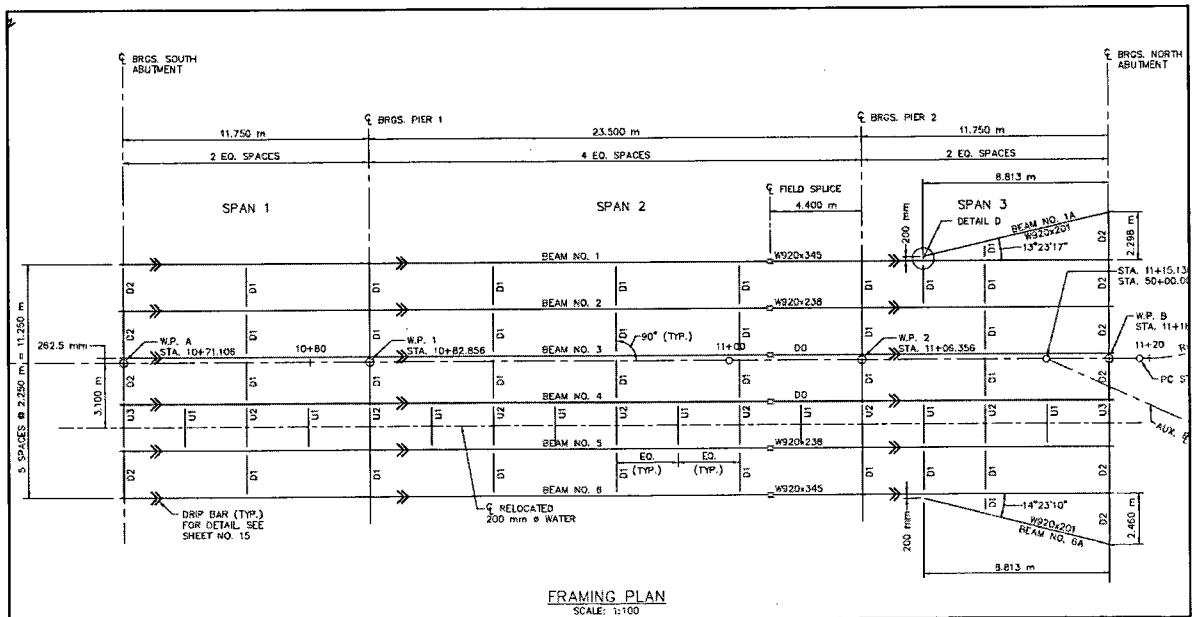


Figure 12. Framing Plan of the VAB ((FST, 2007)

All the steel girders on the bridge are wide-flange shapes made of weathering steel conforming to AASHTO M270M Grade 345W (Grade 50). The interior girders are W920x238 (W36x160), the exterior girders are W920x345 (W36x232), and the fascia

girders are W920x201 (W36x135). There are steel channel-shaped diaphragms for bracing between the girders at the quarter points for the mid-span and at the half point for the end-spans. Between girders 4 and 5 is a utility bay with extra diaphragms to support the weight of a water pipe, shown in Figure 13. At the abutments, the steel diaphragms are encased in concrete, and are poured integrally with the deck concrete. The water pipe and integral end diaphragms are unique points of interest in the study of the performance of the VAB.

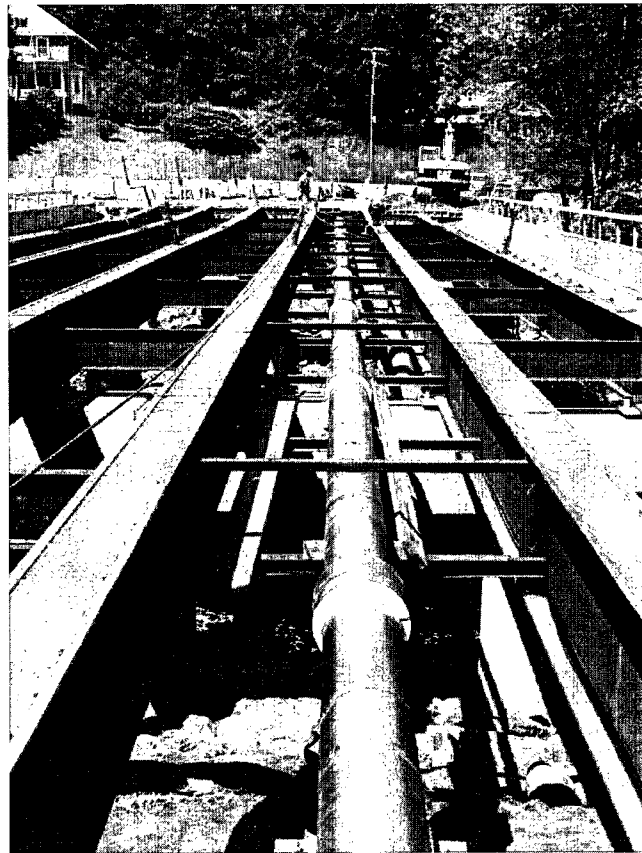


Figure 13. Water main crossing the bridge between girders 4 and 5

Each girder is supported by elastomeric bearing pads at the abutments and at the piers. The pads are circular in shape with a 350mm (13.8 in) diameter and a 61mm (2.4 in) thickness. There are 4 internal 11ga steel shims with 13mm (0.52 in) spacing between the shims. There is a 5mm (0.20 in) cover of elastomer on all sides of the pad.

The shims are A1011 Gr250 steel and the elastomer was a neoprene rubber with a design hardness of durometer 60 grade 3, which is a standard for the geographical region concerned the extreme temperature variation over the course of the year. The shop drawing detail of the abutment pad is shown in Figure 14. The placement of these bearing pads prior to steel erection is shown in Figure 15.

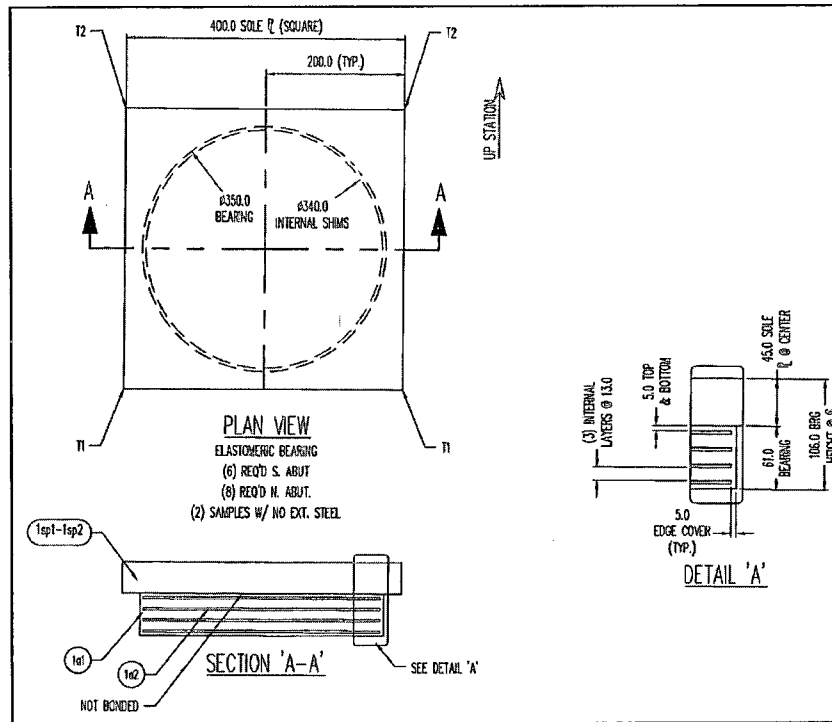


Figure 14. Elastomeric bearing pad cross sections from shop drawings(DS Brown, 2008).

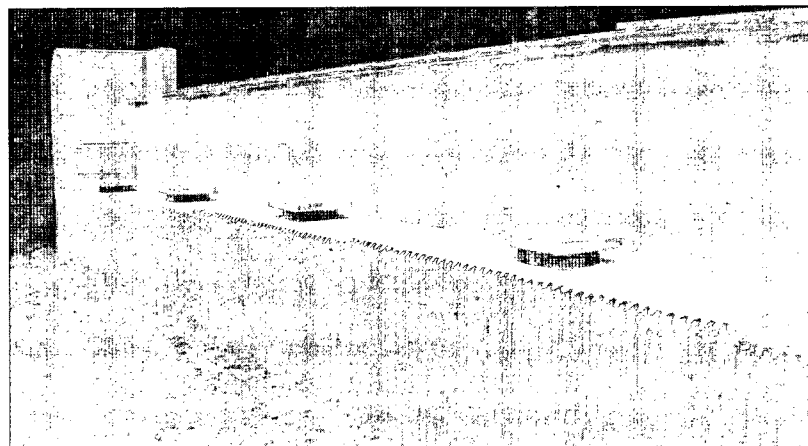


Figure 15. Sole plates on top of the elastomeric bearing pads at the south abutment prior to steel erection.

The substructure consists of the concrete abutments and two concrete piers. Each pier consists of three columns with a 915mm (36 in) diameter circular cross-section beneath a pier cap of rectangular cross section 1.2 m (47 in) wide by 1.0 m (39.4 in) tall. The bridge seats on which the bearing pads are placed are perpendicular to the bridge layout line, which for modeling purposes is considered the equivalent of a fixed base.

### **2.3 Summary**

The VAB is a two-lane three-span continuous steel girder bridge with composite reinforced concrete deck located in Barre MA. The VAB is owned and managed by the Town of Barre, was designed by Fay, Spofford, and Thorndike, Inc., and was constructed by ET&L Construction under the supervision of MassDOT. The bridge was instrumented by researchers at Tufts University and the University of New Hampshire under the guidance of previous in-house research, research at other institutions, and with the professional advice of instrumentation and structural monitoring experts at Geocomp Corp.

## CHAPTER 3

### INSTRUMENTATION

The instrumentation of the VAB consisted of two phases: planning and installation, and testing and data acquisition. There were not only many details to consider about sensor choice and placement for SHM, but there were also issues relating to the logistics of installation during construction, approvals by ownership and management, legal and safety considerations, and concerns of vandalism that needed to be considered in the plan. During the course of installation, many details that were not considered during the planning phase needed to be addressed, including intricate details of power and permanent cabling.

#### **3.1 Preliminary Modeling**

The instrumentation planning began with preliminary modeling. A single beam model, continuous over three spans, and supported by pins and rollers, was used to determine rough sensor placement across the length of the bridge. The frame cross section was assumed the same as an interior girder (a W920x238, or a W36x160 in US Customary units) and the span lengths of the girder were as in the VAB. This basic model was analyzed for response due to self weight, as seen in Figure 16.

The purpose of this simplified modeling was to guide the selection of sensor placement to ensure a meaningful response in the collected data. The location was dependent on the type of sensor to be installed. For example, if rotational data was of interest, the deflected shape was analyzed to determine areas of maximum rotation.

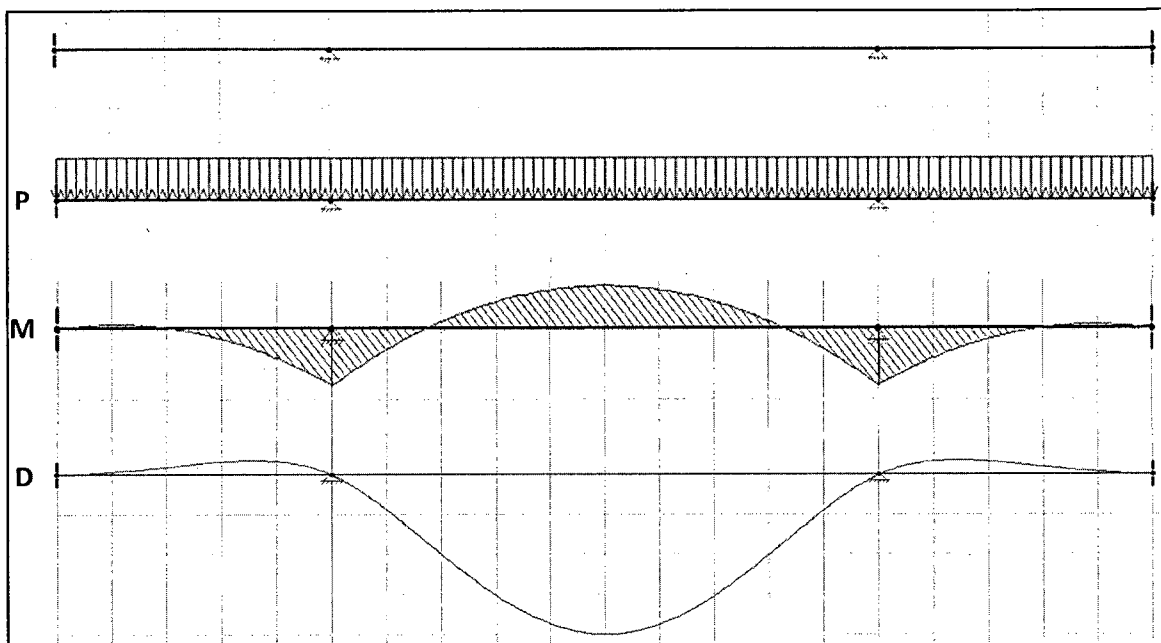
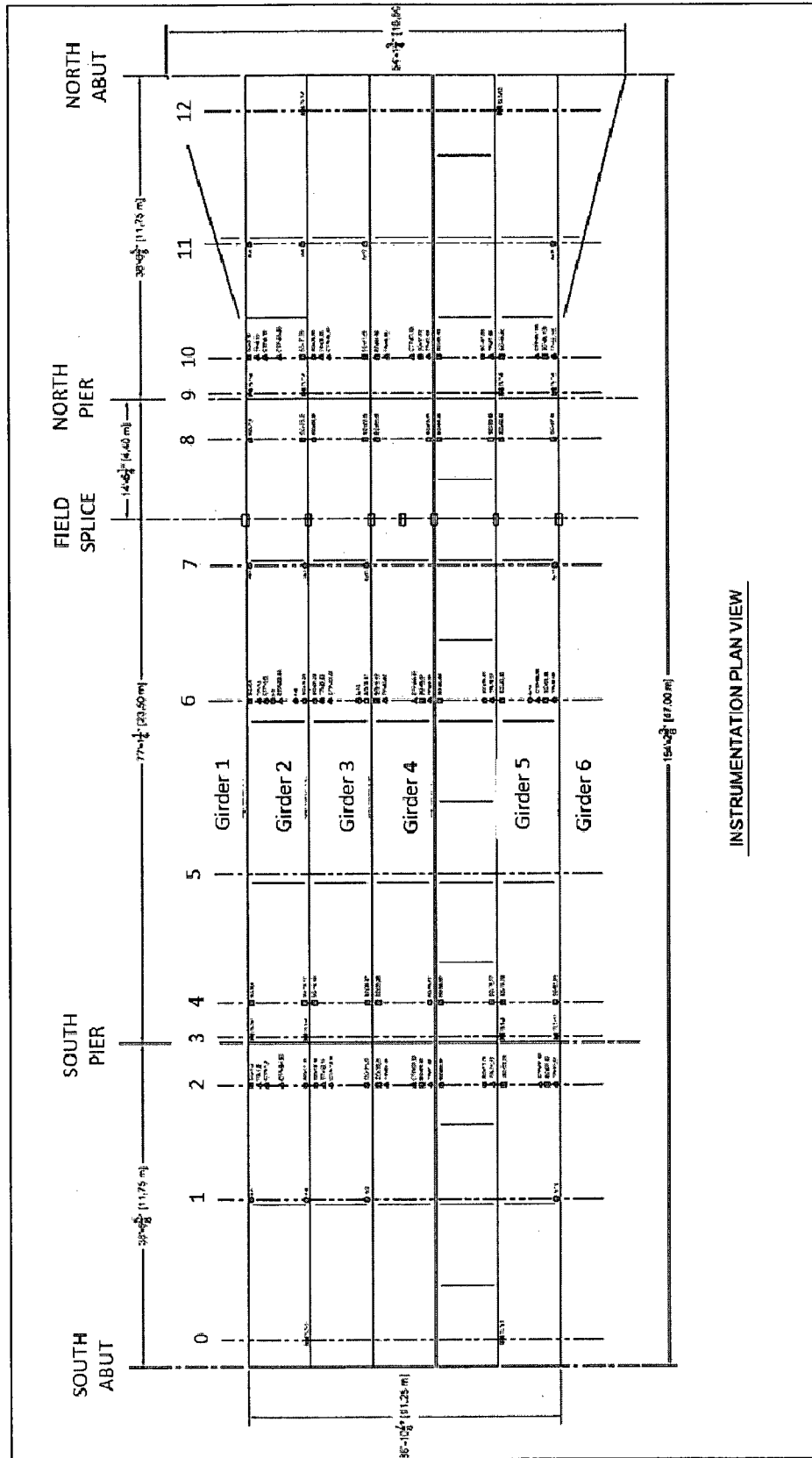


Figure 16. Preliminary modeling and analysis for the planning of instrumentation

The complete instrumentation plan included considerations for static measurements of strain, temperature, and rotation, and the dynamic measurements of acceleration. Each measurement type and location will be discussed individually below. A framing plan marked with station numbers can be seen in Figure 17 and an example elevation showing instrumentation of the north section of girder 2 is shown in Figure 18. The complete version of the instrumentation plan, including an elevation of each girder can be found in Appendix H.



INSTRUMENTATION PLAN VIEW

Figure 17. Annotated framing plan with instrumentation station numbers marked along the top of figure



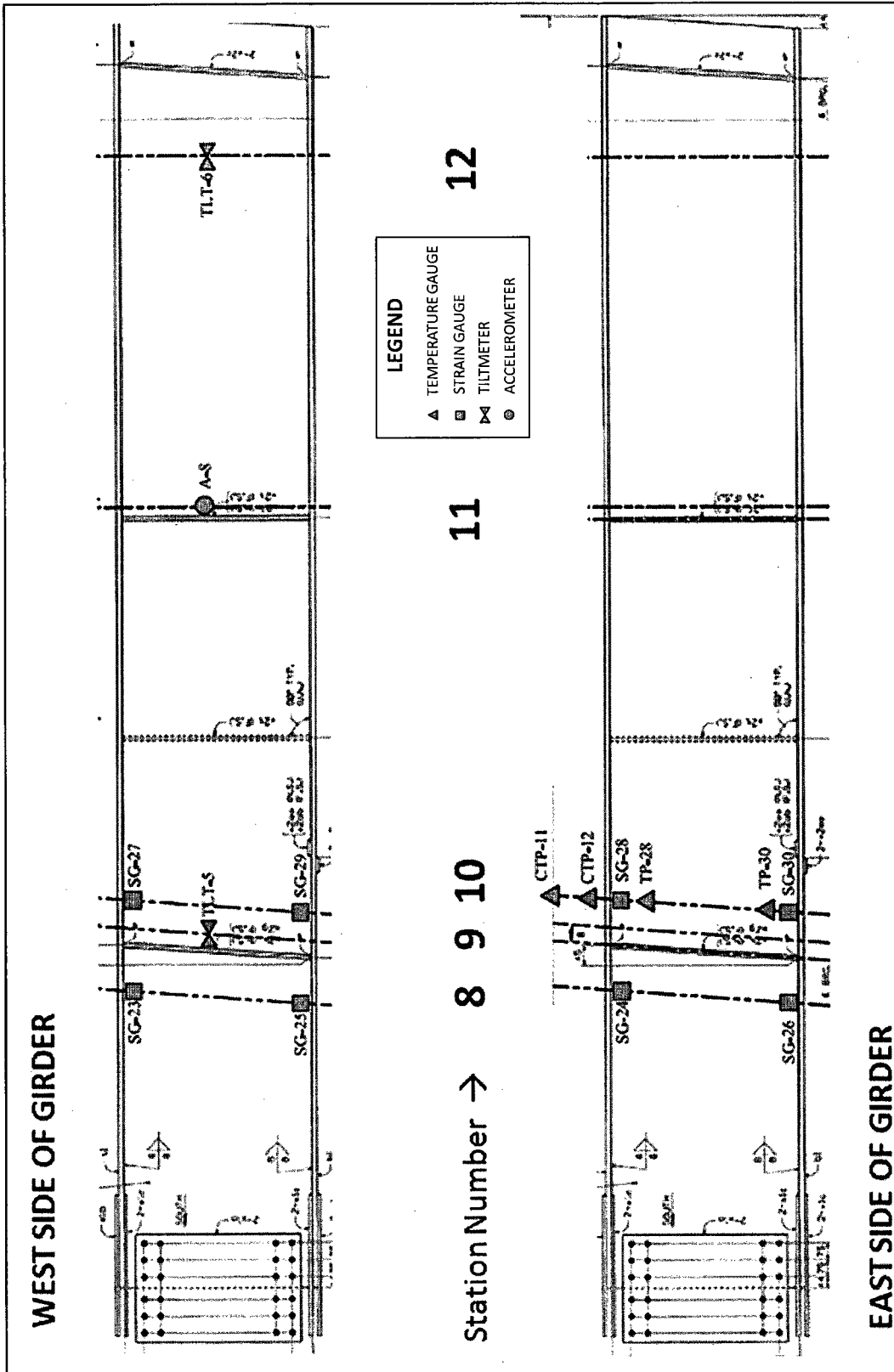


Figure 18. Sample girder elevation showing instrumentation of the north section of girder 2

## **3.2 Instrumentation Plan by Sensor Type**

### **3.2.1 Strain Gauges**

Strain gauges are a simple and inexpensive form of instrumentation, and commonly used for measurement of strain. An Omega® 3-wire uniaxial strain gauge, model # KFG-5-350-C1-11L3M3R, was used on the VAB instrumentation plan at costs of approximately \$20 each. Strain is measured electrically through a change in resistance which can be captured using data acquisition. The strain can be converted to stress, and then into forces using properties of the cross section. The forces can then be converted to bending moment, and is therefore appropriate for use with the instrumentation of a braced beam, where the primary response is bending.

The strain gauges were installed on all six steel girders at locations where the largest bending moments were expected. These locations were above both piers for negative moment and at the midpoint of the center span for positive moment. These locations refer to stations 2, 4, 6, 8, and 10 in Figure 17. At each location, 4 strain gauges were installed: two on the top side of the bottom flange, and two on the underside of the top flange, as shown in Figure 19. The only exception to this pattern is on the exterior girders. Strain gauges were installed only on the inner side of the exterior girders to protect the gauges from the weather, hide the instrumentation from the public to discourage vandalism, and for aesthetic purposes.

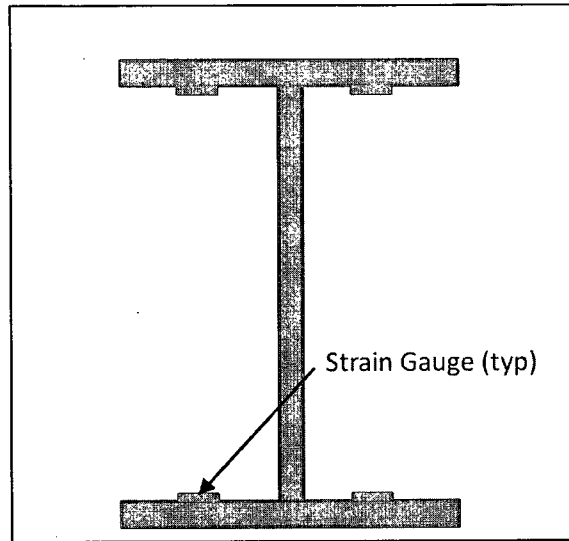


Figure 19. Typical strain gauge locations on top and bottom girder flanges (depiction is of an interior girder)

This configuration was installed at each location for multiple reasons. Strain readings on both sides of the web would verify the reliability of each gauge and also help to determine the presence of weak axis bending or torsional effects in the girders. Lastly, having gauges on both the top and bottom flanges can help to determine the location of the composite neutral axis: By assuming a linear strain distribution across the composite section, two measurements of strain across the section can be used to determine where strain is zero and therefore locate the neutral axis. This concept is illustrated in Figure 20 and the results of this study are shown in Chapter 5. A major assumption of the linear strain distribution is that the applied loading will cause only linear elastic responses.

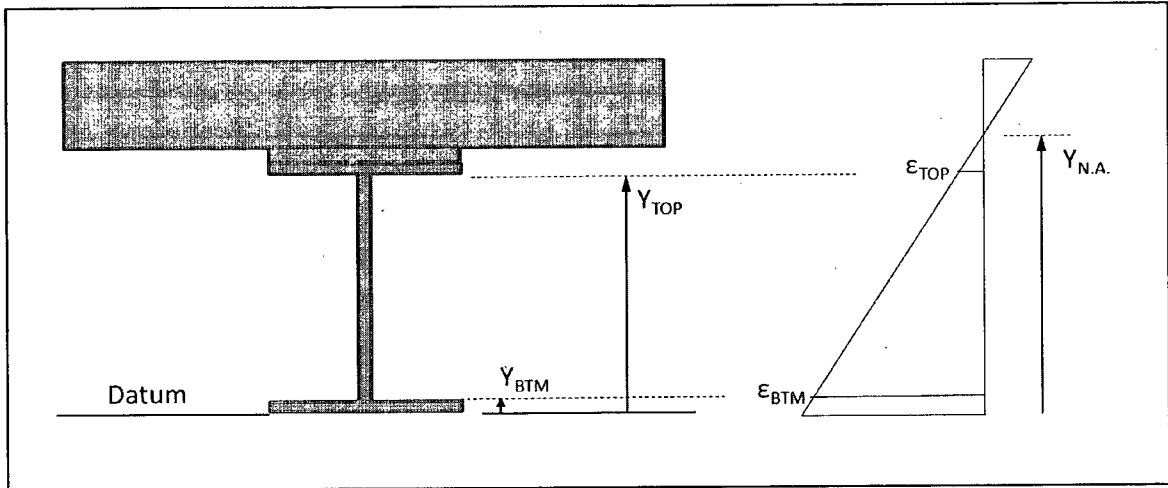


Figure 20. Illustration of neutral axis of a composite section

### **3.1.2 Temperature Gauges**

YSI 44000 Series temperature gauges, or thermistors, were installed across the depth of the composite section to capture the temperature distribution and therefore account for the contribution of strain due to thermal load. Capturing the temperature across the section required embedment of thermistors in the concrete deck as well as attachment of thermistors to the steel girders. On the steel, the sensors were placed adjacent to strain gauges as possible at stations 2, 6, and 10. It was assumed that the temperature on either side of the girders would not differ, and therefore only two gauges were used per station: one on the top flange and one on the bottom.

Two thermistors were tied to the rebar cage in the concrete as shown in Figure 21. The location of the concrete thermistors was at stations 2, 6, and 10 above girders 1, 2, 4, and 6, and in the bay between girders 1 and 2. The purpose of the thermistors was to determine the temperature distribution across the composite section at all strain gauge stations, but it was assumed that direct exposure of the deck to the weather would create a uniform temperature across the exposed surface. Thus, it was not necessary to install thermistors at every strain station. The thermistors in the bay

between girders 1 and 2 were installed to determine if the exposure of the underside of the deck to shaded conditions affected the temperature in the concrete. This could be compared to the typical location where the thermistor was directly above a girder. Collected temperature data was not processed during the course of this research and was set aside for future work.

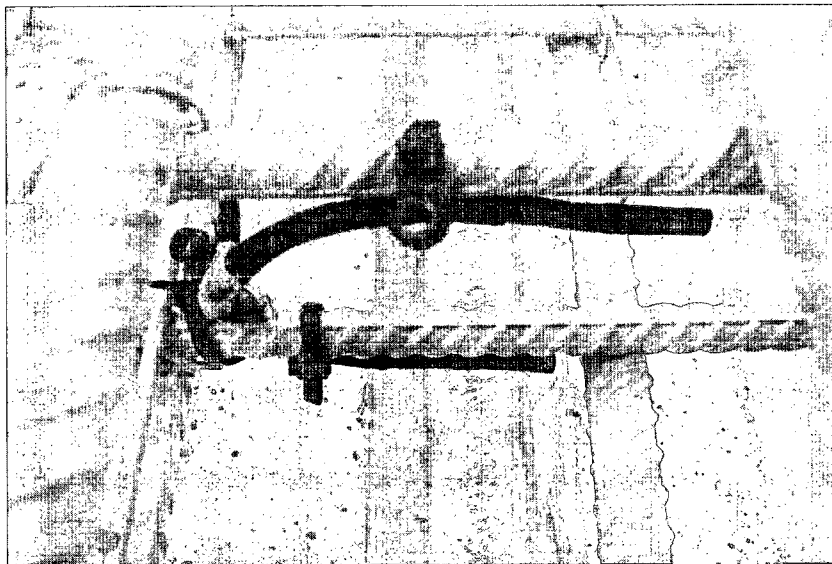


Figure 21. Location of thermistors on longitudinal reinforcing steel

### **3.1.3 Tiltmeters**

Dual axis tiltmeters, or inclinometers, (VTI Technologies inclinometer model # sca121t) were installed at a variety of locations in order to determine changes in rotation in the girders, on the face of the abutments, and on the face of the piers. These tiltmeters were placed to measure rotation about the weak axis of the girders (about the line perpendicular to the layout line) and were installed at the center of the web of girders on girders 2 and 5 at stations 0, 3, 9, and 12. On girders 1 and 6, the tiltmeters were installed at the piers, stations 3 and 9, only. Additional tiltmeters were installed on the substructure locations (abutments and piers) in order to determine any relative

rotation of the superstructure with respect to the substructure. The substructure tiltmeters were placed to measure rotation about the weak axis of the girders and also about the strong axis (about the bridge layout line). These sensors can verify the assumption that the abutments and piers function as fixed ends in the structural modeling of the bridge by measuring the rotational rigidity transferred to the superstructure elements from the foundation elements. The tiltmeters were not processed as part of this research due in part to noise found in the data. An in depth study into the source of the noise in the datasets is set aside for future work.

#### **3.2.4 Accelerometers**

Accelerometers (Dytran model #7521A1) were installed to study the dynamic response of the VAB. Accelerometers capture accelerations that can be used to determine dynamic properties of the structure, such as the bridge's natural frequency. Sensors were placed on girders 1, 2, 3, and 6 at stations 1, 5, 7, and 11 in Figure 17. Modal analysis of the initial course model predicted that the accelerometers at these stations would best capture behavior relating to the primary bending mode of the structure. These sensors were not post-processed for this research.

#### **3.2.5 Pressure Cells**

Two earth pressure cells, Geokon series 3500 with a 250 kPa (36 psi) capacity, were installed in the sub-base aggregate of the approach. Both cells were installed in the south approach, one in each lane: In the southbound lane, the cell is installed under the passenger-side wheel path; in the northbound lane, the cell is installed under the driver-side path. The top surface of both cells was in direct contact with the asphalt. Figure 22 is an annotated site plan view from the design drawings showing the proposed location of pressure cell installation.

The pressure cells can act as vehicle identification system or traffic counter for the determination of annual average daily traffic (AADT) and annual average daily truck traffic (AADTT) counts. The sensing of a heavier vehicle can act as a trigger for the data acquisition system activation. Conversely, the sensing of a period of no-loading can allow for the study of environmental effects. Finally, the cells can provide a dataset into the research of asphalt pavements and the distribution of load through the pavement. The cells were not used in this research, but information on installation location and purpose was important for future work.

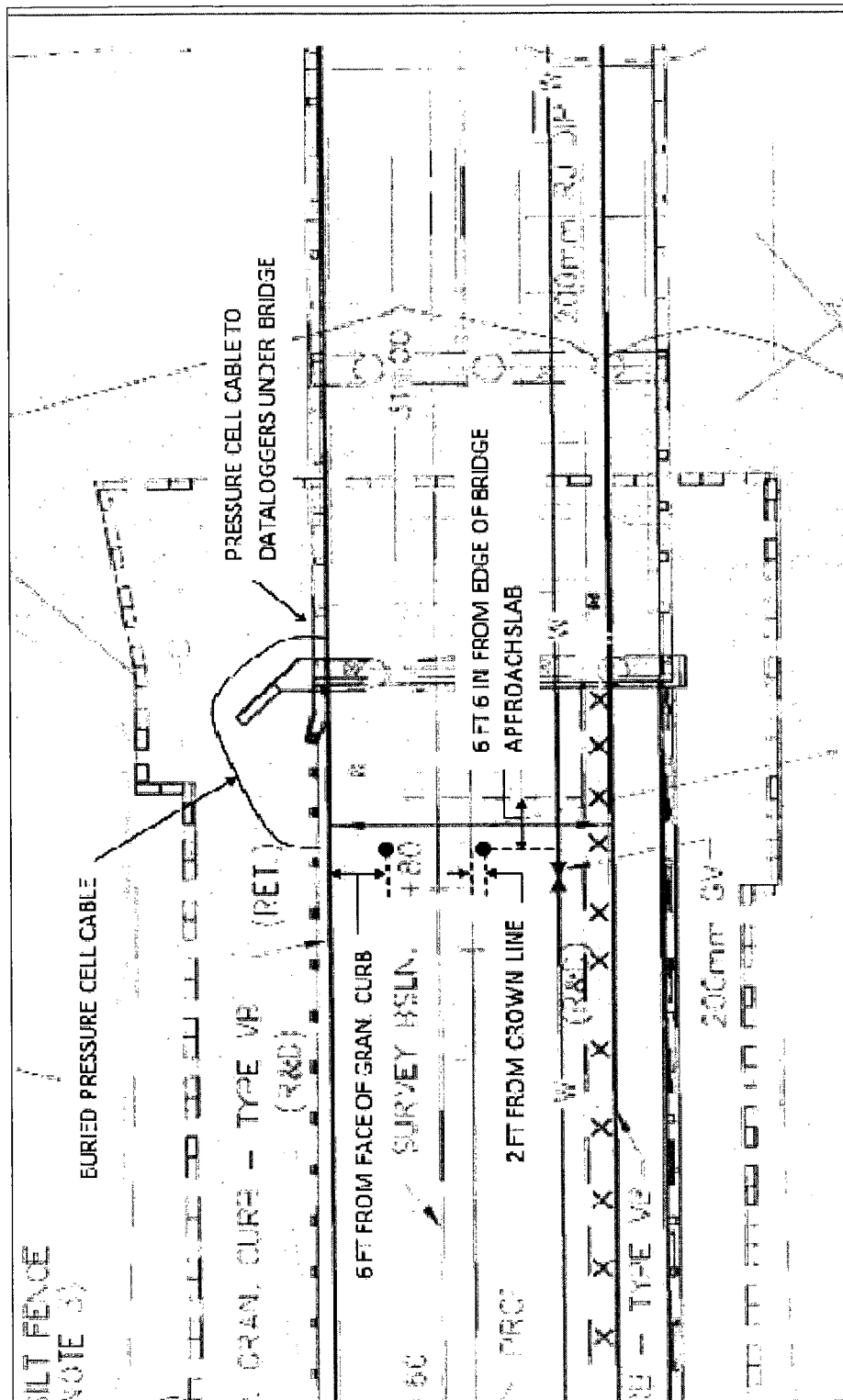


Figure 22. Plan view of pressure cell installation location.



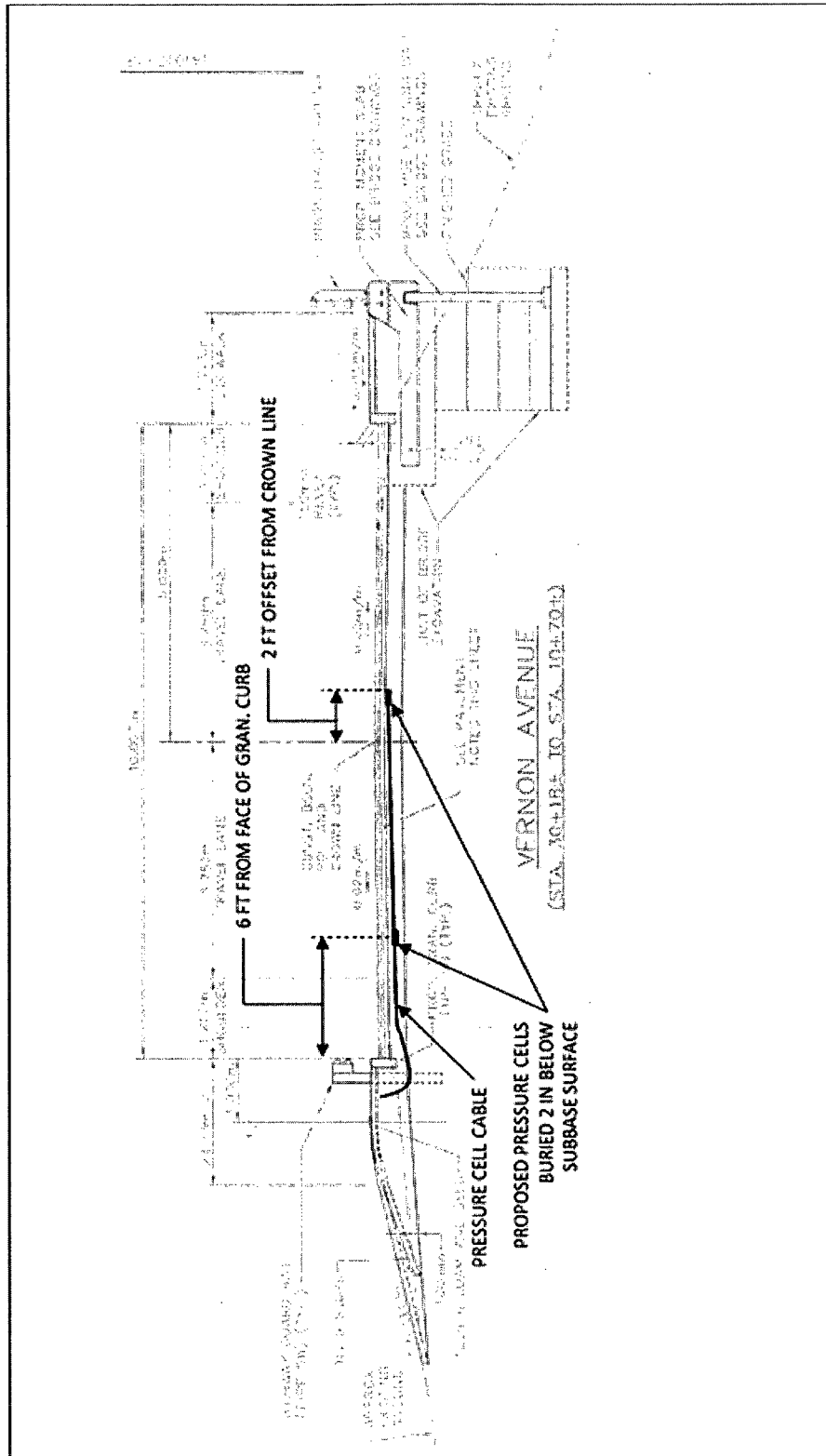


Figure 23. Cross Section of Vernon Ave Approach with pressure cell installed locations

### **3.2.6 Datalogging**

The datalogging system for DAQ was a set of 16 linked multichannel dataloggers called iSites. They were designed by Geocomp Corp. especially for outdoor applications since each was housed in its own rugged and environmentally protected box (see Figure 28). Combined with an internet connection, Ethernet hub, computer, the system provides a completely remote DAQ system. Geocomp also has a website called iSite Central to allow for 24-7 monitoring of the structure, automatic post processing of raw data, and an adjustable trigger alarm system to notify the user of potential emergencies. The VAB monitoring site can be found at <http://isite8.geocomp.com/NSF/>. The username and password can be obtained from Erin Bell at UNH or Masoud Sanayei at Tufts University. Figure 24 shows the iSite Central web-based interface, with SG22 displaying strain readings over 1 week. The strain due to temperature is clearly evident in the cyclic nature of the measured strain. Figure 25 is a schematic describing the process of data collection.

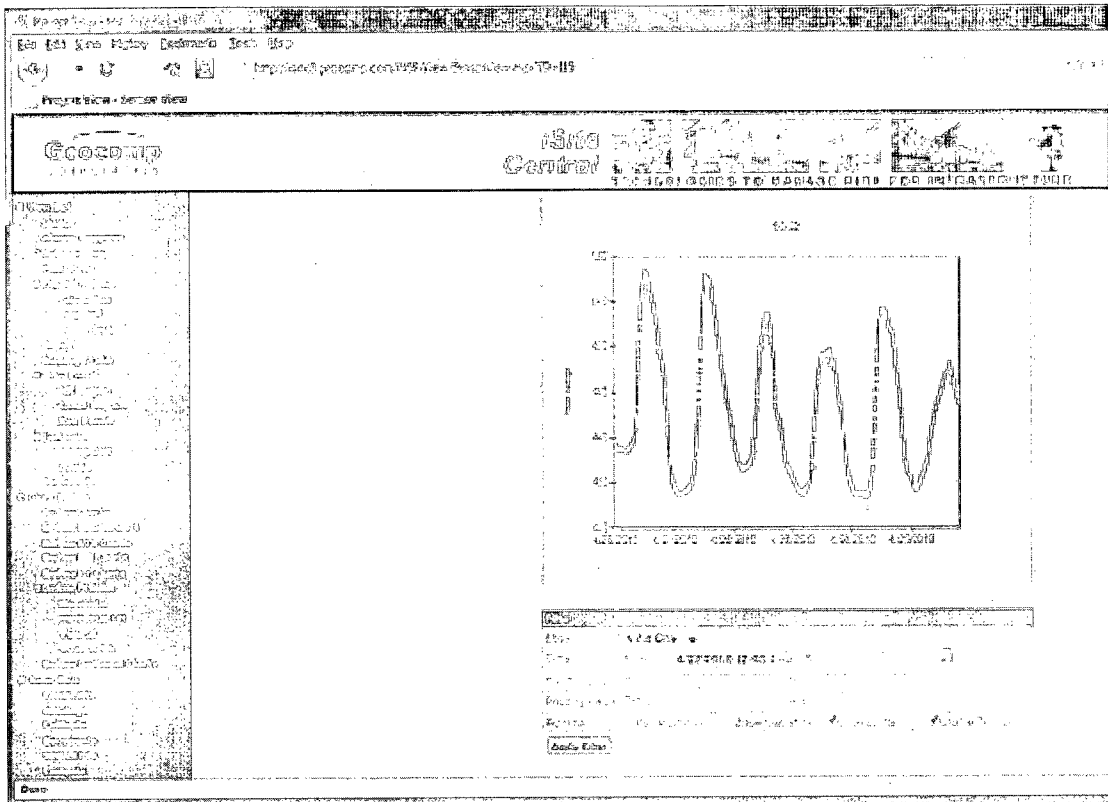


Figure 24. iSite Central Internet-based remote monitoring system

Two types of loggers were installed at the VAB. The first is a low-speed datalogger called the iSite-V3, which capable of sampling at a rate of 5 Hz (5 samples per second). These iSites have 16 channels each and were used for sampling of temperature data, which is not expected to need a high sampling rate. The other type of iSite logger is the iSite-HS which has 8 channels and is capable of sampling at rates to 200 Hz. 13 iSite-HS dataloggers were used to collect data from strain gauges, tiltmeters, accelerometers, and pressure cells. Each different type of sensor required different internal programming of the iSite logger, and was completed by Geocomp in conjunction with researchers at Tufts University as part of the collaborative effort within this project.

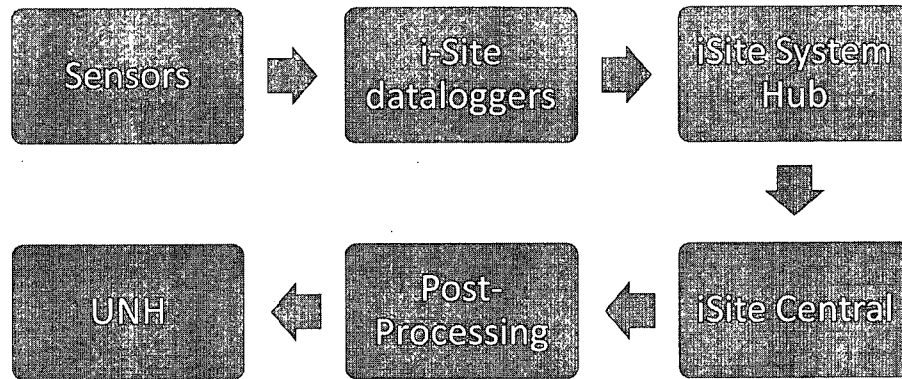


Figure 25. Schematic describing data collection process

### **3.3 Installation**

The installation of the instrumentation system took place over three months during construction and chronologically, there were four phases to the installation process:

1. Prior to steel erection (May, 2009).
2. After steel erection but prior to the installation of the concrete formwork (June, 2009).
3. After deck reinforcement installation, but prior to the concrete deck pour (July, 2009).
4. After the deck pour but prior to bridge opening and controlled load test (August, 2009).

#### **3.3.1 Installation Prior to Steel Erection**

The first phase was strain gauge installation on the girders. Strain gauging is a time consuming process, with each installation taking approximately 30 minutes to complete, from surface preparation to environmental protection. Installation over a river or at heights only reachable by ladder or scaffolding would add additional time.

Therefore, the installation of strain gauges occurred at the High Steel fabrication plant in Lancaster, Pennsylvania. In the steel yard, sensors could be installed at ground level, saving valuable time (see Figure 26). A team of six researchers from Tufts University, UNH, Geocomp Corporation, and FST spent six days completing the installation of 100 strain gauges, 36 steel-mounted thermistors, and related cabling.

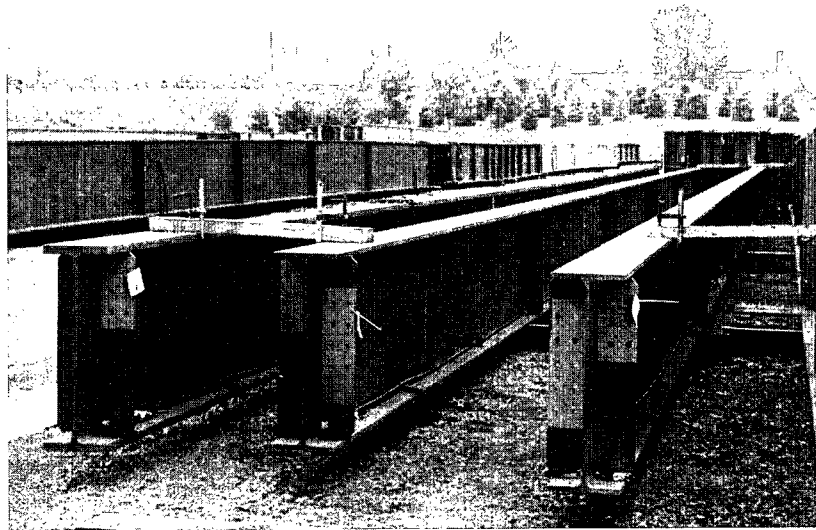
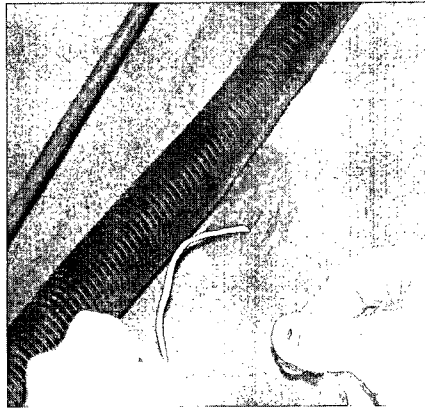


Figure 26. Three of the steel girders at the steel fabrication plant in Lancaster, PA.

The procedure first involved surface preparation by grinding, sanding with fine grit sand paper, and cleaning with acetone. Then the strain gauge was attached to the steel with Loctite Super Bonder Instant Adhesive #496. The installed location was recorded relative to the nearest web stiffener plate along the length and to the edge of the flange widthwise. Next, the strain gauge wire was spliced to the DAQ cabling using Grainger insulation displacement wire connectors, (Grainger P/N 4FE28). Then, the cabling close to the gauge was secured to the girder using Oatey Fix-it-Stick epoxy putty (Oatey P/N 31270) to prevent the gauge from being disturbed. Finally, the assembly was environmental protected by first covering the gauge with silicone caulking, then covering with aluminum tape. Each completed installation was marked for sensor identification. The procedure for installation of steel-mounted thermistors was similar,

but required less surface preparation since their functionality was not dependent on adhesion to the surface like strain gauges. The procedures for all instrumentation installations were courtesy of Geocomp Corporation, and details of the installation can be found in Appendix H. Figure 27 shows a strain gauge mounted to the prepared steel surface and Figure 28 shows a completed installation of a strain gauge with thermistor, including environmental protection. All sensors were also checked for functionality using a multimeter. This process ensured that the gauges were functional by measuring resistance through the gauge. All other DAQ cabling was run along the girders in preparation for the remaining sensor installation after steel erection, and was gathered in a split wire loom wiring harness for security during transport. Following the completion of the installation, the girders were loaded on trucks for delivery to the VAB site.



**Figure 27. Strain gauge installed on prepared surface**



Figure 28. Strain gauge and steel-mounted thermistor installation with environmental protection and labeling

### **3.3.2 Installation Prior to Concrete Formwork**

Once erection of the steel girders was completed, the construction process could continue to welding of angle supports for concrete stay-in-place formwork, installation of wooden formwork on exterior girders for the deck overhang, and installation of the water pipe that is supported by the diaphragms between girders 4 and 5 (shown in Figure 29). The process of the water pipe installation took about a week, which allowed plenty of time for the instrumentation process to continue. First, the sensor cabling from the two girder pieces could be spliced together. This involved tying in to the steel erector's fall safety system and beam walking to the location of the field splice in the girders, in the center span near the north pier. A plank was dropped on to the bottom flanges of the girders and researchers from UNH, with permission and training from the steel erectors at Atlantic Bridge & Engineering and the general contractors from ET&L, spliced the cables for all sensors located on the north side of the bridge. Researchers walking the steel beams can be seen in the background of Figure 29.

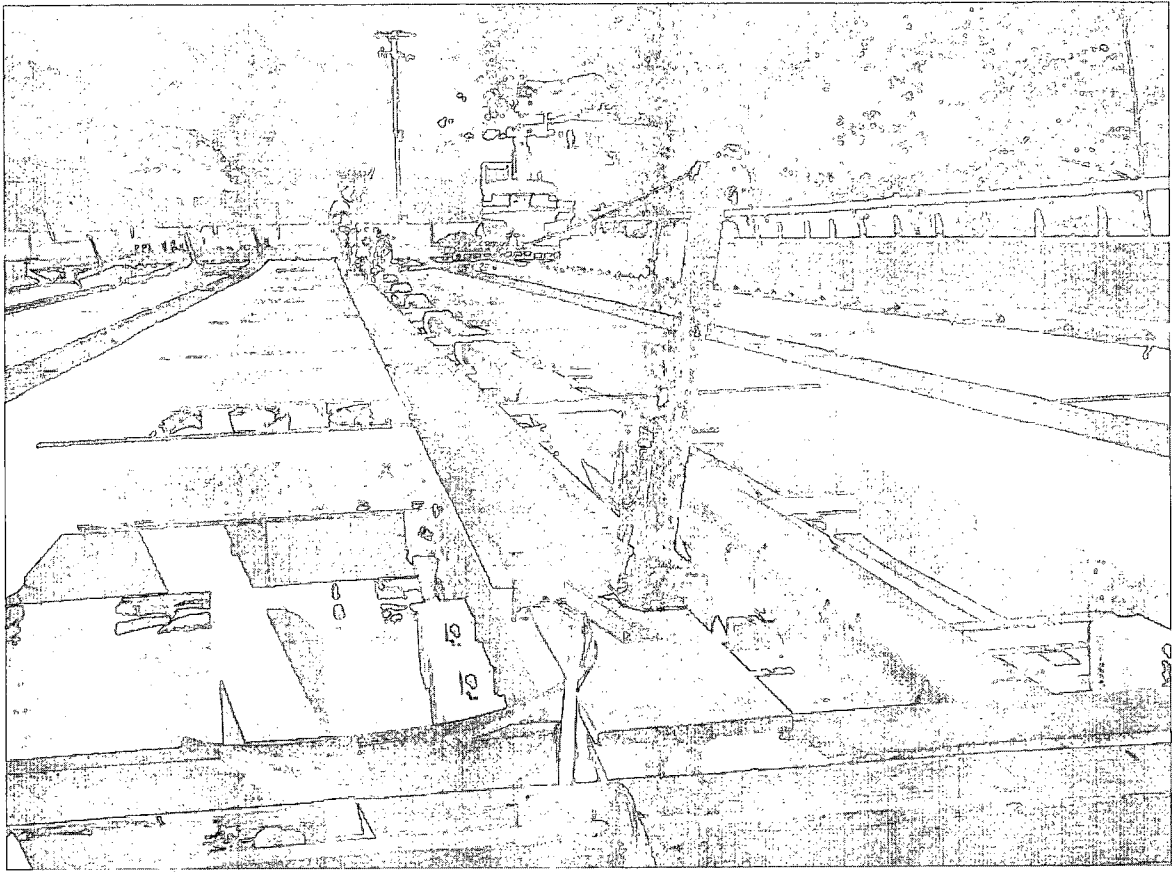


Figure 29. Water pipe between girders 4 and 5. Researchers can be seen in the background splicing the DAQ cabling over the steel field splice.

While the wiring was being spliced, the iSite data loggers could be installed. All six girders were used for placement of a total of 19 iSite boxes. The boxes themselves were bolted to steel angle, zinc-oxide coated to minimize impact to weathering steel, and the angle was mounted to the bottom flange of the girders using c-clamps (Figure 30).



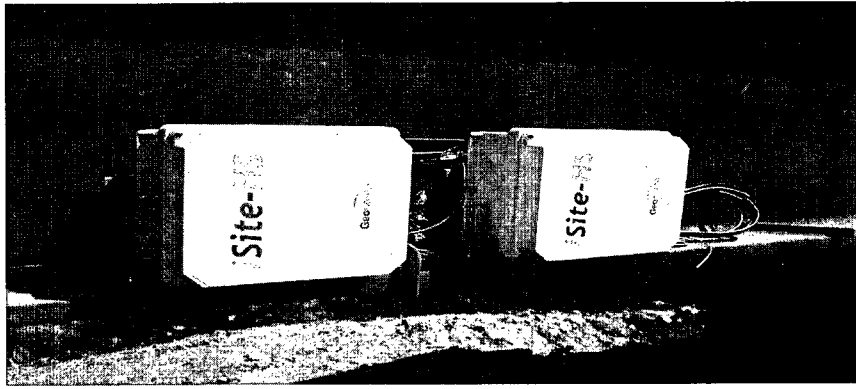


Figure 30. Installed iSite boxes with completed cabling, angle mounting, and c-clamp installation

Once the boxes were installed and the DAQ cabling was spliced, the cabling could be organized and grouped by iSite box, sensor and girder. It became inevitable that some cables needed to be run across diaphragms to adjacent girders in order to accommodate the placement of iSite boxes. The cables were grouped together with zip ties at these locations and many others along the length of the girders to keep the instrumentation wiring as neat and tight as possible. See Figure 31.

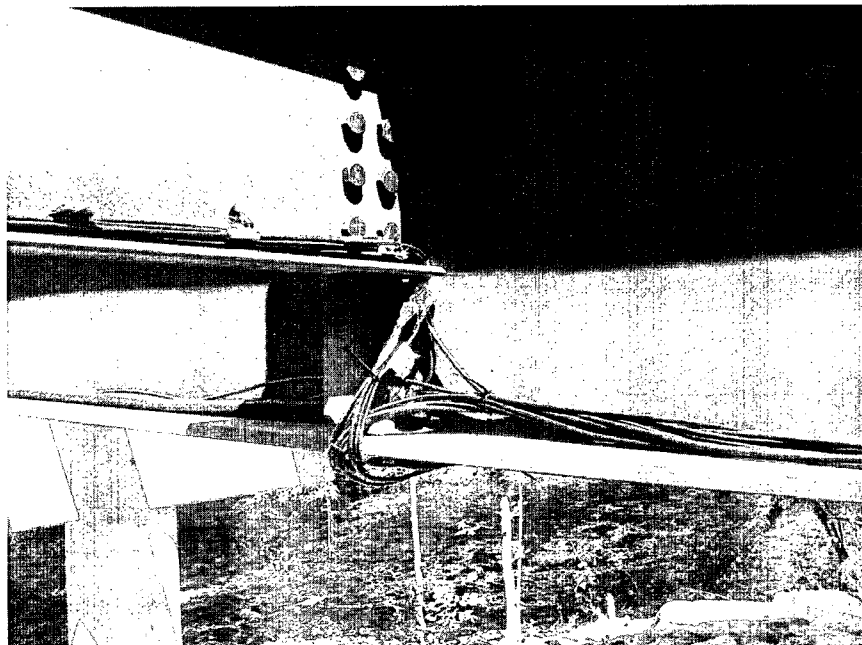


Figure 31. Cabling grouped across girders to accommodate iSite placement

After the wiring was labeled and organized, the iSite boxes were wired with the cables from each of the sensors. This involved a lot of wire-stripping and cataloging. The life of the instrumentation system was planned to coincide with the life of the bridge, which is why well-organized and user-friendly records were vital. Each cable contained the wires for as many as four gauges or as few as one. And each cable contained 8 wires that needed to be stripped and inserted into the appropriate iSite channel. A researcher from UNH is seen in Figure 32 performing the wire installation and sensor channel cataloging for an iSite box.

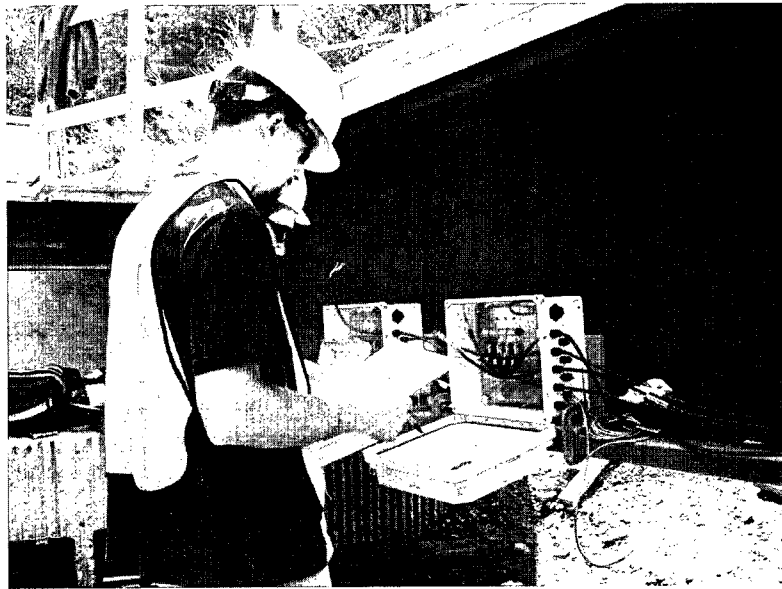


Figure 32. Book-keeping for 200 gauges during iSite installation

### **3.3.3 Installation Prior to Concrete Pour**

Once the stay-in-place formwork was installed, ET&L's construction crews worked to lay out the concrete deck reinforcement cage. As was noted before, thermistors were tied to the longitudinal bars above some of the strain gauge stations to capture the full temperature distribution across the composite section. The cabling was then threaded under the stay-in-place forms, as seen in Figure 33, to be linked with the rest of the wiring harness and then back to the iSite-V3 loggers.

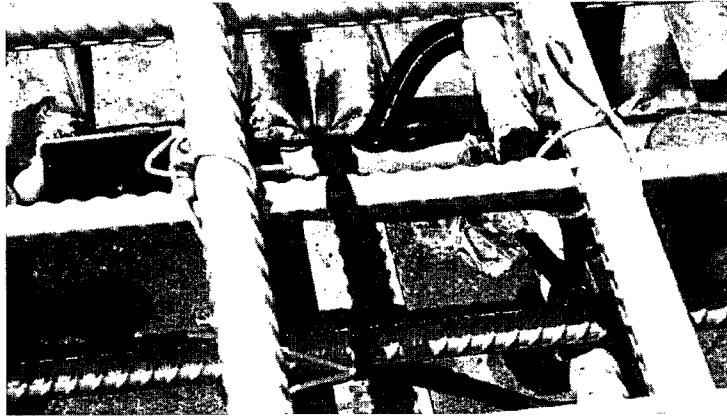


Figure 33. Installation of concrete thermistor on deck rebar

### **3.3.4 Installation Prior to Load Test**

Due to the sensitivity of the instruments and cost of replacement, accelerometers and tiltmeters were installed on girders after concrete pour and prior to load testing. The concrete formwork provided protection from weather and construction debris, assuring that they would not be accidentally damaged. The installation process is very similar to that of strain gauges in terms of surface preparation and environmental protection. They were affixed in a slightly different manner though, as epoxy putty was used as the adhesive to the girder surface (Figure 34 and Figure 35). The detailed procedure for installation of tiltmeters and accelerometers can be found in Appendix H.



Figure 34. Accelerometer adhered to girder with epoxy putty

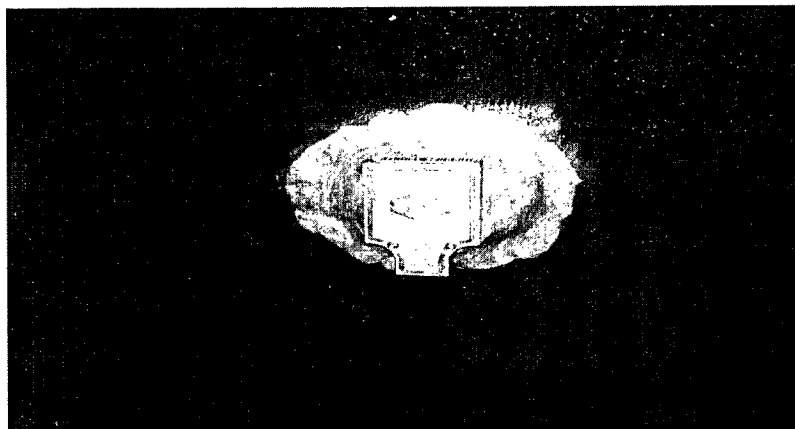


**Figure 35.** Tiltmeter adhered to girder with epoxy putty, prior to application of environmental protection

The pressure cells were the last to be installed since the last stage of construction was the asphalt pavement and wearing surface. The pressure cells were installed in the subgrade of the bridge approach roadway on a specially prepared surface within the aggregate using stone dust to ensure even distribution of loads to the cells (Figure 36 and Figure 37). If large aggregate were to be in direct contact with the cell, it could cause a stress concentration at the point of contact, which would compromise the accuracy of the collected data. Hot asphalt was carefully hand tamped by construction workers atop the cells to ensure full surface contact of the asphalt to the top surface of the cells. This was done immediately prior to the paving of the approach roadway to ensure that the hand-tamped asphalt would adhere to the wearing surface.

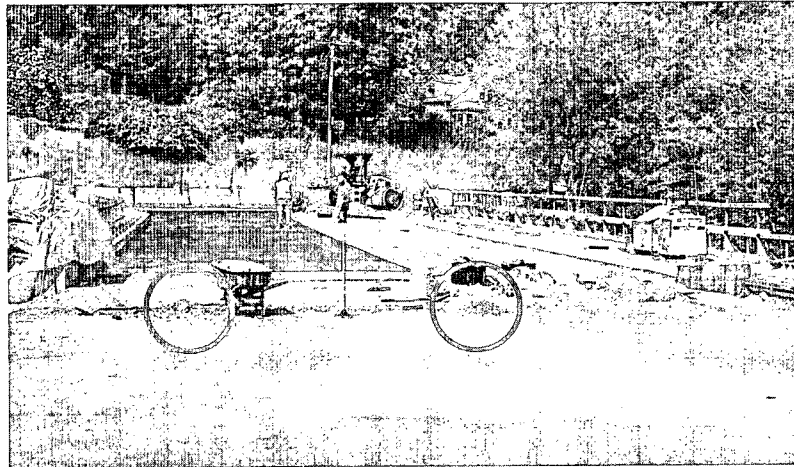


Figure 36. Pressure Cell Layout prior to Installation



Figure 37. Pressure cells installed in subgrade prior to paving

### **3.5 Logistical Considerations**

#### **3.5.1 Legal Concerns**

Due to the multifaceted nature of the project, some logistical considerations were expected; some were not. In either case, the situations all had to be dealt with accordingly. Many of the concerns came from involvement during the construction process. Bridge construction is a very expensive one, and no involved parties wanted

cost or schedule overruns. In the end, it took an agreement among all parties that the research team would remain conscious of construction deadlines and would not impact the construction process. Despite the agreement, the construction team at ET&L was very understanding and sympathetic to the goals of the research team, and was able to accommodate reasonable requests.

### **3.5.2 Power and Internet**

Throughout the process, the issue of getting power and internet capabilities to a bridge was a problem. A permanent power and internet source was not available until well after the September 3 load test, so until that point extension cords were laid for power from a town-owned pump house approximately 200 ft south of the bridge and uploading of collected data had to be conducted manually using a laptop. The local utility company was unable to supply service to a facility that did not have an address or bill a party (Tufts University) that was not the owner or renter of the property. Eventually, the utility companies allowed installation of the services as long as a licensed electrician approved the design and oversaw the installation. The town of Barre supplied their town electrician, Glen Tattan of Tattan Electric. He ensured the installation of a safe, long lasting wiring system for the electric and internet supply. Some of the permanent setup can be seen in Figure 38, Figure 39, and Figure 40.

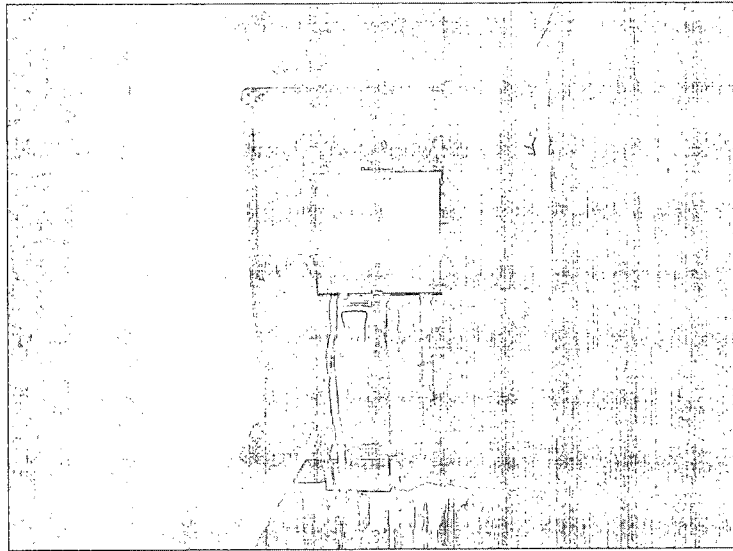


**Figure 38. Meter box just before power hook-up**

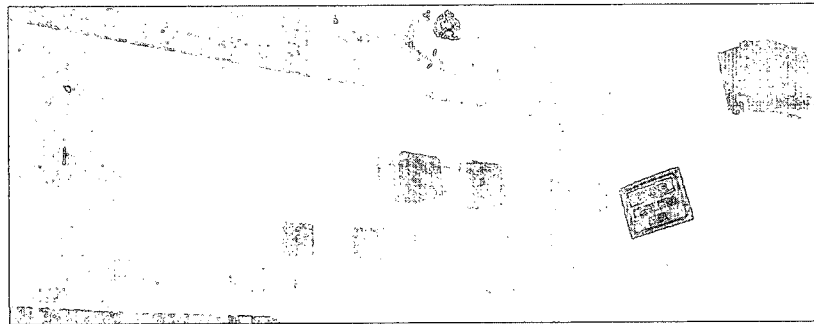


**Figure 39. iSite-HS boxes distributed across all six girders**

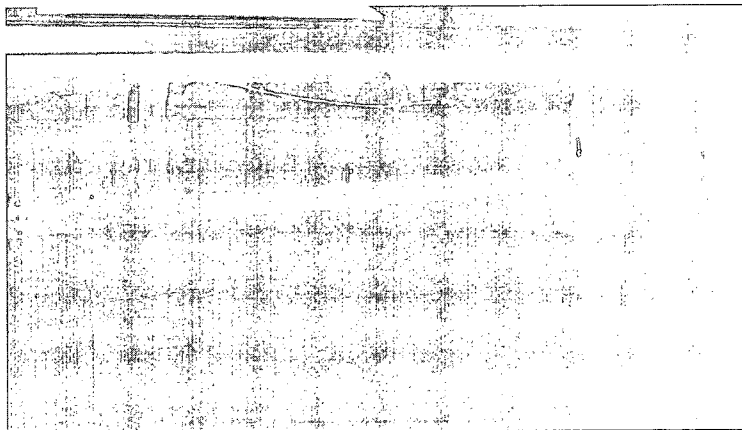


**Figure 40. Permanent cabling attached to abutment wall**

### **3.6 Instrumentation Summary**

In total, nearly 200 sensors were included in the instrumentation plan, including 100 strain gauges, 36 thermistors installed on steel girders, 30 thermistors installed in the concrete deck, 16 tiltmeters on both the superstructure and substructure, 16 accelerometers on the steel girders, and 2 pressure cells on the south approach. Table 1 displays a summary of the number of sensors by type. Table 2 and Table 3 show the distribution of sensors with respect to each girder for all stations. Datasheets, literature, and manufacturer calibrations for each sensor are included in Appendix G.

**Table 1. Instrumentation breakdown by type**

<b>Quantity</b>	<b>Instrument Type</b>
100	Strain Gauges
36	Girder Temperature Sensors
30	Concrete Temperature Sensors
16	Accelerometers
16	Tiltmeters
2	Pressure Cells



Table 2. Distribution of sensors w.r.t. girder # for stations 1 to 6

	Station 0	Station 1	Station 2	Station 3	Station 4	Station 5	Station 6
<b>Girder 1</b>	Deck		2 Concrete Thermister				2 Concrete Thermister
	Top Flange		1 Strain		1 Strain		1 Strain
	Web		1 Thermister				1 Thermister
	Bottom Flange		1 Accel	1 Tiltmeter		1 Accel	
<b>Girder 2</b>	Deck		1 Strain		1 Strain		1 Strain
	Top Flange		1 Thermister				1 Thermister
	Web		1 SWP				1 SWP
	Bottom Flange						2 Concrete Thermister
<b>Girder 3</b>	Deck		2 Concrete Thermister				2 Concrete Thermister
	Top Flange		2 Strain		2 Strain		2 Strain
	Web		1 Thermister				1 Thermister
	Bottom Flange		1 Accel	1 Tiltmeter		1 Accel	
<b>Girder 4</b>	Deck		2 Strain		2 Strain		2 Strain
	Top Flange		1 Thermister				1 Thermister
	Web		2 Concrete Thermister				2 Concrete Thermister
	Bottom Flange		2 Strain		2 Strain		2 Strain
<b>Girder 5</b>	Deck		1 Thermister				1 Thermister
	Top Flange		2 Strain		2 Strain		2 Strain
	Web		1 Thermister				1 Thermister
	Bottom Flange		1 Accel				1 Accel
<b>Girder 6</b>	Deck		2 Strain		2 Strain		2 Strain
	Top Flange		1 Thermister				1 Thermister
	Web		2 Concrete Thermister				2 Concrete Thermister
	Bottom Flange		2 Strain		2 Strain		2 Strain
<b>Abutment Pier Cap</b>	Deck		1 Thermister				1 Thermister
	Top Flange		2 Strain		2 Strain		2 Strain
	Web		1 Thermister				1 Thermister
	Bottom Flange		1 Accel	1 Tiltmeter		1 Accel	
							1 Bi-Axial Tilt

Table 3. Distribution of sensors w.r.t. girder # for stations 7 to 12

Vernon Ave. Bridge Instrumentation Schedule							
	Station 7	Station 8	Station 9	Station 10	Station 11	Station 12	Totals
Girder 1	Deck			2 Concrete Thermister			6 Concrete Thermister
	Top Flange	1 Strain		1 Strain			5 Strain
	Web	1 Accel	1 Tiltmeter		1 Accel		3 Thermister
	Bottom Flange		1 Strain		1 Strain		4 Accel, 2 Tiltmeter
Girder 2	Deck			1 Thermister			5 Strain
	Top Flange			1 Thermister			3 Thermister
	Web	1 Accel	1 Tiltmeter		1 SWP		3 SWP
	Bottom Flange			2 Concrete Thermister			6 Concrete Thermister
Girder 3	Deck			2 Strain			10 Strain
	Top Flange			1 Thermister			3 Thermister
	Web	1 Accel		1 Thermister	1 Accel		4 Accel
	Bottom Flange		2 Strain		2 Strain		10 Strain
Girder 4	Deck			2 Concrete Thermister			6 Concrete Thermister
	Top Flange			2 Strain			10 Strain
	Web	1 Accel		1 Thermister	1 Accel		3 Thermister
	Bottom Flange		2 Strain		2 Strain		4 Accel
Girder 5	Deck			1 Thermister			10 Strain
	Top Flange			2 Strain			3 Thermister
	Web			2 Concrete Thermister			6 Concrete Thermister
	Bottom Flange		2 Strain		2 Strain		10 Strain
Girder 6	Deck			1 Thermister			3 Thermister
	Top Flange			2 Strain			4 Tiltmeter
	Web	1 Accel	1 Tiltmeter				10 Strain
	Bottom Flange		2 Strain		1 Thermister		3 Thermister
Abutment	Deck			2 Concrete Thermister			6 Concrete Thermister
	Top Flange			1 Strain			5 Strain
	Web	1 Accel	1 Tiltmeter		1 Accel		3 Thermister
	Bottom Flange		1 Strain		1 Thermister		4 Accel, 2 Tiltmeter
				1 Strain			5 Strain
				1 Thermister			3 Thermister
				1 Strain			4 Accel, 2 Tiltmeter
				1 Thermister			5 Strain
				1 Thermister			3 Thermister
				1 Strain			2 Bi-Axial Tilt

## CHAPTER 4

### FIELD DATA COLLECTION

In order to capture the behavior of the bridge, data was collected from the sensors at various stages of construction. Since strain gauges were installed on the girders prior to erection, this allowed many opportunities for the collection of data that are not normally attainable. One of the original goals of the research team was to capture the stress that would be locked into the girders during construction. After construction, a controlled non-destructive load test was conducted in order to verify bridge design assumptions and calibrate the structural models. Finally, the DAQ was programmed to collect data continuously into the future for long-term structural health monitoring. The procedures for data collection are outlined here, and a brief summary of the datasets is outlined in Table 4.

**Table 4. Data Collection Summary**

Date	Stage of Construction	Collection Method	Measurements Collected
5-Jun-09	After Steel Erection	P3500	Strain
16-Jun-09	After SIP form installation	P3500	Strain
25-Jun-09	During Rebar Cage Installation	P3500, iSite	Strain
10-Jul-09	During Deck Pour	iSite @ 200Hz	Strain, Tilt
3-Sep-09	Controlled Load Test	iSite @ 200Hz	Strain, Tilt, Accel., Temp., Pressure Cells
Present	In Service	iSite @ 0.002 Hz	Strain, Tilt, Accel., Temp., Pressure Cells

## **4.1 Data Collection During Construction**

Attempts to obtain strain data during benchmark stages of construction were essential to the fundamental goals of the collaborative research project. The data obtained in this time frame can provide information on stresses locked into the girders due to applied loads during construction, which can later be used in the development of a baseline condition for structural modeling. For example, girder self weight, temporary formwork, SIP formwork, rebar, and wet concrete all contribute to the state of stress in the girders prior to the curing of the concrete deck and the onset of composite behavior.

### **4.1.1 Data Collection Prior to Concrete Pour**

SIP formwork is welded to the top flange of the girders and may provide additional bracing against lateral-torsional buckling which is not considered during design of bracing. Other formwork, typically made of wood, is removed after the concrete deck has cured. Some temporary formwork for the bridge deck overhang can be seen in Figure 41. The weight of the formwork applies a distributed load to the girders which induces a state of stress to the girders. This is similar to other dead loads from construction such as girder self-weight, only the formwork load, and therefore the contribution to the state of stress, is removed.

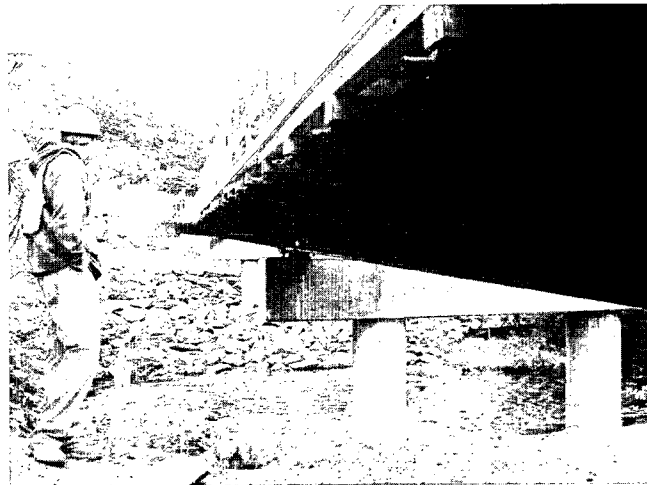


Figure 41. Temporary concrete formwork on exterior girder for deck overhang.

It is a reasonable assumption that as more components were added to the bridge, the more complicated a system the bridge would become. Therefore, strain measurements were collected after steel erection for comparison to hand-calculated dead load measurements. Strain data was collected during construction at two other stages as well: after installation of SIP formwork, and during installation of reinforcement cage.

The iSite dataloggers, the permanent data acquisition system for the bridge, were not available until during the rebar placement construction stage, nearly three weeks after steel erection. Therefore data collection prior to their delivery was conducted using two Vishay model P3500 Strain Indicators supplied by the structures lab at Tufts University. Researchers would later conduct a calibration of P3500 strain readings to iSite strain readings after the iSite dataloggers were installed. This was accomplished by collecting data from the iSite boxes, then manually connecting each gauge to the P3500. It was thought that there would be a direct correlation between two readings that would be evident upon data analysis. A researcher conducting the calibration measurement can be seen in Figure 42.



Figure 42. A researcher measures strain using the P3500 for calibration to iSite strain readings

An initial analysis revealed that there was little to no correlation between successive readings. The researchers theorized many possibilities for the poor correlation. First of all, the P3500, although conveniently portable and battery-powered, was typically used to measure changes in strain over a period of a few seconds in a controlled lab environment. Changing environmental conditions such as temperature and humidity had an adverse effect on the repeatability of the readings and therefore could not be used for long term data acquisition. Secondly, the researchers were sampling strain of a poorly defined load case. All three datasets were taken during the course of a construction day and significant vibrations were felt in the girders due to construction loads as small as a worker walking along a beam.

The combination of poorly defined load cases with questionable data acquisition created a low level of confidence in the reliability of the measurements, and the three datasets were therefore abandoned. It is still possible that future work into the behavior of the P3500 in changing environmental conditions may shed some light on the apparent unreliability of the readings, but P3500 data was abandoned as part of this research.

#### **4.1.2 Data Collection During Concrete Pour**

The last opportunity for strain collection of a non-composite structural system was the day of concrete deck pour, which occurred on July 10, 2009. It was assumed that the wet concrete would not act compositely with the girders, but instead as an area dead load that would distribute uniformly to the girders. Additionally, the deck thickness and width were known from the design plans, and the density of the concrete was calculated from the aggregate plant mix design.

The assumption of non-composite behavior combined with a well-defined load case created an excellent opportunity for researchers to attempt to compare measured changes in strain with modeled results. This comparison could help determine the repeatability of strain measurements and the reliability of the DAQ system. It also provided an opportunity to observe the performance of the bridge's elastomeric bearing pads, which could then be used to calibrate the bridge model boundary conditions. Strain data was sampled at 5 Hz over the course of the entire day while construction teams poured the concrete (Figure 43). Temperature was also recorded in order to take into account the strain due to temperature. A sample of the concrete pour data is also shown in Figure 43. In the sample data, the symmetry of strain magnitudes in the top and bottom flange shows that the slab initially acts as a dead load to the girders. Therefore, the neutral axis for the beam is the centerline of the girder and strains in the top and bottom flanges are equal and opposite in magnitude. Due to the particular importance of this data set in terms of monitoring the change of behavior from non-composite to composite, the dataset collected during the concrete pour was set aside for future work.

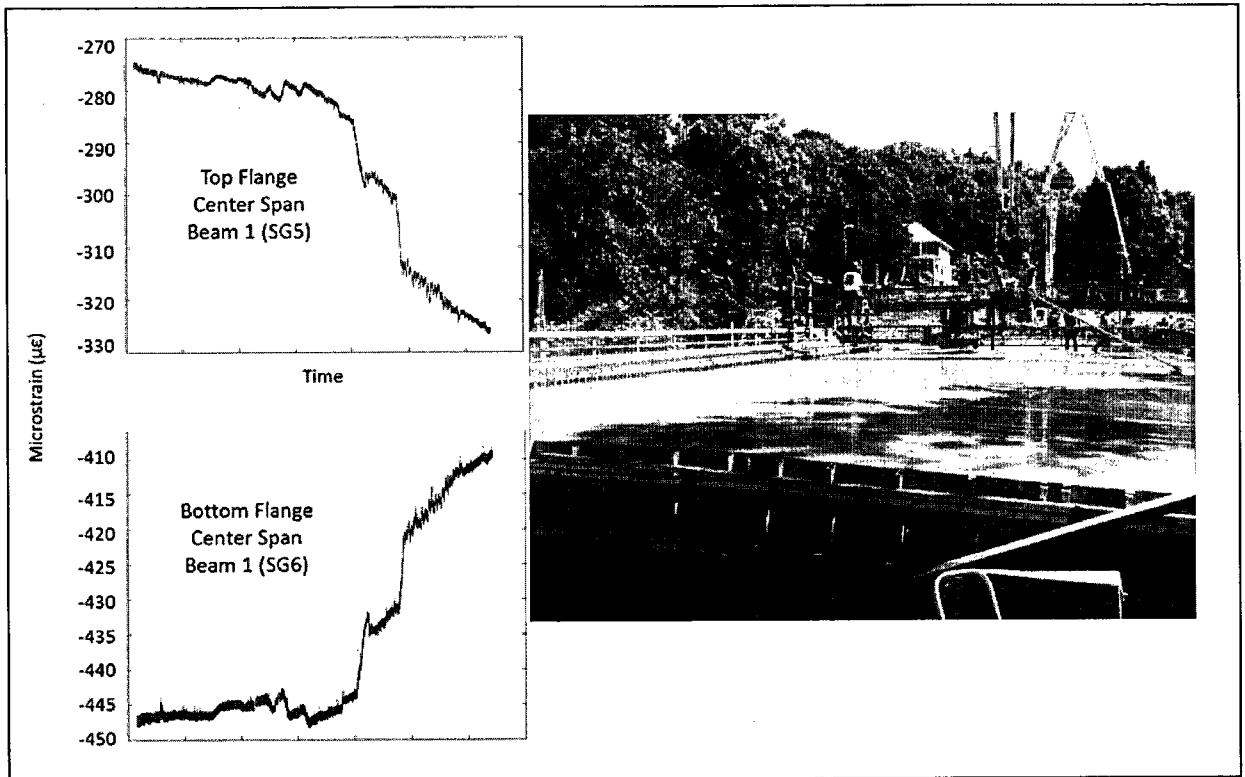


Figure 43. To the left is a sample of collected strain data from concrete pour of deck. To the right is a photo of the construction crew conducting the pour.

#### **4.1.3 Data Collection After Concrete Pour**

Once the deck was poured, data acquisition was slowed to 0.002 Hz (1 sample every 5 minutes) and set to record continuously. The purpose of this dataset was to attempt to observe the change in bridge behavior from a non-composite system into a composite one. No construction equipment would be allowed on the bridge during this time, and therefore the only loading change that would occur would be due to environmental impacts, both ambient weather conditions and heat of hydration in the concrete. This data set was successfully collected but has not yet been analyzed. It is one of the suggestions for future work.



## **4.2 Controlled Load Test**

The load test was conducted on September 3, 2009, which was one day before the bridge was opened to traffic. This time was ideal because there was a 48 hour window between asphalt lay-down and the lanes could be painted. Therefore the bridge would not yet be opened to traffic. The load test was attended by researchers at Tufts and UNH, as well as representative from FST, ET&L, and Geocomp. The original purpose of the load test was to calibrate the baseline structural model for long-term SHM. It was later determined that the same dataset could be used for verification of the design of composite behavior. The load test consisted of a tri-axle dump truck loaded with local aggregate driven across the bridge. Three different tests were conducted: static truck stop tests, constant-velocity rolling truck tests, and dynamic speed bump tests. The static tests were studied in this research, and the rolling truck and impact tests were set aside for future work.

### **4.2.1 Test Truck Specifications**



Figure 44. Test Truck for Sept. 3 Load Test

The truck used to conduct the load tests was rented by D&P Leasing, courtesy of the general contractor ET&L. Don Pelley, the owner of D&P leasing, regularly hauled

material for ET&L throughout the construction of the bridge, and was very familiar with the site. The truck was a tri-axle Mack dump truck with tandem wheels in the rear and the first rear axle raised, as seen in Figure 44, to assist in the concentration and simplification of wheel loads. The spacing of the front axle wheels was 2.13 m (7 ft) on center and the spacing of the rear axles was 1.85 m (6 ft-1 in) on center. The axle spacing was 5.05 m (16 ft-7 in) on center between the front axle and first rear axle, and 1.42 m (4 ft-8 in) on center between the first and second rear axles. Each of the front tires had a contact patch of 203 mm (8 in) long by 292 mm (11.5 in) wide and each tandem pair of rear tires had a contact patch of 203 mm long by 546 mm (21.5 in) wide. These truck dimensions are summarized in Table 5.

**Table 5. Test Truck Wheel Size and Axle Spacing Dimensions**

Vehicle Type	Mack Tri-Axle Dump Truck	
Tires Patch Dimensions (LxW)	Front: 203x292mm	Rear: 203x216mm (each)
		203x546mm (tandem)
Width – Axle 1:Front	2.13m On Center	
Width - Axles 2,3,4: Rear Tandem Pair	1.85m On Center	
Spacing: Axle 1 - Axle 3	5.05m On Center	
Spacing: Axle 1 – Axle 4	6.48m On Center	

The truck was filled with borrowed aggregate, courtesy of RJ McDonald of Barre, MA. The truck was also weighed prior to arrival at the bridge site. RJ McDonald reported the truck weight to be 72 kips, with a distribution of 19.8kips to the front axle and 52.2 kips to the rear axles. Truck weights were also conducted on site for each wheel in contact with the surface. Four Cas RW-S wheel scales were used to weigh each wheel of the truck. Since there were 10 wheels to be measured, wooden “dummy scales” were placed under the other 6 wheels in order to assure the correct distribution of wheel loads. Figure 45 shows researchers conducting wheel load measurement. The dummy scales can be seen under the both wheels of the front axle. Each wheel was

weighed three times before the load test and an average of the three weights calculated. The wheel weights were again recorded after the test to determine if weight had shifted during the test. A summary of the wheel loads can be found in Table 6.



Figure 45. Researcher recording wheel weights.

Table 6. Average test truck wheel weights

Wheel # (From L to R)	Prior To Test (lbs)	After Test (lbs)	Average Wheel Wt (lbs)
Front Axle 1-1	10025	10103	<b>10,064</b>
Front Axle 1-2	9560	9413	<b>9,487</b>
Axle 2	N/A	N/A	N/A
Axle 3-1	6032	6340	<b>6,186</b>
Axle 3-2	7647	7250	<b>7,448</b>
Axle 3-3	7463	7407	<b>7,435</b>
Axle 3-4	5493	5610	<b>5,552</b>
Axle 4-1	6510	6710	<b>6,610</b>
Axle 4-2	7220	6957	<b>7,088</b>
Axle 4-3	7223	7370	<b>7,297</b>
Axle 4-4	5613	5490	<b>5,552</b>

#### 4.2.2 Load Test Plan

The load test plan layout design was lead by Jesse Sipple, a doctoral student funded by this project at Tufts University, with feedback and assistance from the

research group. The truck was run across the bridge in three separate lanes, numbered 1-3, always from the south abutment to the north abutment in order to avoid interfering with traffic to the north of the bridge. Lane #1 was the west lane, with the left front tire of the truck centered on a line 0.61 m (2 ft) from the west safety curb. Lane #2 was the center lane, with the left front tire 3.93 m (12.9 ft) from the west safety curb. Lane#3 was the east lane, with the right front tire 0.762 m (2.5 ft) from the sidewalk and east curb. The lane layout can be seen in Figure 46.

As was mentioned before, three types of tests were performed. The first was a designed to be a static load test. The truck was to stop at 15 predetermined locations across the bridge with each stop 12 feet from next. The first stop location, stop 0, was 22 feet south of the saw cut at the south bearing centerline. Stop 0 was designed as a starting point to begin data acquisition. Stop 1 was also off of the bridge, but fell on the concrete approach slab, and was designed to identify whether loading of the approach slab and abutment affected the response of the bridge superstructure. The remaining 13 stops were spaced evenly across the length of the bridge. The layout of the stops can be seen in Figure 46. With 3 lanes and 15 stops, a total of 45 distinct load cases were performed on the bridge. Three iterations of each run were performed for quality assurance for a total of 9 truck stop tests. The data collected during the stop tests is the primary focus of this research.

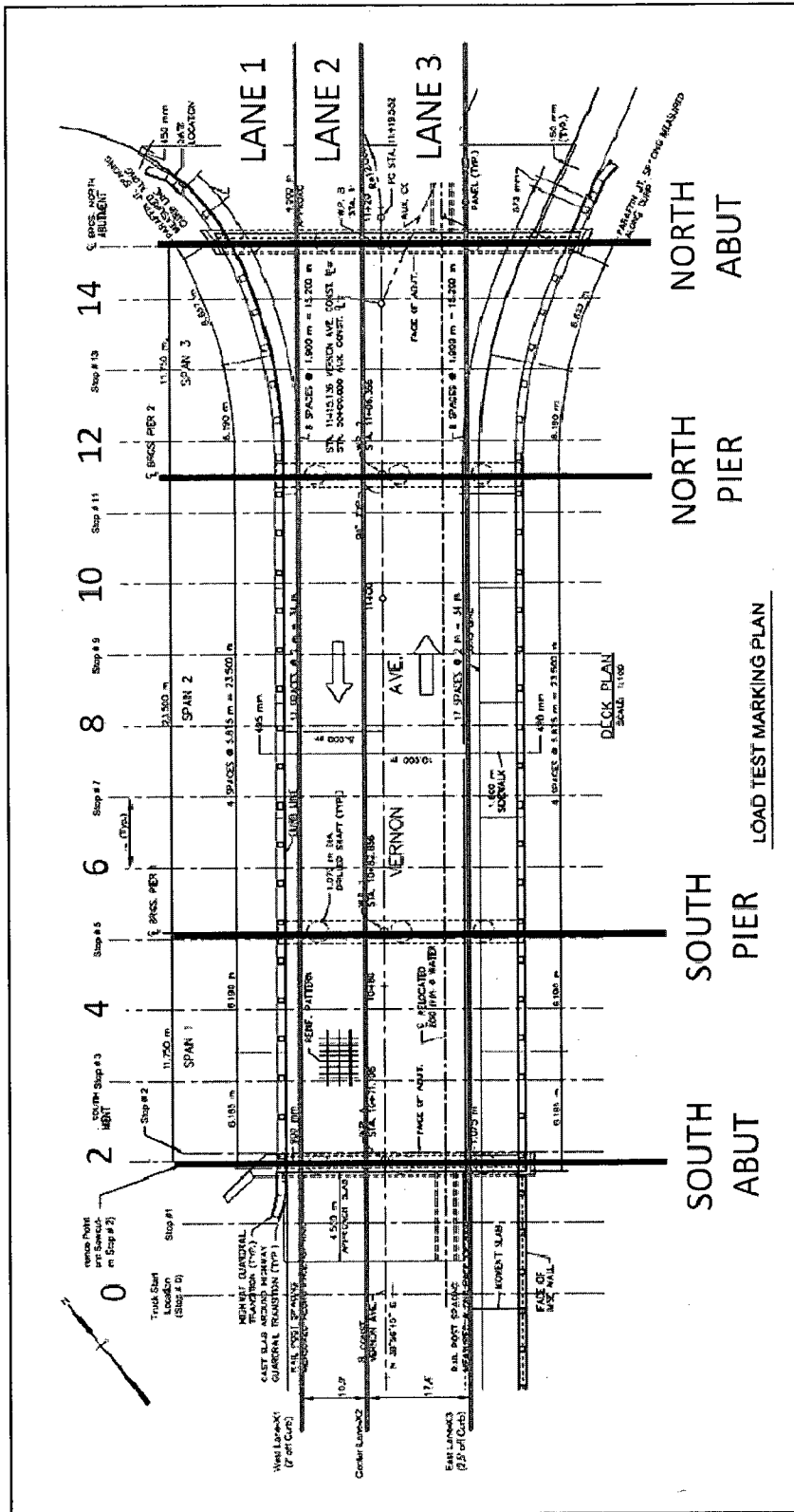


Figure 46. Load test lane and stop location layout

The second type of test was a rolling test. This test was designed to be quasi-static, in that if the truck rolled at a constant velocity, the dynamic effects of the truck would be negligible. The purpose of this test was two-fold. First, researchers wished to prove the theory that the dynamic impact of the slow-moving vehicle was negligible. Second, a constantly moving truck would allow for the development of bridge influence lines for comparison to design calculations and model results. The static tests also produced gross influence lines for strain, but the rolling truck tests were continuous as long as the truck rolled at a constant speed. In this test, the truck was run 3 times in each lane, as in the stop tests, but was moved at a near constant velocity of about 0.61 m/sec (2 ft/sec). The rolling truck test results would be analyzed in future work.

The third type of test that was performed was an impact test. The purpose of this type of test was to compare the bridge response to the predicted static response multiplied by the impact factor assumed in the design of live load distribution to girders. In this test, the truck was driven at a safe speed over two of the dummy scales used when weighing the truck. The dummy scales were to act as speed bumps. The speed bumps were placed at stop #7, which corresponds to the stop closest to the center of the bridge. One impact test was conducted in each of the lanes. Figure 47 shows the truck as it approaches the speed bumps in lane #3. The marking of "stop 7" on the pavement can be seen in the foreground. The impact tests would be analyzed in future work.



**Figure 47. Truck approaching “dummy scales” during impact test**

In addition to the 9 stop tests, 9 crawl speed tests, and 3 impact tests, ambient conditions in between tests were also recorded. In this test, all traffic, foot or vehicle, was removed from the bridge in order to monitor the bridge at a state of rest. The purpose of this test was to sample data when only environmental conditions could provide an excitation to the bridge. These tests also provided a way to examine a state of pure “noise” in the data. This test was performed once in the morning, prior to the stop tests, and twice in the afternoon. The two versions in the afternoon were conducted consecutively and differed only in the fact that noise was limited as well: The motors of the test truck and any other vehicles were shut down to investigate if the bridge was in any way excited by the vibration of the running motor. This data set was set aside for future study.

#### **4.2.3 Data Acquisition**

For each test, the truck was placed in the appropriate lane at stop #0. Once all researchers were ready, data acquisition at a speed of 200 Hz was initiated and the truck was held at stop 0 for 10 seconds to confirm activation of all 19 iSite dataloggers. The truck spent 10 seconds at each station before traveling to the next one to allow any

dynamic excitation to dissipate. After 10 seconds at the final stop (#14), the truck rolled forward until the rear axles were clear of the bridge. At the start of each test the temperature and humidity were recorded. The time of truck arrival and departure from each truck stop was recorded to the nearest second, including the time data acquisition was initiated, the time the truck cleared the bridge, and the time it was terminated. The times and environmental conditions were recorded by two separate researchers for quality assurance. Researchers were able to coordinate truck movement and data acquisition via two-way radios.

In addition to the sensors installed on the bridge, digital imaging was used by other researchers at UNH to collect deflection data on the bridge. In this data collection technique, a pair of cameras recorded movement of pixels within a given image from the initial position of a pixel captured in a reference image. The cameras' positions from the girder are obtained by triangulation, and then pixel movement within an image is post-processed to a measurement of deflection. Two sets of cameras recorded deflections due to truck loads on the south span and center span of girder 1 (the west exterior girder) during the both stop tests and crawl speed tests. The test setup for center span can be seen in Figure 48. A comparison between deflections in the structural model and deflections measured using digital imaging is briefly discussed as a possible metric for model response verification in Chapter 6.



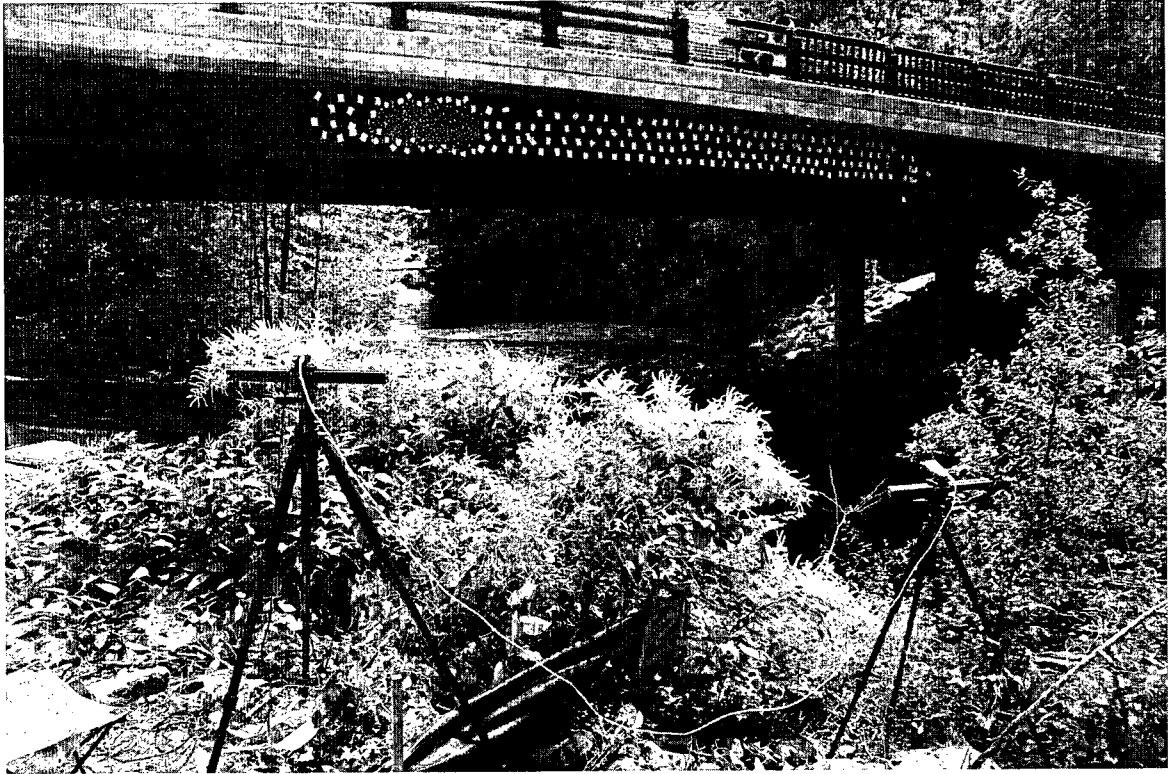


Figure 48. Center span digital image correlation test setup.

#### **4.2.4 Load Test Summary**

In total, 24 tests were conducted on the bridge on September 3, 2009. Strain, temperature, accelerations, rotations, pressure, and deflection measurements were collected for all tests. Due to the overall size of the dataset, the focus of this research was limited to the analysis of strain measurements during the 9 truck stop tests. Therefore, post-processing and discussion shall also be limited to strain readings of the 9 stop tests. Despite the limited focus, the dataset for analysis is still very large: In total 3 repetitions of 45 load cases on 100 strain gauges were analyzed for initial verification of the model. The remaining datasets will be used in future work to further assess the validity of the calibrated model.

#### **4.3 Field Data Post Processing**

The original dataset obtained from the iSite loggers was a daunting one: 19 dataloggers containing 8 channels sampled at 200 Hz for an average test time of over 5

minutes. This gave a total of over 60,000 measurements per channel per test. It was quickly realized that processing of datasets of this size using typical spreadsheets such as Microsoft Excel® was not practical. Instead, Matlab® was used to process strain data at nearly every stage of the analysis process. Matlab® is a technical computing program that uses matrices and matrix algebra along with computer programming to perform computations of very large datasets.

The strain data was post-processed using a filtering program written by Jesse Sipple at Tufts. The processing method and results were scrutinized by the principal investigators at Tufts and UNH, and the processed strain measurements were then used by all researchers. A visual inspection of the post-processed data revealed very clean data sets. Plots of the strain with respect to time revealed distinct plateaus corresponding to stops of the truck. The magnitude of SG22 measurements at the truck stops from the three lane 2 tests, as shown in Figure 49, show early evidence of good repeatability in strain response. SG22 is located on the bottom flange of girder 2 at the midpoint of the center span. To further investigate this, the entire set of strain readings was analyzed for repeatability and quality control, as discussed in Chapter 5.

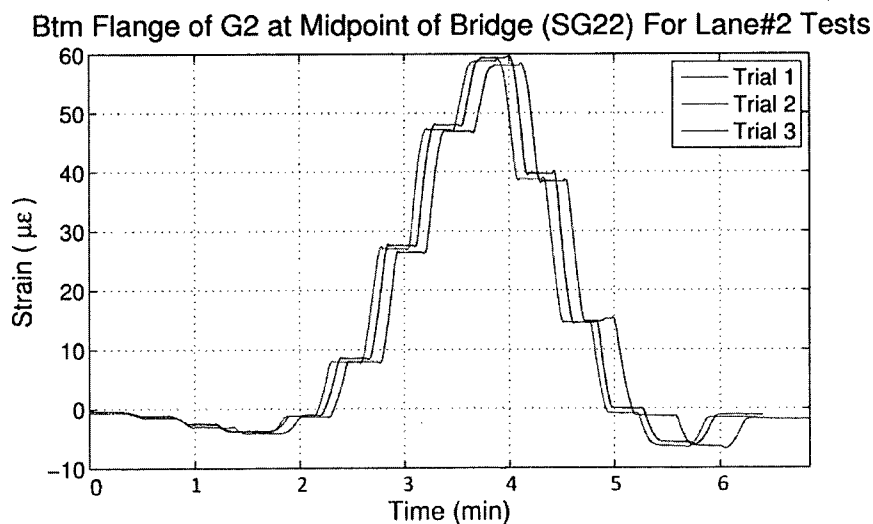


Figure 49. Repeatability of strain measurements for 3 repetitions of the lane #2 truck runs, for strain in the bottom flange of girder 2 at the midspan (SG22)

## CHAPTER 5

### FIELD DATA QUALITY ASSURANCE AND QUALITY CONTROL

The first step in analysis of the NDT strain data was to determine if the data was reasonable. This was part of the filtering program during field data post processing, but it is appropriate to discuss the range of strain values for some different locations across the bridge to see if the values made sense. To determine this, strain in each gauge for all 9 tests were plotted with respect to time. The quality of the collected data was verified in three distinct methods. The 100 gauges were analyzed for functionality after installation by visual inspection. Next the measured strain was analyzed for repeatability due to sensor installation symmetry. Finally, the strain measurement sign, magnitude, and time of occurrence were studied.

#### **5.1 Functionality of Strain Gauges**

The first example of field data quality control was to determine which gauges were malfunctioning. Strain gauges are very sensitive instruments and the quality of the measurement easily impacted. The splice connecting the strain gauge wire to the main cabling is also quite fragile. It was determined through visual inspection of the plots that 10 strain gauges were not functioning properly or at all during NDT data collection. The gauges that were malfunctioning as of Sept. 3 2009 are listed in Table 7 by girder, station, and location within the section.

**Table 7. Location of Faulty Gauges from Sept 3 Load Test**

<b>Strain Gauge #</b>	<b>Girder #</b>	<b>Station #</b>	<b>Location in Section</b>
40	3	6	Top East
41	3	6	Btm West
62	4	6	Top East
65	4	8	Btm West
72	5	2	Top East
81	5	6	Btm West
84	5	8	Top East
97	6	8	Top West
98	6	8	Btm West
100	6	10	Btm West

Secondly, it was necessary to confirm that post processing produced a clean data set for model calibration assessment. As was mentioned before, the original signal was filtered by researchers at Tufts. A visual inspection of all gauges revealed that strain gauges in two dataloggers, iSite3 and iSite9, produced noise in all eight of their channels that was not filtered in the processing program. Figure 50 depicts an example of the difference between the clean data and the noisy data. SG87 and SG88 are two sensors on the top flange of girder 5, located at station 10. SG87 is wired to iSite 3, but SG88 is wired to iSite 2. The variation in the signal was still relatively small, and did not appear to worsen with amplitude; therefore the collected data was still considered relatively clean and was included in the analysis.

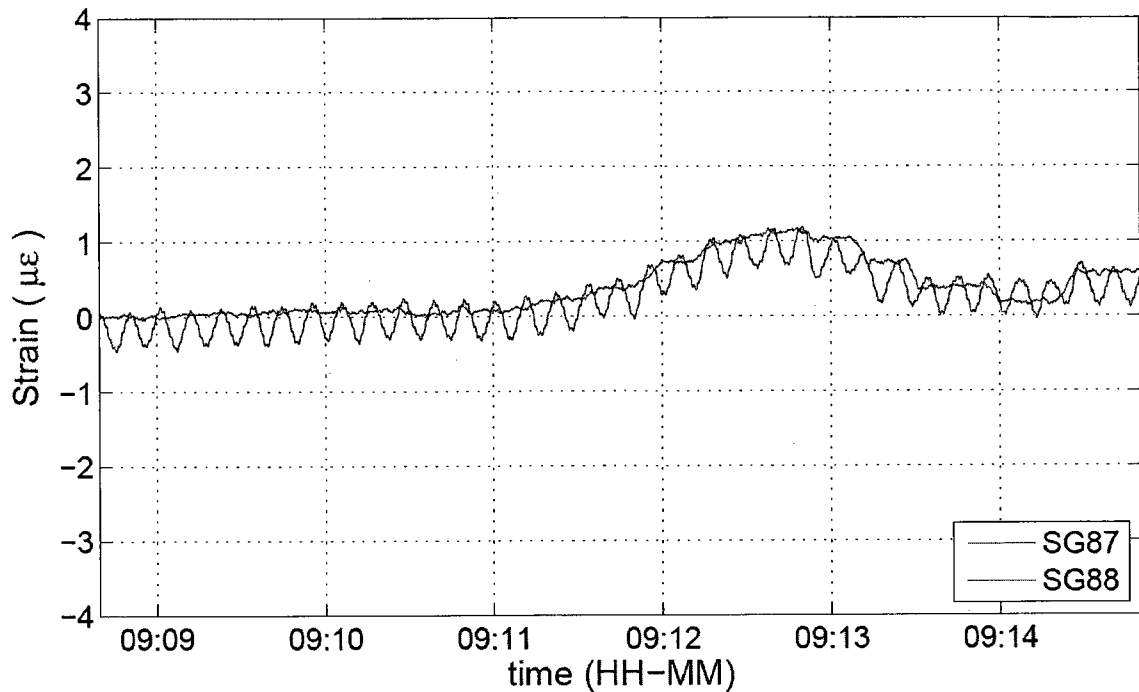


Figure 50. Comparison of Clean and Noisy Collected data

## **5.2 Symmetry of Sensor Placement**

Three main observations were supported from a visual inspection of the graphs. First, the symmetry of sensor placement was used to observe that sensors were working properly. Since interior girders were instrumented on both sides of the web, it was expected that strain readings from both sensors would be relatively close. Visual inspection of plots of parallel sensors showed that in general the strain felt by a gauge on one side of the girder was felt by the gauge on the other side. Figure 51 shows four sets of “parallel” measurements on girder 3. The odd-numbered gauges are on the west side of the web and the even gauges are on the east. It is worth noting that the noise in girder 3 is virtually scaled out, further evidence that the noise does not severely affect the data quality.

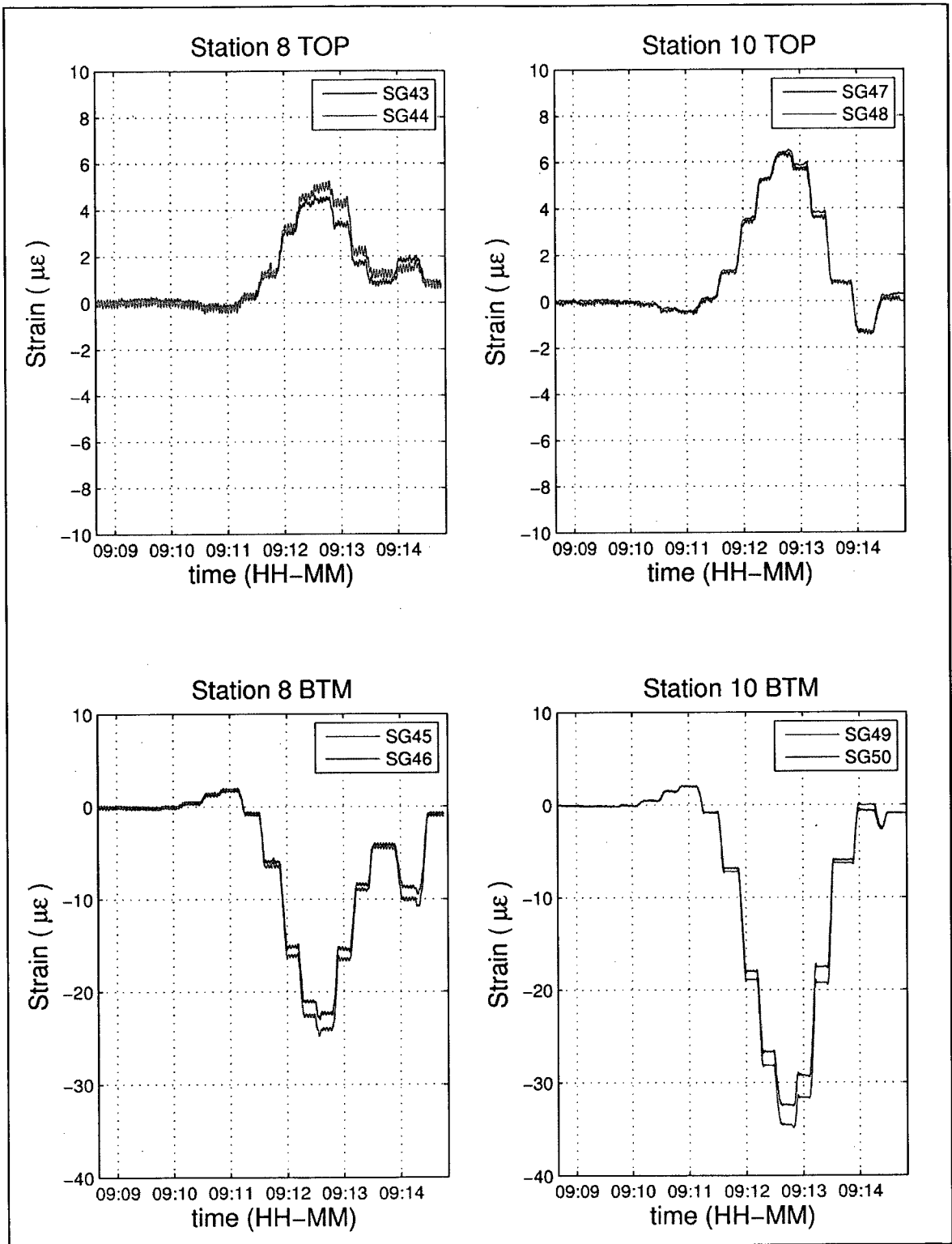


Figure 51. Comparison of parallel sensors on Girder 3 Stations 8 and 10 during a west lane test.

### **5.3 Measurement Sign, Magnitude, and Time of Occurrence**

A final test of measurement quality included in this research examined the strain measurements in terms of sign and relative magnitude when correlated to expectations based on engineering judgment. Design calculations predicted that the neutral axis of the composite steel girder-concrete deck system would be located in the web of the girder, slightly below the top flange and top flange strain gauges (see Figure 58 later in this chapter). The structural mechanics of beams in bending assumes that axial strain in the beam near the neutral axis should be close to zero. Assuming that the design calculations would be reflective of true bridge behavior, it was expected to see very small values of strain in the top flange compared to that of the bottom flange. It was also expected that strain in the top flange would have the opposite sign from that of the bottom flange. As seen in Figure 51, strain in the bottom flange is near 4 times the magnitude of that in the top flange. Additionally, the Figure 51 gauges are located at stations 8 and 10, which are above the north pier. Therefore, negative bending is expected and observed when the truck is in the center span. This would put the bottom flange in compression (negative strain), and the top flange in tension (positive strain). The opposite effects were observed at station 6, at the midpoint of the center span: Figure 52 shows that the bottom flange is in tension and the top flange in compression.

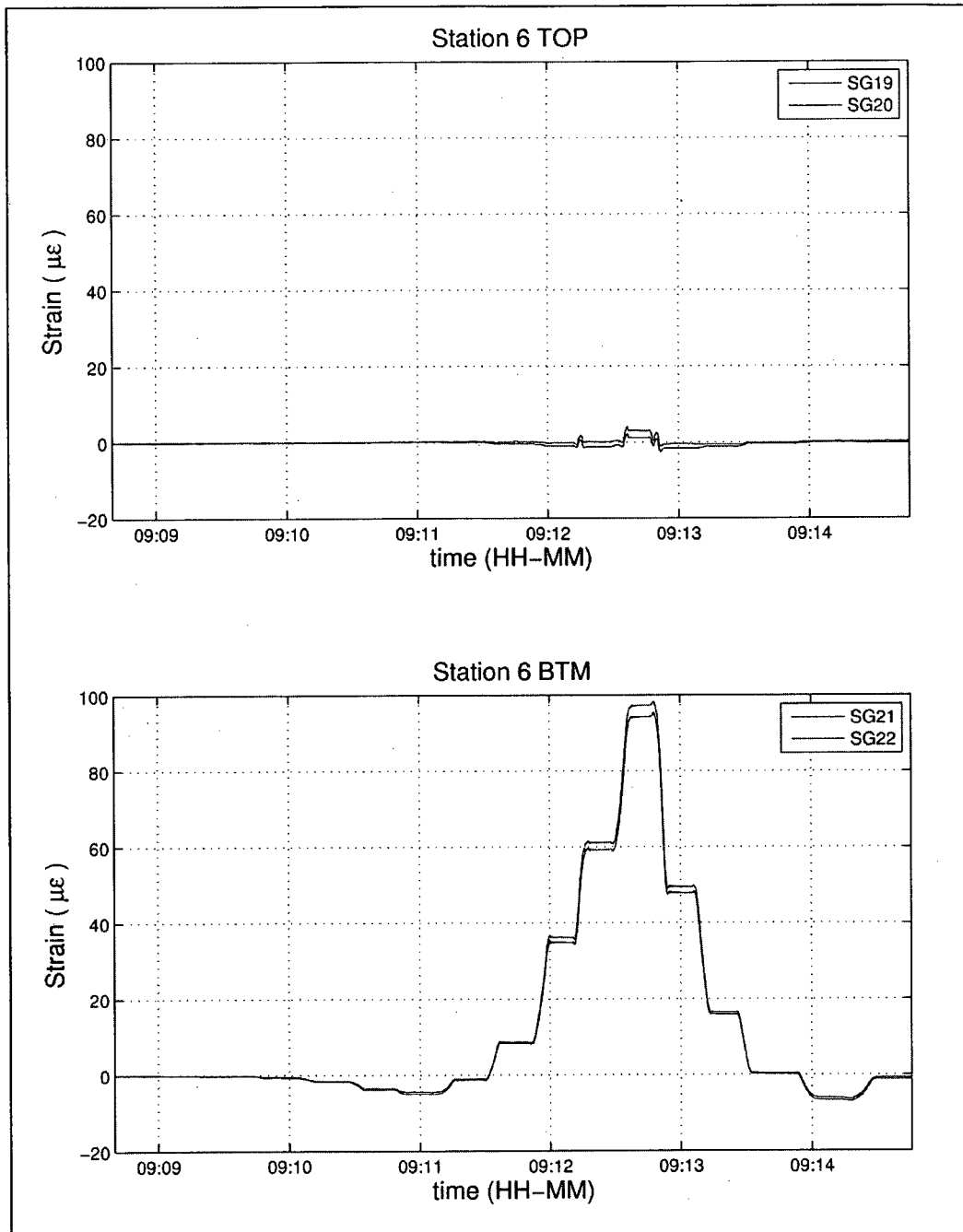


Figure 52. Comparison of Magnitude and Sign of Measured Strain for Locations in Positive Flexure.

It was also necessary to determine if stop locations were easily identifiable in the plots. Figure 51 to Figure 54 all show that “plateaus” of strain are clearly identified when the truck was paused at a stop location. A closer look at Figure 52 also shows the bottom flange in slight compression when the truck is in the north span near the end of



its run: the truck weight in the north span lifts up on the center span, creating compression in the bottom flange.

Finally, it was necessary to confirm that all load cases were evident as plateaus in the data. 15 stops of the truck occurred, but only 13 of them actually occurred with the truck on the bridge, and only 12 of them occurred with the full weight of the truck on the bridge (For the third stop, only the front truck axel had passed the abutment). Therefore 13 plateaus should be evident in each gauge where a significant measurement was expected, in particular bottom flange measurements. Figure 53 demonstrates that overlapping the field recorded truck stop times with the strain plots identifies the plateaus for all truck stops where the full weight of the truck is on the bridge (stops 3-14).

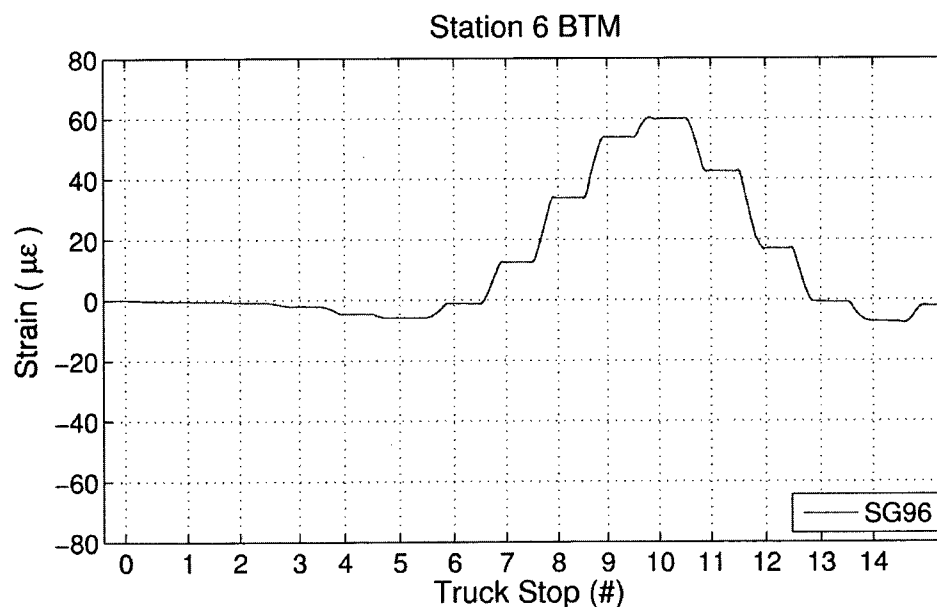


Figure 53. Truck Stops Numbered for Identification of Strain Plateaus

#### **5.4 Additional Quality Assurance and Quality Control Measures**

Once the initial QA/QC was complete, two additional steps were taken to assure that only relevant data used for analysis. The first step was to extract a measured value

of strain for each load case for each strain gauge. This was done to have a measurement with which to compare to the predicted strains in the structural model. The second step was to use the strain gauges placed along the depth of the bridge cross section to determine the measured neutral axis location for post processing of model output as well as for design verification of composite action as a metric of bridge behavior.

#### **5.4.1 Extraction of Strain Values for Model Comparison**

With 15 truck stops over three lanes, there were 45 distinct load cases conducted during the NDT. With three repetitions of each truck stop, there were a total of 135 distinct stops of the truck. Across 100 strain gauges, this totaled 13,500 distinct measurements for evaluation. The main step in quality control for model comparison was to extract a value of strain from the time domain that a gauge measured due to a particular stop of the truck and then determine the repeatability of the measurements over the three repetitions of each of the 45 load cases. To accomplish this, strain measurements from each truck stop “plateau” were removed from the continuous data set, as demonstrated in Figure 54. The middle 8 seconds of data from the 10 seconds of sampling at each stop test was used to compute a mean strain value in each gauge for each stop. In addition to the mean, the number of samples in the 8 second window was recorded, and the standard deviation was calculated. Figure 55 displays the standard deviations of the plateau windows for all 90 functioning strain gauges with respect to the 135 distinct load cases. The average standard deviation of the plateau windows was only  $0.09\mu\epsilon$ , the maximum spread was just under  $2\mu\epsilon$ , and the vast majority was well below  $0.5\mu\epsilon$ .

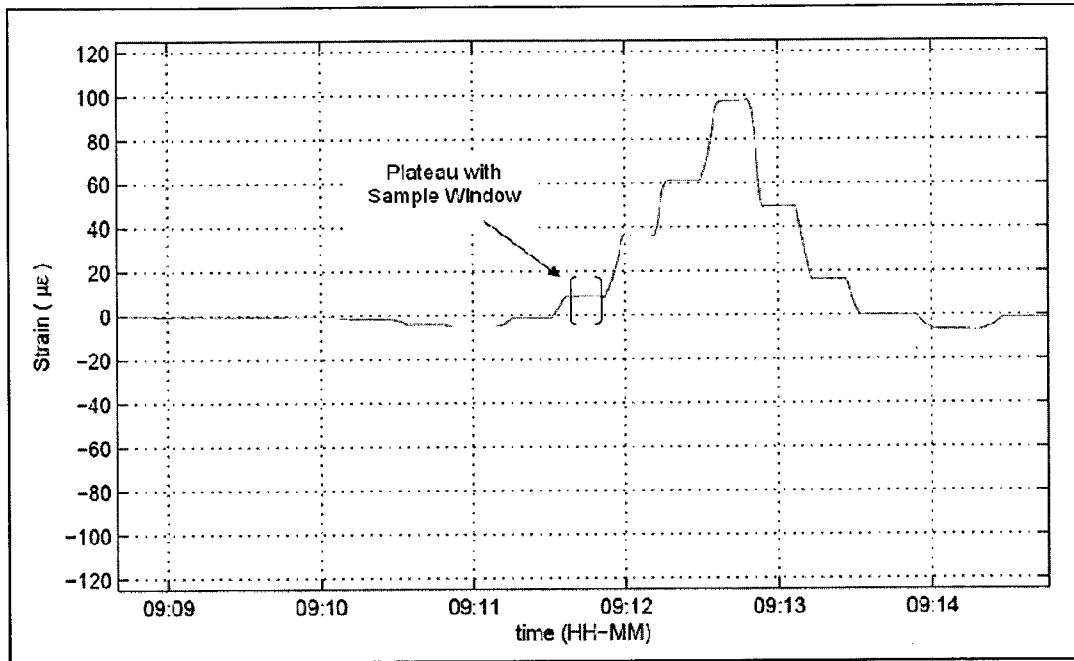


Figure 54. Typical plot of filtered strain data from a load test with truck stop "plateau" and sampling window

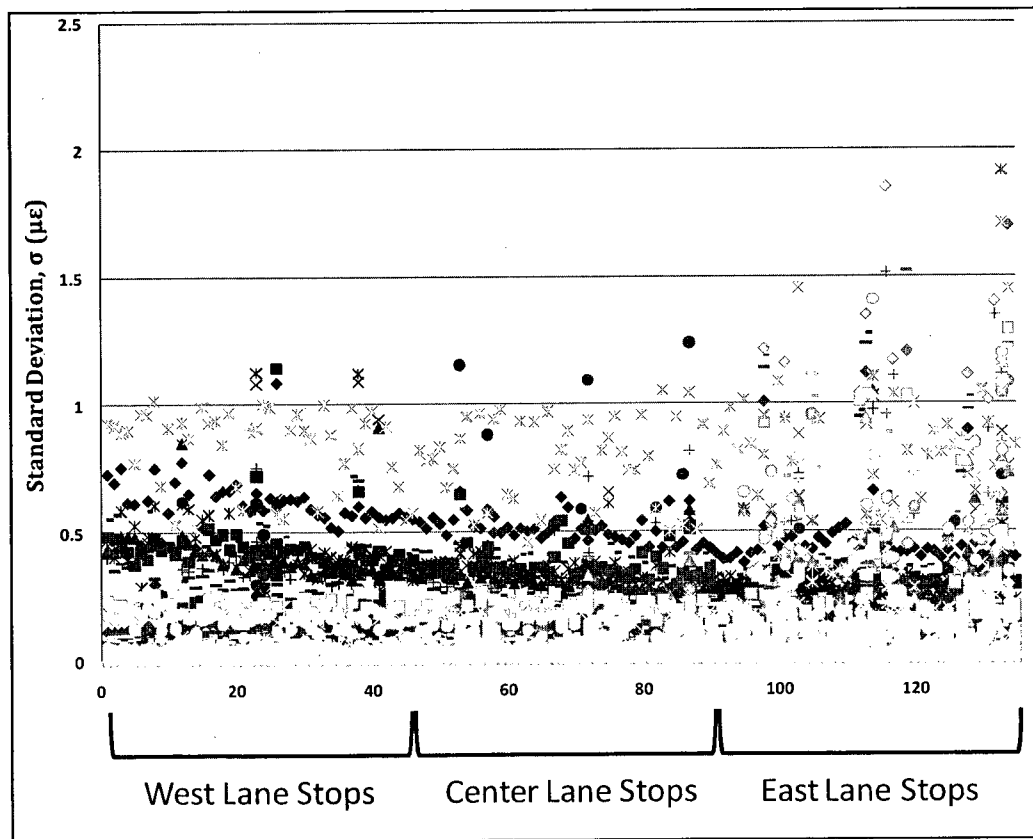


Figure 55. Plot of standard deviations of 100 strain readings with respect to each of the 135 truck stops.

With confidence in the quality in the collected data, the three trials of each load case were combined to one weighted mean, as demonstrated by Equation 1 (Pagano & Gauvreau, 2000)

$$\mu = \frac{n_1x_1 + n_2x_2 + n_3x_3}{n_1 + n_2 + n_3} \quad (1)$$

where  $n$  is the number of samples and  $x$  is the mean of the measured strain in each of the three plateaus. The mean was weighted because the sample sizes were not necessarily the same: As was mentioned before, each sample consisted of about 10 seconds of data sampled at 200 Hz; therefore each sample size was approximately 2000 but some were slightly larger than others. A weighted mean was used so that the mean with the larger sample size was counted more than the smaller samples. Since the samples were taken from the same sensor under the same loading condition, it was assumed that the three sample means were the same. Changes in temperature and humidity were assumed to be negligible during the short time between the three trials for each lane.

The next step was to analyze the spread of the weighted means. This was done using a pooled standard deviation, as demonstrated in equation 2 (Navidi, 2008). The pooled standard deviation is nothing more than a weighted average of the sample standard deviations. A plot of the pooled standard deviations for the 90 functioning strain gauges with respect to the 45 load cases can be seen in Figure 56. The vast majority of the pooled standard deviations were under  $0.5\mu\epsilon$  with a maximum value of  $1.39\mu\epsilon$  and an average value of  $0.1\mu\epsilon$ . As can be seen in the comparisons of Figure 55 and Figure 56, the increase in the standard deviations by using one grouped mean is negligible.

$$\sigma_p = \sqrt{\frac{(n_1 - 1)\sigma_1^2 + (n_2 - 1)\sigma_2^2 + (n_3 - 1)\sigma_3^2}{n_1 + n_2 + n_3 - 3}} \quad (2)$$

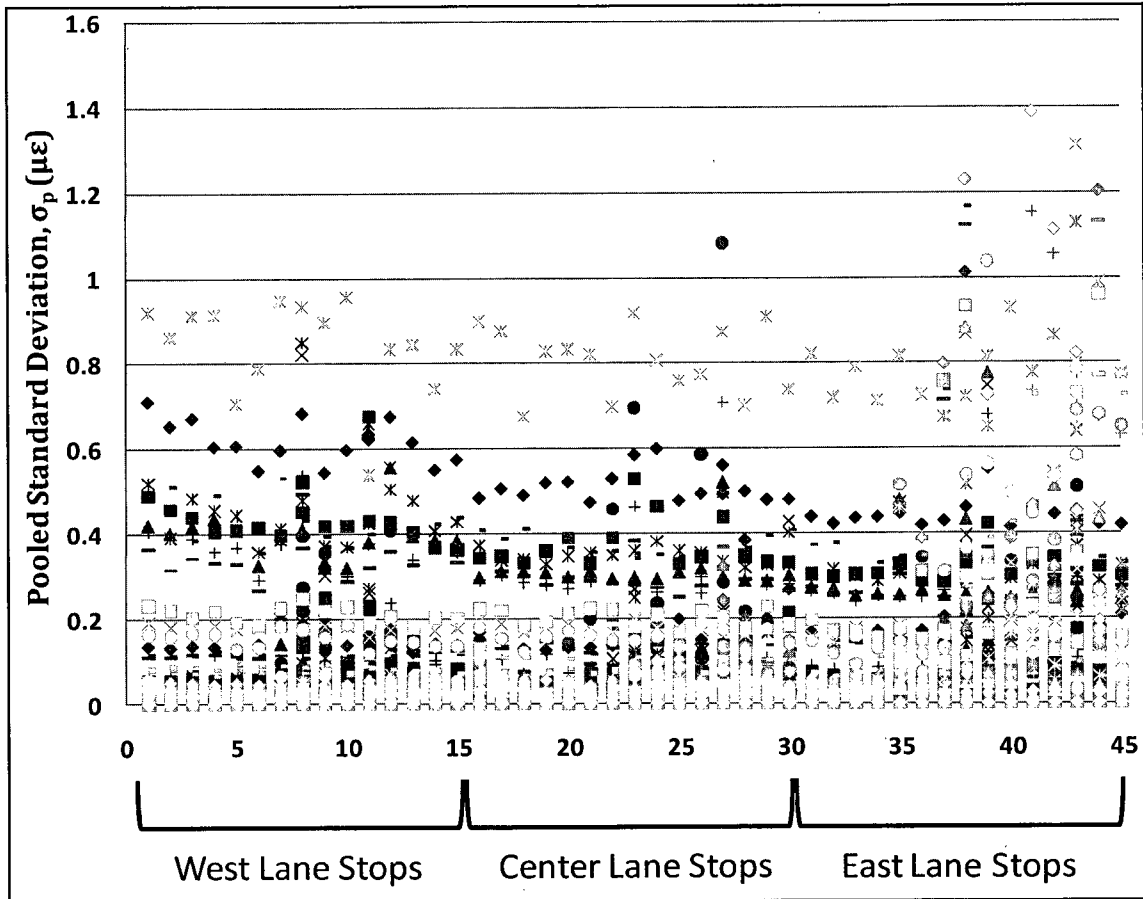


Figure 56. Plot of Pooled Standard Deviations of collected strain with respect to load case.

A final test of the quality of measured strain was done to determine if reliability of the measurements varied with amplitude. To do this, the pooled standard deviation was plotted as a function of the corresponding grouped mean for all measurements, as shown in Figure 57. In this figure, the standard deviation does not appear to be dependent on the magnitude of the measurement. Most measurements are between 20  $\mu\epsilon$  and -20  $\mu\epsilon$ , and the standard deviations range mostly between 0  $\mu\epsilon$  and 0.5  $\mu\epsilon$ . This is also

true for the less occurring measurements greater than  $20 \mu\epsilon$ . Therefore, there is no relationship between the spread of the data and the amplitude of the mean.

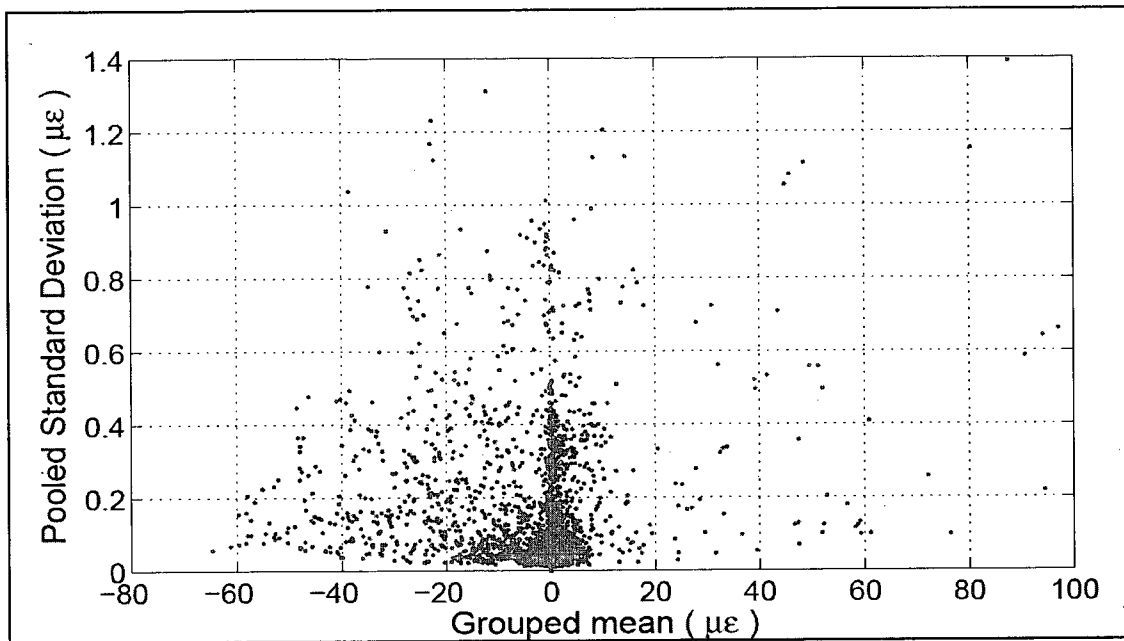


Figure 57. Plot of variation of Pooled Standard Deviation of Collected Strain with respect to Amplitude

Such low error in the plateaus supported a high level of confidence in the grouped mean strains for a later comparison to predicted values from the structural model. The combining of the 9 tests into 3 also made dealing with the data sets much easier.

#### **5.4.2 Extraction of Composite Section Neutral Axis for Model Strain Calculation and Design Verification**

The final step of data QA/QC was to relate the strain in the top flange to that in the bottom flange in order to determine the neutral axis of the composite girder-deck system. This was done for two purposes. First, in order to calculate strain from the force output in the model, it was necessary to determine the location about which to sum forces and also about which to calculate strain from moment. By simple beam

mechanics, the axial strain at a given depth in the cross section of a beam in bending is a function of its distance from the neutral axis, and thus determining this location is essential for proper calculation of strain in the model. More about the calculation of strain can be found in the section on the post processing of model output in Chapter 6. Second, determination of the composite neutral axis can be used as a metric of design verification that the bridge performance is composite.

In order to determine the location of the neutral axis, it was necessary to assume that strain varied linearly across the depth of the bridge composite section. This was reasonable assumption since the truck weight was below the nonlinear range for bridge behavior. When a beam section is bent, the top fibers of the section are in compression, exhibiting negative strain, and the bottom fibers of the section are in tension, exhibiting positive strain. Therefore, a point of zero strain should exist, identifying the neutral axis. The development of an equation for identification of the neutral axis was a simple process of fitting a line to two points, illustrated in Figure 58 and Equation 3.

$$N.A. = \frac{-\varepsilon_{BTM}(d - 2 * t_f)}{\varepsilon_{TOP} - \varepsilon_{BTM}} + t_f \quad (3)$$

The coordinates were equal to the location of strain gauges within the depth of the composite section and the measured strain at those locations. The location of the neutral axis with respect to these values is given by Equation 3, where N.A. is the depth from datum to the neutral axis,  $\varepsilon_{BTM}$  and  $\varepsilon_{TOP}$  are measurements of strain on the bottom and top flanges, respectively,  $d$  is the depth of the steel cross section, and  $t_f$  is the thickness of the top flange of the girder. One benefit of this calculation is that it is independent of the section properties of the concrete deck, which can vary due to construction.

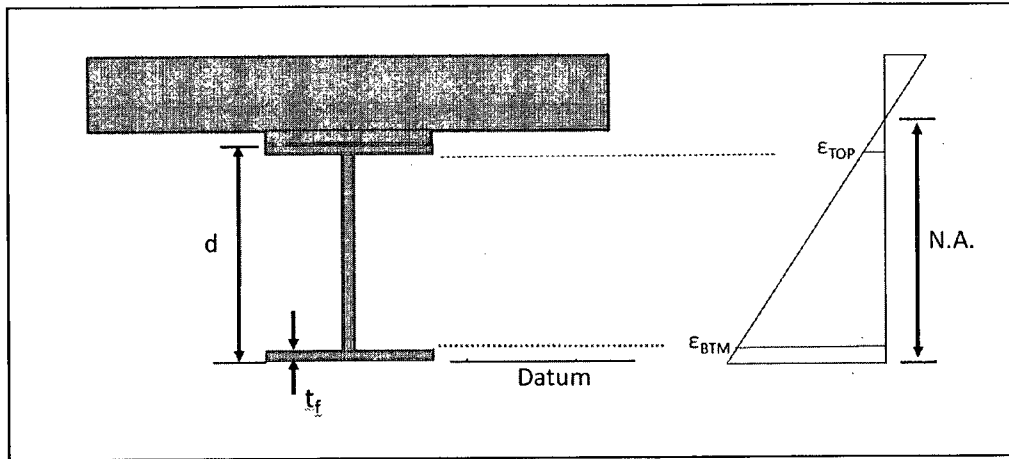


Figure 58. Calculation of Neutral Axis from Strain in Top and Bottom Flange

With an equation for neutral axis calculation, the original strain data was used to calculate a continuous neutral axis for each pair of top-and-bottom strain gauges. Figure 59 shows a plot of the neutral axis for all top-and-bottom strain gauge pairs of girder 2 during a Lane 1 test. A thick horizontal black line representing the depth to the designed bridge neutral axis was also shown in the figure.

The plot is extremely noisy for two reasons, both of which have to do with the sensitivity of Equation 3 to loading conditions that cause measured strains in the top and bottom strain flange strain gauges to be approximately equal and denominator of the formula approaches zero. Therefore when the loading is near zero such as at stops 0, 1 and 2, the neutral axis calculation is inaccurate. Secondly, when bending moment is not the primary internal force, such as when the truck is directly over a bearing or directly over the station being measured, we see the same effect.



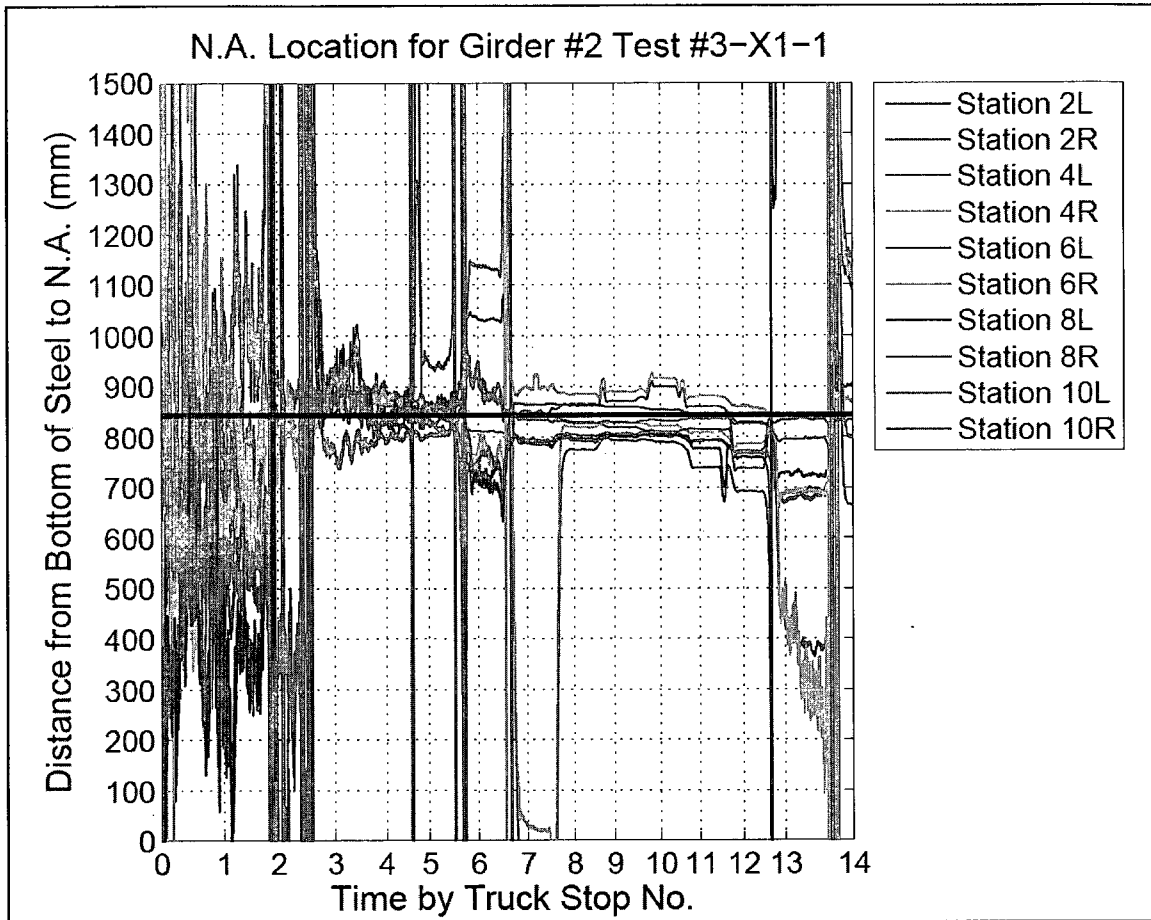


Figure 59. Original Plot of Neutral Axis Location for Girder 2 during a Lane 1 Test.

Conversely, the equation is most accurate for loading conditions where the difference between top and bottom strain gauge readings is the largest. Since readings in the top flange are almost always near zero, this should occur when the truck is at the midpoint of the center span, when the largest internal moments are experienced by the bridge and the largest strains occur in the bottom flange. The truck stops that best correspond to this situation are stops 8, 9, and 10. When the window between these stops is sampled, as shown in Figure 60, the neutral axis calculation is much cleaner. Evidence of the local loading effects on the station 6 pairs is also visible in the form of a rising neutral axis at stops 9 and 10. This is due to an increase in axial strain in the top flange based on the truck placement above station 6. This concept is illustrated in

Figure 61. Finally, proof of concept is evident in that that the measurements show a neutral axis close to the design neutral axis for fully composite action.

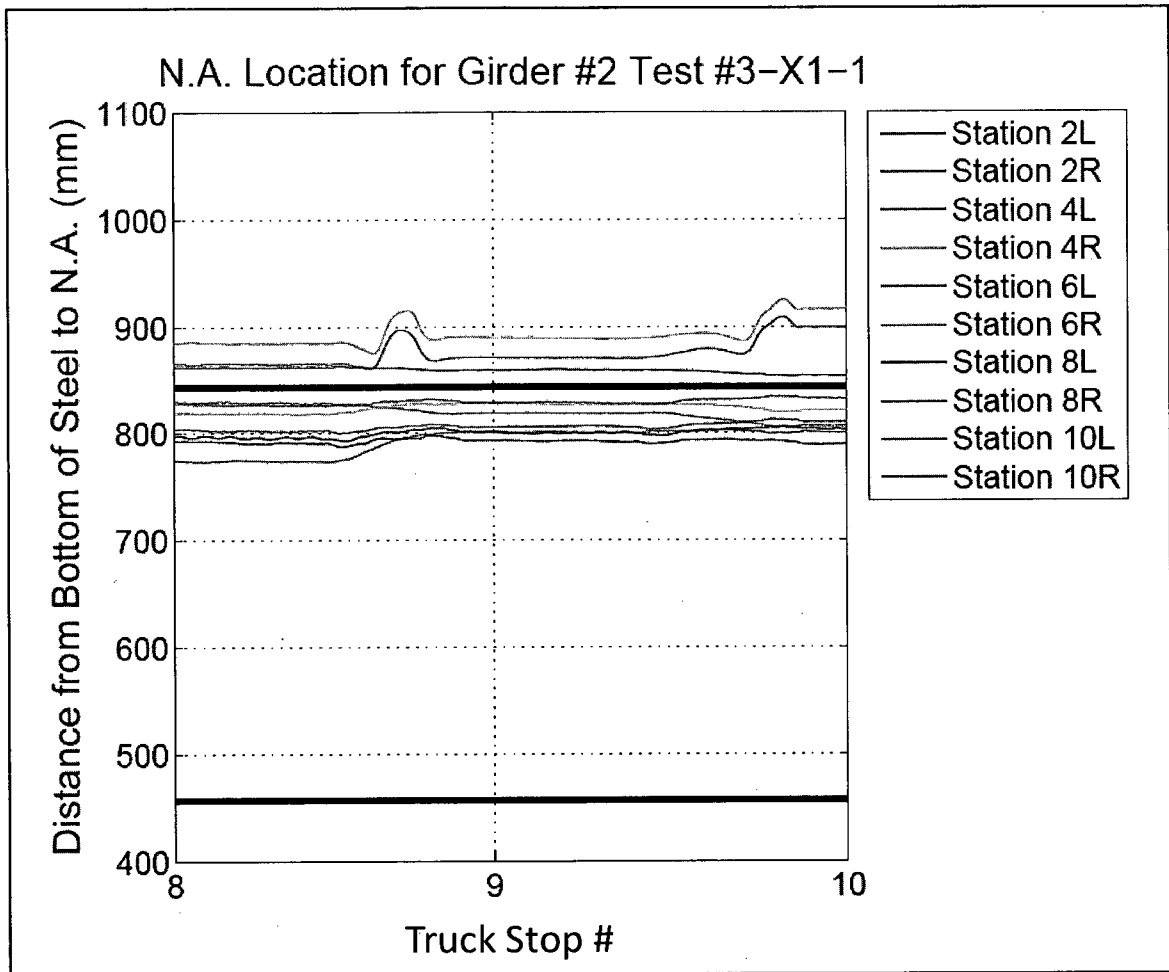


Figure 60. Filtered Plot of Neutral Axis Location for Girder 2 Stations during a Lane 1 Test. The black line at the top represents the neutral axis for a fully composite bridge. The black line at the bottom represents the centerline of the girder and the neutral axis of a fully non-composite girder.

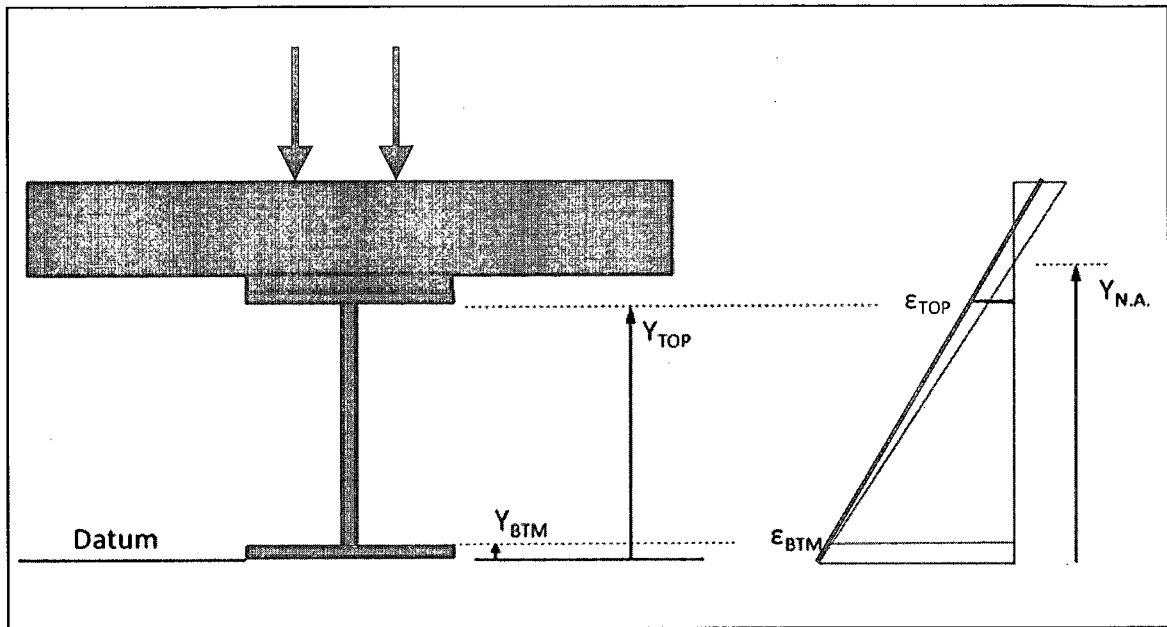


Figure 61. Illustration of local loading effects on top flange axial strain.

The final step in quality assessment of the neutral axis data is to examine the repeatability of the measurements. A list of the mean measured neutral axis for each station on each girder is listed in

Table 8. The results show a fairly dependable measurement. It can be seen that the pooled standard deviation of the grouped means is larger than what was observed in the pure strain measurements. This can be expected, however, given the level of measurement manipulation that the neutral axis calculation undergoes. Given the typical amplitude between 800 mm and 900 mm, a maximum spread of 37mm (station 4 of girder 3) is only 5% of the measurement. Therefore, it seems reasonable to conclude that the mean neutral axis measurements are acceptable for use in the calculation of strain from model output as well as for a comparison to design criteria. It is worth noting that at measurement stations which included a malfunctioning strain gauge, such as station 6 of girder 3, the design neutral axis value shall be used in its place. The calculation of design neutral axis measurements can be found in Appendix B.

Table 8. Analysis of Measured Neutral Axes for Strain Stations on all Six Girders

Girder	Station	Measured Neutral Axis (Grouped Mean) (mm)	Pooled Standard Deviation (mm)	Girder	Station	Measured Neutral Axis (Grouped Mean) (mm)	Pooled Standard Deviation (mm)
1	2	859.00	2.35	4	2	846.76	0.99
	4	817.58	2.83		4	878.41	5.68
	6	801.30	5.90		6	889.35	6.76
	8	863.54	2.17		8	806.56	8.65
	10	816.43	2.26		10	808.18	2.06
2	2	839.30	4.95	5	2	859.82	2.25
	4	807.05	10.52		4	871.64	0.63
	6	883.02	11.28		6	890.51	7.64
	8	795.84	3.30		8	879.65	4.66
	10	817.49	2.84		10	889.35	6.76
3	2	773.15	8.78	6	2	921.14	1.62
	4	723.06	36.90		4	851.26	8.92
	6	0.00	0.00		6	821.35	16.41
	8	793.60	3.41		8	0.00	0.00
	10	797.57	2.12		10	0.00	0.00

The second purpose of the calculation of the composite section neutral axis was to determine if the bridge was acting compositely, as it was designed to. Table 9 displays the mean neutral axis measurements compared to the design neutral axis. Two measurements of the design neutral axis are present in the table. The first neutral axis assumes that each girder bends independently of the others, which is the assumption for the strength load case in design. The second set of design calculations assumes that the entire bridge section bends as a whole, and thus the neutral axis is consistent with the section properties of the entire bridge section.

The percent errors from design values are also shown for both sets of calculations. It can be seen from Table 9 that the majority of the errors from the bridge neutral axis are smaller than those for the girder neutral axis. In fact, the average absolute error for the measured from the girder neutral axis is 1% more at 5.2% than for

the bridge neutral axis at 4.27%. The variation from the bridge neutral axis is also smaller, with a standard deviation of 2.94% than for the girder neutral axis (standard deviation of 3.85%). Both statistics suggest that the bridge is performing compositely as designed and also that the girders are bending about the bridge neutral axis. Plotting the data of Table 9 for each station with respect to girder displays some conflicting evidence to this conclusion however. Stations 8 and 10 (Figure 65 and Figure 66, respectively) show that measured neutral axes are very close to the design neutral axis for individual girders.

**Table 9. Measured Distance versus Design Distance to Neutral Axis from Bottom Flange of Steel**

Girder Number	Station	Measured Neutral Axis (Grouped Mean) (mm)	Design Neutral Axis (Girder) (mm)	% Error	Design Neutral Axis (Bridge) (mm)	% Error
1	2	859.00	796.49	7.85	843.68	1.82
	4	817.58	796.49	2.65	843.68	-3.09
	6	801.30	796.49	0.60	843.68	-5.02
	8	863.54	796.49	8.42	843.68	2.35
	10	816.43	796.49	2.50	843.68	-3.23
2	2	839.30	855.35	-1.88	843.68	-0.52
	4	807.05	855.35	-5.65	843.68	-4.34
	6	883.02	855.35	3.23	843.68	4.66
	8	795.84	855.35	-6.96	843.68	-5.67
	10	817.49	855.35	-4.43	843.68	-3.10
3	2	773.15	855.35	-9.61	843.68	-8.36
	4	723.06	855.35	-15.47	843.68	-14.30
	6	0.00	855.35		843.68	
	8	793.60	855.35	-7.22	843.68	-5.94
	10	797.57	855.35	-6.76	843.68	-5.47
4	2	846.76	855.35	-1.00	843.68	0.37
	4	878.41	855.35	2.70	843.68	4.12
	6	889.35	855.35	3.98	843.68	5.41
	8	806.56	855.35	-5.70	843.68	-4.40
	10	808.18	855.35	-5.51	843.68	-4.21
5	2	859.82	855.35	0.52	843.68	1.91
	4	871.64	855.35	1.91	843.68	3.31
	6	890.51	855.35	4.11	843.68	5.55
	8	879.65	855.35	2.84	843.68	4.26
	10	889.35	855.35	3.98	843.68	5.41
6	2	921.14	796.49	15.65	843.68	9.18
	4	851.26	796.49	6.88	843.68	0.90
	6	821.35	796.49	3.12	843.68	-2.65
	8	0.00	796.49		843.68	
	10	0.00	796.49		843.68	

Further conclusions can also be drawn by looking at the sign of the % error in Table 9. A negative error suggests that the measured neutral axis at the strain station is physically below that of the design neutral axis for a fully composite section, as in stations 8 and 10 on girders 2, 3, and 4 (see Figure 65 and Figure 66). This can be explained as follows.

As the section becomes less composite, the neutral axis drops to a theoretical minimum at the centerline of the steel girder. A measured neutral axis here would suggest a fully non-composite section where the concrete deck bends independently of the girders, the interface between them slipping like the pages of a magazine. If the cross section geometry, and thus the design neutral axis location, was constructed as designed, then the design neutral axis location for the composite behavior is a maximum. Furthermore, obtaining pure 100% composite behavior between steel and concrete is physically unattainable. Therefore, it is not surprising that many of the % errors are negative. The cause for this could be because the shear studs welded to the girders are not fully preventing slippage between the deck and girder. Another reason for the lower neutral axis could be that the concrete cracks under tension, reducing the effective moment of inertia of the composite section and shifting the neutral axis downward in the section.

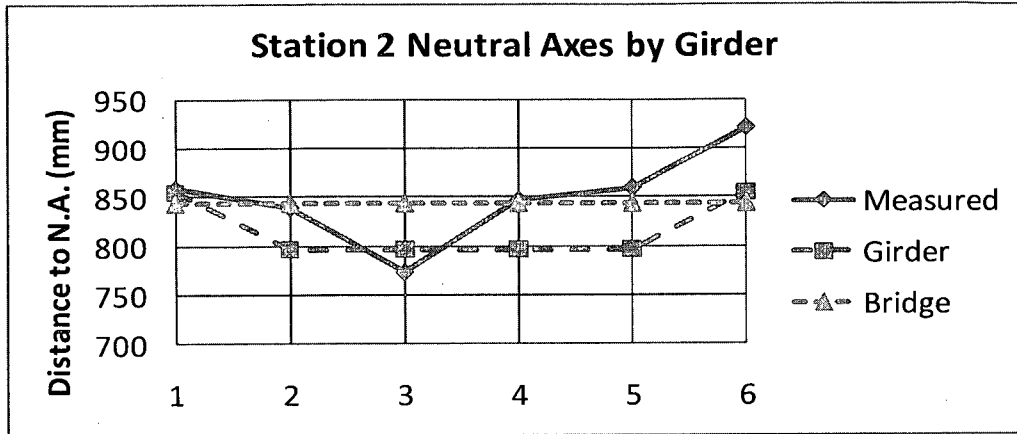


Figure 62. Measured and Calculated Neutral Axes for each Girder at Station 2

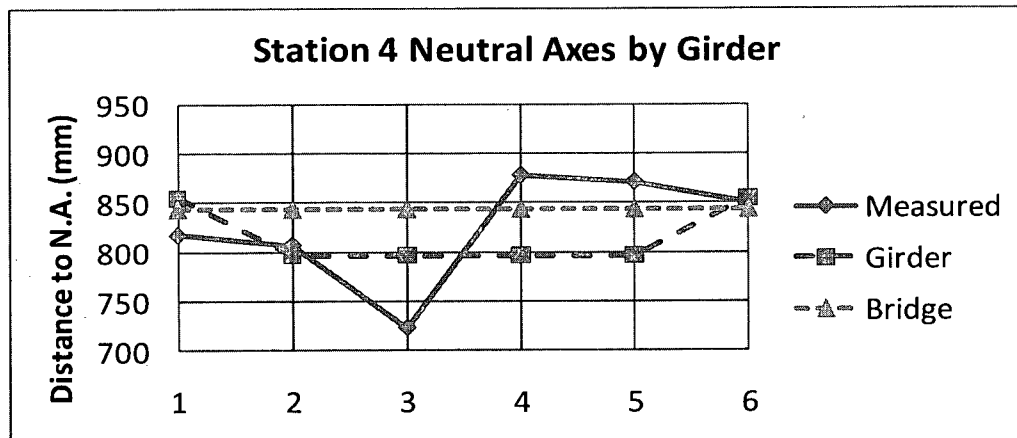


Figure 63. Measured and Calculated Neutral Axes for each Girder at Station 4

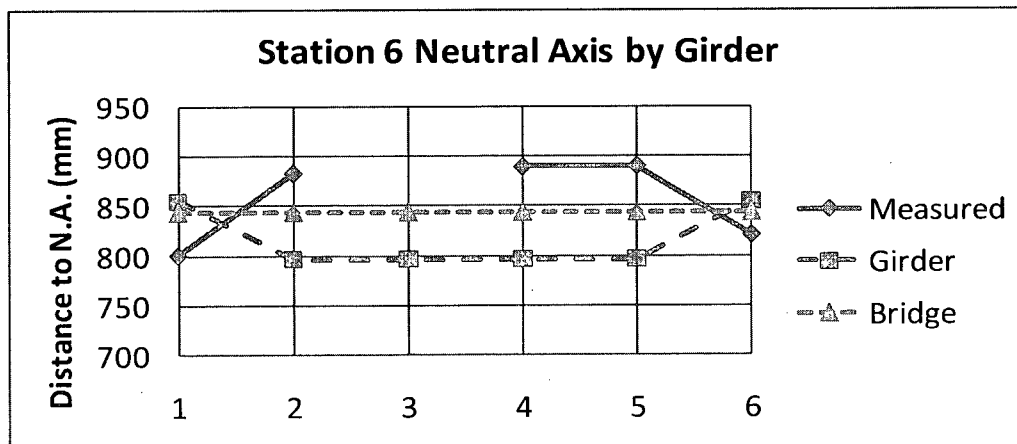


Figure 64. Measured and Calculated Neutral Axes for each Girder at Station 6

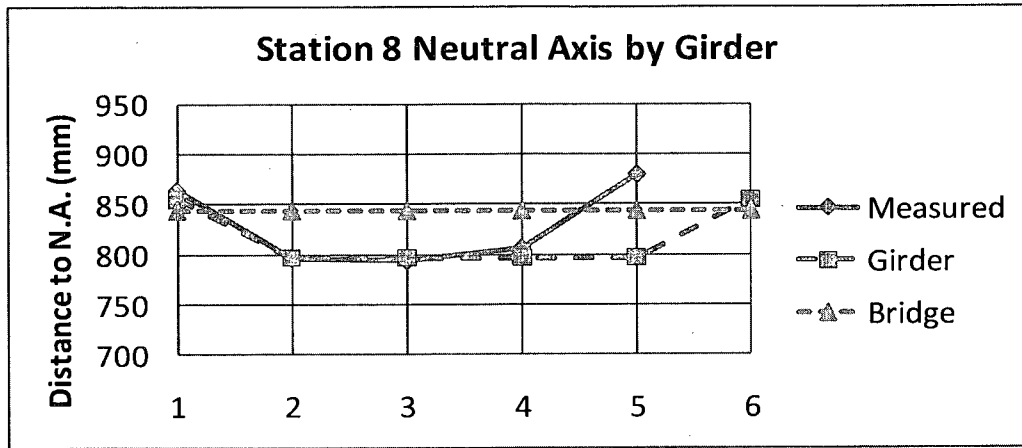


Figure 65. Measured and Calculated Neutral Axes for each Girder at Station 8

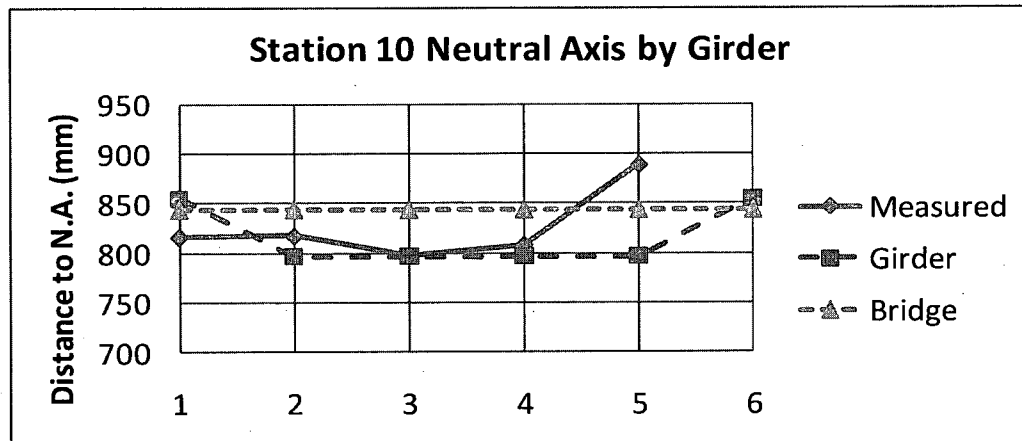


Figure 66. Measured and Calculated Neutral Axes for each Girder at Station 10

A positive error suggests that the neutral axis at the strain station is physically above the design value. Since a neutral axis above the design value is theoretically unattainable, the positive error suggests that the cross sectional properties in the design calculations underestimate the stiffness of the section. Many of the positive errors occur at stations on girders 1, 5 and 6 (see Figure 62 to Figure 66). Missing measured neutral axes in these figures is due to faulty sensors. The west edge of the deck above girder 1 has a safety curb that was poured separate from the deck but whose reinforcement is integral with the deck. If the safety curb is acting compositely with the girder-slab



system, it could provide additional stiffness to the deck thus raising the measured neutral axis (see Figure 81 in Chapter 6 for a photo of integral curb reinforcement). Similarly there is a concrete sidewalk above girder 6 and partially above girder 5. The sidewalk was also poured separate from the deck pour and its reinforcement integral with the deck. Thus, the same conclusions may be drawn with respect to neutral axis measurements on girders 5 and 6.

### **5.5 Summary of QA/QC Efforts**

The assessment of the quality of collected data during the load test consisted of multiple procedures and analyses. First, the strain gauges were individually inspected for functionality and proper post-processing. A list of faulty gauges and noisy data loggers was noted. The measurements were then analyzed to determine if the response seemed reasonable. Tests for this analysis included visual inspection if sign, magnitude, time of occurrence and length of occurrence. Second, the strain measurements were analyzed for repeatability and reliability. It was determined that the three truck runs in each lane could be combined to one, and that a single value of strain for each truck stop could be used for comparison to predicted results.

Finally, the neutral axis location was calculated for each top-and-bottom strain gauge pair on all six girders. The formula was found to be sensitive to loadings in which strain in the top and bottom gauges were approximately equal and when bending moment was not the primary force effect felt by the gauges. To account for this, the only neutral axis calculations used were from load cases where the truck inhabited the center span of the bridge. Neutral axis values were compiled in a similar way to the strain plateaus, and were determined acceptable for use in model strain calculation and for verification of design criteria. The bridge was also determined to be acting compositely as designed. Some measurements suggest errors in the assumption of the bridge cross

section and some suggest a nearly composite section. In either case, the monitoring of neutral axis location can provide a metric for bridge health assessment.

The Load test on September 3, 2009 produced a dependable measured dataset of strain across the length, width, and depth of the bridge, which can be confidently used in the comparison to the structural bridge model, the creation of which is discussed in the next chapter.

## CHAPTER 6

### STRUCTURAL MODELING

One of the major purposes of this research was to create a baseline enhanced designer's model (EDM) of the VAB. An EDM is defined here as a structural model of the full bridge that accounts for system behavior, but can be created in a relatively short period of time. If the design paradigm is to consider modeling and instrumentation as a requirement for submission, the modeling process must be specified to serve the purpose of long-term design without severely affecting the cost-to-benefit ratio. One of the future goals of this research project is to conduct a feasibility study from the perspective of bridge ownership and management to determine the relative benefits of instrumentation and modeling.

Modeling a large civil engineering structures can be a complicated process, depending on a variety of factors including the modeler's experience with FE software packages and the concepts of FE analysis. Even the most experienced bridge designer may struggle with the modeling program's graphical user interface (GUI) or with verifying the results of the model analysis.

#### **6.1 Modeling Program Selection**

The first step of the modeling process was to choose a program that could satisfy the requirement of a simple user interface combined with quick model creation. SAP2000® by Computers and Structures, Inc. (CSI) is a FE modeling program with a

built-in bridge information modeler (BrIM). The program was already owned by UNH and Tufts University and it had been used in previous research at UNH (Sipple, 2008). Additionally, SAP2000® is a popular FE modeling and analysis package used by many bridge design and management offices, such as FST, a partner in the project, and the NHDOT.

The SAP2000® BrIM was appropriate for many reasons. First, the model could be created in a matter of hours for someone familiar with the program, and involves a process similar in order to the design process itself. There is a bridge modeler wizard that walks the user through all the necessary steps of model creation, beginning with the layout line and grade, the definition of material properties, superstructure cross section definition, boundary conditions of the superstructure, and finally abutment and pier definition. The creation of the model is illustrated by the menu in Figure 67.

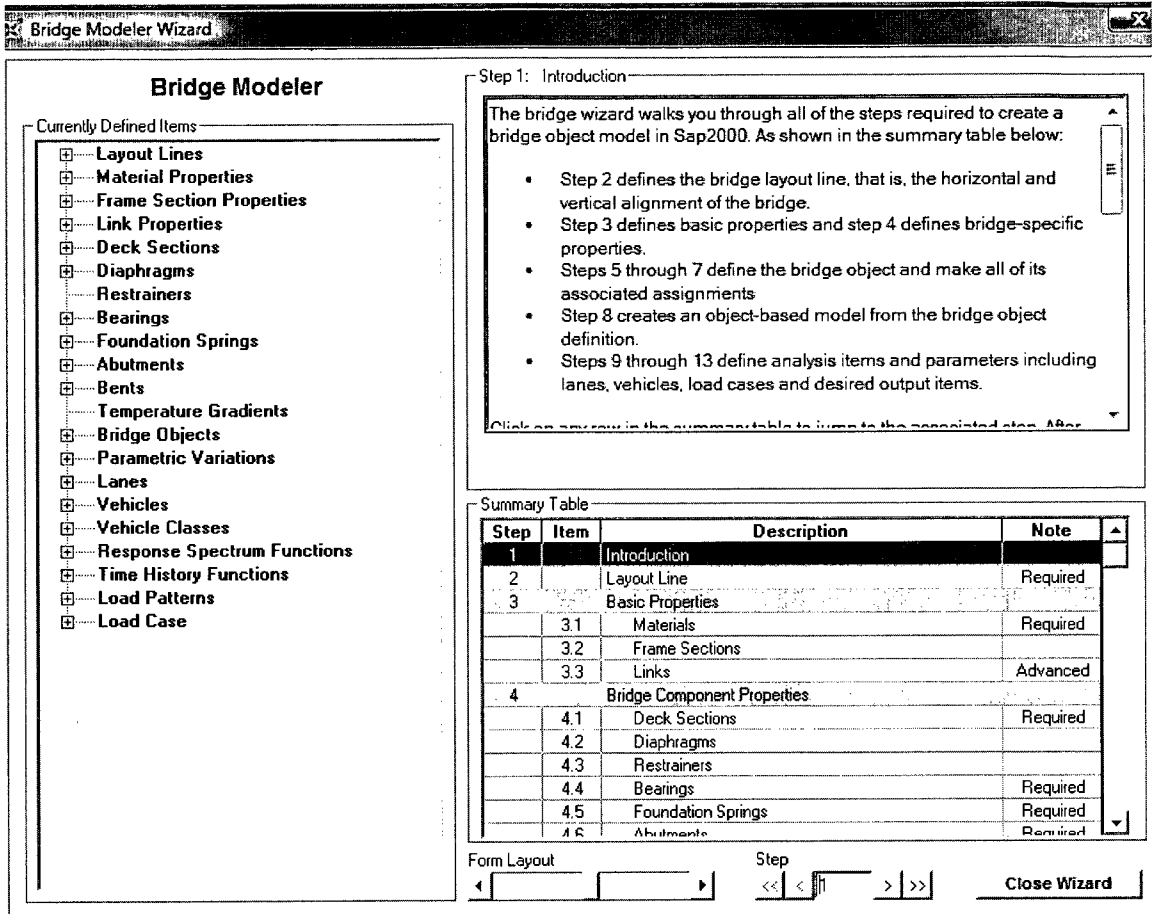


Figure 67. SAP Bridge Modeler Wizard User Interface (SAP2000 ® v14.1)

SAP2000® was also chosen for its advanced programming interface (API) and its compatibility with MUSTANG, a Matlab®-based parameter estimation and model updating program under development at UNH. One of the future goals of the research project is to use the model as a case study for verification of damage indices using MUSTANG.

A third reason for the choice of SAP2000® as the modeling program was to be able to compare the UNH baseline model with one created at Tufts University (Phelps, 2010). The model created at Tufts was to be a “perfect” FE model, i.e. one that attempts to replicate the true behavior of the bridge as closely as possible. In the Tufts model, the amount of time necessary to create the model was not a concern. As was previously

mentioned, cost-to-benefit is a major concern the Research group. Future research will study the results from the FE model at Tufts with the EDM created through the BrIM. A few factors for comparison will be speed of model creation, computing time, ease of post-processing, access to required strains, and model accuracy. SAP2000® was chosen because it can accomplish the goals of both models. This chapter is written so as to guide future researchers in the creation of a model using all the options available in the modeling software.

## **6.2 Initial Baseline EDM Creation**

The Bridge Modeling Wizard in SAP2000® walks the user through all the steps necessary to create the bridge model. This began with the layout of the bridge. Here, the initial and end stations were defined and the 3.5% grade of the bridge was applied between them. The direction of the bridge was assumed to run from due south to due north in order to keep local and global coordinates systems the same.

The second step in the process was to define the base materials to be used in the bridge. First was the concrete in the deck. The base material was a 30MPa (4 ksi) high performance concrete with a density of 2403 kg/m<sup>3</sup> (150 pcf) and a modulus of elasticity of 24.9 MPa (3600 ksi). The steel girders were defined using the predefined ASTM A992 Gr50 steel with a density of 7850 kg/m<sup>3</sup> (490 pcf) and a modulus of elasticity of 200MPa (29000 ksi). It is worth noting that the VAB used weathering steel, AASHTO M 270M Gr345W (Gr50W), but an investigation of material properties such as modulus of elasticity, unit weight, and coefficient of thermal expansion showed that there was no difference from those of A992 Steel for the purposes of modeling and linear elastic analysis.

Next, the deck section was defined. This involved defining the spacing of the steel girders, the thickness of the deck, the thickness of the concrete haunch, and the

geometry of the deck overhang. There were two deck sections to define. The first was the typical section of 6 girders spaced at 2.25m (7.38 ft) and the second was the deck section in the north span where the two fascia girders joined to support the widening deck section. The deck section definition form is shown in Figure 68.

The screenshot shows the 'Define Bridge Section Data - Steel Girder' dialog box. At the top left is a cross-section diagram of a bridge deck with 6 girders. The diagram labels the 'Left Exterior Girder', 'Interior Girder 1', 'Interior Girder 2', and 'Right Exterior Girder'. It also shows 'S1', 'S2', and 'S3' for girder spacing, 'L1', 'L2', and 'L3' for overhangs, and a 'Ref Pt' (Reference Point). Below the diagram is the text 'Constant or Variable Girder Spacing'. To the right of the diagram is a smaller diagram showing the bridge layout with a coordinate system (X, Y) and a 'Do Snap' checkbox. Below this is the text 'Section is Legal' and a 'Show Section Details...' button.

The main part of the dialog is a table titled 'Section Data' with columns 'Item' and 'Value'. The table is divided into sections: 'General Data', 'Girder Spacing Definition', and 'Slab Thickness'.

Item	Value
<b>General Data</b>	
Bridge Section Name	6Girders
Slab Material Property	4000Psi
Number of Interior Girders	4
Total Width	12715
Girder Longitudinal Layout	Along Layout Line
Constant Girder Spacing	No
Constant Girder Haunch Thickness (t2)	Yes
Constant Girder Frame Section	No
<b>Girder Spacing Definition</b>	
Girder Space S1	2250
Girder Space S2	2250
Girder Space S3	2250
Girder Space S4	2250
Girder Space S5	2250
<b>Slab Thickness</b>	
Top Slab Thickness (t1)	200
Concrete Haunch + Flange Thickness (t2)	79.878

At the bottom right of the dialog are buttons for 'OK' and 'Cancel'. There are also buttons for 'Girder Output' (Modify/Show Girder Force Output Locations...), 'Materials', 'Frame Sects...', and a 'Units' dropdown menu set to 'ENGR (mm, kN)'. A 'Show Section Details...' button is also present.

Figure 68 SAP BrIM Bridge Cross Section Definition (SAP2000 ® v14.1)

The next major step was the creation of bridge objects. The bridge object definition form, displayed in Figure 69, was where the previously defined bridge elements were combined to create the full bridge model. The location of the piers and the location of the deck section were defined here, as well as the locations of diaphragms within each span, boundary conditions for the superstructure, and boundary conditions for the abutments and piers. The bridge object definition form also allowed the user to force discretization points along the length of the bridge, which was necessary for correlation with collected data from bridge sensors.

Bridge Object Data

Bridge Object Name: [BOBJ1]    Layout Line Name: [BLL1]    Coordinate System: [GLOBAL]    Units: [Kip, in, F]

Define Bridge Object Reference Line

Span Label	Station in	Span Type
South Abutment	0	Start Abutment
South Span	462.5984	Full Span to End Bent
Center Span	1387.7953	Full Span to End Bent
North Span6	1503.4449	Span Segment 1
North Span8	1850.3937	Span Segment 2 to End Abutment

Modify/Show Assignments

- Spans
- User Discretization Points
- Abutments
- Bents
- In-Span Hinges (Expansion Jts)
- In-Span Cross Diaphragms
- Superelevation
- Prestress Tendons
- Staged Construction Groups
- Temperature Load Assigns

Note: 1. Bridge object location is based on bridge section insertion point following specified layout line.

Bridge Object Plan View (X-Y Projection)

OK    Cancel

Figure 69. SAP BrIM Bridge Object Data Definition (SAP2000® v14.1)

Several of the details of the model that were defined in the bridge object definition form were unique aspects of the VAB and/or important to the understanding of how the BrIM is formed. These details are discussed individually below.

### 6.2.1 Variation of Deck Section

At the quarter point of the north span, the deck section of the VAB changes from a 6 girder deck section with a constant deck width to one with an 8-girder deck section with varying deck width. In the bridge design plans, the two fascia girders widen linearly from their southern attachment to the exterior girders to their northern completion at the north abutment (Figure 70). SAP2000® allows the user to define parametric variations of model properties in order to accomplish the varying deck width. The parametric variation defined here was accomplished in two parts. First the creation of an 8 girder



deck section was performed such that there was a seamless integration with the 6 girder system. The design drawings call for an initial spacing of 200 mm (7.9 in) between the exterior girders and the fascia girders, with the flanges of the fascia girders coped to allow connection to the exterior girders. When the 200 mm spacing in the model was attempted, however, the deck section was reported as erroneous because the flanges in the model overlap. Coping of the flanges was not an option in the model, and therefore the initial spacing of 306.2 mm was used. This was the closest spacing that the program would allow. In this base 8-girder deck section, the deck width was held to the 12.5 m (41 ft) width of the 6-girder section, the spacing of the original six girders was kept at 2.25 m, and the deck overhang was decreased to allow for the placement of the fascia girders.

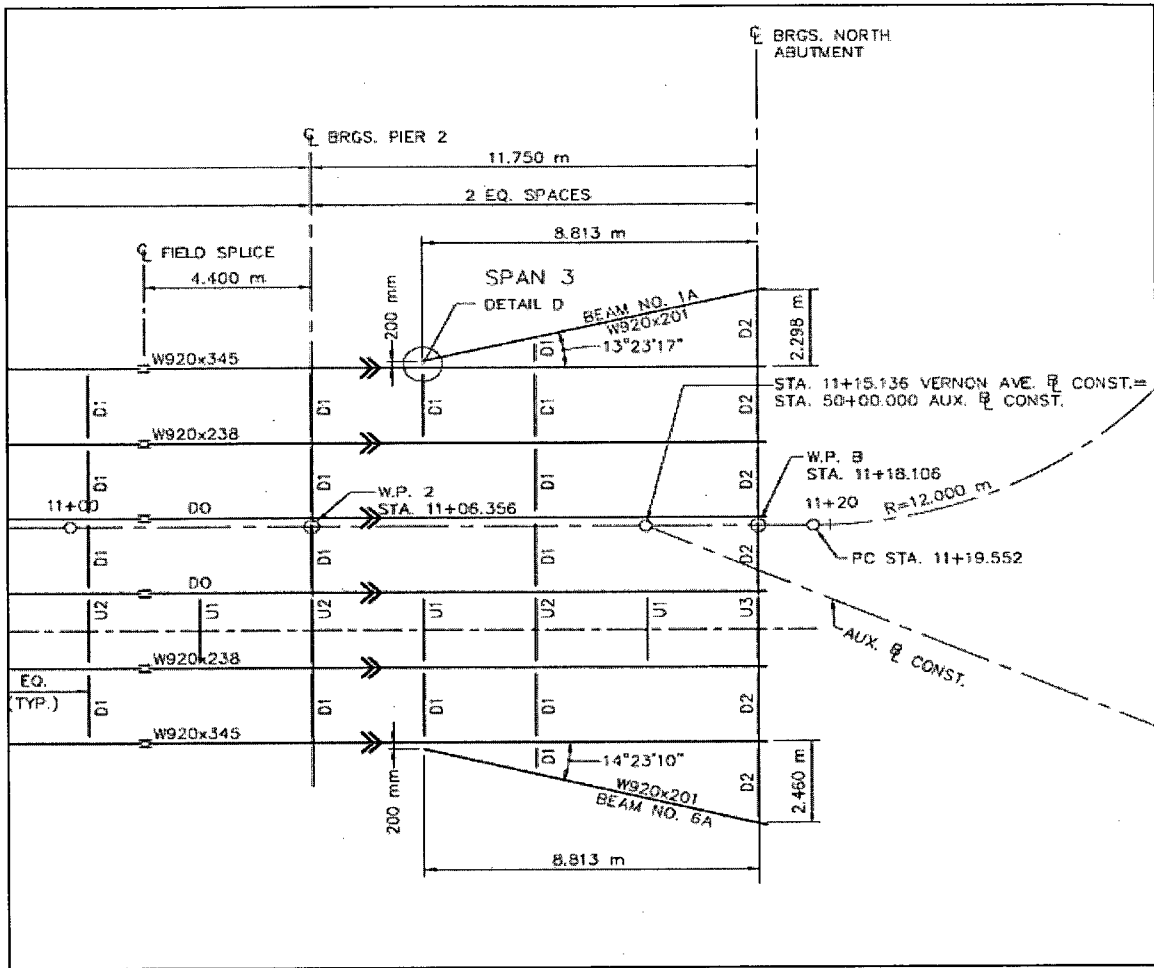


Figure 70. Varying deck section as given by design framing plan (FST, 2007)

Once the base section was created, the second step was to define parametric variations to account for the widening deck width and widening fascia girder spacing. The girder spacing increased linearly. The connection of the fascia girders to the exterior girders was modeled with a rigid link. The rigid link is fixed for all degrees of freedom to accomplish a full force and moment transfer between the two girders.

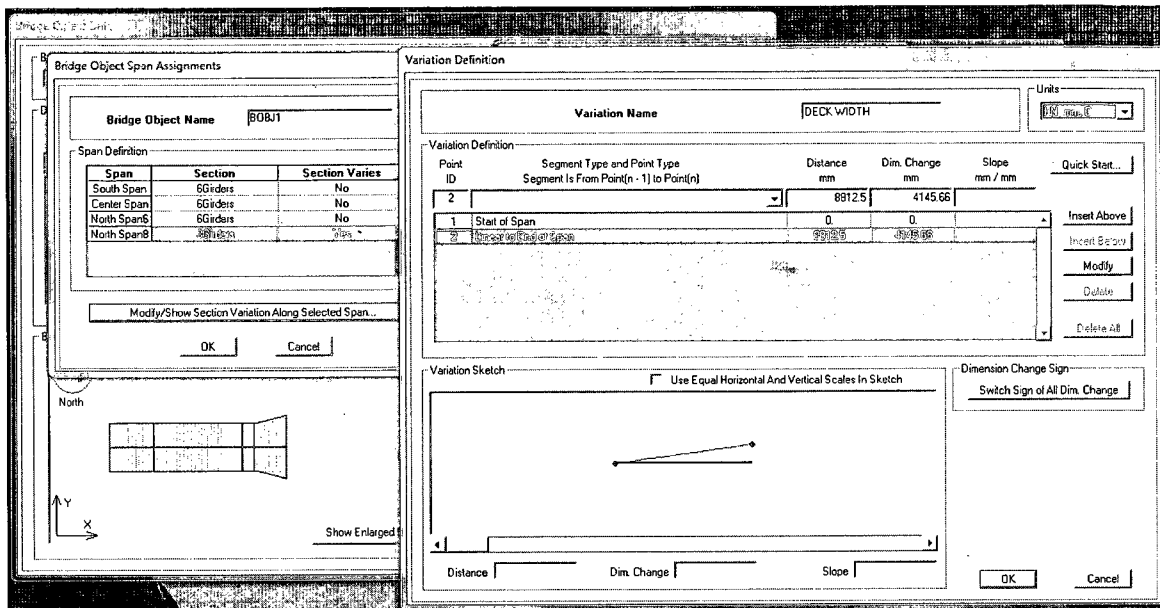


Figure 71. Display of section variation definition form for deck width variation (SAP2000® v14.1)

The deck was assumed to widen linearly as well. In reality, the deck increased width according to a radial arc that was not reported in the design plans. The radius was very large, however, and it was determined that the error would be acceptable if the deck reasonably encompassed the widening girder layout and was geometrically sound at both its start and finish. It can be seen from Figure 71 that the definition of a parametric variation is a simple process of defining what varies, and then how it varies. It is worth noting that variation by a radius, as is typical for roadway design, is not one of the variation types available in SAP2000®.

### 6.2.2 Bridge Deck Mesh

An appropriate FE mesh is an important characteristic of any FE model. The mesh of the VAB was chosen such that there was a balance between detail and efficiency. Loads that are applied to the interior of a shell element are distributed to the nodes of that element according to load's location with respect to the node locations. Therefore, a poorly meshed model will not provide enough detail to accurately capture the response of the structure. Furthermore, if the mesh of the model is too fine, the program can be

overburdened and the analysis can take too long for practical purposes. Recalling that efficiency was an important characteristic of the model, the shell elements were discretized to a maximum element length of 1 m along the length of the bridge. As previously mentioned, five locations along the length of the bridge were identified as user-defined discretization points in order to obtain model output at strain gauge locations. The mesh of the deck is predetermined along the width of the bridge so that the shell elements end at the centerline of the girder spacing. This corresponds to the effective width of a composite girder in bridge design and is not adjustable due to the BrIM analysis methodology within the SAP2000 programming.

The final lengthwise mesh discretized the frame elements of the steel girders and shell elements of the concrete such that a node existed at all connection points such as diaphragms connections, girder bearings, strain gauge locations, and finally such that no elements were longer than 1 m. The final widthwise mesh discretized the shell elements such that a node existed at the centerline of the girder spaces, above each girder, and at any change in shell element thickness such as at the deck overhang. After discretization the model had almost 800 shell elements and almost 400 frame elements. The bridge mesh can be seen in Figure 72.

The mesh of the model is also important for accurately modeling of composite behavior. The BrIM uses joint constraints to connect the frame elements of the girders with the shell elements of the deck. Many different types of joint constraints are available in SAP2000®, but the BrIM uses what SAP2000® calls a body constraint. In a body constraint, all participating joints move together as a 3-dimensional rigid body. In this case the participating joints are a frame joint and the corresponding shell joint directly above it. This concept is important in a composite bridge model because the joint constraints allow for the transfer of applied live and dead loads from the deck into the frame elements and vice versa. These constraints serve to represent the shear studs of

the bridge, transferring shear forces through the deck to the girders, creating the composite stiffness and moment of inertia that makes a composite section so efficient.

### **6.2.3 Insertion Points of Girders**

In addition to connectivity between the deck and girder, the BrIM must provide connectivity between the girders, bridge bearings, and bridge foundation. SAP2000® uses variable insertion points and links to accomplish this. Figure 72 shows the superstructure with three links labeled 1, 2 and 3 to represent connectivity between the frame and bearing pad, the bearing pad itself, and the foundation. An extruded view of the model can also be seen to given a visual aid to the description that follows.

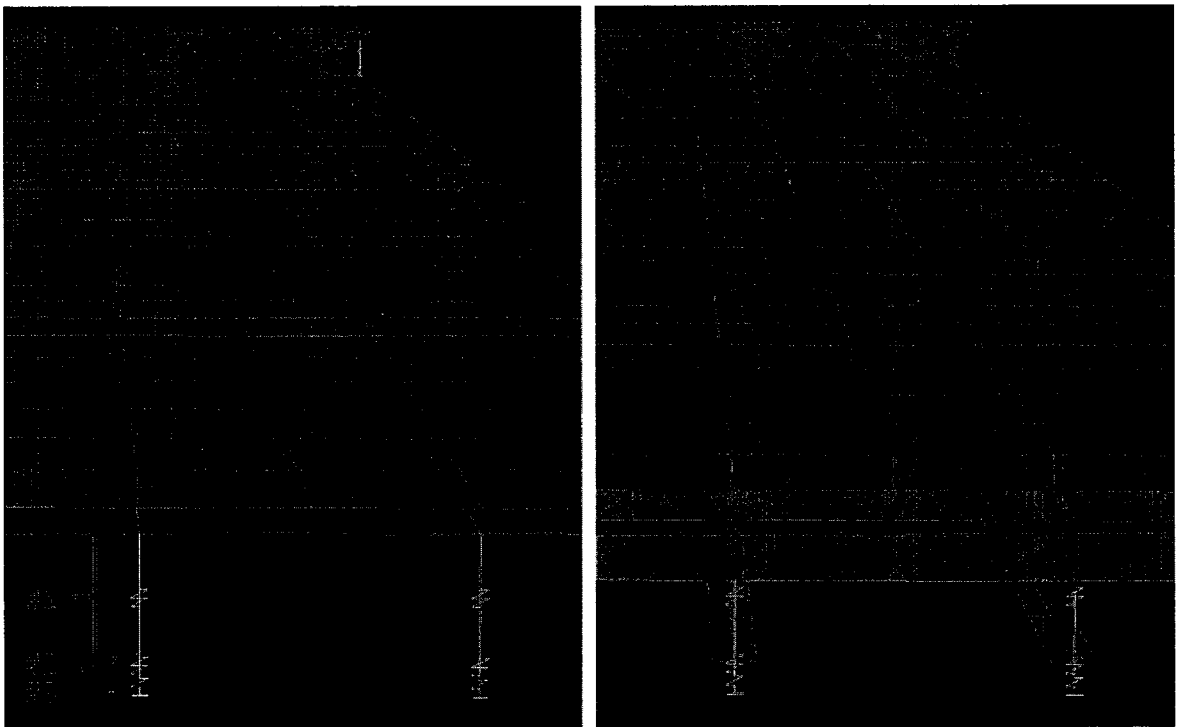


**Figure 72. Three links are used to create the connectivity between girder, bearing, and foundation.**

A frame element is a 1-dimensional element and its neutral axis is typically used to model its location within the structure. In order to limit the distance between the constrained joints between the girder and deck, SAP2000® offsets the location of the

modeled element to bottom of the top flange of the girder, and transforms the stiffness of the frame to account for the offset from its centroid.

In a typical modeling process, boundary conditions are applied to a girder at the frame's neutral axis. In reality, a girder is supported at its base. In order to account for the fact that the girder is not supported at its centerline, a two-node link is used to connect the frame element with the geometrically correct elevation of the bearing pad. This can be seen by the red bracket marked #1 in Figure 72. The link makes the frame element deflect appropriately with respect to its boundary conditions.

The boundary conditions of the bridge are steel reinforced elastomeric bearing pad as was described in the VAB introduction. Elastomeric bearing pads are designed with some flexibility to allow the bridge to expand and contract due to thermal loading, similar to a pin-roller boundary condition of the typical modeling process. The bearing definition in the BrIM can allow any of the six degrees of freedom to be fixed, free, partially restrained using a specified spring constant. At the time of the original model creation, limited information of bearing pad stiffnesses was available, therefore the bearings were modeled with the design assumption that the bridge should be free to expand, and a roller-roller-roller-pin boundary condition was defined, with the north abutment bearings arbitrarily chosen for the pin locations. The #2 bracket in Figure 72 marks the location of the link representing the bridge bearing.

Bridge Bearing Name:  Units:

Bridge Bearing Is Defined By:

Link/Support Property

User Definition

User Bearing Properties

DOF/Direction	Release Type	Stiffness
Translation Vertical (U1)	Fixed	
Translation Normal to Layout Line (U2)	Fixed	
Translation Along Layout Line (U3)	Fixed	
Rotation About Vertical (R1)	Free	
Rotation About Normal to Layout Line (R2)	Free	
Rotation About Layout Line (R3)	Free	

OK Cancel

Figure 73. BrIM bearing definition form. A “roller” bearing type is defined here (SAP2000® v14.1).

The bearings sit on the bridge abutment or pier cap, and represent the foundation for the superstructure. The foundation is modeled as a 1-node link beneath each of the bearings, as shown by the link labeled #3 in Figure 72. The foundation can be defined in the BrIM in the same fashion as the bearing pads: the 6 degrees of freedom are defined as fixed, free, or partially restrained. The bridge foundation was modeled as fully fixed in all directions since the stiffness of the abutments and piers relative to the superstructure is very high, and any movement in the abutments and piers would be negligible next to that of the superstructure. Tiltmeters were installed on the abutments and piers to test this hypothesis in future work.

### **6.3 Load Application**

In order to analyze the response of the BrIM due to the load truck, fifteen truck stops across three lanes were defined, for a total of 45 load cases. The first step in this definition was to define the truck dimensions and wheel loads. There are a number of

predefined trucks in the BrIM, so one truck was simply adapted to have the dimensions and wheel loads of the test truck. It can be seen from Figure 74 that the wheel loads are applied as 6 point loads, 2 for each axle. The on-center distances between axles and between wheels were used as was previously defined in Table 5 and the point loads were defined according to the average wheel loads as was previously defined in Table 6.

Figure 74 also shows that there is an option to apply uniform lane loads in addition to the truck loads, but this option was not used in the analysis. The bridge was loaded with only the weight of the truck and dead load was ignored in the model to be consistent with the fact that in the NDT, strain readings were zeroed prior to the start of each test. The response of the bridge was assumed to be linear elastic during application of the truck loads. Therefore the principle of superposition applied and it was determined that application of dead load then removal of the response due to deal load would only complicate model output post-processing.



**General Vehicle Data**

Vehicle name:  Units:

**Floating Axle Loads**

	Value	Width Type	Axle Width
For Lane Moments	<input type="text" value="0."/>	<input type="text" value="One Point"/>	<input type="text"/>
For Other Responses	<input type="text" value="0."/>	<input type="text" value="One Point"/>	<input type="text"/>

Double the Lane Moment Load when Calculating Negative Span Moments

**Usage**

Lane Negative Moments at Supports  
 Interior Vertical Support Forces  
 All other Responses

**Min Dist Allowed From Axle Load**

Lane Exterior Edge:   
Lane Interior Edge:

**Length Effects**

Axle:    
Uniform:

**Load Plan**

**Load Elevation**

**Loads**

Load Length Type	Minimum Distance	Maximum Distance	Uniform Load	Uniform Width Type	Uniform Width	Axle Load	Axle Width Type	Axle Width
Leading Load	Infinite		0.	Zero Width		19.551	Two Points	84.
Leading Load	Infinite		0.	Zero Width		19.551	Two Points	84.
Fixed Length	199.		0.	Zero Width		26.621	Two Points	73.
Fixed Length	56.		0.	Zero Width		26.547	Two Points	73.

Vehicle Applies To Straddle (Adjacent) Lanes Only    Straddle Reduction Factor:   
 Vehicle Remains Fully In Lane (in Lane Longitudinal Direction)

Figure 74. SAP BrIM Truck Load and Dimension Definition (SAP2000® v14.1)

The second step in the application of truck loads was to define the travel lanes for the truck in accordance with the load test layout plan. As can be seen in Figure 75, this process simply involved defining the location of the lane centerline with respect to the bridge layout line, and then defining the lane width.

**Bridge Lane Data**

Lane Name: X1 Lane

Coordinate System: GLOBAL

Units: Kip, in, F

Maximum Lane Load Discretization Lengths:

Along Lane: 19.685

Across Lane: 19.685

Additional Lane Load Discretization Parameters Along Lane:

Discretization Length Not Greater Than 1/ [ ] of Span Length

Discretization Length Not Greater Than 1/ [ ] of Lane Length

Lane Data

Bridge Layout Line	Station in	Centerline Offset in	Lane Width in	Move Lane...
BLL1	0	-164.8071	84	Add
BLL1	1850.3937	-164.8071	84	Insert
BLL1				Modify
				Delete

Plan View (X-Y Projection)

North

Layout Line: [ ]

Station: [ ]

Bearing: [ ]

Radius: [ ]

Grade: [ ]

X: [ ]

Y: [ ]

Z: [ ]

Snap To Layout Line

Snap To Lane

Objects Loaded By Lane:

Program Determined

Group: [ ]

Lane Edge Type:

Left Edge: Exterior

Right Edge: Interior

Display Color: [ ]

OK Cancel

Figure 75. SAP BrIM Lane Definition (SAP2000® v14.1)

The third and final step of load application was to define the load pattern and load case. The load pattern definition is shown in Figure 76. The load pattern type used was a bridge live load type, and proved to be very convenient for truck load case application. It is worth noting that this load type is only optioned if the structure was created using the bridge modeler. The bridge live load pattern discretizes the truck load within a given lane as a function of time. A truck "speed" is defined here, along with a truck starting location, length of time for the truck run, and time to apply the load to the bridge. The bridge live load pattern definition is a static load application, and only uses "speed" and time as a method to define the truck location across the length of the bridge. The load case associated with the bridge live load pattern is a linear multi-step static

load case. This load case allows for the application of the truck load at the discretization points defined by the bridge live load pattern definition. These points are correlated with stop locations from the load test.

The image shows two overlapping dialog boxes from the SAP2000 software. The background dialog is 'Define Load Patterns', and the foreground dialog is 'Multi Step Bridge Live Load Pattern Generation'.

**Define Load Patterns Dialog:**

Load Pattern Name	Type	Self Weight Multiplier	Auto Lateral Load Pattern
Truck Lane 1	BRIDGE LIVE	0	
Truck Lane 2	BRIDGE LIVE	0	
Truck Lane 3	BRIDGE LIVE	0	
DEAD	DEAD	1	

Buttons on the right: Add New Load Pattern, Modify Load Pattern, Modify Bridge Live Load..., Delete Load Pattern, Show Load Pattern Notes...

**Multi Step Bridge Live Load Pattern Generation Dialog:**

Vehicle	Lane	Start Dist	Start Time	Direction	Speed	
Load Truck	X1 Lane	-22.	0.	Forward	2.	Add
Load Truck	X1 Lane	-22.	0.	Forward	2.	Modify
						Delete

Note: Vehicles that are defined using a uniform load will not be included in the program generated multi-step load case. Click this note to see a list of vehicles defined using uniform loads.

Load Pattern Discretization Information:

Duration of Loading is: 84. seconds

Discretize Load every: 6. seconds

Units: (dropdown menu)

Buttons: OK, Cancel

Figure 76. Load Pattern Definition Form (SAP2000® v14.1).

One of the added benefits to using the BrIM during load application is that SAP2000® allows a visual interpretation of the truck at locations of load application. This is convenient for visual verification of the truck stop discretization within the load pattern definition and also for presentation purposes, as shown in Figure 77. The presentation of a truck on the bridge is more useful for visual communication than 6 vertical arrows representing the point loads applied.

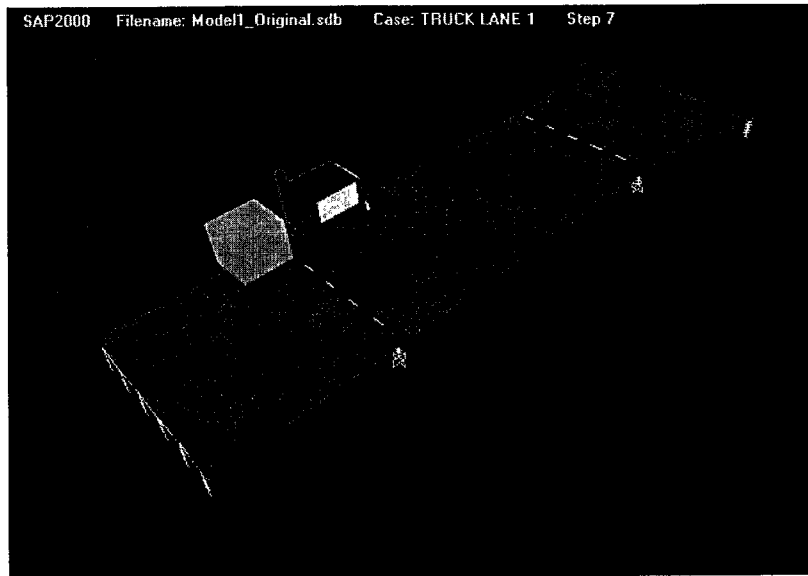


Figure 77. Modeled Load Truck at Stop #6 of Lane 1 (SAP2000® v14.1)

## **6.4 Post Processing of Model Output**

In order to obtain strains from the bridge model, the structural response required post-processing. The nature of the element types—shell elements for the deck and frame elements for the girders—did not allow the extraction of strain directly. Instead, strain was calculated from force components in the bridge using equations from elementary structural mechanics. The explanation of the process consists of two parts. First, it is necessary to understand how the forces are determined in the model for a composite section consisting of different element types. Secondly, the forces must be appropriately processed into strain using the strain compatibility method from structural mechanics. The post-processing methodologies are described below.

### **6.4.1 Output of Composite Section Forces**

On the first run of the model, the BrIM created predefined section cuts to calculate forces for the composite section. The section cuts are a grouping of selected elements and nodes. In this case, there is a section cut for every composite girder and deck. For an interior girder, for example, this includes two shell elements and one frame

element. Nodes are selected at these elements to define where on the selected elements the forces should be reported. In this example, there are three shell nodes to make up the deck portion of the section cut, and one frame node. This concept is illustrated in Figure 78. There is a section cut for each composite girder-and-effective-deck cross section, across the width of the bridge, and also one for the entire bridge cross section.

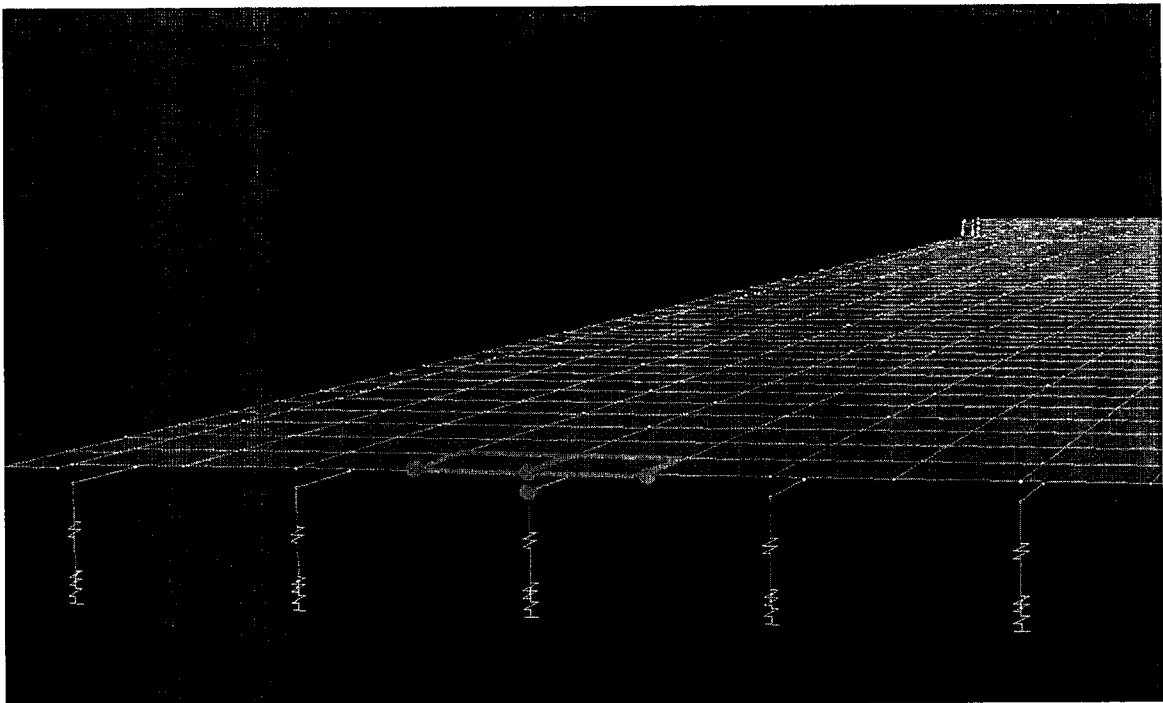


Figure 78. Section cut concept illustrated with red elements and respective nodes (SAP2000® v14.1)

The purpose of the section cuts is to calculate forces and moments at an individual section across the bridge for a particular composite girder. This is accomplished by summing the model forces at given nodes according to the section cut definition. For shear and axial forces, the calculation is simply the summing of respective force components at each node in the section cut definition. For moments, the force components are multiplied by a moment arm which is the perpendicular distance from the node to the centroid of the section cut. This centroid can be user

defined, and a study into the effects of changing this centroid is discussed later on in this chapter.

The results of the summing of forces in the section cut is conveniently displayed in the SAP2000® BrIM Bridge Forces graphical display, and can be outputted to a table as well. The graphical display is a shear, axial, moment, and torsion diagram across the length of the bridge for any of the analyzed load cases. The discretization of the diagram across the bridge is dependent on the mesh size along the length. As mentioned before, the mesh across the width is programmed defined, but the mesh along the length can be adjusted according to user preference. The moment diagram for the entire bridge section under the truck load can be seen in Figure 79.

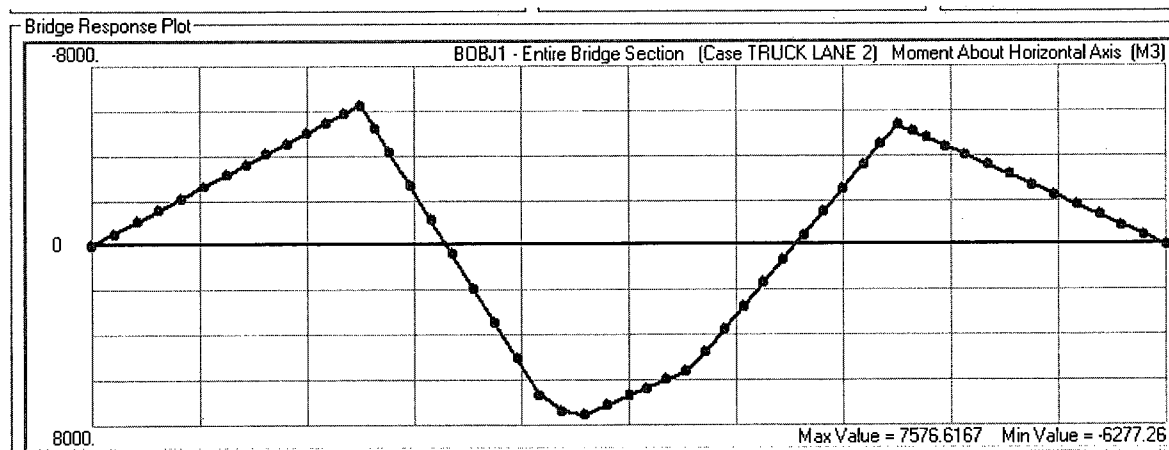


Figure 79. BrIM Object Response displaying the moment diagram for the full bridge section for Truck Stop #9 in Lane 2 (SAP2000® v14.1)

#### **6.4.2 Calculation of Strain from Model Forces**

The calculation of axial strain from the model output consisted of the summation of strain due to two force effects. The first is axial strain due to axial force effects and the second is axial strain due to strong axis bending moment. The strong axis bending of the bridge is bending about the line perpendicular to the bridge layout line, in other words perpendicular to the layout of the girders. Other force effects of shear, weak axis bending and torsion were not included for the following reasons. First, the strain gauges

on the bridge only measure strain along the bridge layout line. Therefore, strain due to shear would not be measured in the bridge, and thus should not be measured in the model. Secondly, torsional and lateral bending may have an effect on the axial strain measurements in both the model and the actual bridge, but the magnitude of these force effects were assumed to be less relative to the magnitude of axial forces and strong axis bending because bracing provided by diaphragms, web stiffeners, and the concrete deck. These force effects are also less understood and more complicated to confidently quantify, especially in the case of torsion. The addition of other force effects may be a consideration for future work where NDT's can be specifically designed to investigate such effects.

$$\varepsilon = \frac{P}{EA} + \frac{M_x y}{EI_y} \quad (4)$$

The formation of the conglomerate strain calculation can be seen in Equation 4 where P is the axial force, A is the cross sectional area, E is the modulus of elasticity,  $M_x$  is the strong axis bending moment,  $I_y$  is the strong axis moment of inertia, and y is the distance across the depth of the section from the neutral axis to the location of interest. The section properties used in the strain calculation are summarized in Table 10. In this calculation, the Parallel Axis Theorem was performed on a transformed section corresponding to an equivalent section made entirely of steel. The calculation of these properties is detailed in Appendix B.

**Table 10. Transformed section properties of composite section for model strain calculation**

Section Type	E (Mpa)	A mm <sup>2</sup>	I mm <sup>4</sup>	NA <sub>girder</sub> mm	NA <sub>bridge</sub> mm	NA <sub>measured</sub> mm
Interior Girder	199.948	88,286	1.160E+10	312.63	338.66	varies
Exterior Girder	199.948	97,392	1.499E+10	385.85	338.66	varies

The first term in the equation is the strain due to axial forces and is independent of the measurement location within the cross section. This term did not require any

adjustment during post processing. In the axial strain term,  $P$  is the axial force at the section cut,  $E$  is the elastic modulus of the transformed composite section, and  $A$  is the cross sectional area of the transformed composite section. The cross sectional area used in the calculation was that of the cross section of the girder, along with that of the effective deck width above the steel girder. The assumption of an effective deck width is consistent with AASHTO design procedures and the SAP2000® BrIM section cut (AASHTO, 2008). The formulation of strain due to axial force effects is detailed through the subscripts of Equation 5.

$$\epsilon_{AXIAL} = \frac{P_{SAP2000}}{E_{STEEL}A_{EFFECTIVE,TRANSFORMED}} \quad (5)$$

The bending moment portion of the strain calculation was the larger of the two strain components, and therefore the most important. Furthermore, the calculation of strain due to bending was dependent on the location of the measurement within the depth of the cross section with respect to the neutral axis. Although  $E$  and  $I$  were calculated in a similar fashion to that of the axial component, the choice of a neutral axis was not as clear. Three versions were compared to determine which best matched the collected data and therefore the true behavior of the bridge. The first was based on the design assumption that each girder acts independent of the other girders, and thus each girder-deck section would bend about its own neutral axis. The distance from the top of the concrete deck to this neutral axis is given by  $NA_{girder}$  in Table 10.

The second version of strain calculation assumed that all the girders of the bridge would bend about the neutral axis of the entire bridge, regardless of the section properties of each composite girder.

The third version of the strain measurement used the neutral axis that was measured from the bridge response. In this case, the calculation of the model strain was



dependent on its location on the bridge. As was seen in Chapter 5, the measured neutral axis was slightly different for each of the 5 strain measurement stations across the length of the bridge, and also varied from one girder to the next. Table 9 in Chapter 5 displays all 30 of the measured neutral axes measurements along the bridge, and how the measurements compare to bridge design neutral axis and girder design neutral axes. The measured neutral axis was determined the most appropriate for the calculation of model strains because the results of a comparison of all three versions of model data with respect to the measured data showed that the measured neutral axis values produced calculated strains with the closest agreement to collected strains. An example of the comparison is illustrated in Figure 80 using strain gauge SG25, which is located on the bottom flange of Girder 2 at station 6.

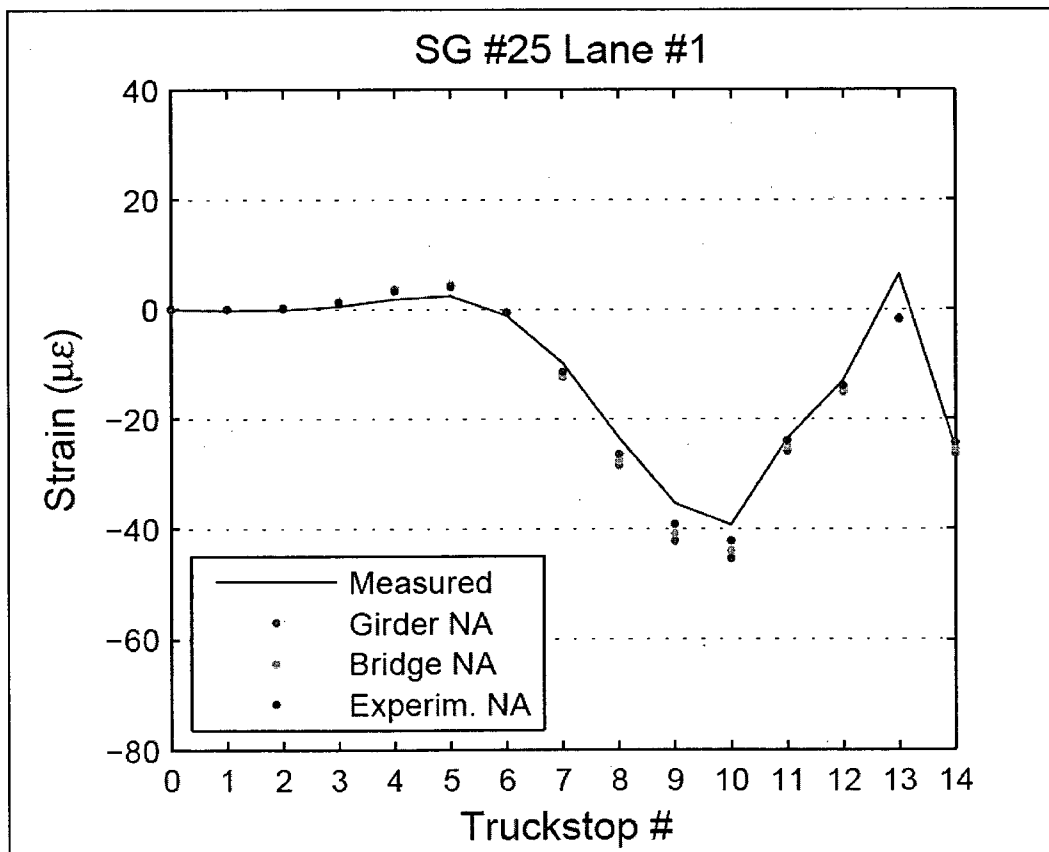


Figure 80. Example of Model Improvement by Model Post-Processing Update

The use of the girder neutral axis assumes that each girder acts independent of the others. This is appropriate for strength design so that if one girder fails, the remaining girders should not, but in terms of behavior, the girders and deck are all tied together after construction, and should not behave this way. Elementary structural mechanics teaches that a composite cross section should bend about its neutral axis, regardless of how many components are included in the section.

Secondly, the distribution of strain across the composite section depends on the level of composite behavior. A fully composite system with distribute strains to its extreme fibers differently than a section that acts 90% compositely. Therefore, the calculations of strain should be dependent on the level of composite behavior. The formation of strain due to strong axis bending is detailed through the subscripts of Equation 6.

$$\epsilon_{BENDING} = \frac{M_{x,SAP2000} * Y_{MEASURED}}{E_{STEEL} I_{EFFECTIVE,TRANSFORMED}} \quad (7)$$

### **6.5 Model Updating**

Four manual model updates were made to improve the accuracy of the model to as-built conditions. The updates were based on a detailed review of design drawings and from data collected and observations made during construction. It was expected that these updates would also improve the calibration of the model with collected data. Updates were made to the model in the order shown in Table 11: First, material properties of the concrete deck were updated based on mix design criteria from the aggregate plant. Second, a concrete safety curb was added to the deck at the edge of the deck overhang based on a field observation that the curb was heavily reinforced and the reinforcement was integral with the deck. Third, the boundary conditions were

adjusted based on literature on the stiffness of elastomeric bearing pads. Finally, reinforcement was added to the previously homogeneous concrete deck based on design drawings.

**Table 11. Description and basis for manual model updates in order of confidence**

<b>Number</b>	<b>Description of Update</b>	<b>Basis for Update</b>
1	Concrete Deck Material Properties	Testing of as-built material. Calculations from concrete Mix Design
2	Addition of Concrete Safety Curb	High level of reinforcement. Reinforcement integral with deck.
3	Spring Boundary Condition Stiffness	Literature on stiffness of elastomeric bearing pads.
4	Addition of steel reinforcement in concrete deck	Design plans

The updates were made to the model in order of increasing degree of uncertainty because the changes made to the model were not independent of one another. For example, the changing of the boundary conditions to spring stiffnesses may allow more flexibility in the bridge, since vertical deflections are no longer held to zero as was the case with the roller-pin boundary condition combination. Conversely, the addition of the reinforcement was expected to increase the stiffness of the bridge, thus decreasing the vertical deflections.

### **6.5.1 Updating of Concrete Deck Material Properties**

The original model was first updated to include the results of concrete cylinder laboratory testing and the aggregate mix design to update material properties of the concrete deck. This update was important because the values used in the original model were based off of design assumptions. The degree of uncertainty with this update was the lowest of the four because it was based testing by MassDOT in a controlled laboratory environment. Three parameters were updated in the model. First, the density of the concrete was updated from a typical design assumption for reinforced concrete of

2403 kg/m<sup>3</sup> (150 pcf) to the density specified in the concrete mix design supplied by Aggregate Industries plant that mixed the concrete, plant #288 in Lunenburg, MA. The mix design from which the densities were taken can be found in Appendix C.

The second updated parameter was the unconfined compressive strength of the concrete. Bridge strength was not studied in this research, so the value was not directly necessary, but concrete strength was used along with density in the empirical calculation of the modulus of elasticity, which is very important to this research.

The original model used a material with nominal unconfined compressive strength of 30 MPa (4000psi). MHD sampled concrete for cylinder break testing throughout the day of the deck pour. These cylinders were tested for typical 28 day strength and the results for each break recorded. The results of the testing were obtained by MHD and can be found in Appendix C. To determine a strength parameter to be used in the bridge model, the average compressive strength for four reported strengths was calculated. It was found that the strength of the in place concrete was about 35 MPa, which was much stronger than the designed compressive strength.

The third parameter updated in the model was the modulus of elasticity. This parameter was perhaps the most important because it in part defines the stiffness of the material, which affects deflections and force distributions in the model, and therefore would affect stress and strain distributions in the steel girders. In design, the modulus is given by a formula which is a function of its density and its compressive strength, as shown in Equation 7. The formula was based in part on the slope of the compressive stress-strain curve from a stress of 0 to 45% of the strength (American Concrete Institute, 2008). The original model used a concrete with an elastic modulus of 24,850 MPa, and the updated model used a value of 26,790 MPa, an increase of nearly 10%.

$$E_c = 0.043(w_c^{1.5})\sqrt{f'_c} \quad [MPa] \quad (7)$$

**Table 12. Comparison Original and Updated Concrete Material Properties**

	Units	Original	Reference for Original	Updated
Density, $w_c$	kg/m <sup>3</sup>	2402.8	Typical (150 pcf)	2235.9
Unconfined Compressive Strength, $f'_c$	MPa	27.579	Design (4000 psi)	34.725
Modulus of Elasticity, E	MPa	24855.6	Design Calc: $f(w_c, f'_c)$	26789.8

### **6.5.2 Addition of Safety Curb**

The second update to the model was to include the safety curb as part of the deck. The safety curb was also made of concrete, measured 495mm (19.5 in) in width by 200mm (7.9 in) high, and ran the length of the bridge. The concrete for the curb was poured a number of weeks after the pour of the deck concrete, once the deck was cured enough for carpenters to build the formwork for the curb. This update was done because the curb was so heavily reinforced, and because that reinforcement was integral with the main deck, as seen in Figure 81. It was determined that even though the curb was poured separate, it would act as part of the composite section. This would increase the stiffness of the deck at the deck overhang, and thus affect the performance of the bridge as a whole. The update was performed by selecting the deck shell elements that created the deck overhang, and increasing their thickness from 200mm to 400mm.

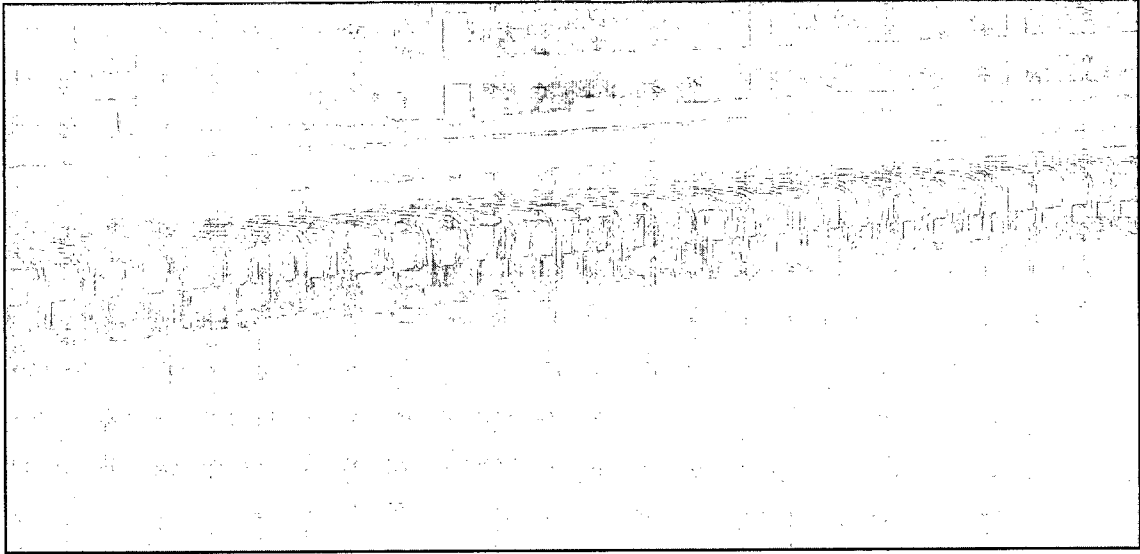
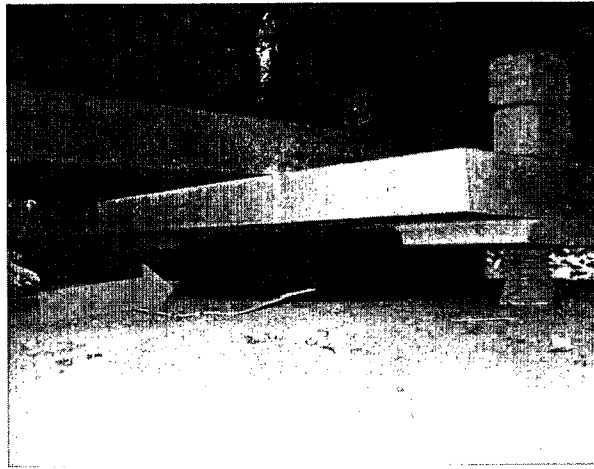


Figure 81. The safety curb reinforcement was integral with main deck

### **6.5.3 Updating of Boundary Conditions**

Each girder on the bridge was supported by elastomeric bearing pads. The pads are placed on top of the piers and abutments, topped with galvanized steel sole plates, and then the girders sit on top of the sole plates. At the piers, anchor bolts secure the sole plate to the pier, as seen in Figure 82. This update was done because the original model used a “Roller-Roller-Roller-Pin” boundary condition, based on a performance evaluation of different boundary condition combinations from data during the concrete pour.

The original boundary conditions for the model were replaced by springs with stiffness coefficients that were calculated based on recommendations published in NCHRP Report 12-68 (Stanton, Roeder, & Mackenzie-Helnwein, 2004). These recommendations were also used by other researchers at UNH for calibration of a single span precast concrete girder bridge in Rollinsford, NH (Sipple, 2008). The stiffness coefficients calculated for use in the Rollinsford Bridge were found to improve the agreement between collected data and modeled data.



**Figure 82. Elastomeric bearing pad supporting one of the girders. This location is at a pier, characterized by the anchor bolts.**

There were three main reasons why the degree of uncertainty with the spring stiffness coefficients was more than the curb and concrete material property updates. First, it is noted in the literature that updating boundary conditions can have a profound effect on model results (Schlune, Plos, & Gylltoft, 2009), (Sipple, 2008). Therefore the updating of boundary conditions should be made with extreme care and consideration.

Second, the stiffness of the pads was calculated based on an empirical design formula, and even though the research was based on testing results of many different bearing pads geometries, circular pads were not among them. It would be preferable to do lab testing in-house on a bearing pad with the same geometry and from the same batch of elastomer to determine stiffness coefficients in all six degrees of freedom.

Third, while investigating the formulas given by Stanton et al (2004), it was determined that the stiffness coefficients were highly sensitive to changes in assumptions of the material properties of the elastomer. The shear modulus was obtained from laboratory testing of the bearing pad elastomer (see Appendix D), but a second parameter was necessary to determine the bulk modulus of the elastomer. This parameter was Poisson's ratio which is a measure of longitudinal strain to lateral or radial strain. A typical assumption is that rubber is incompressible, which gives a

Poisson's ratio of 0.5 (Eisenberg, 1980), but a typical value used in practice is 0.49 to avoid mathematical instability between conversions of elastic moduli. Stanton et al used a value of 0.49985. In a study on the effect of bearing pads on precast concrete bridges, Yazdani et al used a Poisson's ratio of 0.4985 (Yazdani, Eddy, & Cai, 2000). As shown in Table 13, this researcher found that trying different values from 0.4985 to 0.4999 had a very large effect on the value of the bulk modulus, which is directly used in the calculation of Stanton stiffness calculations. A Poisson's ratio of 0.49975 was determined a reasonable balance between the published values and was chosen for use in the model.

**Table 13. Comparison of bulk moduli, K, for changing values of Poisson's ratio**

	<b>Yazdani</b>	<b>Sipple</b>	<b>Stanton et al</b>	<b>Maximum</b>
<b>v</b>	0.4985	0.4998	0.49985	0.4999
<b>G (kPa)</b>	1.0142	1.0142	1.0142	1.0142
<b>K (MPa)</b>	338	2535	3380	5071

The formulas for axial and rotational stiffnesses in the research by Stanton et al were given as a function of the geometry of the bearing pad and the material properties of the elastomer. No recommendations were given for shear and torsional stiffnesses, so researchers determined values based on other methods. The shear stiffness was calculated based on mechanics of materials, and torsional stiffness was assumed to be 10% of the rotational stiffness. It was assumed that torsional movement was not a major component of the overall movement of the superstructure of the bridge with respect to the bearings pads, and was chosen to maintain mathematical stability in the model analysis. The values for stiffness for all six degrees of freedom can be seen in Table 14, and the calculation of the stiffnesses can be seen in the Appendix D.



Table 14. Updated model boundary condition stiffness coefficients for SAP2000® model

Degree of Freedom	Original Pin Conditions	Original Roller Conditions	Updated Stiffness Coefficient	Units
Axial, $U_z$	Fixed	Fixed	560.469	kN/mm
Shear, $U_y$	Fixed	Free	0.992	kN/mm
Shear, $U_x$	Fixed	Free	0.992	kN/mm
Rotational, $R_x$	Free	Free	1.77E+06	kN-mm/rad
Rotational, $R_y$	Free	Free	1.77E+06	kN-mm/rad
Torsional, $R_z$	Free	Free	1.77E+05	kN-mm/rad

The addition of the stiffness coefficients to the model was as simple an update as the concrete material properties. The springs are modeled as links in the model, just like the original boundary conditions, but there is an option to use an advanced definition menu where individual stiffness coefficients can be entered. A screen shot of the menu with stiffness coefficients entered can be seen in Figure 83. The subscripts 1, 2 and 3 refer to x, y and z directions, respectfully.

**Linear Link/Support Directional Properties**

Link/Support Name:

Directional Control

Direction: Fixed

U1   

U2   

U3   

R1   

R2   

R3   

Stiffness Values Used For All Load Cases

Stiffness Is Uncoupled     Stiffness Is Coupled

U1	U2	U3	R1	R2	R3
560.469	0.992	0.992	176500.	1765000.	1765000.

Damping Values Used For All Load Cases

Damping Is Uncoupled     Damping Is Coupled

U1	U2	U3	R1	R2	R3
0.	0.	0.	0.	0.	0.

Shear Distance from End J

U2:

U3:

Units:

Figure 83. Boundary condition stiffness definition form (SAP2000® v14.1)

#### 6.5.4 Addition of Deck Reinforcement

The last update to the model was to change the concrete deck from a homogeneous cross section to one that included the steel reinforcement. This update was done to accurately account for the stiffness of the deck in negative moment regions. In order to do so, the longitudinal and containment steel reinforcement were accounted for as defined in the design drawings. The general layout of the longitudinal reinforcement was two layers of #13 rebar (#4 US Customary) every 120 mm (4.7 in) across the width of the deck. The general layout of the containment reinforcement was two layers of #16 bar (#5 US Customary) every 127 mm (5 in). A minimum of 50 mm (2

in) cover was required above the reinforcement, and a minimum of 10 mm (0.4 in) was required between the SIP formwork and the bottom reinforcement layer.

The deck reinforcement was included in the model by changing the homogeneous shell elements to layered shell elements, as was described in previous research (Sipple, 2008). The layered shell definition form in SAP2000® is shown in Figure 85. The typical cross section in the design plans were used to determine the depth to each layer of steel and total area of steel in each layer. The depth of each layer within the deck was appropriately defined so that the behavior of the reinforcement in bending was appropriate. The steel area was smeared into a layer of constant thickness by dividing the area of steel by the width of the deck. Both the longitudinal and containment steels were defined in this same fashion. This concept is illustrated in Figure 84.

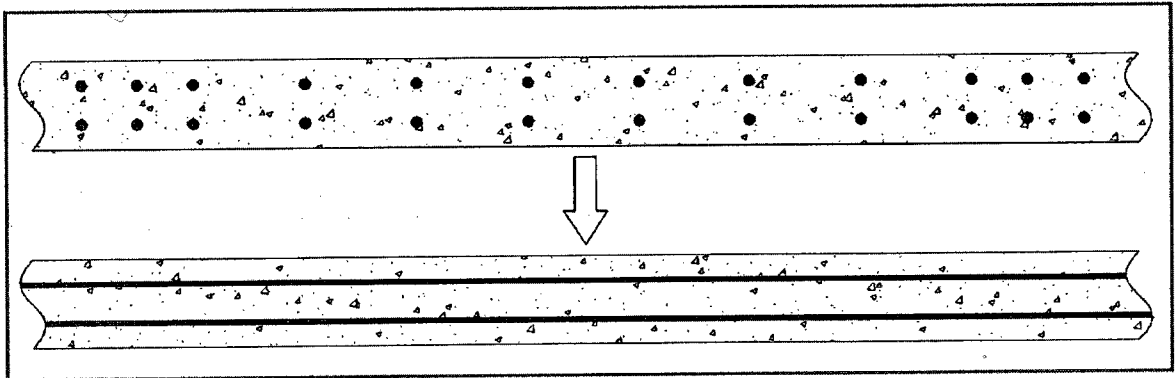


Figure 84. Modeling of steel reinforcement using SAP2000 layered shell element (Sipple, 2008).

Shell Section Layer Definition

Layer Definition Data

Layer Name	Distance	Thickness	Type	Num Int. Points	Material	Material Angle	Material S11	Material S22	Material Behavior S12
ConcS	0.	7.874016	Shell	2	Updated Concrete	0.	Linear	Linear	Linear
TopBar1	1.096457	0.035472	Shell	1	A615Gr60	0.	Linear	Inactive	Linear
TopBar2	1.656004	0.061772	Shell	1	A615Gr60	90.	Linear	Inactive	Linear
BotBar1	-2.67126	0.035472	Shell	1	A615Gr60	0.	Linear	Inactive	Linear
BotBar2	-3.230807	0.061772	Shell	1	A615Gr60	90.	Linear	Inactive	Linear

Quick Start | | | Add | Insert | Modify | Delete

Highlight Selected Layer

Transparency Control

Section Name: Interior

Order Layers By Distance:

Calculated Layer Information:

Number of Layers	5
Total Section Thickness	7.874
Sum of Layer Overlaps	0.1945
Sum of Gaps Between Layers	0.

Distance

Figure 85. SAP BrIM Layered Shell Definition

The resulting cross section had an equivalent area of steel within the deck. The layered shell definition form also supplied the option to define the behavior of each layer in each direction. This was important so that the longitudinal steel only affected deck behavior in the longitudinal direction (defined as S11 direction in Figure 85) and the containment steel only affected deck behavior in the lateral direction (defined as S22).

This update was the least dependable among the four updates for multiple reasons. First, it is commonly accepted that concrete can be assumed linear elastic in compression, but this is far from the truth when in tension. Given that the VAB is a 3-span continuous girder bridge, negative moment regions are found above both piers, which would put the concrete deck in tension with the steel reinforcement taking the tension force. But the concept that concrete behaves differently in tension than in

compression is a non-linear analysis, which is beyond the scope of the EDM. It can be seen in Figure 85 that linear behavior was selected for all materials and for all active degrees of freedom. It will be part of the recommendations for future work that the next researcher considers the effect of considerations of non-linear behavior in the deck.

The second reason for the limitations of the update is its accuracy with as-built conditions. The layout of rebar in the deck is dependent on the location along the deck: In negative moment regions, the number of longitudinal bars doubles; Along the curb, additional layers of longitudinal bars are present; the containment steel layout also changes above the exterior girder layout with the addition of the hoop steel around the edge of the deck; At the abutment, the deck reinforcement ties in with the reinforcement in the end diaphragm. The level of detail involved in the modification of reinforcement in each individual shell element is beyond the scope of the EDM, although a study into what, if any, of these details is especially important should be considered in future updates.

## **6.6 Baseline Model Evaluation**

There were 100 strain gauges measuring 15 load cases in 3 different lanes. Influence lines proved the best way of displaying the comparison, and the comparison between predicted and measured for each strain gauge could be conveniently displayed in 3 plots, 1 for each truck run. The result is 300 plots of comparison, which is too many to attempt a visual interpretation of goodness-of-fit and a mathematical method of evaluation is therefore necessary. In general, both the original model and the updated model matched well to collected measurements. Selected plots (Figure 86 to Figure 90) of comparison between modeled and collected data have been included in the following pages for illustration of particular problems model evaluation

and model update evaluation on a global scale. The captions describe the particular problems that are mentioned below. See Appendix J for a full Model-to-NDT-Data comparison for all 100 strain gauge locations.

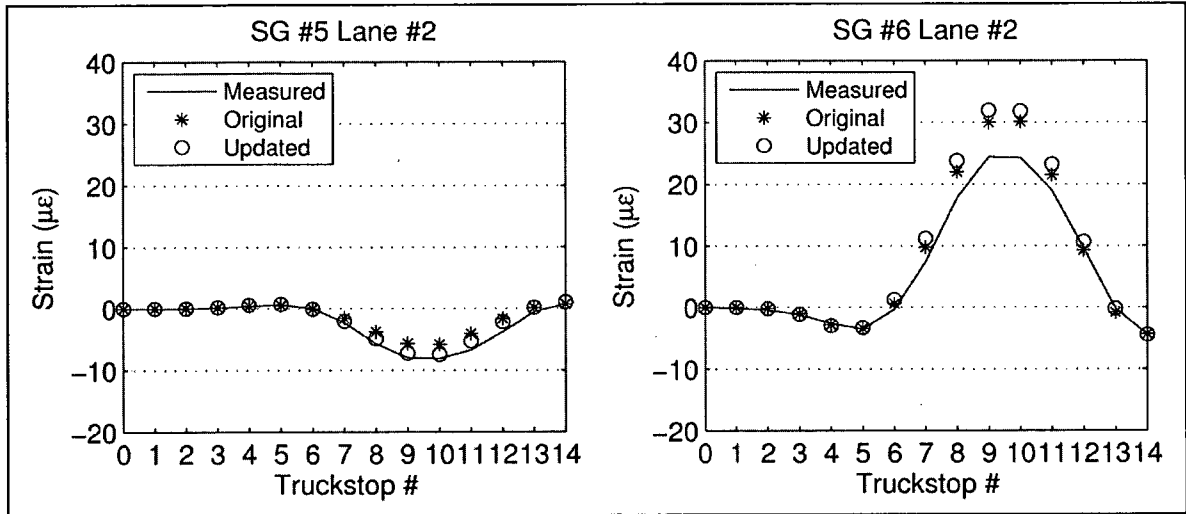


Figure 86. The center span station of girder 1 shows updated model closer to collected measurement in top flange (SG5) and farther from collected measurement in bottom flange (SG6).

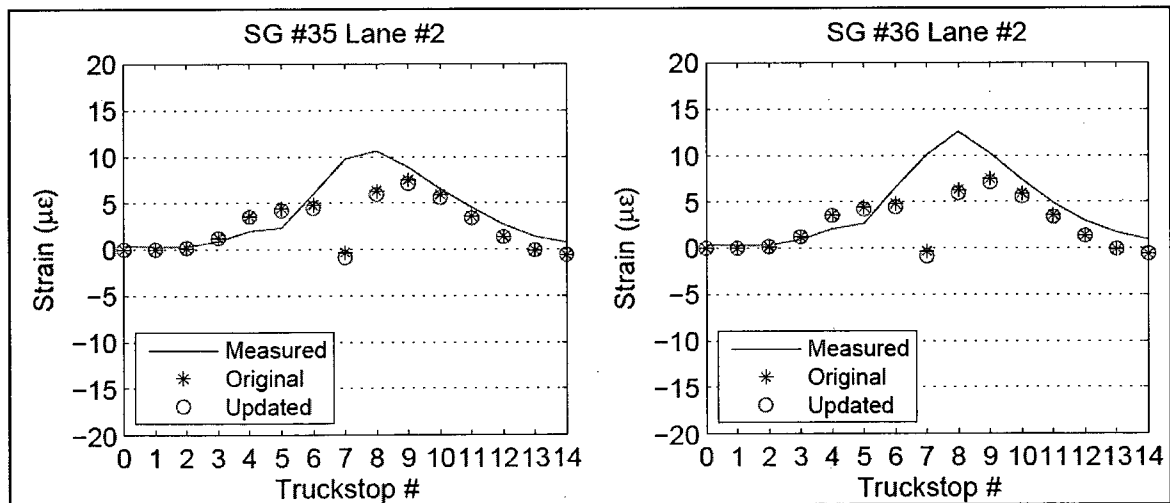


Figure 87. Measurements on the bottom flange of girder 3 just to the north of the south pier illustrate the effects of local loading on bending moment strain. Truck stop 7 is located directly above SG35 and SG36.

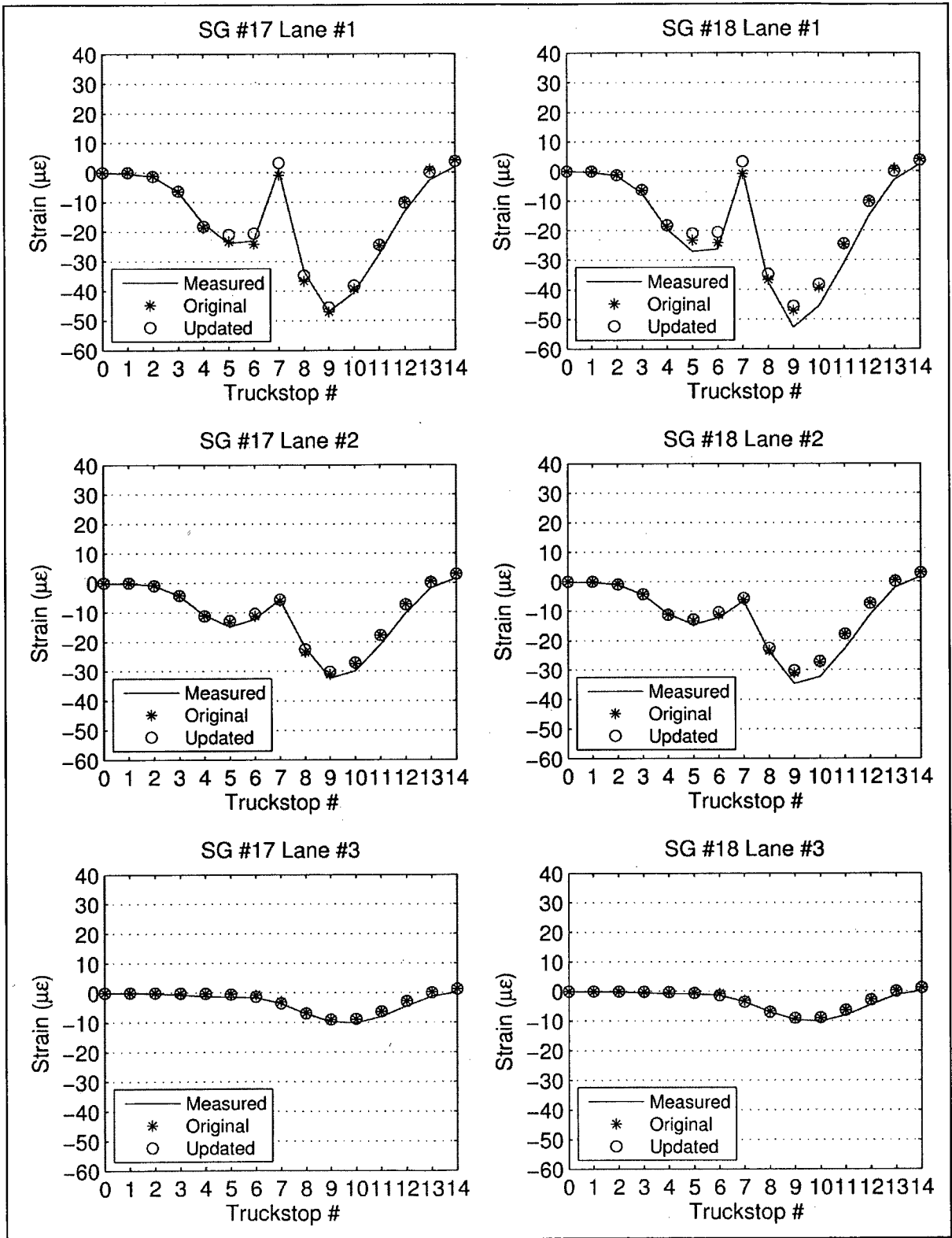


Figure 88. Varying strain magnitude with lane is illustrated by south pier strain gauges on the bottom flange of girder 2 (SG17 and SG18). The largest amplitudes are found when the truck is directly overhead (lane 1), and the smallest amplitudes when truck is on the opposite side of the bridge (lane 3). The original model better predicts the measured response in the lane 1 test and the updated in the lane 3 test.

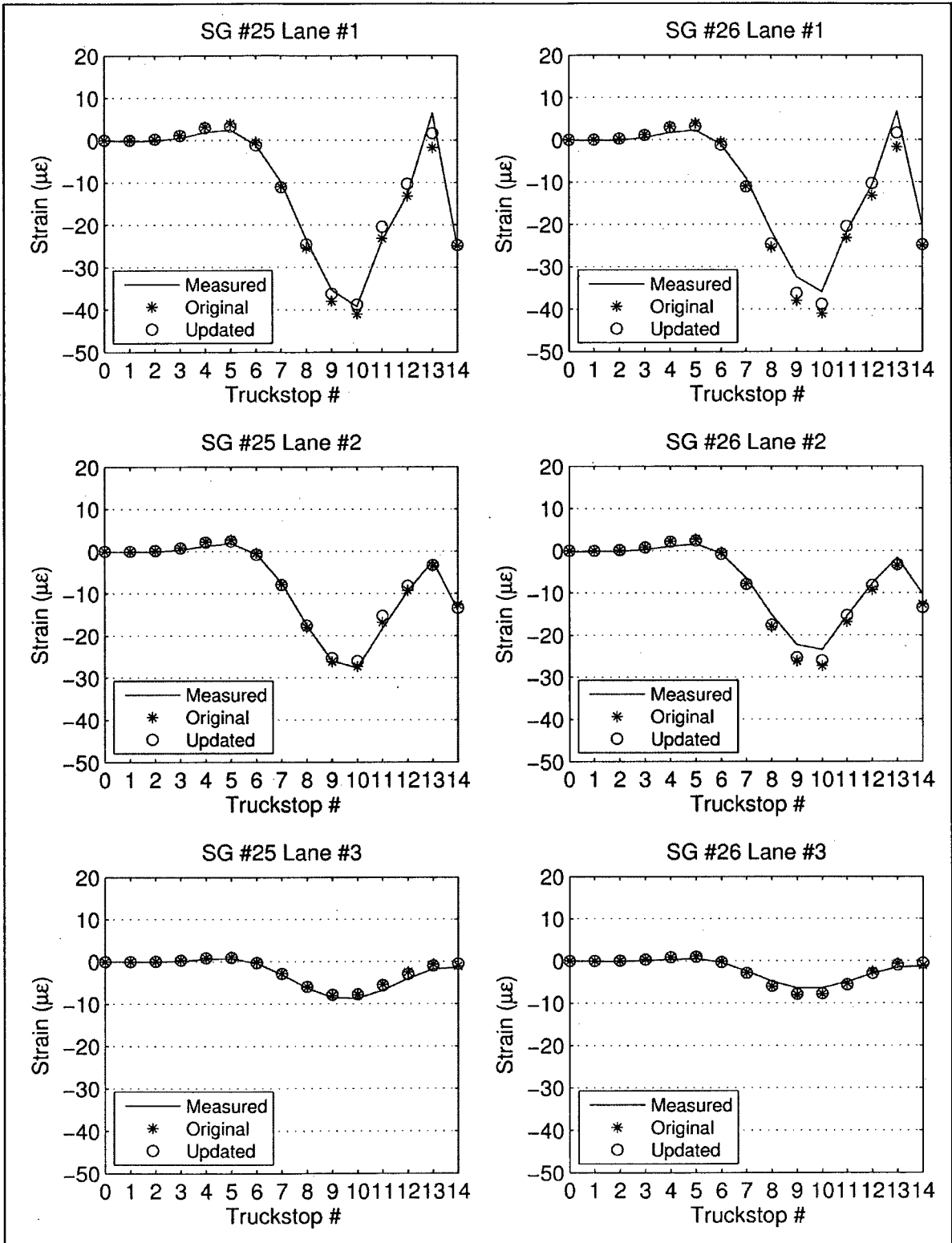


Figure 89. Mixed results are shown in the comparison of modeled to collected strains in SG25 and SG26, which are strain gauges on the bottom flange of girder 2 at the north pier. Also depicted here are the small strains for southern truck stops for a measurement on the north pier.



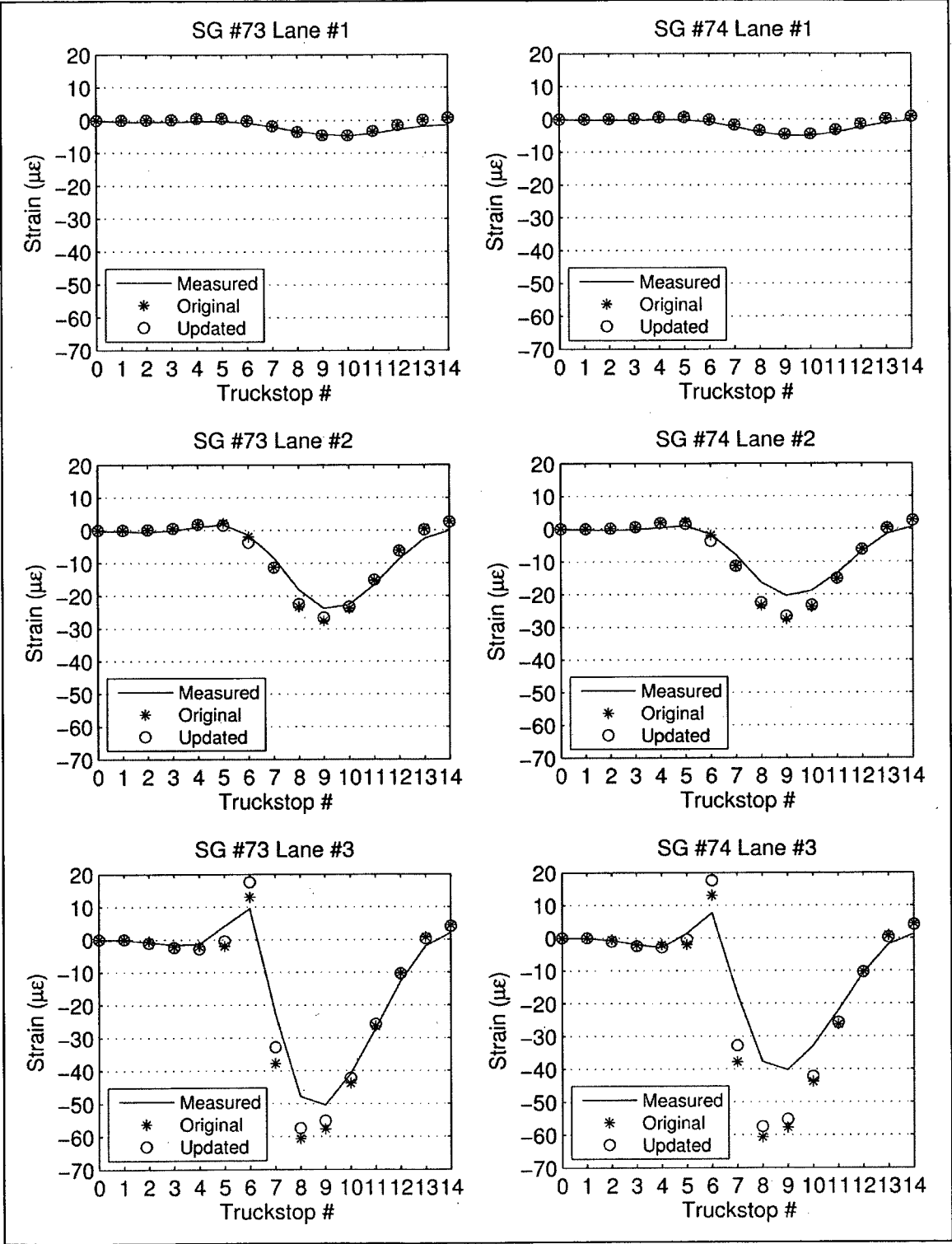


Figure 90. Strain on the bottom flange of girder 5 at the south pier. The modeled data is much closer to measurements on the left side of the web (SG73) than the right side (SG74).

Determination of a global metric for comparison was problematic, primarily because of the variation in measurement magnitude and importance. Some examples are the following: Top flange measurements were typically smaller when compared to bottom flange measurements because of proximity to the neutral axis; Truck loads in the west lane would give small strain measurements on the east side of the bridge; Truck loads in the southern truck stops would give small readings on north span strain gauge locations; Local effects caused by truck loads over the piers or directly over strain gauge locations were not necessarily accounted for in the model results; As was seen in Figure 50 in Chapter 6, some of the collected measurements were “cleaner” measurements and thus more dependable and more important than others.

Conversely, an argument can be made that all measurements are important, regardless of amplitude. For example, small measurements may be just as important in determining the goodness-of-fit of the model. If the model and measured data agree on a reading of  $1\mu\epsilon$  in a gauge on the left side of the bridge for a load case for the truck in the right lane, this might signify an extremely accurate model.

Despite the arguments that can be made for determining which measurements to use in a comparison between modeled and collected measurements, another issue is how to quantify the comparison between the collected measurements and different model updates. Furthermore, it is necessary to quantify if a model is “good enough”. It was determined that a comparison of three different metrics would be used to determine the accuracy of the original model and of the updates to the model. The first method used a scalar objective function called J, which was a published method to determine model improvement relative to previous versions of a model. A second method was to use a percent error technique with various minimum measurement thresholds. A third technique was to look at average differences between measured and modeled data.

These differences will be referred to as residuals in the remaining pages of this document.

### **6.6.1 J-Value Metric**

The first metric used to determine the accuracy of the model to collected measurements was based on research into FE model updating through non-linear optimization. In the paper, Schlune et al (2009) discussed many versions of an objective function, termed J, to determine a metric that could quantify the model's performance compared to the collected data. J was to be a single unitless value that attempted to be as unbiased as possible. The function used in this research is given by Equation 8, where n is the number of load cases (45, using the September 3<sup>rd</sup> NDT plan) and s is the number of sensors (100). The scalar objective function J was used for multiple reasons. First, smaller residuals are weighted significantly less than larger residuals and normalization of the residual by the standard deviation of the measured data allows cleaner data to have a larger weight. Since the standard deviation was typically less than 1µε, the sum of 4500 terms tends to be a very large number. Therefore the size of the number was controlled by normalizing the sum by the number of measurements. The second reason for using J was based on the fact that researchers at tufts University had used the metric for model updating (Sanayei, Imbaro, McClain, & Brown, 1997), (Sanayei & Saletnik, 1996). Regardless of how the metric performed within this research, J would provide a means of comparison between the detailed FE model at Tufts and the EDM created in this research.

$$J = \frac{1}{n} \frac{1}{s} \left( \sum_{i=1}^n \sum_{j=1}^s \frac{(\epsilon_{xx,measured} - \epsilon_{xx,modeled})^2}{(\sigma_{measured})^2} \right) \quad (8)$$

Figure 91 shows the comparison of J-values from the original baseline model and with each successive update. It can be seen that using J as a metric of model improvement shows that the model updates improve the agreement between modeled and collected data, with the update of boundary conditions providing the greatest jump in improvement. In terms of percent improvement in the value of J, however, the final update showed just under a 10% improvement to the value of J. One of the problems with J is determining what value would indicate a “good” model. Clearly, a value of zero would indicate that the difference between all predictions and measurements would be zero, but it is reasonable to assume that obtaining a perfect match is unobtainable. Therefore, the choice of the normalization term becomes very important, especially for small standard deviations. The average pooled standard deviation of the collected data was  $0.1 \mu\epsilon$ . If the residual is  $1 \mu\epsilon$ , then the J-value for that measurement would be 100; if the residual was  $2 \mu\epsilon$ , then the J-value would be 400. This example illustrates that in the case of clean measured data with small standard deviations, the use of J as an objective measure of goodness of fit may not be the best option.

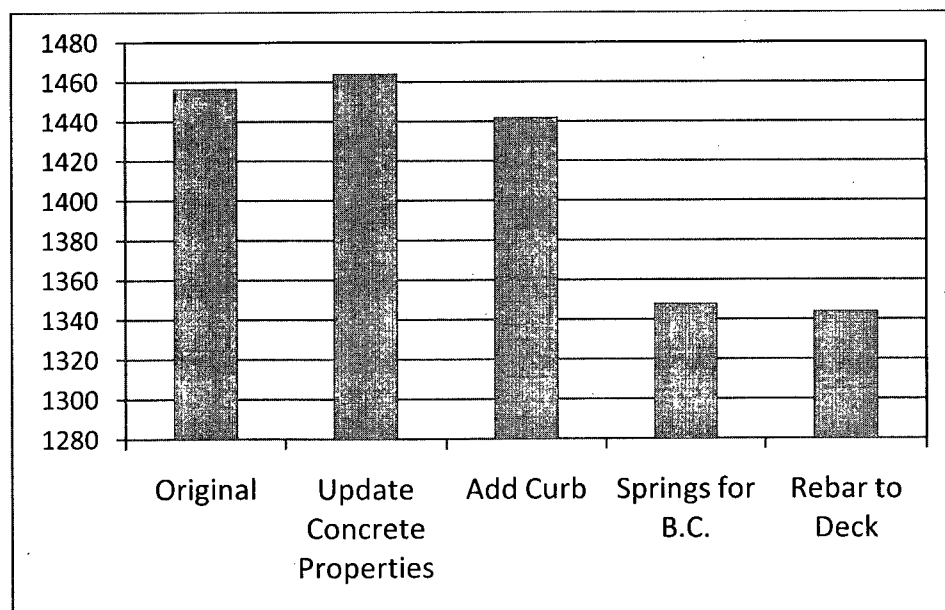


Figure 91. J-value of all measurements

### **6.6.2 Percent Passing Metric**

The second metric for judging the agreement of predicted response with measured response was to consider the percent error of the predicted response from the measured response. The purpose of the test was to determine how well the individual model measurements were performing compared to the collected measurements by attempting to determine what measurements should be considered significant. Model measurements that had less than 10% error from the collected were considered “good” and those with more than 10% were skipped. Additionally, a minimum threshold of the collected measurement was used in order to prevent the “good” count from being dominated by small measurements. This was done because small measurements can add bias to a judge of model agreement. Small measurements can make the model look better in the case where both modeled and measured data read zero because of the distance from the applied load to the location of the measurement. This is sometimes the case when the truck is in the west lane, but the measurement is taken from the east lane. In this case, it is possible to have a near 0% error but the measurement may be insignificant.

Conversely, small measurements can also make the model look worse than it is. A predicted measurement of 2  $\mu\epsilon$  compared to a collected of 1  $\mu\epsilon$  would show a 100% error. If the measurement is an important one, then a difference of 1  $\mu\epsilon$  should not be considered as equally poor as a 100% error on a collected measurement of 50  $\mu\epsilon$ . It was assumed that the bias in either case would offset, and the decision was made to consider minimum collected measurement thresholds of 5, 10, 20, 30 and 40  $\mu\epsilon$  to be included in the percent error evaluation. It is also noted that absolute residuals and measurements were used to eliminate bias due to sign. The final step in the algorithm was to count the residuals that passed the test. Therefore, a larger value shows improvement. Figure 92 summarizes the algorithm for the Percent Passing metric.

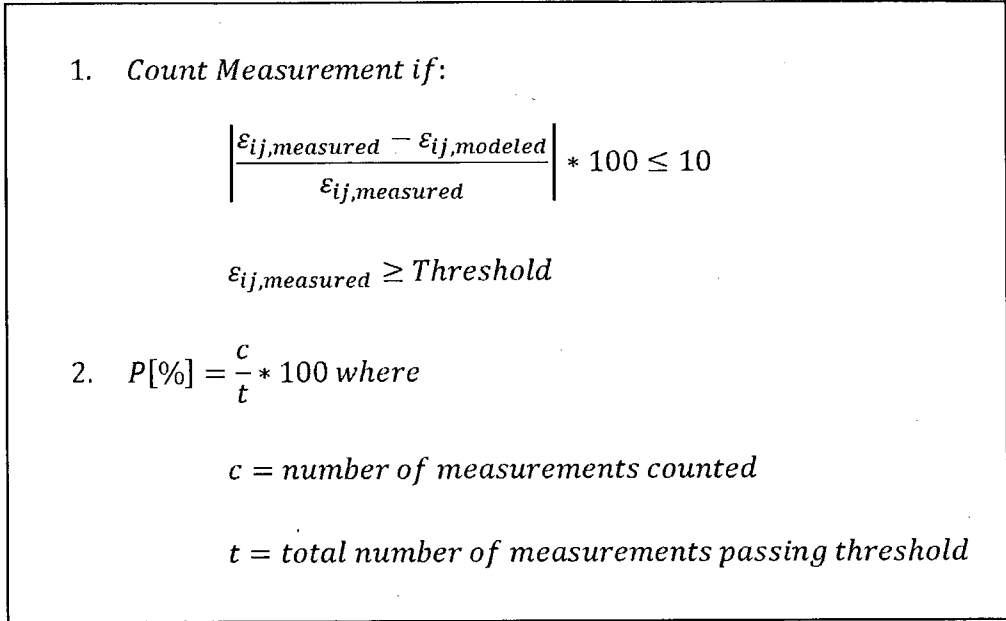


Figure 92. Algorithm for percent passing metric

Figure 93 displays the percentage of measurements greater than the minimum measurement threshold that had residuals with less than 10% error from collected data. The results for 5 different thresholds are displayed for each of the 5 model updates. First it can be seen that only about 35% of measurements greater than 10  $\mu\epsilon$  have an error of less than 10%, but more than 60% of measurements greater than 40  $\mu\epsilon$  have an error less than 10%. Finally, it is clear that the % error metric shows conflicting results to the J values in terms of the model updates. J showed that the addition of springs for boundary conditions improved the model, while % error tests consistently show that the new boundary condition definition worsens the comparison between modeled and collected, regardless of measurement threshold. Despite this update, the final model is improved from the original, which is consistent with the J-value test.

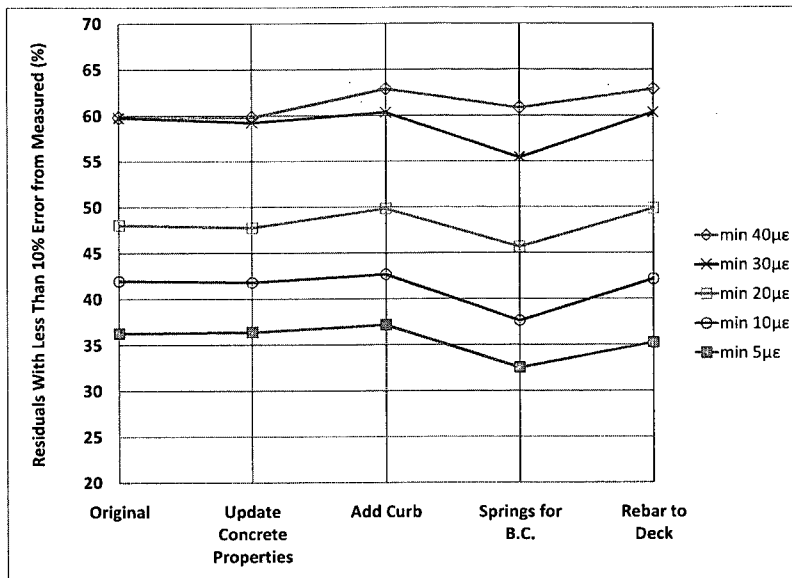


Figure 93. Residuals with less than 10% error from measured for varying minimum measurements

### **6.6.3 Average Residual Metric**

The third metric for model comparison was similar to the % error metric, but instead of normalizing residuals by the magnitude of the measurement, the residuals were normalized by the number of measurements greater than the threshold, as seen in Figure 94. In other words, the metric calculated an average residual for measurements passing the minimum measurement threshold. Again, absolute measurements were used to avoid bias due to signs. This was done in order to get a better feeling for the actual residuals at different magnitudes, regardless of how close the residuals were to the collected measurements. A smaller value in this metric would represent a closer match between measured and modeled data.

Figure 95 shows the results of this metric for the original model and each of the model updates. The average residual greater than 5  $\mu\epsilon$  was about 3.3  $\mu\epsilon$  for the original model and about 3.25  $\mu\epsilon$  for the final model. In the 40  $\mu\epsilon$  threshold test, the average residual improved from 5.25  $\mu\epsilon$  to about 5.1  $\mu\epsilon$ . The average residual metric also showed that the bearing pad update decreased model agreement with the collected data. The fact that both the % passing and average residual metrics show decreased model agreement suggests that J may be biased toward small measurements.

$$\begin{aligned} \text{Avg Residual} &= \left| \frac{\epsilon_{ij,measured} - \epsilon_{ij,modeled}}{n} \right| \\ \epsilon_{ij,measured} &\geq \text{Threshold} \\ n &= \#(\epsilon_{ij,measured}) \text{ passing threshold} \end{aligned}$$

Figure 94. Algorithm for average residual metric



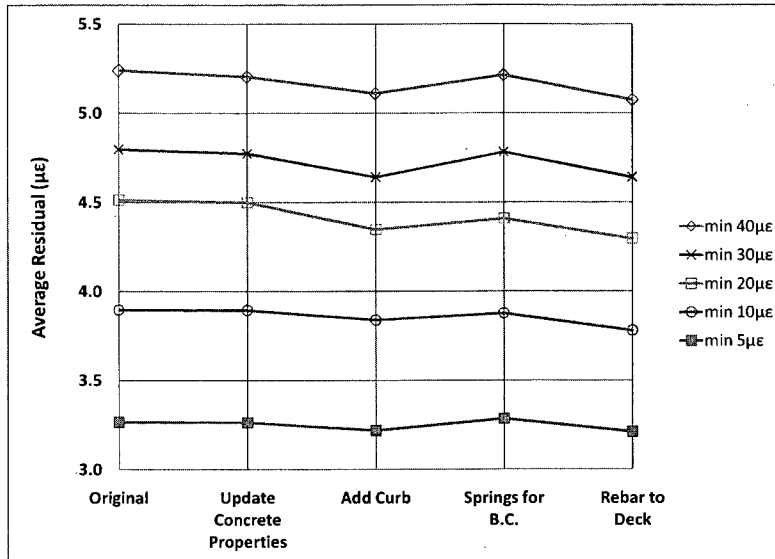


Figure 95. Average Residual for varying minimum measurements

#### **6.6.4 Deflection Comparison**

A final measure of model evaluation was done using measurements of deflection collected using digital image correlation (DIC) by Phil Brogan, a fellow graduate researcher at UNH. Brogan's research was a feasibility study on using highly sensitive digital cameras to record deflections. DIC is used in practice in controlled laboratory settings where the cameras can be placed very close to a small specimen with controlled lighting conditions. The research attempted to use the cameras to measure vertical deflections from a far distance (approximately 50 ft) on large specimens (the web of the Girder 1 or the west exterior girder) under variable ambient lighting. Two sets of cameras were placed on the site. The first set observed vertical deflections on the south

span of girder 1 from a distance of about 5 feet; the second set captured vertical deflections on the center span from about 50 feet away. The camera setup for center span deflection measurements was previously shown in Figure 48, and the setup for the south span is shown in Figure 96.



Figure 96. South Span Camera Setup Location

Deflection measurements are reported directly on the SAP2000® GUI, which made for a quick comparison of modeled to collected data. Since the DIC method of deflection measurement on large civil engineering structures was a feasibility study, the results cannot be weighted as highly as the model comparison with collected strain data. With this consideration, the comparison between camera deflections in Brogan's research and modeled deflections from this research show a good correlation. The comparison also improves with the updated model. Figure 97 to Figure 100 give a snapshot of the comparison between collected vertical deflections using DIC and both the original and final updated model. In the collected data, the "plateaus" of data in the time domain are again visible, evidence of the truck stops.

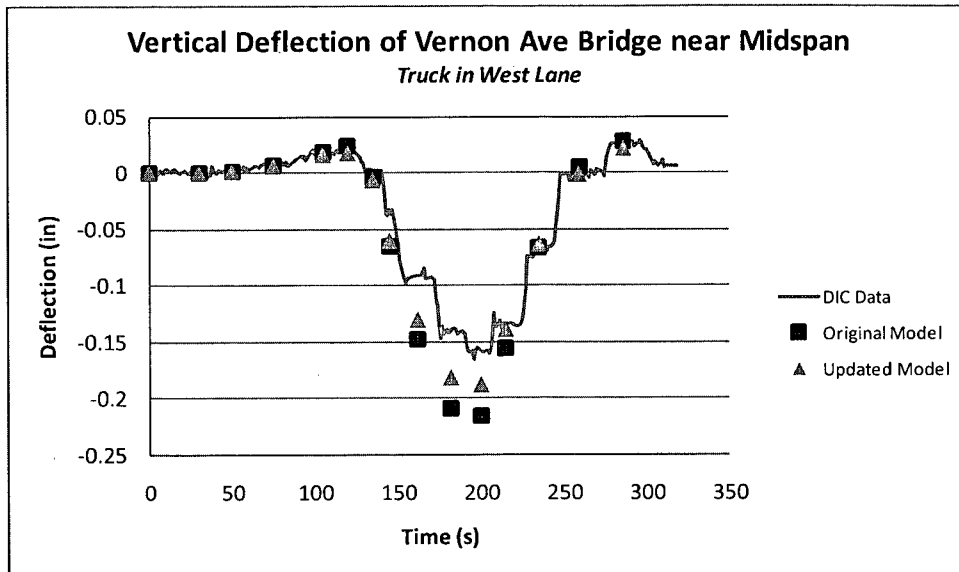


Figure 97. Comparison of Vertical Deflections near midspan of west exterior girder for truck in west lane

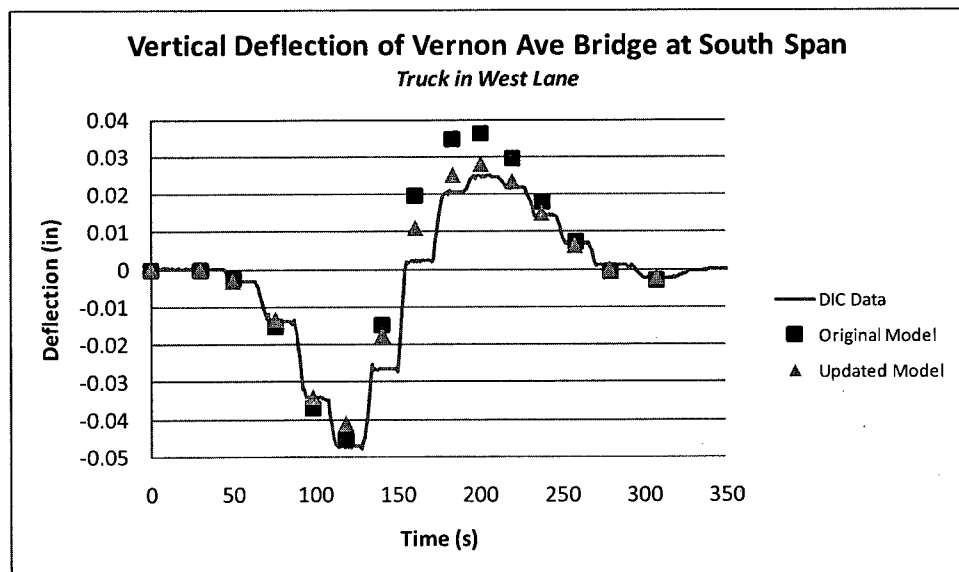


Figure 98. Comparison of Vertical Deflections in south span of west exterior girder for truck in west lane

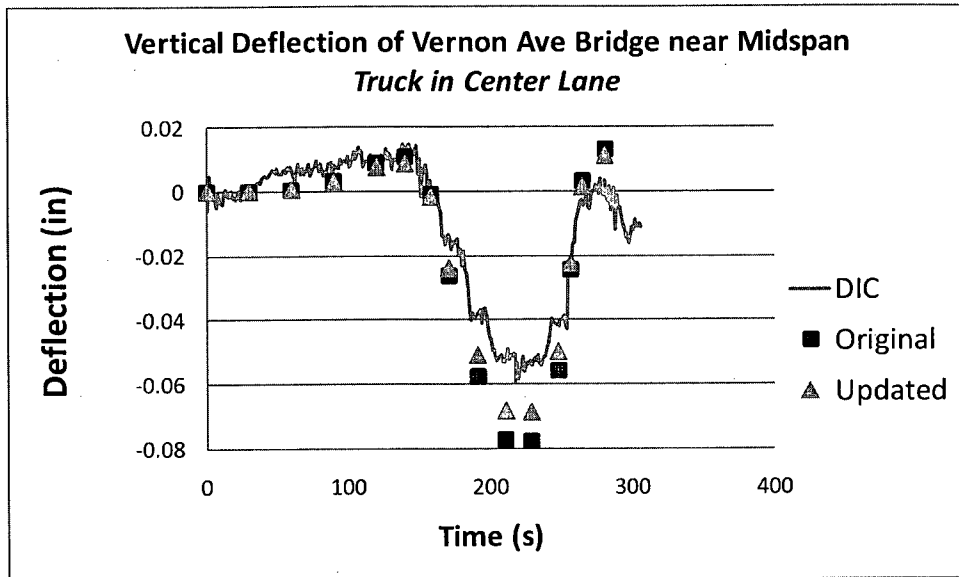


Figure 99. Comparison of Vertical Deflections near midspan of west exterior girder for truck in center lane

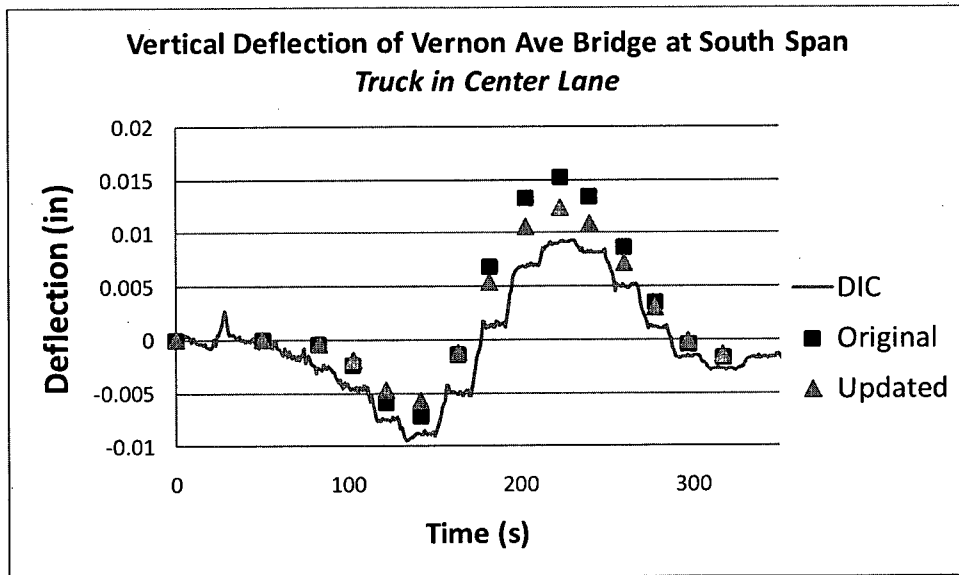


Figure 100. Comparison of Vertical Deflections in south span of west exterior girder for truck in center lane

### 6.6.5 Summary of Baseline Model Evaluation

The baseline EDM was found to correlate well with collected strain and deflection measurements. However quantifying the goodness-of-fit was inconclusive using three separate metrics. Each of the metrics provides some pros and cons. The J-value can

be used in conjunction with other data types, future tests, parameter estimation, model updating, and comparison with other models. It is convenient to define the goodness of fit of a model through one value, but it is difficult to determine what a good value would be, especially with small standard deviations. An even more abstract question would be how good is good enough to claim that the model reasonably represents the response of the bridge. The Percent Passing metric provides information as to the percentage of modeled measurements that are within 10% of collected measurements for given minimum thresholds. The Average Residual metric provides information about the actual difference between modeled and collected measurements beyond the same thresholds. All three metrics provide information about how the model updates have improved the original model, although there is some discrepancy between metrics as to whether the individual updates improved the model, specifically in the case of the boundary condition update. A major problem with the metrics studied is that none of them have the ability to locate problematic areas on the bridge. For example, exterior girders measurements could be far less accurate than measurements on the interior girders. Compartmentalizing areas of the bridge prone to error, or load cases that appear to be problematic is a major component of future work, and is further discussed in Chapter 8.

Although the quantification of model fit was inconclusive, the model was found to reasonably predict bridge behavior. Thus the model can be used as a baseline for further studies, including model updating studies by parameter estimation using MUSTANG and comparison to the FE model of the VAB at Tufts University. In the next chapter, the model will be shown useful for bridge management decision-making such as load rating.

## CHAPTER 7

### BASELINE MODELING FOR BRIDGE MANAGEMENT

After the bridge construction has been completed and the owner accepts the bridge, it begins its life of public service that often lasts more than 50 years (Jaramilla & Huo, 2005). Bridge management decisions are mainly based on visual inspection. Every two years a team of qualified personnel conducts a routine inspection of the bridge for evidence of damage and corrosion. (FHWA-2, 2010).

#### **7.1 Bridge Inspection**

All public bridges must be inspected according to National Bridge Inspection Standards (NBIS) (AASHTO, 2008-C). The NBIS routine bridge inspection practice involves visual inspection of bridge components, field measurement and meticulous documentation of structural member section loss and other damage, and a condition rating. The rating is a number from 0 to 9 where zero is a failed component and nine is a component in excellent condition. The old VAB was inspected twice prior to its replacement in 2009 due to severe corrosion in the deck and girders. A page from the routine inspection report is found in Figure 102. The deck was given a condition rating of 3, or in “serious” condition. The superstructure had a rating of 4 for a “poor” condition. The substructure had a rating of 6 which corresponds to a “satisfactory” condition. For the full definitions of the condition ratings and other coding in the MassDOT inspection report, see Appendix E. The bottom flange of girder #5 was found to have experienced

noticeable section loss, with the remaining thickness recorded as 9/16 in, as seen in Figure 101.

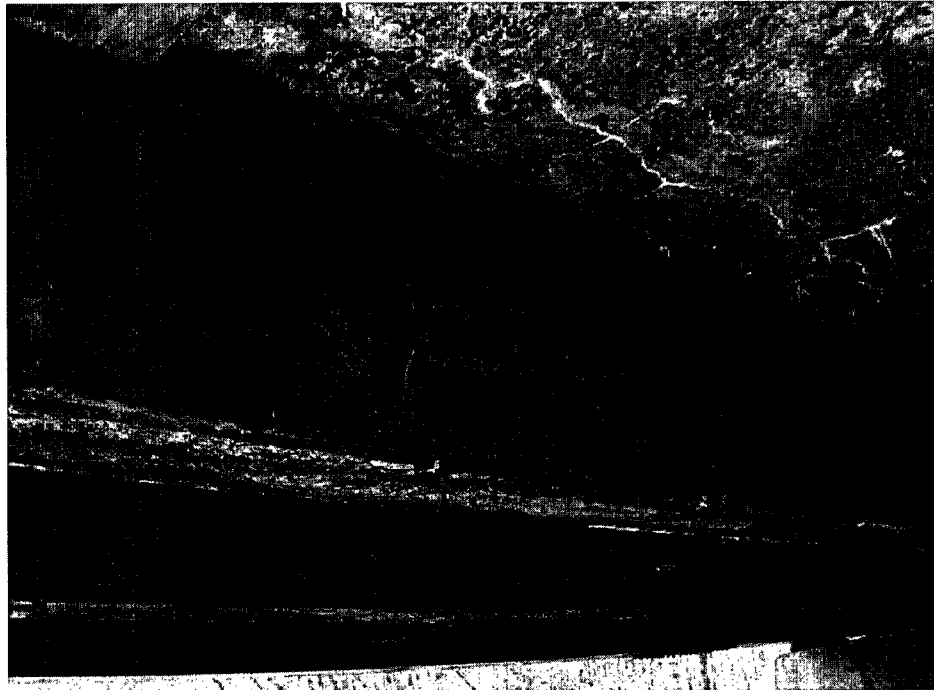


Figure 101. Photo from VAB inspection reporting section loss in beam lower flange(MHD, 2007).

Although bridge inspectors are highly trained, and every attempt is made to obtain objective reports, bridge inspection is still a highly subjective process, and results can be highly irregular. A study into the reliability of bridge inspections showed that visual inspection is the most common form of bridge inspection, bridge inspectors are not required to undergo any vision testing, and professional engineers typically do not conduct the inspections (Phares et al, 2000). In fact, the study showed that for one particular bridge, the superstructure rating ranged from a low of 4, indicating major section loss, to a high of 8, indicating no noticeable problems (Phares et al, 2001). Load ratings are calculated based on the results of inspection condition ratings (AASHTO, 2008-C). Load ratings are a more objective measure of bridge health, but nevertheless are still calculated based on the results of subjective observations.

MASSACHUSETTS HIGHWAY DEPARTMENT

STRUCTURES INSPECTION FIELD REPORT

ROUTINE & SPECIAL MEMBER INSPECTION

2-DIST  
02

B.I.N.  
15H

BR. DEPT. NO.  
B-02-012

CITY/TOWN <b>BARRE</b>		R-STRUCTURE NO. <b>B02012-15H-MUN-NBI</b>		11-KM POINT <b>005.182</b>	41-STATUS <b>A:OPEN</b>	90-ROUTINE INSP DATE <b>JAN 24, 2007</b>
37-FACILITY CARRIED <b>HWY VERNON AVE</b>		MEMORIAL NAME/LOCAL NAME <b>POWDER-MILL BRIDGE</b>		27-YR BUILT <b>1937</b>	106-YR REBUILT <b>0000</b>	YR REHAB'D (NON 106) <b>0000</b>
36-FEATURES INTERSECTED <b>WATER WARE RIVER</b>		26-FUNCTIONAL CLASS <b>Major Collector</b>		DIST. BRIDGE INSPECTION ENGINEER <b>E. R. Henning</b>		
43-STRUCTURE TYPE <b>Steel continuous Stringer/Girder</b>		22-OWNER <b>Town Agency</b>	23-MAINTAINER <b>Town Agency</b>	TEAM LEADER <b>J. A. Mankowsky</b>		
107-DECK TYPE <b>Concrete Cast-in-Place</b>		WEATHER <b>Cloudy</b>	TEMP (air) <b>-6°C</b>	TEAM MEMBERS <b>L. R. LYNCH</b>		

<b>ITEM 53</b>		
<b>DECK</b>	<b>3</b>	<b>DEF</b>
1. Wearing surface	4	S-P
2. Deck Condition	3	S-A
3. Stay in place forms	N	-
4. Curbs	6	M-P
5. Median	N	-
6. Sidewalks	4	S-P
7. Parapets	5	M-P
8. Railing	4	S-P
9. Anti Missile Fence	N	-
10. Drainage System	4	M-P
11. Lighting Standards	N	-
12. Utilities	5	M-P
13. Deck Joints	N	-
14.	N	-
15.	N	-
16.	N	-
CURB REVEAL (In millimeters)		
	N	S
	215	230

<b>APPROACHES</b>		
a. Appr. Pavement Condition	6	M-P
b. Appr. Roadway Settlement	5	M-P
c. Appr. Sidewalk Settlement	N	-
d.	N	-

<b>OVERHEAD SIGNS</b> (Attached to bridge)		
	(Y/N)	N
<b>DEF</b>		
a. Condition of Welds	N	-
b. Condition of Bolts	N	-
c. Condition of Signs	N	-

<b>ITEM 59</b>		
<b>SUPERSTRUCTURE</b>	<b>4</b>	<b>DEF</b>
1. Stringers	N	-
2. Floorbeams	N	-
3. Floor System Bracing	N	-
4. Girders or Beams	4	S-P
5. Trusses - General	N	-
a. Upper Chords	N	-
b. Lower Chords	N	-
c. Web Members	N	-
d. Lateral Bracing	N	-
e. Sway Bracings	N	-
f. Portals	N	-
g. End Posts	N	-
6. Pin & Hangers	N	-
7. Conn Plt's, Gussets & Angles	5	M-P
8. Cover Plates	N	-
9. Bearing Devices	4	S-P
10. Diaphragms/Cross Frames	4	S-P
11. Rivets & Bolts	5	S-P
12. Welds	N	-
13. Member Alignment	5	-
14. Paint/Coating	3	S-P
15.	N	-
Year Painted <b>X</b>		

COLLISION DAMAGE: Please explain  
None (X) Minor ( ) Moderate ( ) Severe ( )

LOAD DEFLECTION: Please explain  
None (X) Minor ( ) Moderate ( ) Severe ( )

LOAD VIBRATION: Please explain  
None ( ) Minor ( ) Moderate (X) Severe ( )

Any Fracture Critical Member: (Y/N) **N**

Any Cracks: (Y/N) **N**

<b>ITEM 60</b>		
<b>SUBSTRUCTURE</b>	<b>6</b>	<b>DEF</b>
<b>1. Abutments</b>		
a. Pedestals	N	N
b. Bridge Seats	N	7
c. Backwalls	N	6
d. Breastwalls	N	6
e. Wingwalls	N	7
f. Slope Paving/Rip-Rap	N	N
g. Pointing	N	N
h. Footings	N	H
i. Piles	N	H
j. Scour	N	N
k. Settlement	N	7
l. Erosion	N	5
m.	N	N
<b>2. Piers or Bents</b>		
a. Pedestals	N	N
b. Caps	N	6
c. Columns	7	7
d. Stems/Webs/Pierwalls	N	N
e. Pointing	N	N
f. Footing	H	H
g. Piles	X	X
h. Scour	6	H
i. Settlement	8	7
j.	N	N
k.	N	N
<b>3. Pile Bents</b>		
a. Pile Caps	N	N
b. Piles	N	N
c. Diagonal Bracing	N	N
d. Horizontal Bracing	N	N
e. Fasteners	N	N

UNDERMINING (Y/N) IF YES please explain **N**

COLLISION DAMAGE: None (X) Minor ( ) Moderate ( ) Severe ( )

SCOUR: Please explain  
None (X) Minor ( ) Moderate ( ) Severe ( )

A60 (Dive Report): **6** A60 (TNS Report): **6**

93B-UW (DIVE) Insp **08/10/2005**

X=UNKNOWN N=NOT APPLICABLE H=HIDDEN/INACCESSIBLE R=REMOVED

08/01/06

Figure 102. Sample page from MassHighway routine inspection of the former VAB



## 7.2 Load Rating

The accuracy of a bridge inspection report dictates the allocation of funding for repairs, and it is therefore important for the report to be conservative in its ratings of the bridge under load rating and overload permitting. The measured section loss in an inspection report is also used to update live load rating factors (RF). A live load RF is a ratio of a bridge's live load capacity to a worst case scenario load condition. The 2008 AASHTO Manual for Bridge Evaluation defines two types of ratings:

*Inventory Level RF: "Rating at the design level of reliability for new bridges in the AASHTO LRFD Design Specifications, but which reflects the existing bridge and material conditions with regard to deterioration and loss of section."*

*Operating Level RF: "Maximum load level to which a structure may be subjected."(AASHTO, 2008-C)*

The calculation of the load rating using the Load and Resistance Factor Rating (LRFR) method of the 2008 AASHTO Manual for Bridge Evaluation is given by Equation 1.

Equation 1. Formula for Bridge Structural Element Load Rating Factor (AASHTO, 2008-C)

$$RF_{LRFR} = \frac{C - \gamma_{DC}DC - \gamma_{DW}DW - \gamma_P P}{\gamma_{LL}LL(1 + IM)}$$

In this equation, RF is the rating factor of a structural element; C is its capacity in terms of a given force effect; DC is the effect of dead load structural components of the element; DW is the effect of dead load wearing surfaces and utilities; P is the effect of other permanent or superimposed dead loads; LL is the effect of a worst-case live load condition. IM and each of the  $\gamma$ -factors are the dynamic load allowance and LRFD load

factors, respectively, according to AASHTO LRFD bridge design specifications (AASHTO, 2008-C). The calculation of Inventory and Operating RF's differ only in the value of the live load factor,  $\gamma_{LL}$ .

In the example that follows, an Inventory rating will be calculated for the new VAB for bending moment under the Strength I limit state as defined by the 2008 LRFD bridge design specifications. Therefore, the load factors also correspond to moment under Strength I, as summarized in Table 15. The Inventory rating will also be extracted from the response of the EDM under the same live load conditions. In order to make a direct comparison between the RF's, the dead load components included in all calculations are limited to the components included in the model, as described below. Therefore, there the DW and P components in Equation 1 are zero.

Three different versions of the Inventory rating will be determined for both the LRFR hand calculations and the EDM. First, an Inventory rating will be calculated for the bridge assuming that a bridge inspection has reported new conditions for all components. A second rating will be calculated based on a fictitious field inspection reporting a 10mm section loss to the thickness of the bottom flange of an exterior girder. The third rating will use the same section loss assumption, but for an interior girder.

It is important to note that in current bridge management practice, load ratings are calculated for each structural member—an elemental approach, just like the design process—and does not consider system wide behavior. Although the baseline structural model may not enhance the accuracy of the bridge inspection process, it can provide insight into the capacity of a bridge in terms of a RF by inputting the structural deficiency noted in the inspection into the structural model.

### **7.2.1 Inventory Load Rating Using LRFR Method**

To determine the feasibility of using the model for load rating purposes, the bridge load rating was first calculated using traditional design protocol as specified in the

2008 AASHTO LRFD Bridge Design Specifications. The calculated loads and moments that follow can be seen in detail in Appendix F. The first step in this process was to determine the capacity of each of the girders. Since the geometry of the exterior girder-slab system differed from that of the interior, two capacities were calculated. The capacity of the element as a composite section was calculated at its plastic moment,  $C = M_p$ , using the strain compatibility method. The capacities for both interior and exterior girders can be seen in Table 15. These capacities are used for the calculation of load rating factors in both the LRFR and the EDM rating.

**Table 15. LRFD load factors and plastic moment capacities of interior and exterior girders used in the calculation of all Inventory rating factors.**

<b>Girder Type</b>	<b>Dead Load Factor, <math>\gamma_{DC}</math></b>	<b>Live Load Factor for Inventory Rating, <math>\gamma_{LL}</math></b>	<b>Dynamic Impact Factor, (1+IM)</b>	<b>Plastic Moment Capacity, <math>M_p</math> (kN-m)</b>
Exterior	1.25	1.75	1.33	7414
Interior	1.25	1.75	1.33	6150

After the capacities were calculated, the applied loads were back calculated to obtain the maximum applied moment on the bridge, starting with dead loads. A number of assumptions are built in to these calculations. First, it was necessary to calculate only those dead loads that were included in the EDM. The structural components that were included in the model include the steel girders and diaphragms, the concrete haunch, deck, and safety curb. A number of other components that exist on the actual bridge but are not in the EDM were not included in the dead load calculation, such as the steel railing, the concrete sidewalk, the water pipe that runs between girders 4 and 5 (however, its bracing was included), and the asphalt wearing surface. It is worth noting that adding the weight of these components would increase the dead load moment and thus lower the rating factor, but they were necessarily neglected in order to make a useful comparison between design calculations and the EDM.

The common design assumption is that dead load distributes itself evenly across the girders, and therefore all components can be summed and divided by the number of girders. The dead load was shared by six girders in the south and center spans, and by eight in the north span. The additional dead load of the fascia girders and expanding deck was taken into account, but when the increased load is divided by eight girders instead of six, the resulting load per girder is the same. When multiplied by the dead load factor  $\gamma_{DC} = 1.25$ , the dead load per girder is  $w_u = 18 \text{ kN/m}$  (1230 plf).

After dead loads were calculated, the live loads in the form of a traffic lane load and design truck load could be determined. LRFD Bridge design uses distribution factors to determine the distribution of live load to individual girders. The factors take into account, span length, bridge width, girder spacing, and the depth and relative stiffness of the girders and deck (AASHTO, 2008-B). The distribution factors also differentiate between interior and exterior girders, and the loading of 1 lane of traffic versus multiple lanes. Therefore, four different distribution factors are calculated: two for the interior girders and two for the exterior girders, as shown in Table 16. The code dictates that the maximum distribution factor for each girder type be used in the live load analysis. Therefore, a distribution factor of 0.676 was used for exterior girders and 0.587 was used for interior girders.

Table 16. Live load distribution factors for moment for interior and exterior girders (AASHTO, 2008-B).

Girder type	One Lane Loaded	Two or More Lanes Loaded	Maximum
Interior	0.425	0.587	0.587
Exterior	0.676	0.502	0.676

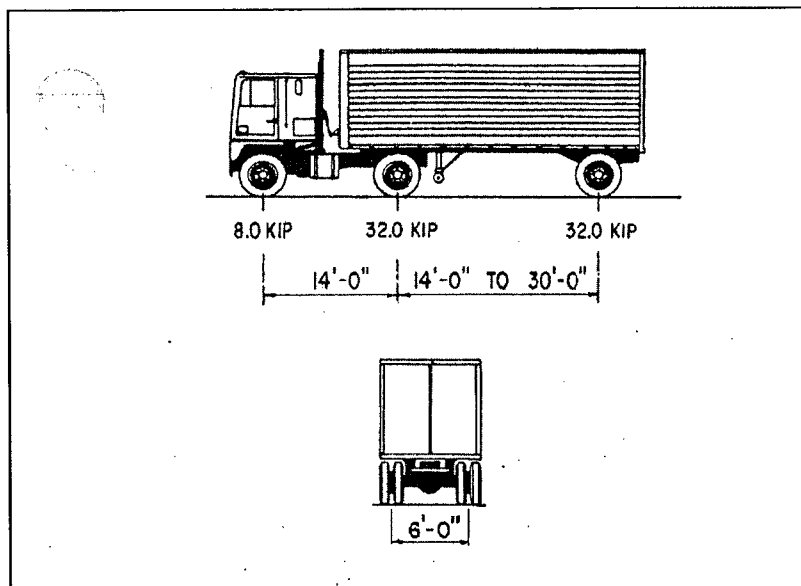


Figure 103. Design Truck (AASHTO, 2008-B)

The live loads to be applied are given in the 2008 AASHTO LRFD bridge design specifications as follows: The live load due to traffic as  $3.06 \text{ kN/m}^2$  (64 psf) over a 3.05 m wide (10 ft) lane, or  $9.352 \text{ kN/m}$  (640 plf). The design truck load is a 3 axle truck with a  $35.6 \text{ kN}$  (8 kip) front axle and two  $142.5 \text{ kN}$  (32 kip) rear axles, as shown in Figure 103. The truck wheels are spaced at 1.83 m (6 ft) laterally. The front axle spacing is fixed at 4.27 m (14 ft) and the rear axle spacing is variable between 4.27 m and 9.14 m (30 ft) to obtain maximum force effects. The loads are multiplied by the load factor of  $\gamma_{LL} = 1.75$ , a dynamic impact factor of 1.33 (1+IM), and the appropriate distribution factor. The resulting factored live loads are summarized in Table 17.

Table 17. Summary of live loads applied to LRFR calculations and EDM for rating factor calculation

	LRFR Factored Live Loads, Interior Girder	LRFR Factored Live Loads, Exterior Girder	EDM Factored Live Loads
Dead	18 kN/m	18 kN/m	N/A
Lane	9.602 kN/m	11.070 kN/m	$5.37 \text{ kN/m}^2$
Truck Front Axle	48.66 kN	56.10 kN	82.93 kN
Truck Rear Axle	194.63 kN	224.38 kN	331.72 kN

The last step is to apply the loads. The dead load must be applied uniformly across the entire girder length. The live loads are patterned for maximum force effect. Using influence lines for bending moment, it was determined that the worst case bending moment occurs at the midpoint of the center span with the lane load applied across the length of the center span and the center axle of the truck at the midpoint of the center span. The smallest axle spacing resulted in the greatest force effects. The influence line is shown in Figure 104. The moments at this location for both the interior and exterior girders are given in Table 18, along with the resulting rating factors at the Inventory level. It can be seen that both the exterior and interior girders are appropriately and safely over designed for bending moment at the strength limit state, with the exterior girders having just over four times the design live load capacity and the interior girders having just under four times capacity.

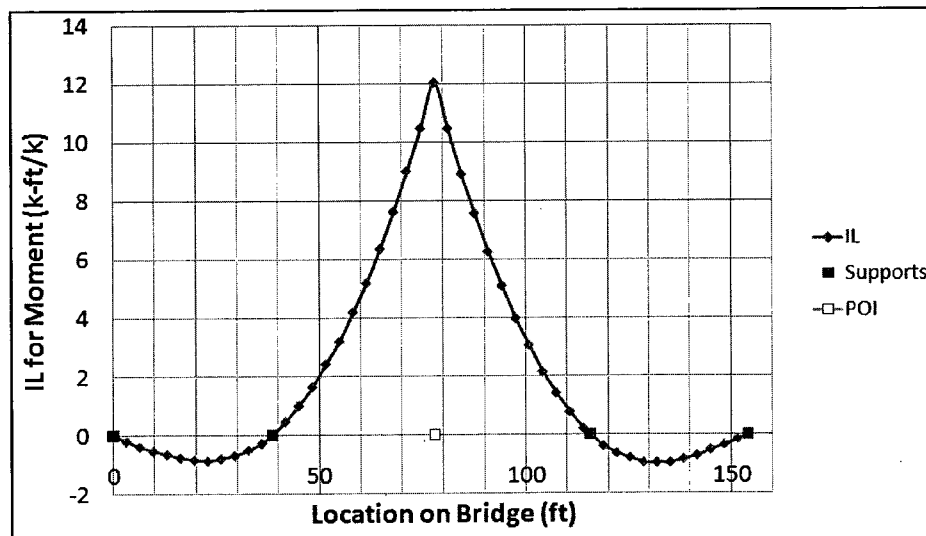


Figure 104. Influence Line for moment at the midpoint of the center span.

Table 18. Moments at the midpoint of the center span due to DL and patterned LL

Girder Type	Moment due to DL (kN-m)	Moment due to LL (kN-m)	Rating Factor,
Exterior	544	1660	4.14
Interior	544	1440	3.89

### **7.2.2 Load Rating Using Baseline EDM**

To verify that the EDM could be used as a tool for load rating, it was necessary to verify that the response of each girder in the model was comparable to that obtained in the LRFR version. Therefore, it was necessary to fully understand the assumptions of the design code and apply an equivalent loading condition. In the structural model, the lane widths, the truck axle and wheel spacings, the unfactored lane load and truck axle loads, and the LRFD load factors are all equivalent to that in the LRFR version. A summary of the following loading conditions is found in Table 17. The self weight of the bridge scaled by  $\gamma_{DC} = 1.25$  was used as a dead load instead of a calculated, assumed dead load. The bridge width inside the curbs is 11.725 m (38.5 ft) and dictates that there are three 10 ft traffic lanes to be loaded. Therefore, three trucks were applied to the bridge, using wheel loads instead of axle loads and without the distribution factor from the factored load calculation. Without a distribution factor, there was no explicit distinction between interior and exterior girder loads in the model, as seen in Table 17. Instead, the distribution was accomplished by the structural behavior in the model. Lengthwise, the trucks were placed with their center axle at the midpoint of the center span. Widthwise, the three trucks were placed within the three lanes. Following LRFD design specifications (2008), the exterior wheels of a truck over the exterior lane shall be placed one foot from the face of the curb. The middle lane was centered along the bridge layout line.

Equation 2. Rating factor equation for EDM Load Rating

$$RF_{Model} = \frac{C - DL_{Model}}{LL_{Model}(1 + IM)}$$

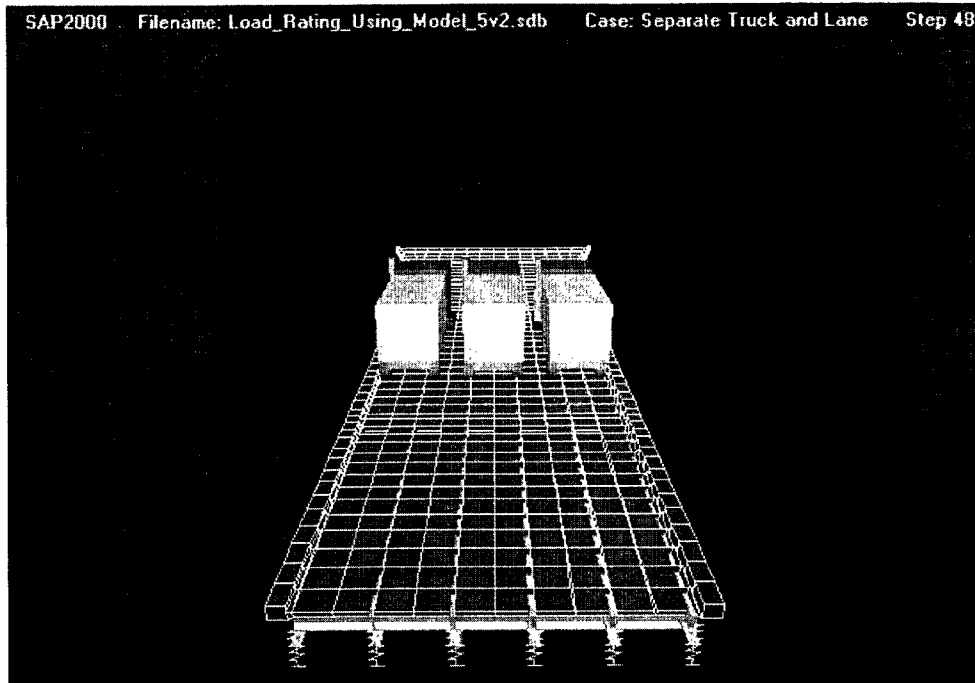


Figure 105. Depiction of truck location for worst-case loading condition at the midpoint of the center span.

The most significant assumptions made in the loading of the bridge were associated with the lane loading. It was necessary to pattern the lane load to only the center span, but due to SAP2000® programming limitations this could not be accomplished within the three design lanes because the widthwise mesh of the bridge is rather coarse, with only 2 elements per span. Therefore, a conservative lane load was applied such that the entire width of the bridge center span minus the safety curbs, as shown in Figure 106, was loaded with a factored traffic load of  $5.37 \text{ kN/m}^2$  (112 psf).



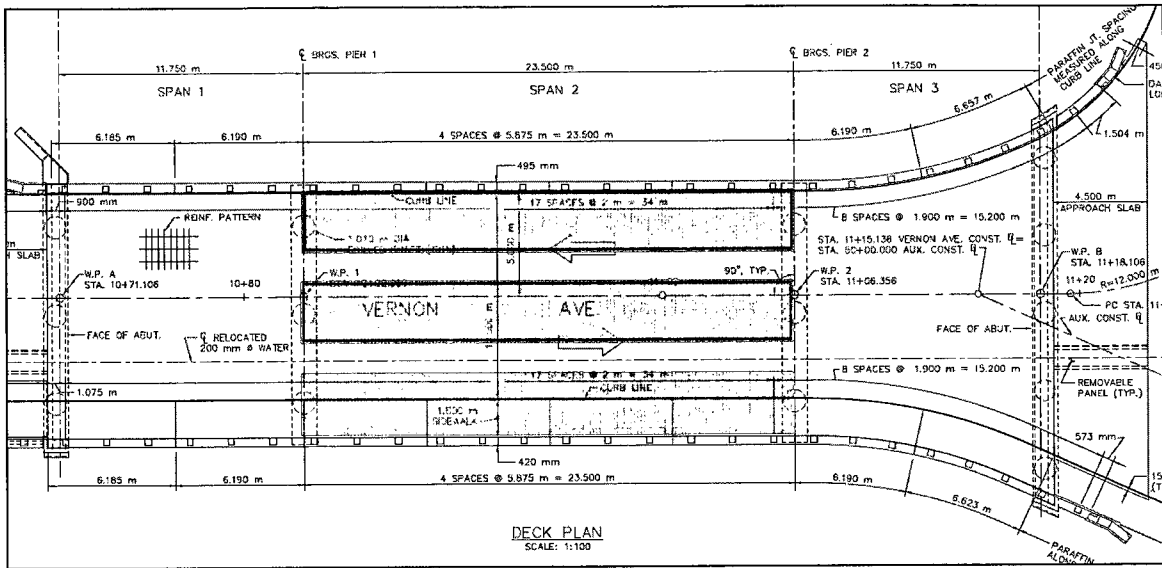


Figure 106. Location for lane loading for maximum force effects according to LRFD design specifications are shaded in black. The EDM lane loading conservatively included the area between the lanes.

As a method of verification that the same loads were being applied in both the LRFR and EDM methods, the total moments due to live load and dead load for all six girders were added and compared to the sum of the design analysis. The total moments for both dead and live loads are reasonably close, as seen in Table 19. One reason for the underestimation of live load when compared to the design calculations is a function of the FE method of analysis used within SAP to approximately distribute point loads applied in the interior of a shell element to the nodes on the shell's corners. The moment response may therefore be reduced at the midspan but accounted for at another location. One possible reason for the overestimation of the dead load response could actually be due to approximation of dead load in the varying deck section of the north span design calculations as previously discussed.

Table 19. Comparison of Total moments at midpoint of center span using both rating methods

	EDM Response	LRFD Design Calculations	% Difference
Total Dead Load Moment (kN-m)	3377	3264	3.46
Total Live Load Moment (kN-m)	8164	9080	-10.09

The resulting moments at the center span from both dead and live load for each of the six girders is found in Table 20. The loadings are nearly symmetrical across the width of the bridge, with girder pairs 1 and 6, 2 and 5, and 3 and 4 each reporting nearly identical responses from both dead and live load applications. The ratings were also found to be close to the LRFR ratings, as seen in Figure 107. The model gives a greater rating than the LRFR method for all girders. On a girder-by-girder basis, the model ratings are also much closer to each other than in the LRFR ratings. The more evenly distributed ratings can be attributed to the system behavior that is accounted for in the model. For example, the deck overhang on the VAB is a relatively small one at 732.5 mm (28.84 in) and the effective overhang is even less at only 237.5 mm (9.35 in). The effective overhang is the deck overhang from the CL of girder to the face of curb (AASHTO, 2008). A small effective overhang corresponds to an exterior girder that is not required to carry much of its own load. In other words, the loading at the curb face is more evenly shared by both the exterior girder and the first interior girder and thus the girder live load response is smaller.

**Table 20. EDM moments and rating factors for each girder**

<b>Girder</b>	<b>Moment due to Dead Load (kN-m)</b>	<b>Moment due to Live Load (kN-m)</b>	<b>Model Rating Factor</b>
1	710	1580	4.24
2	474	1211	4.69
3	499	1291	4.38
4	499	1291	4.38
5	484	1211	4.68
6	710	1579	4.24

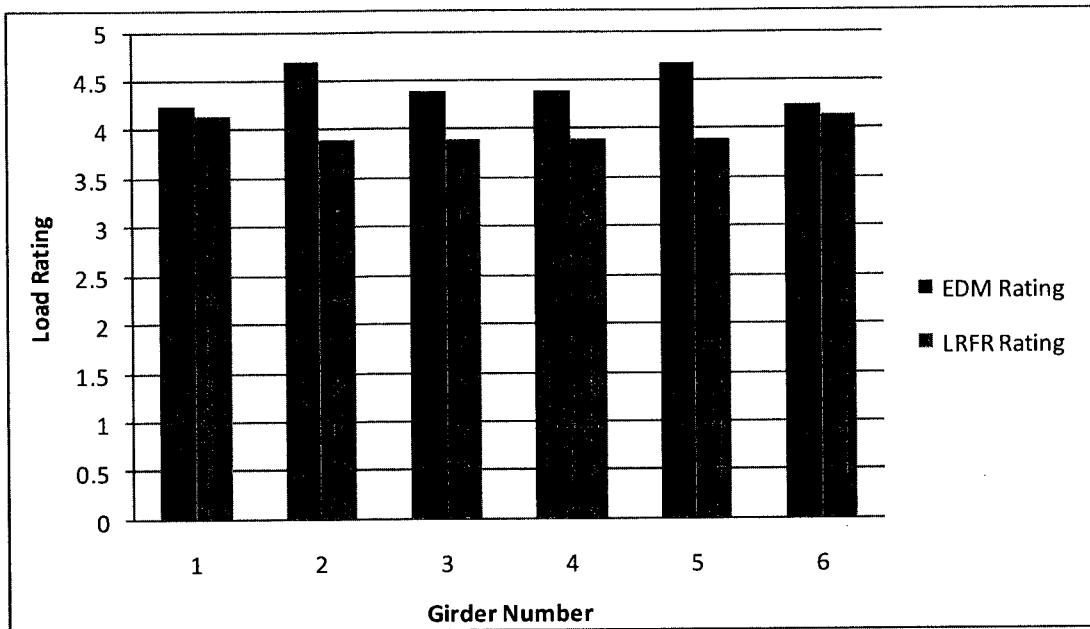


Figure 107. Comparison of LRFR and EDM inventory rating factors for girders 1 to 6

It is important to reiterate that this is a feasibility study to determine if code-based rating factors can be reproduced using the model, and that rating factors obtained here are higher than those that would be obtained by field inspection because not all dead load components were included in the model or the calculations. The live load would also be adjusted to include a sidewalk pedestrian load, further lowering the rating.

Since the load ratings predicted by the EDM reasonably predict the design calculated load ratings, the feasibility study was taken one step further by investigating whether the model can predict an updated load rating if a future field inspection reveals section loss in one of the girders.

### **7.2.3 Load Rating Comparison Considering Girder Section Loss**

To consider if the model can predict LRFR ratings for a girder with a reduced section loss, two fictional inspection reports are considered. The first reports severe deterioration of the bottom flange of girder 1 at the midpoint of the center span has resulted in a section loss of 10mm in the bottom flange thickness. The second case

considered the same loss of section on girder 3. The reduced capacity of the cases was calculated in the same manner as in the original study, but with a bottom flange thickness of 29.878 mm (1.18 in) for the exterior girder and 15.9 mm (0.626 in) for the interior girder. It is worth noting that a 10 mm section loss in the interior girder is equivalent to nearly 40% of its original thickness. The resulting changes in capacity and LRFR rating factors can be seen in Table 21. The exterior girder saw a 10% loss of rating factor to 3.72, and the interior case saw a 17% loss of rating factor to 3.21.

**Table 21. Changes in capacity and LRFR load rating due to 10 mm loss thickness of bottom flange at the midspan**

<b>Girder Type</b>	<b>Original Capacity (kN-m)</b>	<b>Reduced Capacity (kN-m)</b>	<b>% Change in Capacity</b>	<b>Original LRFR Rating Factor</b>	<b>Updated LRFR Rating Factor</b>	<b>% Change in Rating Factor</b>
Exterior	7414	6713	9.46%	4.138	3.72	-10.20%
Interior	6150	5168	15.97%	3.893	3.21	-17.52%

In the EDM, the only capacity that was modified was that of the damaged girder. Just as in the original calculations, the design capacities in Table 21 were used for model rating factor calculation. Two frame sections were “damaged” in the model, one on either side of the center span midpoint, by reducing the thickness of the bottom flange by 10 mm. The resulting changes in load factors for both tests are found in Table 22. It can be seen from both cases that the damaged girder undergoes a significant loss in rating, while the rating factor changes to the undamaged girders are negligible.

Table 22. Changes in EDM load rating due to 10 mm loss of thickness in bottom flange of a girder at the midpoint of the center span

	<b>Girder Num</b>	<b>Original Model Rating Factor</b>	<b>Updated Model Rating Factor</b>	<b>% Change in Rating Factor</b>
<b>Damaged Exterior Girder</b>	1 (damaged)	4.243	3.95	-6.86%
	2	4.687	4.71	0.49%
	3	4.376	4.445	1.58%
	4	4.376	4.452	1.74%
	5	4.679	4.761	1.75%
	6	4.244	4.339	2.24%
	<b>Girder Num</b>	<b>Original Model Rating Factor</b>	<b>Updated Model Rating Factor</b>	<b>% Change in Rating Factor</b>
<b>Damaged Interior Girder</b>	1	4.243	4.32	1.77%
	2	4.687	4.69	0.00%
	3 (damaged)	4.376	3.89	-11.11%
	4	4.376	4.391	0.34%
	5	4.679	4.743	1.37%
	6	4.244	4.332	2.07%

Figure 108 and Figure 109 show comparisons of updated RF's for both the damaged exterior girder and the damaged interior girder. The reduction in RF's for the damaged girders in the EDM are only about 65% of the design reductions. This can be attributed to the benefits of system behavior: although the damaged girder loses capacity and stiffness, the forces are redistributed to the other girders. Using the EDM to calculate the reduction in RF will also show how the damage in one girder affects the response in adjacent girders.

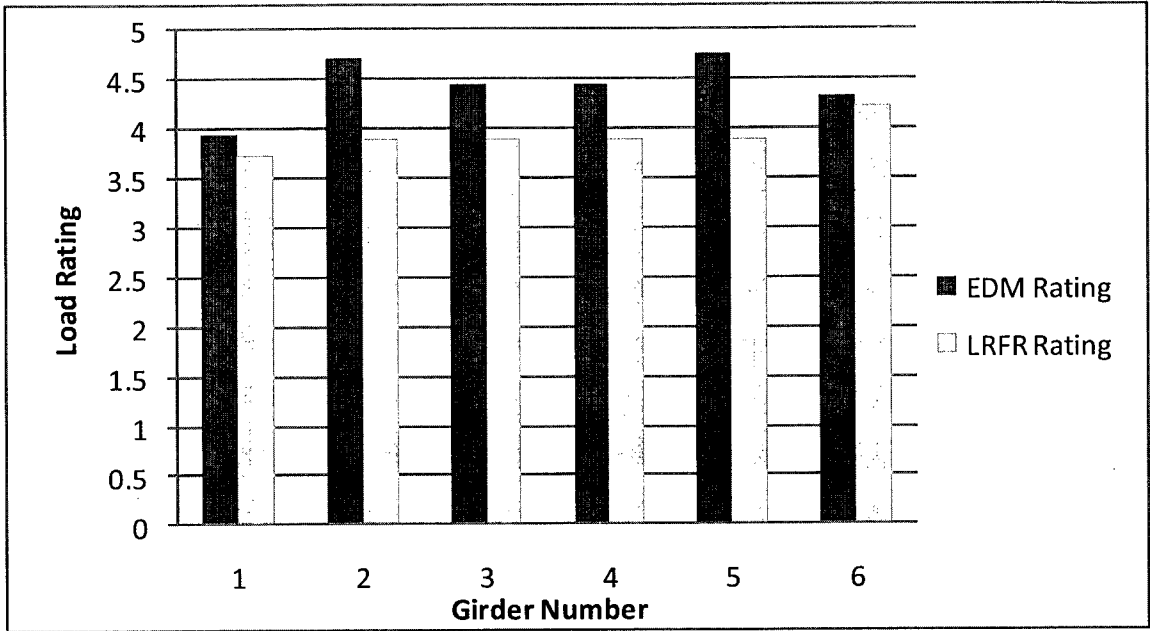


Figure 108. Comparison of EDM and LRFR Inventory ratings for a damaged EXTERIOR Girder (Girder 1)

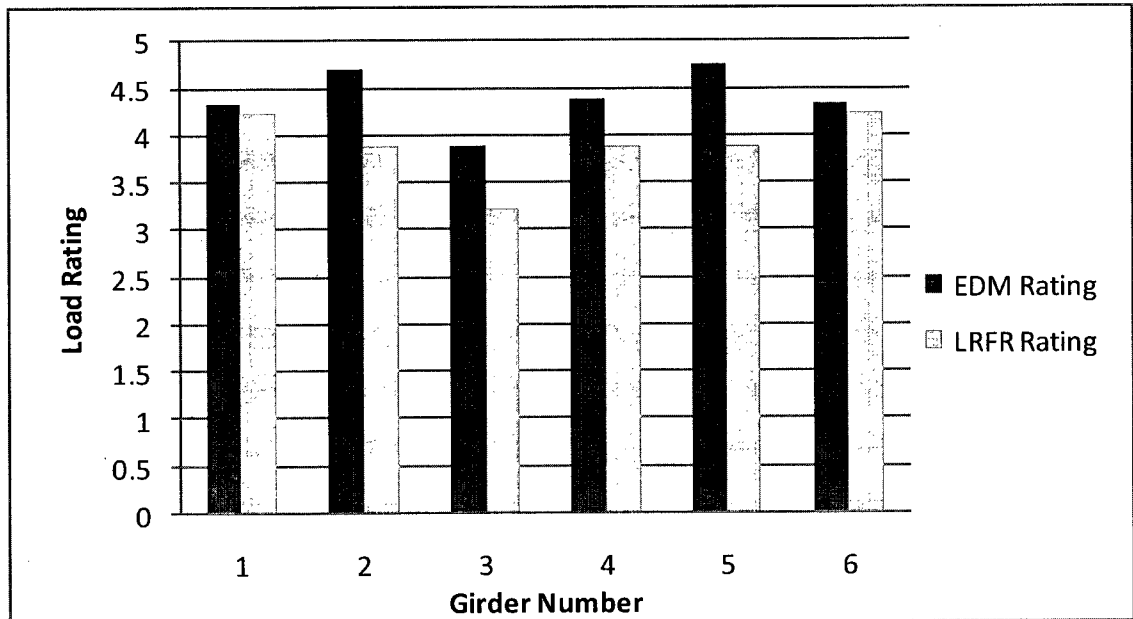


Figure 109. Comparison of EDM and LRFR Inventory Ratings for a damaged INTERIOR Girder (Girder 3)

### 7.3 Results of Baseline EDM usage for Bridge Management

The case study into usage of the baseline model for load rating showed that the model can be used to effectively calculate a baseline load rating for a new bridge.

Further investigation showed that structural member section losses reported in bridge inspections may be effectively applied to the model for updating of load rating factors. It was also evident that the LRFR elemental calculation of load ratings for damaged structural members is more conservative than that obtained from the damaged model, probably because of the added benefit of system behavior in the model. In either case, member capacities must still be calculated using traditional design assumptions.

As was noted in the field inspection report of the old VAB, spalling of concrete can be a problem on some aging bridges, and thus investigation of whether the model can be used for load rating of the deck should be considered in future work.

## CHAPTER 8

### CONCLUSIONS

The VAB is the case study bridge for a NSF-PFI funded research project entitled “Whatever Happened to Long-term Bridge Design.” The overarching goal of the project was to enhance bridge design and management through long-term SHM. The goals of this research project were to design an instrumentation plan for a long-term SHM system, verify design of the bridge during construction, create a baseline structural model of the bridge, collect non-destructive test data prior to bridge commission to obtain a baseline response, refine the baseline model using field observations during construction, and use the refined model for bridge management. A final goal of the NSF-PFI program was to facilitate partnerships between academia, industry, and government agencies while conducting innovative research activities. The research contained herein was successful in its attempts at these goals, each of which is outlined in the following subchapters. The major individual contributions to the civil engineering industry are as follows:

1. A structural baseline model of the VAB was created and verified using collected field data during construction. A study was conducted on different metrics for evaluation of the model’s goodness of fit to NDT data. The study concluded that the metrics did not provide an in depth assessment of model-



to-NDT correlation, and that a true evaluation should be conducted piecemeal with regard to sensor location and load place.

2. The calibrated model can be used for long term performance evaluation. Load ratings were calculated using force output from the calibrated EDM and compared to ratings calculated using the LRFR method as specified by the AASHTO 2010 Manual for Bridge Evaluation. The EDM ratings were found to give higher ratings due to the fact that the model accounts for system behavior that the LRFR ratings do not consider.
3. Bridge performance was verified during construction through a study of the neutral axis location using NDT strain data. The result of this verification was that the bridge was performing as a composite girder-deck system. The investigation of changes to the neutral axis may be used as a metric for structural condition assessment.

### **8.1 Development and Deployment of Instrumentation Plan**

An array of 200 sensors including strain gauges, accelerometers, tiltmeters, temperature sensors, and pressure cells were installed on the VAB during construction for use in a long-term SHM system. Although the majority of instrumentation was completed prior to bridge opening, the strain gauge data was the main focus of the research efforts presented here. The strain gauges were installed at the steel fabrication facility prior to steel erection for ease of access and to avoid interference with construction. One hundred strain gauges were installed at five stations along the length of the bridge on all six girders. At each station, strain gauges were installed on both the underside of the top flange and the top side of the bottom flange. On interior girders, the strain gauge pair was installed on both sides on the web.

In addition to the strain gauges, thirty-six girder temperature sensors were installed at select strain gauge locations to account for thermal effects in long term strain measurements. Thirty concrete temperature sensors were installed above most girder temperature sensors to capture a full temperature gradient across the girder-deck composite section. Sixteen accelerometers were installed at four stations across the bridge to capture dynamic behavior. Sixteen tiltmeters were installed at locations of expected maximum rotation in the superstructure and also at the piers and abutments to determine relative rotation of the superstructure with respect to the abutments. Pressure cells were installed on the south approach span for weigh-in-motion capabilities and as a trigger for remote activation of the DAQ system.

The data acquisition system is a fleet of iSite dataloggers constructed and configured by Geocomp with a permanent power supply, internet connection, and computer. The system can be accessed and sampling rates manipulated via the internet for remote monitoring capabilities. The system records continuously at a rate of 0.0033 Hz (1 sample every 5 minutes), but is capable of sampling at high speed rates in excess of 200 Hz (200 samples per second). Collected data is periodically uploaded to iSite Central, and web-based structural monitoring and management system supported and hosted by Geocomp Corp.

Prior to bridge opening, a non-destructive load test was conducted in order to capture baseline bridge performance, verify design, and calibrate a baseline structural model. A 72 kip, three-axle dump truck was run across the bridge in three lanes. The NDT included a set of static load tests consisting of the truck stopping at 15 distinct locations in each lane for a total of 45 distinct static load cases. Additionally, rolling truck tests and dynamic impact tests were conducted in all three lanes. High speed sampling of strain was conducted using the DAQ system during the course of the static load tests. The results of QA/QC procedures found the strain sensors produced a high quality

signal that could be used for baseline structural model calibration and design verification studies.

## **8.2 Design Verification**

The location of the neutral axis for the composite girder-deck bridge section was chosen as a metric to verify design. The neutral axis was calculated for each of the 50 top-and-bottom strain gauge pairs installed on the girders of the bridge using static excitation from the non-destructive load test. The method of calculation assumed a linear distribution of strain across the composite section. Therefore a point of zero strain could be extrapolated from the two strain gauge measurements, which corresponds to the neutral axis for a section in bending. The method of neutral axis determination was found to be sensitive to loadings in which strain in the top and bottom gauges were approximately equal and when bending moment was not the primary force effect felt by the gauges. Therefore only load cases with the truck in the center span were used for neutral axis extraction. Neutral axis values were analyzed for repeatability and reliability, and were determined acceptable for use in model strain calculation and for verification of design criteria. The bridge was found to act compositely, although some measurements suggest errors in the assumption of the bridge cross section and some suggest a nearly full composite section.

## **8.3 Baseline Structural Modeling**

A baseline structural model was created using the bridge modeler within SAP2000®. The model was created for use as a baseline of bridge condition in long-term SHM and parameter estimation studies. The model consists of frame elements for the steel girders and shell elements for the deck. The frame and shell elements are connected using joint constraints, which allow transfer of load from the deck through the girders and into the bearings, and also give the bridge model the performance of a

composite structure. Four manual updates were made to the original model to complete the creation of a baseline structural model. The updates were made in order of the increasing degree of uncertainty in their definition and method of application, not necessarily to improve correlation with collected data. The four updates performed were as follows:

1. Update material properties of the concrete deck using laboratory test data and concrete mix design data.
2. Install a safety curb along the edge of the bridge in order to improve the accuracy of the bridge cross section.
3. Update boundary conditions using bearing pad laboratory test data and empirical formulas of the stiffness of steel reinforced elastomeric bearing pads.
4. Add steel reinforcement to the concrete deck by changing homogeneous shell elements into layered shell elements.

A linear elastic analysis of 45 static load cases was performed on the model corresponding to the 45 distinct truck stops conducted during the static load test portion of the NDT. Axial strain measurements were extracted from model forces at locations of strain gauges stations using a combination of elementary structural mechanics and collected neutral axis measurements.

The results of the model updates compared to collected strain measurements were evaluated using three distinct model verification metrics, and also evaluated with respect to experimentally collected deflection measurements. Each metric showed that the final model was an improvement from the original model. For measurements greater than  $10 \mu\epsilon$ , the average residual was less than  $4 \mu\epsilon$ . 60% of measurements greater than  $30 \mu\epsilon$  had less than 10% error from field measurements. The boundary condition update provided the most controversy, because one metric showed that the updated boundary conditions improved the model agreement with field data and the other two metrics

showed the opposite. In conclusion, further updates to the model should be considered, as discussed in the future work section of this chapter, but the model shows good agreement with the collected data, and can function as a baseline structural model of the VAB. Future work should be done into metrics for judgment of goodness-of-fit, including a simulated study to verify expected fitness.

One final metric for model verification compared the results of deflections from DIC with both the original model and final model deflections. The DIC data was processed by a fellow researcher at UNH who was studying the feasibility of using DIC for large civil engineering structures. The results of the comparison show good correlation of the original model deflections with DIC measurements, and improved correlation of the updated model deflections. It is worth noting that the experimental deflection measurements were not verified using industry accepted methods such as dial gauges or LVDT's, and thus the comparison of the models to strain data is a more dependable metric for model verification.

#### **8.4 Modeling for Bridge Management**

The typical bridge inspection process involves a visual inspection of structural members for evidence of corrosion and damage. Measured section loss is recorded and used to calculate reduced capacities based on typical elemental design assumptions. Two load ratings are produced that give the ratio of live load capacity to live load applied. The first is the inventory rating which corresponds to a load that can safely use the bridge for an indefinite period of time; the other is the operating rating corresponds to the maximum load the bridge can safely carry. A case study was conducted on the baseline EDM to determine how the model response correlated with the LRFR bridge load rating equation in the 2008 AASHTO Manual for Bridge Evaluation.

The study showed that the baseline EDM can be used to effectively calculate a baseline load rating for a new bridge. Further investigation demonstrated that structural member section losses reported in bridge inspections may be effectively applied to the model for updating of load rating factors. It was also evident that the LRFR elemental calculation of load ratings for damaged structural members is more conservative than that obtained from the damaged model, probably because of the added benefit of system behavior in the model. In either case, member capacities must still be calculated using traditional design assumptions.

### **8.5 Facilitation of Industry Partnerships**

In the course of two years, partnerships were built between industry, academia, and government agencies. MassDOT, the town of Barre, ET&L construction, Atlantic Bridge and Engineering, and Fay, Spofford, and Thorndike Inc. were all witnesses that a bridge can be heavily instrumented during construction without causing delays in the construction process. The most necessary component of success was communication between all involved parties.

### **8.6 Recommendations for Future Work**

During the course of this research, many doors were opened, but the time did not allow for a thorough investigation of what lies behind them. This section aims to guide future research efforts using the lessons and findings contained in this report among others. Two areas of future work are considered here: Recommendations for instrumentation and DAQ and recommendations for model creation, updating and verification protocol.

### **8.6.1 Instrumentation and Data Acquisition**

The first tasks for future work should be to examine the remaining data sets collected during construction, including the load test. High speed data was collected over the course of the day during the concrete pour. Following the end of the construction day, data was continuously collected at 0.2 Hz until the day of the load test. This is a unique dataset that could provide information on the change of the bridge from a non-composite structural system into a composite one. This can also provide an ideal time to study long term thermal effects, concrete heat of hydration, and locked-in construction stresses. Finally, this would provide an opportunity to link temperature and strain data post-processing for removal of strain due to temperature loading in long-term SHM studies. Figure 110 shows the web-based interface of iSite Central displaying SG21 over the course of 1 day. Although the axes are difficult to read, the shape of the graph suggests that a major component of strain collected over time is due to thermal effects.

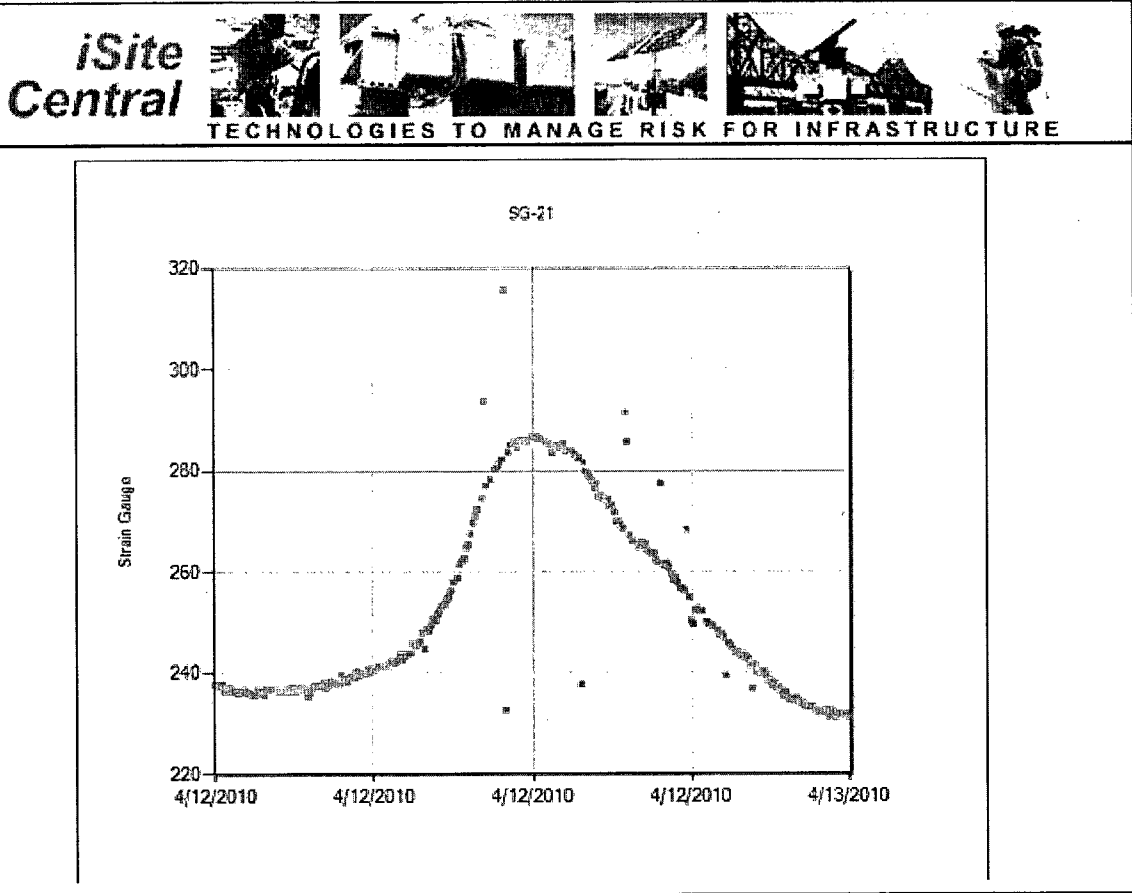


Figure 110. Strain in the bottom flange of Girder 2 at the midspan (SG21) from 4/12/2010 to 4/13/2010 showing large changes in amplitude from the ambient pattern suggesting possible heavy truck loads.

In addition to the concrete pour dataset, tiltmeter, accelerometer, temperature, and pressure cell data sets still need to be analyzed for reliability, repeatability, and other QA/QC protocol. Then, the additional datasets can be applied to the model for further calibration of the baseline model.

One of the more exciting datasets to investigate will be that of the pressure cells during the load test for calibration of lane loads to pressure cells and bridge instrumentation. As previously discussed, it is possible to expand the calibration into the development of a trigger mechanism to activate DAQ. As of now, the DAQ collects data 24 hours per day, 7 days per week, but it might not have to. The pressure cells could sensing a large load about to cross the bridge could activate the DAQ to record a



“meaningful” measurement of a heavily loaded dump truck instead. Lack of any such reading could tell the DAQ to dump the data for the day.

Finally, one of the previous goals of this research was to collect strain measurements prior to steel erection in a zero stress condition, after steel erection, and after formwork installation. The collection of these datasets was not successful for many reasons, but it should be a priority to future instrumentation projects to find a way to complete these goals. For example, the girders were instrumented while still on the ground at the fabrication yard. If a dataloggers were available at this time, they could have been used to capture a baseline strain reading of the girders in very close to an unstressed state. Another one of the major failures in this research was the attempt of using multiple dataloggers (P3500 strain indicators and iSite dataloggers) and trying to back-calibrate baseline readings from just after steel erection. (It was the only option at the time, and unfortunately a calibration between P3500 and iSite readings could not be made).

The application of the load test plan on Sept 3 was successful, but documentation protocol should be addressed. In future load tests, photos of each truck stop and videos of each rolling test should be diligently recorded from an appropriately visible position. The rental of a man lift for the day would be well worth the money. The video and photo would be helpful not only for presentation, interpretation, and communication of load cases, but also to assist in QA/QC of load cases, outliers in the data, and time of test documentation.

In terms of the instrumentation placement, there should be an evaluation of what sensors are truly necessary for long-term SHM. There are 200 sensors installed on the bridge. Even with instrumentation becoming more affordable, this was still a very expensive venture. It is necessary to determine which sensors can be eliminated from future bridge instrumentations projects. This research has found that having strain

gauge pairs on top and bottom flanges is very useful and it is recommended that this concept of instrumentation be continued. It does not seem it is necessary to install gauges on both sides of the flange. On the other hand, the multiple strain readings provided a way to validate to quality of individual readings. With only one gauge at each location, one would need to assume rather than be able to validate strain measurements.

One of the difficulties in post-processing of the collected data came from the fact that the data was captured from a fleet of dataloggers. A major portion of post-processing time was due to aligning of the resulting data sets from each datalogger and further management of the processed data. For example, the data was sampled at “about” 200 Hz during the load test. Not all dataloggers could be initiated at exactly the same time, nor stopped at exactly the same time. The result was a series of data sets that may or may not have the same number of samples, nor have matching starting and ending time stamps. This may prove a particularly difficult problem for processing of dynamic measurements. One possible solution to this problem is to use only one datalogger for the entire system. The University of New Hampshire owns a datalogger manufactured by National Instruments (NI SCXI-1001 datalogger) that is capable of managing the entire VAB instrumentation system. The NI datalogger was not used on the VAB in part due to the partnership with Geocomp, but is worth considering for future instrumentation projects.

### **8.6.2 Modeling**

The results of the modeling chapter mentioned many aspects of the structural modeling protocol that can be studied for further research. The first issue is a matter of the post processing of strain. Although the main components of axial strain in the girders comes from strong axis bending moment and axial force, it is possible that inclusion of weak axis bending forces may provide additional correlation to in-situ

behavior. The inclusion of torsional forces may also help improve the model, but post-processing of strain caused by torsion in a non-symmetrical section may be problematic and not worth the added effort.

The increased meshing of concrete deck shell elements may provide additional accuracy, and studies into the cost-to-benefit ratio of the added time and effort of the highly detailed mesh should be conducted. In this research it was of primary importance to show a model could be constructed in a relatively quick fashion by a designer, but the increasing mesh in the longitudinal direction may improve the disbursement of forces across the bridge.

Additional manual adjustments of the model may be attempted. A few examples of this are the following:

An element by element improvement of concrete deck shell layer definition may prove useful. In the model, all shell elements received the same level of reinforcement. The design plans show that in areas of maximum deck tension, i.e. above the piers longitudinally and above the girders laterally, the longitudinal reinforcement nearly doubles. The plans also show that reinforcement between girders at any location across the bridge is less than above the girders. The level of refinement in layer definition could be made on an element by element basis.

Furthermore, it may be worth investigating a non-linear analysis of the bridge behavior. Figure 111 displays an optional stress-strain curve in the material definition for the behavior of concrete in compression and in tension. This was initially investigated as a model update, but the load patterns and load cases that had been previously defined were for a linear-elastic analysis, and thus switching to a non-linear elastic analysis would not have been consistent with the current results and analysis methodology.

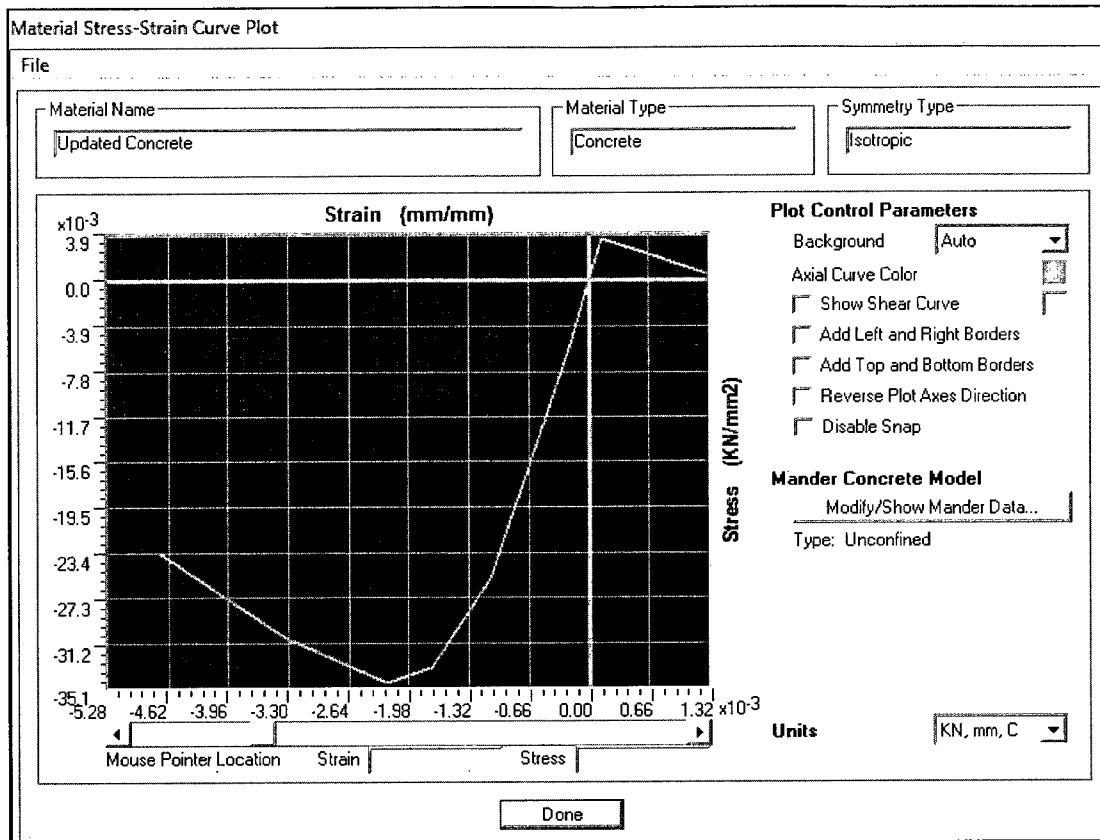


Figure 111. SAP has an option of nonlinear material behavior definition for concrete (SAP2000® v14.1)

Some other updates that are of interest to the potential improvement to the model are inclusion of the field splice connection in the steel girders, the added stiffness of the integral concrete end diaphragms, the added rotational stiffness provided by the anchor bolts at the piers, the effect on performance caused by the water pipe that passes between girders 4 and 5, and the effect on deck stiffness supplied by the asphalt wearing surface, the steel tube safety railing, and the concrete sidewalk. The sidewalk was a candidate for one of the updates in this research, but was abandoned due to the fact that significant refinement of the shell element mesh in the north span deck widening would have been necessary.

As it was determined that the boundary condition update provided the most controversy in terms of the update evaluation metrics, it would be preferable to conduct

in-house laboratory testing on the as-built pads. To add an additional pad to the quantity for the purpose of testing is not a very expensive venture, but would provide enhanced capabilities in the determination of pad stiffness characteristics. An alternative to obtaining a pad would be to request determination of Poisson's ratio during required lab testing, since this was the number that severely affected the values in the bearing pad spring stiffness calculation.

Finally, one of the main conclusions of this research was that an objective measure of model fitness was not obtained and a further study of alternative metrics should be conducted. It may be necessary to determine the performance of the model piecemeal. In other words, it would be interesting to see if error in the model was concentrated at specific locations across the bridge. For example, how does the model perform in negative moment regions versus positive moment regions, or on interior girders versus exterior girders, or finally top flange measurements versus bottom flange measurements?

### **8.1 Summary**

The research conducted herein on the VAB showed that a bridge can be instrumented during construction without causing significant interference to the construction process. It also showed that access to steel prior to erection can be very valuable in obtaining the goal of non-interference.

Recommendations for future work include the further enhancement of the structural model, development of an objective metric for model verification, and development of a long-term SHM protocol for data management and remote activation of the DAQ system using the installed pressure cell installation.

## REFERENCES

- AASHTO. (2008-A). *Bridging the Gap-Restoring and Rebuilding the nation's Bridges*. Washington DC: American Association of State Highway and Transportation Officials.
- AASHTO. (2008-B). *LRFD Bridge Design Specifications*. Washington: AASHTO.
- AASHTO. (2003). *Manual for Condition Evaluation of Bridges*. Washington: American Association of State Highway and Transportation Officials.
- AASHTO. (2008-C). *Manual for Bridge Evaluation*. Washington: AASHTO.
- American Concrete Institute. (2008). *Building code requirements for Structural concrete (ACI 318-08)*. Farmington Hills: ACI.
- Andringa, M., Neikirk, D., Dickerson, N., & Wood, S. (2005). Unpowered Wireless Corrosion Sensor for Steel Reinforced Concrete. *IEEE Sensors* , 155-158.
- ASCE. (2009). *Report Card for America's Infrastructure*. Reston, VA: American Society of Civil Engineers.
- Baker, M. (2003). *Development of a Comprehensive Design Example for a Steel Girder Bridge with Commentary*. Washington DC: Federal Highway Administration/National Highway Institute.
- Brenner, B., Bell, E., Sanayei, M., Pfeifer, E., & Durack, W. (2010). Structural Modeling, Instrumentation, and Load Testing of the Tobin Memorial Bridge in Boston, Massachusetts. *Structures Congress* (pp. 729-740). Orlando: ASCE.
- Brenner, B., Sanayei, M., Santini-Bell, E., & Abriola, L. (2007). *Whatever happened to Long Term Bridge Design*.
- Brogan, P. (2010). *Thesis*. Durham: University of New Hampshire.
- Chajes, M., Mertz, D., & Commander, B. (1997). Experimental Load Rating of a Posted Bridge. *Journal of Bridge Engineering* , 1-9.
- DS Brown. (2008). *Elastomeric Bearing Pad Shop Drawing*. North Baltimore: DS Brown.
- Eisenberg, M. (1980). *Introduction to the Mechanics of Solids*. reading: Addison-Wesley.

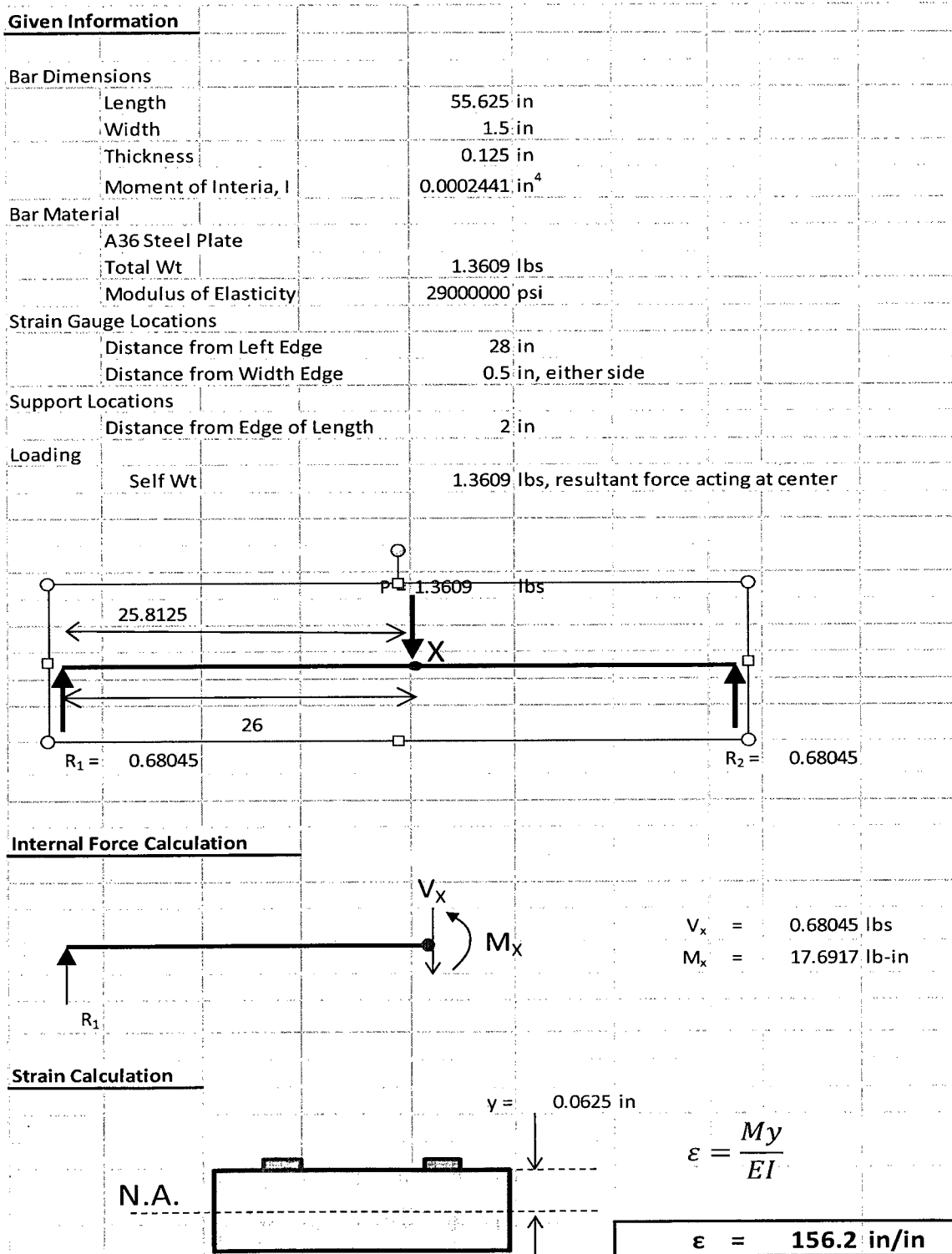
- Federal Highway Administration. (2009, December). *FHWA Bridge Programs NBI Data*. Retrieved March 25, 2010, from <http://www.fhwa.dot.gov/bridge>
- Feng, M. Q., Doo, K. K., Jin-Hak, Y., & Yangbo, C. (2004). Baseline Models for Bridge Performance Monitoring. *Journal of Engineering Mechanics* , 562-569.
- FHWA. (2010). *American Recovery and Reinvestment Act of 2009*. Retrieved March 26, 2010, from United States Department of Transportation - Federal Highway Administration: <http://www.fhwa.dot.gov/economicrecovery/index.htm>
- FHWA. (2010). *Traffic Volume Trends*. Washington D.C.: FHWA.
- FHWA-2. (2010, 5 21). *Questions and Answers on the National Bridge Inspection Standards*. Retrieved from <http://www.fhwa.dot.gov/bridge/nbis/index.htm>
- FST. (2007). *Bridge Replacement #B-02-012 Vernon Avenue over the Ware River*. Boston: Massachusetts Highway Department.
- Fu, G., Feng, J., & Dekelbab, W. (2008). *NCHRP Report 495. Effect of Truck Weight on Bridge Network Costs*. Washington: Transportation Research Board.
- Ghasemi, H. (2009, January). FHWA Long-Term Bridge Performance Program--A flagship initiative. Washington, D.C., USA.
- Howell, D. A., & Shenton, H. W. (2006). System for In-Service Strain Monitoring of Ordinary Bridges. *Journal of Bridge Engineering* , 673-680.
- ISHMII. (2010, March 31). *International Society for Structural Health Monitoring of Intelligent Infrastructure* . Retrieved March 31, 2010, from Definitions: <http://www.ishmii.org/Literature/SHMGlossaryDefinitions.html#S>
- Jaramilla, B., & Huo, S. (2005). *Public Roads: Looking to Load and Resistance Factor Rating*. Washington: FHWA.
- Kim, D.-H. (2008). A fiber-optic tiltmeter system based on the moire-fringe effect. *Measurement Science and technology* , 1-6.
- Liu, C., DeWolf, J., & Kim, J.-H. (2009). Development of a baseline for structural health monitoring for a curved post-tensioned concrete box girder bridge. *Engineering Structures* , 3107-3115.
- Liu, C., Olund, J., Cardini, A., D'Attilio, P., Feldblum, E., & DeWolf, J. (2008). Structural health Monitoring of Bridges in the State of Connecticut. *Earthquake Engineering and Engineering Vibration* , 427-437.
- MHD. (2007). *Structures Inspection Field Report for Powder Mill Bridge*. Boston: Massachusetts Highway Department.
- Navidi, W. (2008). *Statistics for Engineers and Scientists 2nd ed*. New York: McGraw-Hill.

- NYSDOT. (2007). *Reliability Study of the NYS Bridge Inspection Program (C-07-17)*. Albany: NYSDOT Engineering Division, Office of Structures.
- Pagano, M., & Gauvreau, K. (2000). *Principles of Biostatistics 2nd ed.* Pacific Grove: Duxbury.
- Phares, B. M., Rolander, D. D., Graybeal, B. A., & Washer, G. A. (2001). *Reliability of Visual Bridge Inspection*. McLean: Turner-Fairbank Highway Research Center.
- Phares, B. M., Rolander, D. D., Graybeal, B. A., & Washer, G. A. (2000). *Studying the Reliability of Bridge Inspection*. McLean: Turner-Fairbank Highway Research Center.
- Phelps, J. (2010). *Instrumentation, nondestructive testing, and finite element model updating for bridge evaluation*. Medford: Tufts University.
- Ren, W.-X., Peng, X.-L., & Lin, Y.-Q. (2005). Experimental and analytical studies on dynamic characteristics of a large span cable-stayed bridge. *Engineering Structures*, 535-548.
- Sanayei, M., & Saletnik, M. (1996). Parameter estimation of structures from static strain measurements. I: Formulation. *Journal of Structural Engineering*, 555-562.
- Sanayei, M., Imbaro, G., McClain, J., & Brown, L. (1997). Structural model updating using experimental static measurements. *Journal of Structural Engineering*, 792-798.
- Schlune, H., Plos, M., & Gylltoft, K. (2009). Improved bridge evaluation through finite element model updating using static and dynamic measurements. *Engineering Structures*, 1477-1485.
- Sipple, J. (2008). *Structural Modeling and Monitoring of the Rollins Road Bridge for Condition Assessment*. Durham: University of New Hampshire.
- Stanton, J., Roeder, C., & Mackenzie-Helwein, P. (2004). *NCHRP 12-68 Rotational Limits for Elastomeric Bearings Appendix F*. Seattle: Transportation Research Board.
- TRIP. (2010). *Key Facts about America's Surface Transportation System and Federal Funding*. Washington: TRIP.
- Wang, M. L. (2008). Long term Health Monitoring of Post-Tensioning Box Girder Bridges. *International Journal of Smart Structures and Systems*, 711-726.
- Wiberg, J. (2006). *SAMCO Final Report - The New Arsta Railway Bridge - Sweden*. Structural Assessment Monitoring and Control.
- Yazdani, N., Eddy, S., & Cai, C. (2000). Effect of Bearing Pads on Precast Prestressed Concrete bridges. *Journal of Bridge Engineering*, 224-232.
- Zhang, Z., & Aktan, A. E. (1997). Different Levels of Modeling for the Purpose of Bridge Evaluation. *Applied Acoustics*, 189-204.



## APPENDICES

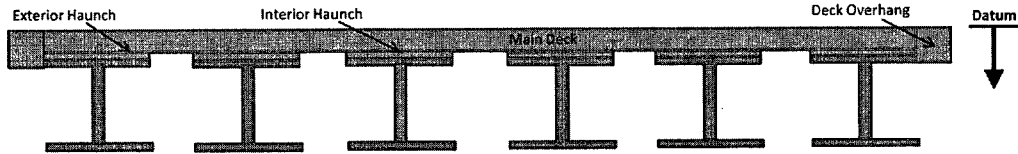
## APPENDIX A: CALCULATION OF STRAIN IN STRAIN GAUGE CALIBRATION



## APPENDIX B: CALCULATION OF VAB COMPOSITE SECTION PROPERTIES

### Full Bridge: Calculation of Section Properties

Ec	3604.9965 ksi	=	24.8556 kN/mm <sup>2</sup>
Es	29000 ksi	=	199.9480 kN/mm <sup>2</sup>
n=Es/Ec	8.044		
Length of Bridge Section 1	38187 mm		
Length of Bridge Section 2	8813 mm		
<b>Interior Girder Properties</b>			
tf	25.9 mm		
bf	305 mm		
Depth	914 mm		
I	4.06E+09 mm <sup>4</sup>		
A	30300 mm <sup>2</sup>		
<b>Exterior Girder Properties</b>			
tf	39.878 mm		
bf	307.34 mm		
Depth	942.34 mm		
I	6.24E+09 mm <sup>4</sup>		
A	43935.4 mm <sup>2</sup>		
<b>North Span Fascia Girder Properties</b>			
tf	20.1 mm		
bf	305 mm		
Depth	904 mm		
I	3.25E+09 mm <sup>4</sup>		
A	25600 mm <sup>2</sup>		
<b>Concrete Typical Properties</b>			
t_deck	200 mm		
t_haunch, Interior	53.978 mm		
t_haunch, Exterior	40 mm		
t_haunch, Fascia	59.778 mm		
<b>Concrete Section 1 Properties</b>			
Deck Width1	12715 mm		
Overhang1 to Girder CL	732.5 mm		
Overhang1 Width	578.83 mm		
<b>Concrete Section 2 Properties</b>			
Deck Width2	16860.66 mm		
Overhang2 to Girder CL	426.33 mm		
Overhang2 Width	273.83 mm		



### Calculation of Deck Section Properties (Datum at T.O. Section, Section transformed to steel)

*Deck Section 1*	Spans 1 and 2 have 6 girders					
	A	y	Ay	d	Ad <sup>2</sup>	I <sub>o</sub>
	mm <sup>2</sup>	mm	mm <sup>3</sup>	mm	mm <sup>4</sup>	mm <sup>4</sup>
Main Deck, transformed	287,339	100	2.87E+07	-238.661	1.637E+10	9.578E+08
Interior Haunches, transformed	8,186	226.989	1.86E+06	-111.672	1.021E+08	1.988E+06
Exterior Haunches, transformed	3,056	220	6.72E+05	-118.661	4.304E+07	4.075E+05
Overhang	40,277	139.939	5.64E+06	-198.722	1.591E+09	2.629E+08
Interior Girders	121,200	710.978	8.62E+07	372.317	1.680E+10	1.624E+10
Exterior Girders	87,871	711.17	6.25E+07	372.509	1.219E+10	1.249E+10
Sums	<b>A_section = 547,930</b>		<b>1.8556E+08</b>		<b>4.7096E+10</b>	<b>2.9949E+10</b>

<b>y_bar (datum at T.O. Section) =</b>	<b>338.66 mm</b>	<b>I_section =</b>	<b>7.705E+10 mm<sup>4</sup></b>
from bottom of girder	843.68 mm		

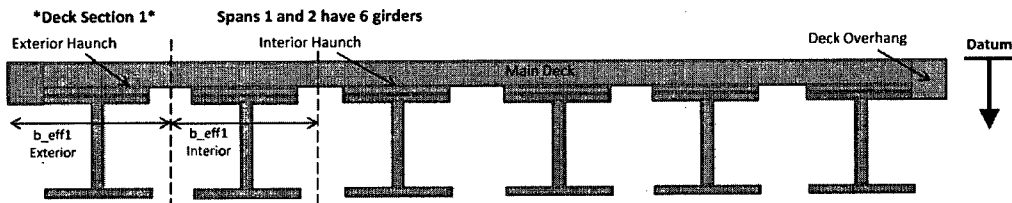
*Deck Section 2*	Span 3 has 8 girders, Section varies linearly to north abutment					
Section Properties are calculated w.r.t. section at north abutment						
	A	y	Ay	d	Ad <sup>2</sup>	I <sub>o</sub>
	mm <sup>2</sup>	mm	mm <sup>3</sup>	mm	mm <sup>4</sup>	mm <sup>4</sup>
Main Deck, transformed	405,575	100	4.06E+07	-230.968	2.164E+10	1.352E+09
Interior Haunches, transformed	8,186	226.989	1.86E+06	-103.979	8.851E+07	1.988E+06
Exterior Haunches, transformed	3,056	220	6.72E+05	-110.968	3.764E+07	4.075E+05
Fascia Haunches, transformed	4,533	229.889	1.04E+06	-101.079	4.631E+07	1.350E+06
Overhang	19,054	139.939	2.67E+06	-191.029	6.953E+08	1.244E+08
Interior Girders	121,200	710.978	8.62E+07	380.010	1.750E+10	1.624E+10
Exterior Girders	87,871	711.17	6.25E+07	380.202	1.270E+10	1.249E+10
Fascia Girders	51,200	711.778	3.64E+07	380.810	7.425E+09	6.500E+09
Sums	<b>A_section = 700,675</b>		<b>2.3190E+08</b>		<b>6.0133E+10</b>	<b>3.6706E+10</b>

<b>y_bar (datum at T.O. Section) =</b>	<b>330.97 mm</b>	<b>I_section =</b>	<b>9.684E+10 mm<sup>4</sup></b>
from bottom of girder	837.01 mm		

## Individual Girders: Calculation of Section Properties

Ec	3604.9965 ksi =	24.85557593 kN/mm <sup>2</sup>		
Es	29000 ksi =	199.9479617 kN/mm <sup>2</sup>		
n=Es/Ec	8.044			
Length of Bridge Section 1	38187 mm	Typical Girder Spacing	2250 mm	1142.078
Length of Bridge Section 2	8813 mm	Max Fascia Spacing	2379 mm	1142.462
				1142.29
<b>Interior Girder Properties</b>		<b>Concrete Properties</b>		0.172
tf	25.9 mm	t_deck	200 mm	
bf	305 mm	t_haunch, Interior	53.978 mm	1142.27
Depth	914 mm	t_haunch, Exterior	40 mm	
I	4.06E+09 mm <sup>4</sup>	t_haunch, Fascia	59.778 mm	
A	30300 mm <sup>2</sup>	<b>Concrete Section 1 Properties</b>		
<b>Exterior Girder Properties</b>		Deck Width1	12715 mm	
tf	39.878 mm	Overhang to CL Girder	732.5	
bf	307.34 mm	Overhang Width1	578.83 mm	
Depth	942.34 mm	b_eff1 Interior	2250 mm	
I	6.24E+09 mm <sup>4</sup>	b_eff1 Exterior	1857.5 mm	
A	43935.4 mm <sup>2</sup>	<b>Concrete Section 2 Properties</b>		
<b>Fascia Girder Properties</b>		(w.r.t. section at north abutment)		
tf	20.1 mm	Deck Width2	16860.66 mm	
bf	305 mm	Overhang to CL Girder	426.33	
Depth	904 mm	Overhang Width2	273.83 mm	
I	3.25E+09 mm <sup>4</sup>	b_eff2 Interior	2250 mm	
A	25600 mm <sup>2</sup>	b_eff2 Exterior	2314.5 mm	
		b_eff2 Fascia	1615.83 mm	

## Calculation of Girder Section Properties (Datum at T.O. Section, Section transformed to steel)



Exterior Girder	A	y	Ay	d	Ad <sup>2</sup>	Io
	mm <sup>2</sup>	mm	mm <sup>3</sup>	mm	mm <sup>4</sup>	mm <sup>4</sup>
Exterior Deck, transformed	31,790	100	3.179E+06	-285.851	2.598E+09	1.060E+08
Exterior Haunch, transformed	1,528	220	3.362E+05	-165.851	4.204E+07	2.038E+05
Overhang1, transformed	20,138	139.939	2.818E+06	-245.912	1.218E+09	1.315E+08
Exterior Girder	43,935	711.17	3.125E+07	325.319	4.650E+09	6.243E+09
Sums	<b>A_section = 97,392</b>		<b>3.758E+07</b>		<b>8.507E+09</b>	<b>6.481E+09</b>

$$y_{\text{bar}} \text{ (datum at T.O. Section) } = 385.85 \text{ mm}$$

$$= 796.49 \text{ mm from bottom}$$

$$I_{\text{section}} = 1.499E+10 \text{ mm}^4$$

Interior Girder	A	y	Ay	d	Ad <sup>2</sup>	Io
	mm <sup>2</sup>	mm	mm <sup>3</sup>	mm	mm <sup>4</sup>	mm <sup>4</sup>
Interior Deck, transformed	55,940	100	5.594E+06	-212.633	2.529E+09	1.865E+08
Interior Haunch, transformed	2,047	226.989	4.645E+05	-85.644	1.501E+07	4.969E+05
Interior Girder	30,300	710.978	2.154E+07	398.345	4.808E+09	4.060E+09
Sums	<b>A_section = 88,286</b>		<b>2.760E+07</b>		<b>7.352E+09</b>	<b>4.247E+09</b>

$$y_{\text{bar}} \text{ (datum at T.O. Section) } = 312.63 \text{ mm}$$

$$= 855.35 \text{ mm from bottom}$$

$$I_{\text{section}} = 1.160E+10 \text{ mm}^4$$

\*Deck Section 2\*

Span 3 has 8 girders, Section varies linearly to north abutment

Section Properties are calculated w.r.t. section at north abutment



**Fascia Girder**

	A	y	Ay	d	Ad <sup>2</sup>	I <sub>o</sub>
	mm <sup>2</sup>	mm	mm <sup>3</sup>	mm	mm <sup>4</sup>	mm <sup>4</sup>
Fascia Deck, transformed	33,365	100	3.336E+06	-230.876	1.778E+09	1.112E+08
Fascia Haunch, transformed	2,266	229.889	5.210E+05	-100.987	2.311E+07	6.749E+05
Overhang2, transformed	9,527	139.939	1.333E+06	-190.937	3.473E+08	6.219E+07
Fascia Girder	25,600	711.778	1.822E+07	380.902	3.714E+09	3.250E+09
Sums	<b>A_section = 70,758</b>		<b>2.341E+07</b>		<b>5.863E+09</b>	<b>3.424E+09</b>

**y\_bar (datum at T.O. Section) = 330.88 mm      I\_section = 9.287E+09 mm<sup>4</sup>**

**Exterior Girder**

	A	y	Ay	d	Ad <sup>2</sup>	I <sub>o</sub>
	mm <sup>2</sup>	mm	mm <sup>3</sup>	mm	mm <sup>4</sup>	mm <sup>4</sup>
Exterior Deck, transformed	57,543	100	5.754E+06	-262.462	3.964E+09	1.918E+08
Exterior Haunch, transformed	1,528	220	3.362E+05	-142.462	3.102E+07	2.038E+05
Exterior Girder	43,935	711.17	3.125E+07	348.708	5.342E+09	6.243E+09
Sums	<b>A_section = 103,007</b>		<b>3.734E+07</b>		<b>9.337E+09</b>	<b>6.435E+09</b>

**y\_bar (datum at T.O. Section) = 362.46 mm      I\_section = 1.577E+10 mm<sup>4</sup>**

**Interior Girder**

	A	y	Ay	d	Ad <sup>2</sup>	I <sub>o</sub>
	mm <sup>2</sup>	mm	mm <sup>3</sup>	mm	mm <sup>4</sup>	mm <sup>4</sup>
Interior Deck, transformed	55,940	100	5.594E+06	-212.633	2.529E+09	1.865E+08
Interior Haunch, transformed	2,047	226.989	4.645E+05	-85.644	1.501E+07	4.969E+05
Interior Girder	30,300	710.978	2.154E+07	398.345	4.808E+09	4.060E+09
Sums	<b>A_section = 88,286</b>		<b>2.760E+07</b>		<b>7.352E+09</b>	<b>4.247E+09</b>

**y\_bar (datum at T.O. Section) = 312.63 mm      I\_section = 1.160E+10 mm<sup>4</sup>**

## APPENDIX C: CALCULATION OF AS-BUILT CONCRETE MATERIAL PROPERTIES

Concrete Density Calculation		Compressive Strength Calculation	
Material	Density (Kg/m <sup>3</sup> )	Deck Cylinder Breaks	Compressive Strength
Aggregate (19mm)	842.00	09-212	35.6
Aggregate (9.5mm)	211.00	09-213	33
Sand	662.00	09-214	33.7
Cement	260.00	09-215	36.6
Fly Ash	87.00		
Water	151.00		
AEA 14	0.14		
CNI	19.31		
Plastiment	0.85		
Visocrete	2.60		
<b>Total Density:</b>	<b>2235.90 kg/m<sup>3</sup></b>	<b>Average Strength:</b>	<b>34.725 MPa</b>
	21.934 kN/m <sup>3</sup>		5036.44 psi
	139.58 pcf		
		<b>Modulus of Elasticity Calculation:</b>	
		$E_c = 0.043(w_c^{1.5})\sqrt{f'_c}$ [MPa]	
		w <sub>c</sub>	2235.90 kg/m <sup>3</sup>
		f' <sub>c</sub>	34.725 MPa
		<b>E<sub>c</sub></b>	<b>26,789.8 MPa</b>

**Barre, Br# B-2-12 - Cement Concrete 28 Day Break Test Results**

SampDate	Contract	ProjLoc	Contractor	ClasConc	Break	P/F	NameMfr	LocaMfr	LabNumbr
22-Jul-09	53932	BARRE, Br B-2-12	ET & L CORP.	30MPa-20mm	35.4	OK	AGG. IND.	LUNENBURG	09-246
17-Jul-09	53932	BARRE, Br B-2-12	ET & L CORP.	30MPa-20mm	35.8	OK	AGG. IND.	LUNENBURG	09-245
16-Jul-09	53932	BARRE, Br B-2-12	ET & L CORP.	30MPa-20mm Core 1 (5/22/09)	34.5	INFO	AGG. IND.	LUNENBURG	C902700 Northeast Wingwall-Core 1
16-Jul-09	53932	BARRE, Br B-2-12	ET & L CORP.	30MPa-20mm Core 2 (5/22/09)	32.0	INFO	AGG. IND.	LUNENBURG	C902700 Northeast Wingwall-Core 2
16-Jul-09	53932	BARRE, Br B-2-12	ET & L CORP.	30MPa-20mm Core 3 (5/22/09)	28.3	INFO	AGG. IND.	LUNENBURG	C902700 Northeast Wingwall-Core 3
10-Jul-09	53932	BARRE, Br B-2-12	ET & L CORP.	30MPa-20mm-HP	33.0	INFO	AGG. IND.	LUNENBURG	09-213 56 Day
10-Jul-09	53932	BARRE, Br B-2-12	ET & L CORP.	30MPa-20mm-HP	28.3	DNC	AGG. IND.	LUNENBURG	09-213
10-Jul-09	53932	BARRE, Br B-2-12	ET & L CORP.	30MPa-20mm-HP	35.6	OK	AGG. IND.	LUNENBURG	09-212
10-Jul-09	53932	BARRE, Br B-2-12	ET & L CORP.	30MPa-20mm-HP	33.7	OK	AGG. IND.	LUNENBURG	09-214
10-Jul-09	53932	BARRE, Br B-2-12	ET & L CORP.	30MPa-20mm-HP	36.6	OK	AGG. IND.	LUNENBURG	09-215
09-Jul-09	53932	BARRE, Br B-2-12	ET & L CORP.	30MPa-20mm	30.7	OK	AGG. IND.	LUNENBURG	09-193
02-Jul-09	53932	BARRE, Br B-2-12	ET & L CORP.	30MPa-20mm	32.0	INFO	AGG. IND.	LUNENBURG	09-190 56 Day
02-Jul-09	53932	BARRE, Br B-2-12	ET & L CORP.	30MPa-20mm	27.2	DNC	AGG. IND.	LUNENBURG	09-190
15-Jun-09	53932	BARRE, Br B-2-12	ET & L CORP.	30MPa-20mm	32.4	OK	AGG. IND.	LUNENBURG	09-146
12-Jun-09	53932	BARRE, Br B-2-12	ET & L CORP.	30MPa-20mm	37.8	OK	AGG. IND.	LUNENBURG	09-145
09-Jun-09	53932	BARRE, Br B-2-12	ET & L CORP.	30MPa-20mm	33.3	OK	AGG. IND.	LUNENBURG	09-144
22-May-09	53932	BARRE, Br B-2-12	ET & L CORP.	30MPa-20mm	24.7	DNC	AGG. IND.	LUNENBURG	09-105B (Cored 7/16/09)
22-May-09	53932	BARRE, Br B-2-12	ET & L CORP.	30MPa-20mm	28.6	INFO	AGG. IND.	LUNENBURG	09-105B 56 Day (Cored 7/16/09)

Figure 112. Concrete Cylinder Break Strengths, Deck Pour values highlighted

COMMONWEALTH OF MASS		CEMENT CONCRETE DESIGN OF MIXES											
MASS HIGHWAY DEPT RESEARCH & MATERIALS SECT RMS 054, METRIC BLDG 6000KAS		COMPANY Aggregate Industries				Factory Date 2/1/2009			City Lunenburg				
		PLANT LOCATION(S) #231 Eastover				No. Grafton Office:			(508) 539-0500				
PLANTS	ID#	Size, Type Mixing (A)	Automatic Controls (X)			Hear Available (X)			CEMENT SILOS				
TO BE	208	7.65 cm, trans, entrl	part, full, X, w/pmt, X	water, X, sand, X, sin, X				1 @ 266 bbl					
USED:	0	8.41 cm, trans, entrl, X	part, full, X, w/pmt, X	water, X, sand, X, sin, X				1 @ bbl					
	0	8.41 cm, trans, entrl, X	part, full, X, w/pmt, X	water, X, sand, X, sin, X				1 @ bbl					
	0	8.41 cm, trans, entrl, X	part, full, X, w/pmt, X	water, X, sand, X, sin, X				1 @ bbl					
COMPONENT MATERIALS (LA= % Wear; SG= Specific Gravity (coarse aggsaturated surface dry))													
CEMENT	LaFarge Blended Silica Fume Cement							SG=	3.06				
FLY ASH ("FASH")	Brayton Point - Somerset, MA					Class F	SG=	2.40					
SAND	Aggregate, LLC - Hubbardston							SG=	2.66				
STONE	3/4"	P.J. Keating - Lunenburg				LA=	17%	SG=	2.70				
STONE	3/8"	P.J. Keating - Lunenburg				LA=	16%	SG=	2.68				
MIX WATER (X)	ADMINES.	A. Air-Entr: AEA 14			C. Water Reducer / Retarder:			Plastiment					
Pvt. X, City X	Kind:	B. Corrosion Inhibitor: CNI			D. HRWR:			Viscocrete 2100					
AGGREGATE ANALYSIS & CONCRETE DESIGN DATA (FM=Fineness Modulus)													
SIEVE	37.5mm	25mm	19mm	12.5mm	9.5mm	4.75mm	2.36mm	1.18mm	600µm	300µm	150µm	75µm	FM
SAND													
Spec.					100	95-100		45-80		10-30	2-10	0-3	2.5-3.0
Analysis					100	99	92	70	49	16	5	1.3	2.69
STONE													
40mm Spec	90-100		35-60		10-25	0-5							
Composite													
STONE													
20mm Spec			90-100		20-50	0-10	0-5						
Composite			97		30	7	1						6.65
STONE													
10mm Spec					100	85-100	10-30	0-10	0-5				
Composite					100	95	28	2	1				5.75
I.T. WT.													
20mm Spec		100	90-100		10-50	0-15							
Composite								0	0	0	0		
I.T. WT.													
10mm Spec					100	50-100	5-30	0-30	0-10				
Composite										0	0		
DESIGN QUANTITIES PER CUBIC METER, @ 150mm SLUMP												TRIAL BATCH	TRIAL AGG.
CLASS OF CONCRETE	37.5mm	19mm	9.5mm	Sand	Cem.	Fly Ash	Water	Admixtures in ml.				Mpa	F.M.
Mpa	kgs.	kgs.	kgs.	kgs.	kgs.	kgs.	L.	A.	B.	C.	D.		
30 20mm SF	0	842	211	662	272	91	163	166	0.0	707.9	2363		5.12
35 20mm SF	0	842	211	599	314	104	168	190	0.0	820.0	2727		5.21
30 10mm SF	0	0	994	685	282	94	170	170	0.0	738.8	2456		4.50
35 10mm SF	0	0	994	622	325	109	174	197	0.0	847.1	2824		4.57
30 20mm HPC	0	842	211	662	272	91	151	143	14853	708	2363		5.12
35 20mm HPC	0	842	211	599	314	104	155	162	14853	820	2727		5.21
30 10mm HPC	0	0	994	685	282	94	157	147	14853	739	2456		4.50
35 10mm HPC	0	0	994	622	325	109	161	170	14853	847	2824		4.57
We agree to furnish mixes to projects of the Massachusetts Highway Department, that are produced from only pre-approved materials. We also understand that designs are to be submitted annually, prior to production for State Work, and any subsequent change in materials or design will require resubmission for approval.													
												Authorized Signature and Title:	
												Richard Fredette QC	

Figure 113. Mix design, Aggregate Industries Lunenburg, MA Plant



## APPENDIX D: CALCULATION OF STIFFNESS COEFFICIENTS FOR MODEL BOUNDARY CONDITIONS

Note: These calculations were completed in coordination with John Phelps at Tufts University.

Paul Lefebvre

VAB-Research

January 25, 2010

### Elastomeric Bearing Pad Stiffness Calculations

**Bearing Pad Properties:** (All dimensions in mm)

$$\begin{aligned}
 D &:= 350 & t_{\text{steelayer}} &:= 3 & G &:= .00101 & \frac{\text{Kn}}{\text{mm}^2} \\
 h &:= 61 & \text{steelayers} &:= 4 & \nu &:= .49975 \\
 \text{Cover} &:= 5 & \text{Aspectratio} &:= 1.0 & t_{\text{inner}} &:= 13 & = \text{thickness of inner elastomer layer} \\
 h_{\text{rubber}} &:= h - \text{steelayers} \cdot t_{\text{steelayer}} = 49
 \end{aligned}$$

**Axial Stiffness Calculation:**

$$\begin{aligned}
 A_i &:= \pi \cdot \left(\frac{D}{2}\right)^2 = 9.621 \times 10^4 & \text{InnerPerimeterArea} &:= 2 \cdot \pi \cdot \left(\frac{D}{2}\right) \cdot t_{\text{inner}} = 1.429 \times 10^4 \\
 A_o &:= \pi \cdot \left(\frac{D}{2}\right)^2 = 9.621 \times 10^4 & \text{CoverArea} &:= 2\pi \cdot \left(\frac{D}{2}\right) \cdot \text{Cover} = 5.498 \times 10^3
 \end{aligned}$$

S = Shape Factor = (Loaded Area)/(Perimeter Area Free to Bulge)

$$S_i := \frac{A}{\text{InnerPerimeterArea}} = 6.731 \quad K_i := \frac{[2 \cdot G \cdot (1 + \nu)]}{3 \cdot (1 - 2 \cdot \nu)} = 2.02 \quad \lambda_i := S_i \cdot \sqrt{\frac{(3 \cdot G)}{K}} = 0.261$$

$$S_o := \frac{A}{\text{CoverArea}} = 17.5 \quad \lambda_o := S_o \cdot \sqrt{\frac{(3 \cdot G)}{K}} = 0.678$$

$$E := 2 \cdot G \cdot (1 + \nu) = 3.029 \times 10^{-3}$$

From Stanton Figure F.3:  $B_{a_i} := 1.75$   $B_{a_o} := 0.95$

From Stanton and Lund,  $A_a = 1.0$  for rectangular bearings, therefore:

Assume  $A_a = 1.0$  for circular bearings

$$A_a := 1.0$$

$$K_{a_i} = \text{axial stiffness for an inner layer} \quad K_{a_i} := \frac{[E \cdot A \cdot (A_a + B_{a_i} \cdot S_i^2)]}{t_{\text{inner}}} = 1.8 \times 10^3 \quad \frac{\text{Kn}}{\text{mm}}$$

$$K_{a_o} = \text{axial stiffness for an outer layer} \quad K_{a_o} := E \cdot A \cdot \frac{(A_a + B_{a_o} \cdot S_o^2)}{\text{Cover}} = 1.702 \times 10^4 \quad \frac{\text{Kn}}{\text{mm}}$$

$$K_a = \text{Total Axial Stiffness} \quad K_a := \frac{1}{\frac{3}{K_{a_i}} + \frac{2}{K_{a_o}}} = 560.469 \quad \frac{\text{Kn}}{\text{mm}}$$

$$\text{If cover is not considered, then} \quad K_{a2} := \frac{1}{\left(\frac{3}{K_{a_i}}\right)} = 599.988 \quad \frac{\text{Kn}}{\text{mm}}$$

**Rotational Stiffness Calculation:**

$$I := \frac{\left[\pi \cdot \left(\frac{D}{2}\right)^4\right]}{4} = 7.366 \times 10^8$$

From Stanton and Lund,  $A_r = 1.0$  for rectangular bearings, therefore:

Assume  $A_r = 1.0$  for circular bearings

$$A_r := 1.0$$

From Stanton Figure F.4:  $B_{r_i} := 0.7$   $B_{r_o} := 0.45$

$K_{r_i}$  = Rotational stiffness of Inner Layer  $K_{r_o}$  = Rotational stiffness of Cover Layer

$$K_{r_i} := \frac{\left[\left[E \cdot I \cdot \left(A_r + B_{r_i} \cdot S_i^2\right)\right]\right]}{t_{\text{inner}}} = 5.615 \times 10^6 \quad \frac{\text{Kn} \cdot \text{mm}}{\text{rad}}$$

$$K_{r_o} := \frac{\left[\left[E \cdot I \cdot \left(A_r + B_{r_o} \cdot S_o^2\right)\right]\right]}{\text{Cover}} = 6.195 \times 10^7 \quad \frac{\text{Kn} \cdot \text{mm}}{\text{rad}}$$

$$K_r = \text{Total Rotational Stiffness} \quad K_r := \frac{1}{\left(\frac{3}{K_{r_i}} + \frac{2}{K_{r_o}}\right)} = 1.765 \times 10^6 \quad \frac{\text{Kn} \cdot \text{mm}}{\text{rad}}$$

$$\text{If cover is not considered, then} \quad K_{r2} := \frac{1}{\left(\frac{3}{K_{r_i}}\right)} = 1.872 \times 10^6 \quad \frac{\text{Kn} \cdot \text{mm}}{\text{rad}}$$

**Shear Stiffness Calculation:**

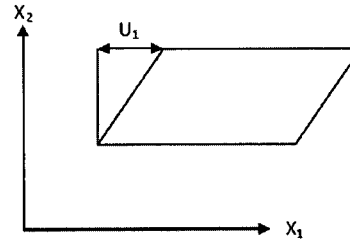
Strain-Displacement Relationship:

$$\epsilon_{ij} := \frac{1}{2} \left( \frac{d}{dx_j} U_i + \frac{d}{dx_i} U_j \right) \quad A_s := A$$

$$U_2 := 0$$

Therefore:

$$\epsilon_{21} := \frac{1}{2} \left( \frac{d}{dx_2} U_1 \right)$$



Where:

$$dU_1 := \Delta u \quad dx_2 := h_{\text{rubber}}$$

Therefore:

$$\epsilon_{21} := \frac{1}{2} \frac{\Delta u}{h_{\text{rubber}}}$$

 $K_{s\_def}$  = Shear Stiffness

$$K_{s\_def} := \frac{F}{\Delta u} \quad F := A_s \cdot \tau \quad \tau := G \cdot \epsilon_{21}$$

Combining equations gives:

$$F := (A_s \cdot G \cdot \epsilon_{21}) \quad \text{Where:} \quad \epsilon_{21} := \frac{1}{2} \frac{\Delta u}{h_{\text{rubber}}}$$

$$F := A_s \cdot G \cdot \left( \frac{1}{2} \frac{\Delta u}{h_{\text{rubber}}} \right)$$

$$K_{s\_def} := \frac{1}{2} \frac{(A_s \cdot G)}{h_{\text{rubber}}}$$

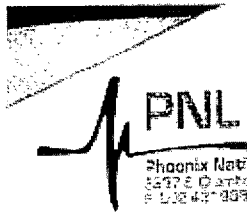
Therefore:

$$K_{s\_i} := \frac{1}{2} \frac{(A_s \cdot G)}{t_{\text{inner}}} = 3.737 \quad \frac{\text{kN}}{\text{mm}}$$

$$K_{s\_o} := \frac{1}{2} \frac{(A_s \cdot G)}{\text{Cover}} = 9.717 \quad \frac{\text{kN}}{\text{mm}}$$

$$K_s = \text{Total Shear Stiffness} \quad K_s := \frac{1}{\left( \frac{3}{K_{s\_i}} + \frac{2}{K_{s\_o}} \right)} = 0.992 \quad \frac{\text{Kn}}{\text{mm}}$$

$$\text{If cover is not considered, then} \quad K_{s2} := \frac{1}{\left( \frac{3}{K_{s\_i}} \right)} = 1.246 \quad \frac{\text{Kn}}{\text{mm}}$$

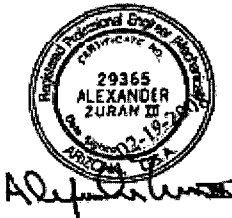


Phoenix National Laboratories, Inc.  
 3477 S. Carbon Street, Phoenix, AZ 85040  
 P: 602.437.9997 • F: 602.437.8083 • www.pnl.com

**LABORATORY REPORT  
 ELASTOMERIC MATERIAL**

CLIENT		COMPOUND NO.	CLIENT ORDER NO.		
D.S. Brown Company		660	78986		
PROJECT DESCRIPTION			MATERIAL DESCRIPTION		
Semi Annual Batch Testing			2 - 6" x 6" slabs and 1 Quad Shear Modulus Fixture		
MATERIAL SUBMITTED BY	DATE SUBMITTED	PNL PROJECT NO.	PNL LAB NO.	REPORT DATE	
Client	01/15/2008	26-208039	ML806139	02/19/2008	
SPECIFICATION	GRADE	DURO	ELASTOMER TYPE	QUALITY REQUIREMENTS	
AASHTO Ch. 18	3	60	Neoprene	Table 18.4.5.1-1A	
SUMMARY OF RESULTS					
ASTM D1149	OZONE RESISTANCE (100 pphm, 100 hours @ 100 °F)		No Cracks	No Cracks	PASS
ASTM D746	LOW TEMPERATURE BRITTLENESS (-40°F)		No Failures	No Failures	PASS
ASTM D1043	INSTANTANEOUS THERMAL STIFFENING (-40°F)		< 4 times stiffness at 73°F	2.50	PASS
ASTM D4014	SHEAR MODULUS - ANNEX A1		130 - 200 psi	147.1	PASS
AASHTO CH 18	LOW TEMPERATURE CRYSTALLIZATION (14 days @ -13°F)		< 4 times stiffness at 73°F	1.7	PASS

The batch material tested complies with the AASHTO Standard Specifications for Highway Bridges 2002, Chapter 18 for all tests noted above as performed by Phoenix National Laboratories, Inc.



PNL warrants that the above services and results were performed under the appropriate standard of care, including the skill and judgment that is reasonably expected from similarly situated technical personnel. No other warranty, guarantee, or representation, whether expressed or implied, is included or intended.

REVIEWED BY Alex Zuran

Figure 114. Elastomeric bearing pad lab test results (1 of 2)



**LABORATORY REPORT  
ELASTOMERIC MATERIAL**



*A. Alexander*

CLIENT	COMPOUND NO.	CLIENT ORDER NO.
D.S. Brown Company	660	78986
PROJECT	PNL LAB NO.	
Semi Annual Batch Testing	ML806139	
SAMPLE SIZE	REPORT DATE	
2 - 6" x 6" slabs and 1 Quad Shear Modulus	02/19/2008	

**SPECIFIC TEST DATA**

OZONE - ASTM D1149 (Mounting Procedure D518, Procedure A)												
HOURS AT 20% STRAIN	TEMPERATURE			PPHM	NO. CRACKS			REQUIREMENT		RESULT		
100	100° F			100	No Cracks			No Cracks		PASS		
LOW TEMPERATURE BRITTLENESS - ASTM D746 (Method B) Mechanical Impact												
SAMPLE SIZE	NO. OF SAMPLES			TEST TEMPERATURE	NO. FAILED			REQUIREMENT		RESULT		
1" x 0.25" x 0.075"	5			-40° F	0			No Failures		PASS		
INSTANTANEOUS THERMAL STIFFENING (-40°F) - ASTM D1043												
	SPAN L (in)	WIDTH a (in)	THICKNESS T (in)	LOAD@T <sub>90</sub> F <sub>1</sub> (grams)	θ <sub>1</sub>	S <sub>1</sub>	LOAD@T <sub>20</sub> F <sub>2</sub> (grams)	θ <sub>20</sub>	S <sub>20</sub>	Ratio	REQUIRED	RESULT
1	2.12	0.265	0.074	10.0	24	0.42	22.7	20	1.14	2.72		
2	2.12	0.263	0.075	10.0	23	0.43	22.7	23	0.99	2.27		
AVG										2.50	Ratio ≤ 4	PASS
Note: S = Relative Stiffness = Load/Rotation (θ)												
SHEAR MODULUS - ASTM D4014 ANNEX A1												
	THICK (in)	WIDTH (in)	WIDTH (in)	AREA (in <sup>2</sup> )	F <sub>max</sub> (Lb)	F <sub>1</sub> (Lb)	X <sub>1</sub> (in)	X <sub>2</sub> (in)	F <sub>2</sub> (Lb)	MODULUS (psi)		
1	0.478	2.024	2.010	4.068								
2	0.478	2.030	2.021	4.103								
3	0.477	2.025	2.008	4.066								
4	0.462	2.031	2.023	4.108								
AVG.	0.474			4.086	570	11.4	0.003	0.240	312	147.1		
REQUIREMENT										130 - 200 psi		
RESULTS										PASS		
LOW TEMPERATURE CRYSTALLIZATION (14 days @ -15°F)												
	THICK (in)	WIDTH (in)	WIDTH (in)	AREA (in <sup>2</sup> )	F <sub>max</sub> (Lb)	F <sub>1</sub> (Lb)	X <sub>1</sub> (in)	X <sub>2</sub> (in)	F <sub>2</sub> (Lb)	MODULUS (psi)		
AVG.	0.474			4.086	1010	20.2	0.003	0.240	522	245.6		
REQUIREMENT										588		
RATIO VALUE										1.7		
RESULTS										PASS		

Figure 115. Elastomeric bearing pad lab test results (2 of 2)

## APPENDIX E: KEY FOR MASSDOT INSPECTION REPORT

<b>CONDITION RATING GUIDE</b>			
(For Items 58, 59, 60 and 61)			
	CODE	CONDITION	DEFECTS
	N	NOT APPLICABLE	
G	9	EXCELLENT	Excellent condition.
G	8	VERY GOOD	No problem noted.
G	7	GOOD	Some minor problems.
F	6	SATISFACTORY	Structural elements show some minor deterioration.
F	5	FAIR	All primary structural elements are sound but may have minor section loss, cracking, spalling or scour.
P	4	POOR	Advance section loss, deterioration, spalling or scour.
P	3	SERIOUS	Loss of section, deterioration, spalling or scour have seriously affected primary structural components. Local failures are possible. Fatigue cracks in steel or shear cracks in concrete may be present.
C	2	CRITICAL	Advance deterioration of primary structural elements. Fatigue cracks in steel or shear cracks in concrete may be present or scour may have removed substructure support. Unless closely monitored it may be necessary to close the bridge until corrective action is taken.
C	1	"IMMINENT" FAILURE	Major deterioration or section loss present in critical structural components or obvious vertical or horizontal movement affecting structure stability. Bridge is closed to traffic but corrective action may put it back in light service.
	0	FAILED	Out of service - beyond corrective action.

<b>DEFICIENCY REPORTING GUIDE</b>	
<b>DEFICIENCY:</b>	A defect in a structure that requires corrective action.
<b>CATEGORIES OF DEFICIENCIES:</b>	
<b>M= Minor Deficiency -</b>	Deficiencies which are minor in nature, generally do not impact the structural integrity of the bridge and could easily be repaired. Examples include but are not limited to: Spalled concrete, Minor pot holes, Minor corrosion of steel, Minor scouring, Clogged drainage, etc.
<b>S= Severe/Major Deficiency -</b>	Deficiencies which are more extensive in nature and need more planning and effort to repair. Examples include but are not limited to: Moderate to major deterioration in concrete, Exposed and corroded rebars, Considerable settlement, Considerable scouring or undermining, Moderate to extensive corrosion to structural steel with measurable loss of section, etc.
<b>C-S= Critical Structural Deficiency -</b>	A deficiency in a structural element of a bridge that poses an extreme unsafe condition due to the failure or imminent failure of the element which will affect the structural integrity of the bridge.
<b>C-H= Critical Hazard Deficiency -</b>	A deficiency in a component or element of a bridge that poses an extreme hazard or unsafe condition to the public, but does not impair the structural integrity of the bridge. Examples include but are not limited to: Loose concrete hanging down over traffic or pedestrians, A hole in a sidewalk that may cause injuries to pedestrians, Missing section of bridge railing, etc.
<b>URGENCY OF REPAIR:</b>	
<b>I = Immediate-</b>	[Inspector(s) immediately contact District Bridge Inspection Engineer (DBIE) to report the Deficiency and to receive further instruction from him/her].
<b>A = ASAP-</b>	[Action/Repair should be initiated by District Maintenance Engineer or the Responsible Party (if not a State owned bridge) upon receipt of the Inspection Report].
<b>P = Prioritize-</b>	[Shall be prioritized by District Maintenance Engineer or the Responsible Party (if not a State owned bridge) and repairs made when funds and/or manpower is available].

## APPENDIX F: CALCULATION OF LOAD RATING FACTORS

Paul Lefebvre

VAB Research

5-18-2010

Calculate Rating Factors for VAB Interior and Exterior Girders using LRFR Rating Factor Equation from 2008 AASHTO Manual for Bridge Evaluation and 2008 AASHTO LRFD Bridge Design Manual

$$RF = \frac{C - \gamma_{DC}DC - \gamma_{DW}DW - \gamma_P P}{\gamma_{LL}LL(1 + IM)} \quad (\text{AASHTO Manual for Bridge Evaluation, 2008})$$

Step 1. Calculate Plastic Moment Capacity, C, for Interior and Exterior girders

### Resistance Factors

$\phi$  = Resistance factor for Strength Limit State for Flexure

$\phi := 1.0$  (2008 Design Manual, 6.5.4.2)

$\phi_C$  = Condition factor for uncertainties increasing with age of bridge

$\phi_C := 1.0$  (New bridge, therefore condition assumed as designed)

$\phi_S$  = System factor for level of redundancy in the bridge

$\phi_S := 1.0$  (No additional information to support otherwise)

### Load Factors

$\gamma_{DC} := 1.25$      $\gamma_{DW} := 1.50$      $\gamma_{LL} := 1.75$  (2008 LRFD Design Manual, 3.4.1)

### Dynamic Load Allowance, IM

$IM := 0.33$  (2008 LRFD Design Manual, 3.6.2.1)

Composite Section Properties For Interior Girder (all units in mm and kN)

$$\begin{aligned}
 t_{\text{deck}} &:= 200 & t_{f\_int} &:= 25.9 & d_{int} &:= 914 \\
 f_c &:= 0.034725 & t_{w\_int} &:= 16.5 & b_{f\_int} &:= 305 \\
 \text{Spacing}_{int} &:= 2250 & f_y &:= 0.34474 \\
 t_{\text{haunch}_{int}} &:= 54 & d_{w\_int} &:= d_{int} - 2 \cdot t_{f\_int} = 862.2
 \end{aligned}$$

$$B_1 := 0.8 \quad (\text{2008 Design Manual, 5.7.2.2})$$

Check for balanced section: T=C (Assume haunch does not contribute to strength)

Assume PNA (plastic neutral axis) is in deck at a depth of 194.827mm from top of deck

$$\text{PNA}_{int} := 194.827$$

Section Forces

$$T_{\text{btm}_{int}} := b_{f\_int} \cdot t_{f\_int} \cdot f_y = 2.723 \times 10^3$$

$$T_{\text{web}_{int}} := d_{w\_int} \cdot t_{w\_int} \cdot f_y = 4.904 \times 10^3$$

$$T_{\text{top}_{int}} := T_{\text{btm}_{int}} = 2.723 \times 10^3$$

$$T_{\text{total}_{int}} := T_{\text{btm}_{int}} + T_{\text{top}_{int}} + T_{\text{web}_{int}} = 1.035 \times 10^4$$

$$C_{\text{total}_{int}} := 0.85 \cdot f_c \cdot B_1 \cdot \text{PNA}_{int} \cdot \text{Spacing}_{int} = 1.035 \times 10^4$$

T = C ok



Calculate  $M_p$  (sum forces about PNA)

$$\text{thickness of compression block } a := \frac{C_{\text{total\_int}}}{0.85 \cdot f_c \cdot \text{Spacing}_{\text{int}}} = 155.862$$

$$\begin{aligned} M_{p\_int} := & C_{\text{total\_int}} \left( \frac{a}{2} \right) + T_{\text{top\_int}} \left( t_{\text{deck}} + t_{\text{haunch\_int}} + \frac{t_{f\_int}}{2} - \text{PNA\_int} \right) \dots = 6.15 \times 10^6 \\ & + T_{\text{web\_int}} \left( t_{\text{deck}} + t_{\text{haunch\_int}} + t_{f\_int} + \frac{d_{w\_int}}{2} - \text{PNA\_int} \right) \dots \\ & + T_{\text{btm\_int}} \left( t_{\text{deck}} + t_{\text{haunch\_int}} + d_{\text{int}} - \frac{t_{f\_int}}{2} - \text{PNA\_int} \right) \end{aligned}$$

Calculate Capacity<sub>interior</sub>

$$\text{Capacity}_{\text{int}} := \phi \cdot \phi_c \cdot \phi_s \cdot M_{p\_int} = 6.15 \times 10^6 \quad \text{kN} - \text{mm}$$

## Section Properties for Exterior Girder

$$t_{f\_ext} := 39.878$$

$$t_{w\_ext} := 22.098$$

$$b_{f\_ext} := 307.34$$

$$d_{ext} := 942.34$$

$$d_{w\_ext} := d_{ext} - 2 \cdot t_{f\_ext} = 862.584$$

$$t_{haunch\_ext} := 40$$

$$b_{overhang\_ext} := 732.5 - \frac{b_{f\_ext}}{2} = 578.83$$

$$Spacing_{ext} := \frac{Spacing_{int}}{2} + b_{overhang\_ext} = 1.704 \times 10^3$$

Check for balanced section: T=C

(Assume haunch and extra overhang do not contribute to strength)

Let PNA (plastic neutral axis) be in top flange at a depth of 263.4mm from top of deck

$$PNA_{ext} := 263.4$$

## Calculate Section Forces

$$T_{btm\_ext} := b_{f\_ext} \cdot t_{f\_ext} \cdot f_y = 4.225 \times 10^3$$

$$T_{web\_ext} := t_{w\_ext} \cdot d_{w\_ext} \cdot f_y = 6.571 \times 10^3$$

$$T_{top\_ext} := T_{btm\_ext} = 4.225 \times 10^3$$

$$C_{c\_max} := 0.85 \cdot f_c \cdot t_{deck} \cdot Spacing_{ext} = 1.006 \times 10^4$$

$$C_s := (PNA_{ext} - t_{deck} - t_{haunch\_ext}) \cdot b_{f\_ext} \cdot f_y = 2.479 \times 10^3$$

$$T_{total\_ext} := T_{btm\_ext} + T_{web\_ext} + T_{top\_ext} - C_s = 1.254 \times 10^4$$

$$C_{total\_ext} := C_{c\_max} + C_s = 1.254 \times 10^4$$

T = C ok

Calculate  $M_p$  (sum forces about PNA)

thickness of concrete compression block:  $a_{ext} := 200$

$$\begin{aligned}
 M_{p\_ext} := & C_{c\_max} \left( PNA_{ext} - \frac{a_{ext}}{2} \right) + C_s \cdot \frac{(PNA_{ext} - t_{deck} - t_{haunch\_ext})}{2} \dots = 7.414 \times 10^6 \\
 & + (T_{top\_ext} - C_s) \cdot \frac{(t_{deck} + t_{haunch\_ext} + t_{f\_ext} - PNA_{ext})}{2} \dots \\
 & + T_{web\_ext} \cdot \left( t_{deck} + t_{haunch\_ext} + t_{f\_ext} + \frac{d_{w\_ext}}{2} - PNA_{ext} \right) \dots \\
 & + T_{btm\_ext} \cdot \left( d_{ext} - \frac{t_{f\_ext}}{2} - PNA_{ext} \right)
 \end{aligned}$$

Calculate Capacity,  $Capacity_{Exterior}$

$$\boxed{Capacity_{Ext} := \phi \cdot \phi_c \cdot \phi_s \cdot M_{p\_ext} = 7.414 \times 10^6} \quad \text{kN} - \text{mm}$$

Step 2. Calculate Dead and Live Loads for Obtaining Maximum Moment  
(All Units in kN and mm)

## Calculate Dead Loads

## Beams

$$\gamma_{\text{steel}} := \frac{76.9729}{10^9} = 7.697 \times 10^{-8}$$

Interior, W920x238

Exterior, W920x345 (W36x232)

$$A_{\text{int}} := 30300$$

$$A_{\text{ext}} := 43935.4$$

$$UW_{\text{int}} := A_{\text{int}} \cdot \gamma_{\text{steel}} = 2.332 \times 10^{-3}$$

$$UW_{\text{ext}} := A_{\text{ext}} \cdot \gamma_{\text{steel}} = 3.382 \times 10^{-3}$$

Fascia W920x201

$$A_{\text{fascia}} := 25600$$

$$UW_{\text{fascia}} := A_{\text{fascia}} \cdot \gamma_{\text{steel}} = 1.971 \times 10^{-3}$$

For Deck Section 1 (Spans 1 and 2), 4 interior and 2 exterior

$$\text{BeamDC}_1 := 4 \cdot UW_{\text{int}} + 2 \cdot UW_{\text{ext}} = 0.016$$

For Deck Section 2 (Span 3), 4 interior, 2 exterior,  
and 2 fascia

$$\text{BeamDC}_2 := 4 \cdot UW_{\text{int}} + 2 \cdot UW_{\text{ext}} + 2 \cdot UW_{\text{fascia}} = 0.02$$

## Deck

$$\gamma_{\text{concrete}} := (140 + 5.0364) \cdot \frac{16.9.81}{10^{12}} = 2.276 \times 10^{-8}$$

(conversion from pcf to kN/m<sup>3</sup>)

$$\gamma_{\text{rc}} := (140 + 5.0364 + 5) \cdot \frac{16.9.81}{10^{12}} = 2.355 \times 10^{-8}$$

For Deck Section 1

$$\text{Width}_{\text{deck1}} := 12715$$

$$A_{\text{deck1}} := \text{Width}_{\text{deck1}} \cdot t_{\text{deck}} = 2.543 \times 10^6$$

$$\text{DeckDC}_1 := A_{\text{deck1}} \cdot \gamma_{\text{rc}} = 0.06$$

For End of Deck Section 2 (North Abutment)

$$\text{Width}_{\text{deck2}} := 16860.662$$

$$A_{\text{deck2}} := \text{Width}_{\text{deck2}} \cdot t_{\text{deck}} = 3.372 \times 10^6$$

$$\text{DeckDC}_2 := A_{\text{deck2}} \cdot \gamma_{\text{rc}} = 0.079$$

## Haunch

$$t_{\text{haunch\_int}} = 54$$

$$t_{\text{haunch\_ext}} = 40$$

$$t_{\text{f\_fascia}} := 20.1$$

$$t_{\text{haunch\_fascia}} := 79.878 - t_{\text{f\_fascia}} = 59.778$$

## For Interior Girder

$$A_{\text{haunch\_int}} := b_{\text{f\_int}} \cdot t_{\text{haunch\_int}} = 1.647 \times 10^4$$

$$\text{HaunchDC}_{\text{int}} := A_{\text{haunch\_int}} \cdot \gamma_{\text{rc}} = 3.879 \times 10^{-4}$$

## For Exterior Girder

$$A_{\text{haunch\_ext}} := b_{\text{f\_ext}} \cdot t_{\text{haunch\_ext}} = 1.229 \times 10^4$$

$$\text{HaunchDC}_{\text{ext}} := A_{\text{haunch\_ext}} \cdot \gamma_{\text{rc}} = 2.895 \times 10^{-4}$$

## For Fascia Girders

$$b_{\text{f\_fascia}} := 305$$

$$A_{\text{haunch\_fascia}} := b_{\text{f\_fascia}} \cdot t_{\text{haunch\_fascia}} = 1.823 \times 10^4$$

$$\text{HaunchDC}_{\text{fascia}} := A_{\text{haunch\_fascia}} \cdot \gamma_{\text{rc}} = 4.294 \times 10^{-4}$$

## For Deck Section 1

$$\text{HaunchDC}_1 := 4 \cdot \text{HaunchDC}_{\text{int}} + 2 \cdot \text{HaunchDC}_{\text{ext}} = 2.13 \times 10^{-3}$$

## For Deck Section 2

$$\text{HaunchDC}_2 := 4 \cdot \text{HaunchDC}_{\text{int}} + 2 \cdot \text{HaunchDC}_{\text{ext}} + 2 \cdot \text{HaunchDC}_{\text{fascia}} = 2.989 \times 10^{-3}$$

## Overhang

For Deck Section 1

$$A_{\text{overhang1}} := b_{\text{overhang\_ext}} \cdot (t_{\text{haunch\_ext}} + t_{\text{f\_ext}}) = 4.624 \times 10^4$$

$$\text{OverhangDC}_1 := A_{\text{overhang1}} \cdot \gamma_{\text{rc}} = 1.089 \times 10^{-3}$$

For Deck Section 2

$$b_{\text{overhang\_fascia}} := 732.5 - \frac{b_{\text{f\_fascia}}}{2} = 580$$

$$A_{\text{overhang2}} := b_{\text{overhang\_fascia}} \cdot (t_{\text{haunch\_fascia}} + t_{\text{f\_fascia}}) = 4.633 \times 10^4$$

$$\text{OverhangDC}_2 := A_{\text{overhang2}} \cdot \gamma_{\text{rc}} = 1.091 \times 10^{-3}$$

## Safety Curb

$$t_{\text{curb}} := 200 + 80 = 280 \quad \text{width}_{\text{curb}} := 495$$

$$A_{\text{curb}} := t_{\text{curb}} \cdot \text{width}_{\text{curb}} = 1.386 \times 10^5$$

$$\text{CurbDC} := 2 \cdot A_{\text{curb}} \cdot \gamma_{\text{rc}} = 6.528 \times 10^{-3}$$

Bracing (Per FST design calcs p.16)

$$\text{Bracing}_{\text{int}} := \frac{0.35}{1000} = 3.5 \times 10^{-4}$$

$$\text{Bracing}_{\text{ext}} := \frac{1}{2} \cdot \text{Bracing}_{\text{int}} = 1.75 \times 10^{-4}$$

For Deck Section 1

$$\text{BracingDC}_1 := 3 \cdot \text{Bracing}_{\text{int}} + 2 \cdot \text{Bracing}_{\text{ext}} = 1.4 \times 10^{-3}$$

For Deck Section 2

$$\text{BracingDC}_2 := 5 \cdot \text{Bracing}_{\text{int}} + 2 \cdot \text{Bracing}_{\text{ext}} = 2.1 \times 10^{-3}$$

Wearing Surface

$$t_{\text{ws}} := 80$$

$$\text{gamma}_{\text{asphalt}} := 140 \cdot \frac{16 \cdot 9.81}{10^{12}} = 2.197 \times 10^{-8}$$

For Deck Section 1

$$\text{width}_{\text{ws1}} := \text{Width}_{\text{deck1}} - 2 \cdot \text{width}_{\text{curb}} = 1.173 \times 10^4$$

$$A_{\text{ws1}} := \text{width}_{\text{ws1}} \cdot t_{\text{ws}} = 9.38 \times 10^5$$

$$\text{WearingDW}_1 := A_{\text{ws1}} \cdot \text{gamma}_{\text{asphalt}} = 0.021$$

For Deck Section 2

$$\text{width}_{\text{ws2}} := \text{Width}_{\text{deck2}} - 2 \cdot \text{width}_{\text{curb}} = 1.587 \times 10^4$$

$$A_{\text{ws2}} := \text{width}_{\text{ws2}} \cdot t_{\text{ws}} = 1.27 \times 10^6$$

$$\text{WearingDW}_2 := A_{\text{ws2}} \cdot \text{gamma}_{\text{asphalt}} = 0.028$$

## Total Factored DL Section 1

$$DC1 := \gamma_{DC} \cdot (\text{BeamDC}_1 + \text{DeckDC}_1 + \text{HaunchDC}_1 + \text{OverhangDC}_1 + \text{CurbDC} + \text{BracingDC}_1) = 0.109$$

$$DW1 := \gamma_{DW} \cdot \text{WearingDW}_1 = 0.031$$

## Total Factored DL Section 2 at North Abutment

$$DC2 := \gamma_{DC} \cdot (\text{BeamDC}_2 + \text{DeckDC}_2 + \text{HaunchDC}_2 + \text{OverhangDC}_2 + \text{CurbDC} + \text{BracingDC}_2) = 0.14$$

$$DW2 := \gamma_{DW} \cdot \text{WearingDW}_2 = 0.042$$

## Factored Load Per Girder:

Note: Wearing Surface, although calculated here, is not included because the element is not in model. The situation is similar to the railing, curb, and utilities, which are also not included in the dead load calculation.

## Section 1

$$w_{uDL1} := \frac{1}{6} \cdot (DC1) = 0.018$$

## Section 2 at North Abutment

$$w_{uDL2} := \frac{1}{8} \cdot (DC2) = 0.018$$



## Calculate Factored Live Loads Using Deck Section 1

(Units in kN and mm, u.o.n)

Calculate Live Load Distribution Factors for Moment, Interior Girder

(Bridge Design Code 4.6.2.2b)

$$E_b := 199.948$$

$$E_d := 26.7898$$

$$n := \frac{E_b}{E_d} = 7.464$$

$$I_{\text{beam\_in}} := 9754.189$$

$$e_{g\_in} := \frac{\left[ t_{\text{haunch\_int}} + \frac{1}{2} \cdot (t_{\text{deck}} + d_{\text{int}}) \right]}{25.4} = 24.055$$

$$A_{\text{int\_in}} := \frac{A_{\text{int}}}{25.4^2} = 46.965$$

$$K_g := n \cdot (I_{\text{beam\_in}} + A_{\text{int\_in}} \cdot e_{g\_in}^2) = 2.756 \times 10^5$$

$$\text{Length} := 23500 \qquad \text{Spacing}_{\text{int\_ft}} := \frac{\text{Spacing}_{\text{int}}}{25.4 \cdot 12} = 7.382$$

$$\text{Length}_{\text{ft}} := \frac{\text{Length}}{25.4 \cdot 12} = 77.1$$

$$m_{g_{\text{int\_1\_lane}}} := 0.06 + \left( \frac{\text{Spacing}_{\text{int\_ft}}}{14} \right)^{0.4} \cdot \left( \frac{\text{Spacing}_{\text{int\_ft}}}{\text{Length}_{\text{ft}}} \right)^{0.3} \cdot \left[ \frac{K_g}{12 \cdot \text{Length}_{\text{ft}} \cdot \left( \frac{t_{\text{deck}}}{25.4} \right)^3} \right]^{0.1} = 0.425$$

$$m_{g_{\text{int\_2\_lanes}}} := 0.075 + \left( \frac{\text{Spacing}_{\text{int\_ft}}}{9.5} \right)^{0.6} \cdot \left( \frac{\text{Spacing}_{\text{int\_ft}}}{\text{Length}_{\text{ft}}} \right)^{0.2} \cdot \left[ \frac{K_g}{12 \cdot \text{Length}_{\text{ft}} \cdot \left( \frac{t_{\text{deck}}}{25.4} \right)^3} \right]^{0.1} = 0.587$$

$$m_{g_{\text{int}}} := \max(m_{g_{\text{int\_1\_lane}}, m_{g_{\text{int\_2\_lanes}}}) = 0.587$$

Calculate Live Load distribution factor for Moment in exterior Beam (Using "level rule") (Units in kN, mm)

...Using Truck Load

$$\text{spacing}_{\text{wheel}} := 6 \cdot 12 \cdot 25.4 = 1.829 \times 10^3$$

$$\text{clear}_{\text{wheel}} := 1 \cdot 12 \cdot 25.4 = 304.8$$

$$d_{\text{left}} := \text{Spacing}_{\text{int}} + 732.5 - \text{width}_{\text{curb}} - \text{clear}_{\text{wheel}} = 2.183 \times 10^3$$

$$d_{\text{right}} := \text{Spacing}_{\text{int}} + 732.5 - \text{width}_{\text{curb}} - \text{clear}_{\text{wheel}} - \text{spacing}_{\text{wheel}} = 353.9$$

$$\text{Reaction}_{\text{wheel}} := \frac{(d_{\text{left}} + d_{\text{right}})}{\text{Spacing}_{\text{int}}} = 1.127$$

$$\text{Reaction}_{\text{axle}} := \frac{\text{Reaction}_{\text{wheel}}}{2} = 0.564$$

$$\text{mult}_{\text{pres}} := 1.2$$

$$\text{mg}_{\text{truck}_{\text{ext}}} := \text{mult}_{\text{pres}} \cdot \text{Reaction}_{\text{axle}} = 0.676$$

...Using Lane Load

$$\text{width}_{\text{lane}} := \text{Spacing}_{\text{int}} + 732.5 - \text{width}_{\text{curb}} = 2.487 \times 10^3$$

$$\text{width}_{\text{full}_{\text{lane}}} := 10 \cdot 12 \cdot 25.4 = 3.048 \times 10^3$$

$$\text{portion}_{\text{lane}} := \frac{\text{width}_{\text{lane}}}{\text{width}_{\text{full}_{\text{lane}}}} = 0.816$$

Check for 2 Lanes Loaded

$$\text{arm}_{\text{lane}} := \frac{\text{width}_{\text{lane}}}{2} = 1.244 \times 10^3$$

$$d_e := 732.5 - \text{width}_{\text{curb}} = 237.5$$

$$\text{Reaction}_{\text{lane}} := \frac{(\text{portion}_{\text{lane}} \cdot \text{arm}_{\text{lane}})}{\text{Spacing}_{\text{int}}} = 0.451$$

$$e_{\text{dist}} := 0.77 + \frac{\left(\frac{d_e}{25.4 \cdot 12}\right)}{9.1} = 0.856$$

$$\text{mg}_{\text{lane}_{\text{ext}}} := \text{mult}_{\text{pres}} \cdot \text{Reaction}_{\text{lane}} = 0.541$$

$$\text{mg}_{\text{ext}_{2\text{lanes}}} := e_{\text{dist}} \cdot \text{mg}_{\text{int}} = 0.502$$

$$\text{mg}_{\text{ext}} := \max(\text{mg}_{\text{truck}_{\text{ext}}}, \text{mg}_{\text{lane}_{\text{ext}}}, \text{mg}_{\text{ext}_{2\text{lanes}}}) = 0.676$$

Calculate Live Loads for Interior Girder

$$w_{\text{lane}} := 640 \cdot \frac{(0.454 \cdot 9.81)}{1000} \cdot \frac{1}{12 \cdot 25.4} = 9.352 \times 10^{-3}$$

$$w_{\text{u\_lane\_int}} := \gamma_{\text{LL}} \cdot m_{\text{gint}} \cdot w_{\text{lane}} = 9.602 \times 10^{-3}$$

$$P_{\text{front\_axle}} := 8000 \cdot \frac{(0.454 \cdot 9.81)}{1000} = 35.63$$

$$P_{\text{u\_int\_front\_axle}} := \gamma_{\text{LL}} \cdot m_{\text{gint}} \cdot P_{\text{front\_axle}} \cdot (1 + \text{IM}) = 48.657$$

$$P_{\text{rear\_axle}} := 32000 \cdot \frac{(0.454 \cdot 9.81)}{1000} = 142.52$$

$$P_{\text{u\_int\_rear\_axle}} := \gamma_{\text{LL}} \cdot m_{\text{gint}} \cdot P_{\text{rear\_axle}} \cdot (1 + \text{IM}) = 194.627$$

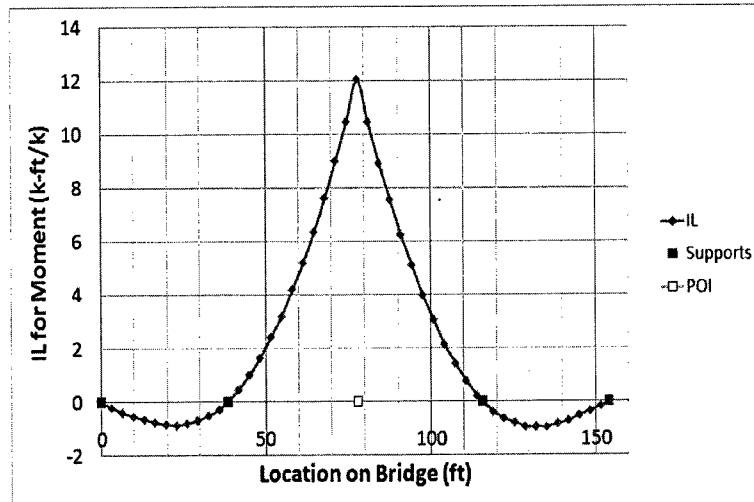
Calculate Live Loads for Exterior Girder

$$w_{\text{u\_lane\_ext}} := \gamma_{\text{LL}} \cdot m_{\text{gext}} \cdot w_{\text{lane}} \cdot 1000 = 11.07$$

$$P_{\text{u\_ext\_front\_axle}} := \gamma_{\text{LL}} \cdot m_{\text{gext}} \cdot P_{\text{front\_axle}} \cdot (1 + \text{IM}) = 56.095$$

$$P_{\text{u\_ext\_rear\_axle}} := \gamma_{\text{LL}} \cdot m_{\text{gext}} \cdot P_{\text{rear\_axle}} \cdot (1 + \text{IM}) = 224.381$$

Step 3. Calculate Maximum Moments,  $M_u$ , and Load Factors for Interior and Exterior Girders



Interior Girder

Exterior Girder

Moment Capacity

$$Capacity_{Int} = 6.15 \times 10^6 \text{ kN} - \text{mm}$$

$$Capacity_{Ext} = 7.414 \times 10^6 \text{ kN} - \text{mm}$$

Moment Due to DL

$$M_{uDead} := 5.44 \cdot 10^5 \text{ kN} - \text{mm}$$

$$M_{uDead} = 5.44 \times 10^5 \text{ kN} - \text{mm}$$

Moment Due to Patterned Live Load

$$M_{uInteriorLive} := 1.44 \cdot 10^6 \text{ kN} - \text{mm}$$

$$M_{uExteriorLive} := 1.66 \cdot 10^6 \text{ kN} - \text{mm}$$

Load Rating

$$RF_{int} := \frac{(Capacity_{Int} - M_{uDead})}{M_{uInteriorLive}} = 3.893$$

$$RF_{ext} := \frac{(Capacity_{Ext} - M_{uDead})}{M_{uExteriorLive}} = 4.138$$

## Step 5: Use Bridge Model to Calculate Load Ratings

## Model Dead Load

Multiply Self Weight of Model by Load Factor:

$$\gamma_{DC} = 1.25$$

## Lane Load for Area Elements

$$a_{lane} := 64 \cdot \frac{(0.454 \cdot 9.81)}{1000} \cdot \frac{1}{12^2 \cdot 25.4^2} = 3.068 \times 10^{-6} \text{ kN/mm}^2$$

$$a_{u\_laneSAP} := \gamma_{LL} \cdot a_{lane} = 5.369 \times 10^{-6} \text{ kN/mm}^2$$

## Truck Loads

$$P_{u\_frontSAP} := P_{front\_axle} \cdot \gamma_{LL} \cdot (1 + IM) = 82.929 \text{ kN}$$

$$P_{u\_rearSAP} := P_{rear\_axle} \cdot \gamma_{LL} \cdot (1 + IM) = 331.715 \text{ kN}$$

	Moment Due to DL	Moment Due to Patterned Live Load	Load Rating
Girder 1 (West Exterior)	$M_{uG1DeadSAP} := 710312$	$M_{uG1LiveSAP} := 1579997$	$RF_{G1SAP} := \frac{(Capacity_{Ext} - M_{uG1DeadSAP})}{M_{uG1LiveSAP}} = 4.243$
Girder 2	$M_{uG2DeadSAP} := 474449$	$M_{uG2LiveSAP} := 1210875$	$RF_{G2SAP} := \frac{(Capacity_{Int} - M_{uG2DeadSAP})}{M_{uG2LiveSAP}} = 4.687$
Girder 3	$M_{uG3DeadSAP} := 498906$	$M_{uG3LiveSAP} := 1291237$	$RF_{G3SAP} := \frac{(Capacity_{Int} - M_{uG3DeadSAP})}{M_{uG3LiveSAP}} = 4.376$
Girder 4	$M_{uG4DeadSAP} := 498907$	$M_{uG4LiveSAP} := 1291256$	$RF_{G4SAP} := \frac{(Capacity_{Int} - M_{uG4DeadSAP})}{M_{uG4LiveSAP}} = 4.376$
Girder 5	$M_{uG5DeadSAP} := 484363$	$M_{uG5LiveSAP} := 1210783$	$RF_{G5SAP} := \frac{(Capacity_{Int} - M_{uG5DeadSAP})}{M_{uG5LiveSAP}} = 4.679$
Girder 6 (East Exterior)	$M_{uG6DeadSAP} := 709904$	$M_{uG6LiveSAP} := 1579452$	$RF_{G6SAP} := \frac{(Capacity_{Ext} - M_{uG6DeadSAP})}{M_{uG6LiveSAP}} = 4.244$

## Total Bridge Dead Load Check at Midspan

$$M_{u\_Dead\_SAP\_Total} := M_{uG1DeadSAP} + M_{uG2DeadSAP} + M_{uG3DeadSAP} \dots = 3.377 \times 10^6$$

$$+ M_{uG4DeadSAP} + M_{uG5DeadSAP} + M_{uG6DeadSAP}$$

$$M_{u\_Dead\_Hand\_Total} := 6 \cdot M_{uDead} = 3.264 \times 10^6$$

## Total Bridge Live Load Check at Midspan

$$M_{u\_Live\_SAP\_Total} := M_{uG1LiveSAP} + M_{uG2LiveSAP} + M_{uG3LiveSAP} \dots = 8.164 \times 10^6$$

$$+ M_{uG4LiveSAP} + M_{uG5LiveSAP} + M_{uG6LiveSAP}$$

$$M_{u\_Live\_Hand\_Total} := 4 \cdot M_{uInteriorLive} + 2 \cdot M_{uExteriorLive} = 9.08 \times 10^6$$

## Summary

## Dead Load

Deck Section 1	Deck Section 2 (at north abutment)	Load Factor for SAP Self Weight
$w_{uDL1} = 0.018 \text{ kN/mm}$	$w_{uDL2} = 0.018 \text{ kN/mm}$	$\gamma_{DC} = 1.25$

## Live Load

Interior Girder	Exterior Girder	SAP Applied
$m_{g_{int}} = 0.587$	$m_{g_{ext}} = 0.676$	
$w_{u_{lane_{int}}} = 9.602 \times 10^{-3} \text{ kN/mm}$	$w_{u_{lane_{ext}}} = 11.07 \text{ kN/mm}$	$a_{u_{laneSAP}} = 5.369 \times 10^{-6} \text{ kN/mm}^2$
$P_{u_{int_{front_{axle}}} = 48.657 \text{ kN}$	$P_{u_{ext_{front_{axle}}} = 56.095 \text{ kN}$	$P_{u_{frontSAP}} = 82.929 \text{ kN}$
$P_{u_{int_{rear_{axle}}} = 194.627 \text{ kN}$	$P_{u_{ext_{rear_{axle}}} = 224.381 \text{ kN}$	$P_{u_{rearSAP}} = 331.715 \text{ kN}$

## Capacity

Interior Girder Capacity	Exterior Girder Capacity
$Capacity_{Int} = 6.15 \times 10^6 \text{ kN-mm}$	$Capacity_{Ext} = 7.414 \times 10^6 \text{ kN-mm}$

## Rating Factors

	Design Calcs	SAP
Girder 1	$RF_{ext} = 4.138$	$RF_{G1SAP} = 4.243$
Girder 2	$RF_{int} = 3.893$	$RF_{G2SAP} = 4.687$
Girder 3	$RF_{int} = 3.893$	$RF_{G3SAP} = 4.376$
Girder 4	$RF_{int} = 3.893$	$RF_{G4SAP} = 4.376$
Girder 5	$RF_{int} = 3.893$	$RF_{G5SAP} = 4.679$
Girder 6	$RF_{ext} = 4.138$	$RF_{G6SAP} = 4.244$

## APPENDIX G: INSTRUMENTATION LITERATURE





MADE IN JAPAN FOR OMEGA ENGINEERING, INC., STAMFORD, CT U.S.A.

TYPE KFG-5-350-C1-11L3M3R

GAGE FACTOR (24°C, 50%RH)	2.10 ± 1.0%	LOT No. Y2337S	BATCH 104A
GAGE LENGTH	5 mm	TEMPERATURE COEFFICIENT OF GAGE FACTOR	+0.008 %/°C
GAGE RESISTANCE(24°C, 50%RH)	351.2 ± 1.2 Ω	APPLICABLE GAGE CEMENT	CC-33A , EP-34B
ADOPTABLE THERMAL EXPANSION	11.7 PPM/°C	QUANTITY	10 P04

## PRE-WIRED STRAIN GAGES

### Strain Gage Instructions

- Follow adhesive instructions for proper mounting procedures. Silverish side with leads attached should be face up.
- After opening package, store in a cool dry place.
- If possible exercise gage prior to taking readings.
- When using a 2 wire strain gage, temperature changes will cause a zero shift beyond what is computed on the enclosed "Engineering Data Sheet" (When using a 3 wire gage, temperature changes will not affect zero drift.) For 2 wire gages compute the zero drift due to lead wire below ( $\epsilon_l$ ) and add it to the apparent strain on the enclosed "Data Sheet" to compensate for zero drift.
 
$$\epsilon_l = \frac{\tau \alpha \Delta T}{K_s R}$$

$\epsilon_l$  = Zero strain drift due to lead wire changing temperature.  
 $\tau$  = Resistance of lead wire alone exposed to a temperature change (ohms).  
 (Wire supplied is 0.22 ohms/meter, therefore if you have 2 leads, 1 meter long,  $\tau = (0.22)(1)(2) = 0.44$  ohms)  
 $\alpha$  = Resistance temperature coefficient of lead wires  
 (copper wire = 0.0038/°C)

R = Total resistance value of gage including lead wires (ohms)  
 (value on front of package).  
 $\Delta T$  = Temperature change (°C)  
 $K_s$  = Gage Factor =  $(R)/(K)(R - \tau)$   
 K = Total gage factor including lead wires (value on front of package).

Typical Example: 2 wire lead gage undergoing a 5°C change.  
 Lead wires are 1 meter long.

$$\epsilon_l = \frac{(0.44)(0.0038/°C)(5°C)}{(2.107)(120)} = \frac{33 \times 10^{-6} \text{ m/m}}{(33 \mu \epsilon)}$$

Where:

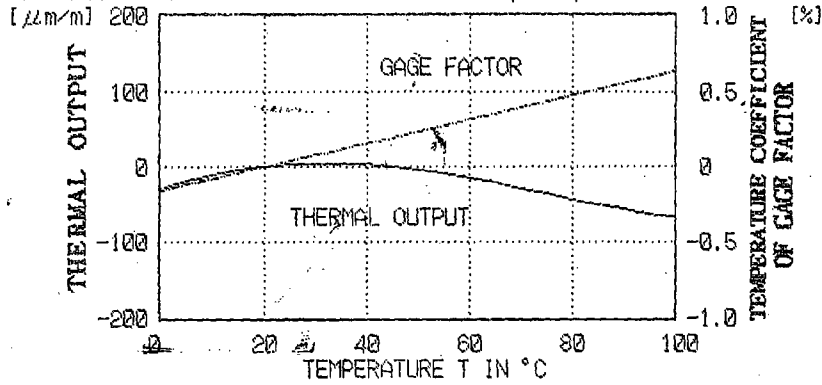
$$\begin{aligned} \tau &= 0.44 \text{ ohms} = (0.22)(1)(2) \\ \alpha &= 0.0038/°C \\ \Delta T &= 5°C \\ R &= 120 \text{ ohms} \\ K_s &= (R)/(K)(R - \tau) = (120)/(2.10)(120 - 0.44) = 2.107 \\ K &= 2.10 \end{aligned}$$



One Omega Drive, Box 4047, Stamford, CT 06907 U.S.A.  
 Phone: (203) 359-1660 FAX: (203) 359-7700

## ENGINEERING DATA SHEET

Gage type : KFG-5-350-C1-11L3M3R / Tested on : SS41  
 Lot No. : Y2337S Batch : 104A Exp. Temp. Coef. :  $11.7 \times 10^{-6} / ^\circ\text{C}$



$$\epsilon_{app} = -0.30 \times 10^{-2} + 0.22 \times 10^{-1} \times T^1 - 0.37 \times 10^{-1} \times T^2 - 0.14 \times 10^{-5} \times T^3 + 0.11 \times 10^{-5} \times T^4 \quad [\mu\text{m/m}]$$

Tolerance :  $\pm 0.85 [(\mu\text{m/m})/^\circ\text{C}]$  (Temperature changes by stages.)

For 2 wire gages the zero drift due to lead wire is added to above equation.

品-086

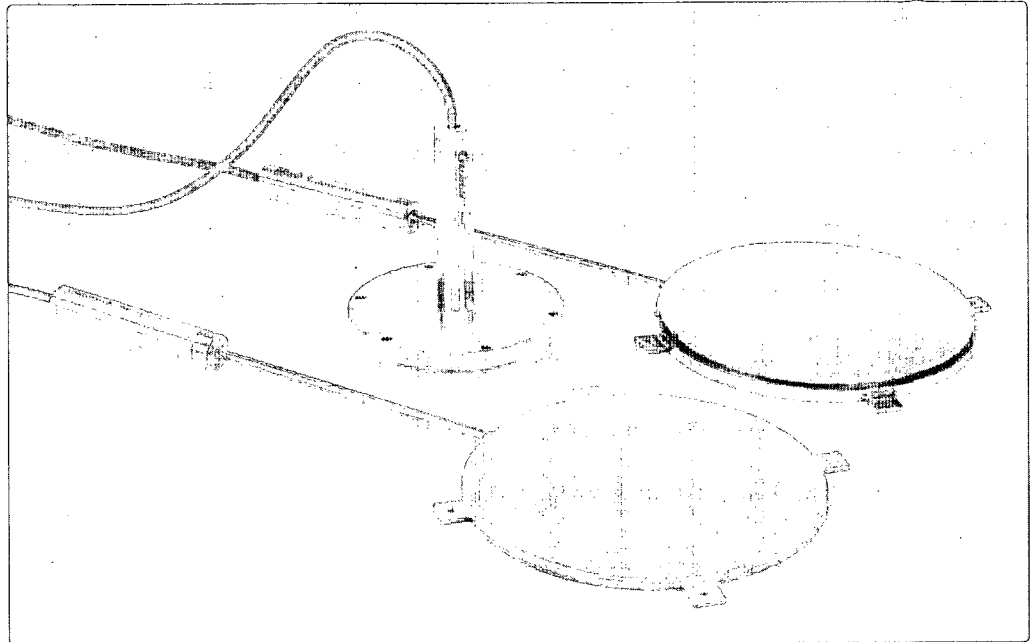
# Earth Pressure Cells

## Applications

Earth Pressure Cells provide a direct means of measuring total pressures, i.e. the combination of effective soil stress and pore water pressure, in or on...

- Bridge abutments
- Diaphragm walls
- Fills and embankments
- Retaining walls surfaces
- Sheet piling
- Slurry walls
- Tunnel linings

They may also be used to measure earth bearing pressures on foundation slabs and footings and at the tips of piles.



○ Model 4800 Earth Pressure Cell (front), Model 4820 Jackout Pressure Cell (center) and Model 4810 Contact Pressure Cell (rear).

## Operating Principle

Earth Pressure Cells are constructed from two stainless steel plates welded together around their periphery and separated by a narrow gap filled with hydraulic fluid. External pressures squeeze the two plates together creating an equal pressure in the internal fluid. A length of stainless steel tubing connects the fluid filled cavity to a pressure transducer that converts the fluid pressure into an electrical signal transmitted by cable to the readout location.

## Advantages & Limitations

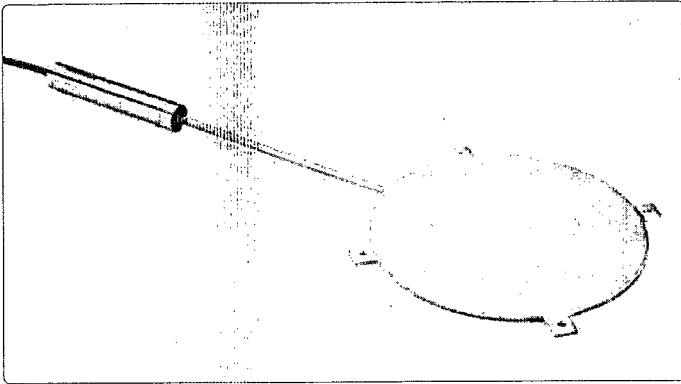
The 4800 Series Earth Pressure Cells use vibrating wire pressure transducers and thus have the advantages of long term stability, reliable performance with long cables and insensitivity to moisture intrusion. All models also include a thermistor for temperature measurements and a gas discharge tube for lightning protection. Where dynamic stress changes are to be measured a semiconductor type pressure transducer is substituted (see Model 3500).

Cell performance depends strongly on the surrounding soil properties. It would be prohibitively expensive to

calibrate a cell in the soil type specific to the application being contemplated. However, studies have shown that the most consistent cell performance is achieved using cells of maximum stiffness with aspect ratios  $D/t > 10$  ( $D$  is the diameter of the cell,  $t$  the thickness). With Geokon cells, maximum stiffness is achieved by using hydraulic oil with less than 2 ppm of dissolved gas and aspect ratios generally greater than 20 to 30. Tests on Geokon cells in various types of soil have shown that the cells over-register the soil pressure by less than 5 percent. This is probably no greater than the inherent variability of the soil pressure distribution in the ground.

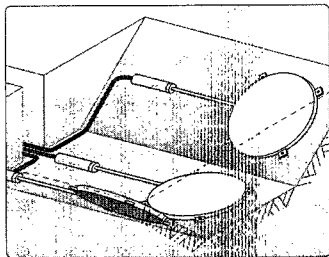
Typical of all closed hydraulic systems, earth pressure cells are sensitive to temperature changes which cause the internal fluid to expand at a different rate than the surrounding soil giving rise to spurious fluid pressure changes. The magnitude of the effect depends to a greater extent on the elasticity of the surrounding soil, i.e., on the degree of compaction and confinement, and is difficult to predict and correct for. The built-in thermistor is helpful in separating these spurious effects from real earth pressure changes.

## Model 4800 Earth Pressure Cells



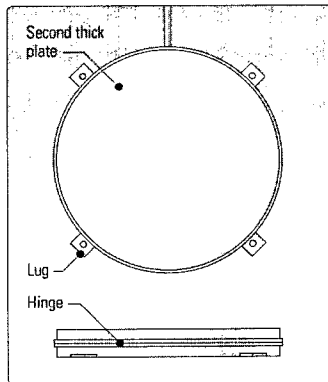
● Model 4800 Earth Pressure Cell.

Cells are constructed from two thin pressure sensitive plates. They can be positioned in the fill at different orientations so that soil pressures can be measured in two or three directions. Special armored cables are recommended in earth dam applications.



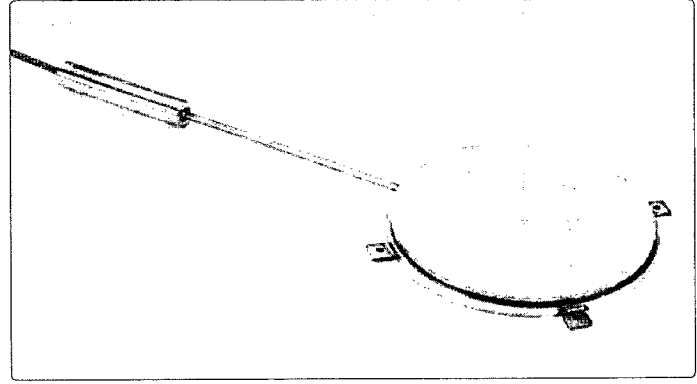
● Model 4800 Earth Pressure Cells installed in fill for soil pressure measurement in three directions.

A special cell modification that effectively reduces the severity of point loading is available for cells when used in granular materials. The modification uses two thick plates welded together at a flexible hinge that helps provide more uniform pressure distribution.



● Modified pressure cell, with two thick plates, for use in granular materials.

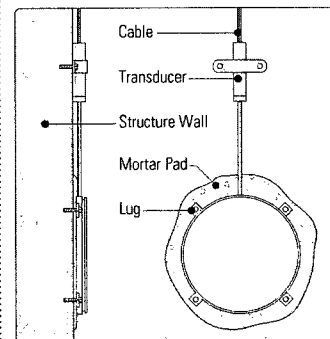
## Model 4810 Contact Pressure Cells



● Model 4810 Contact Pressure Cell for attachment to existing concrete surfaces.

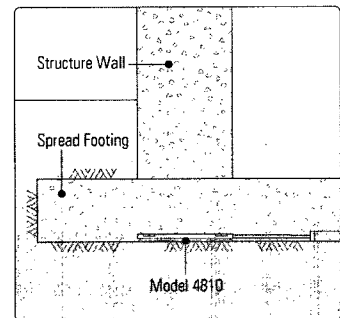
The Model 4810 Contact Pressure Cell is designed to measure soil pressures on structures. The backplate of the cell which bears against the external surface of the structure is thick enough to prevent the cell from warping. The other plate is thin and is welded to the backplate in a manner which creates a flexible hinge to provide maximum sensitivity to changing soil pressures.

Lugs on the side provide a means of mounting the cell to concrete forms or to steel or concrete surfaces. A mortar pad beneath the backplate ensures good contact with the structure surface. Cells are best installed flush with the surface to which they are attached. The fill material next to the cell should be screened to remove pieces larger than 10 mm.



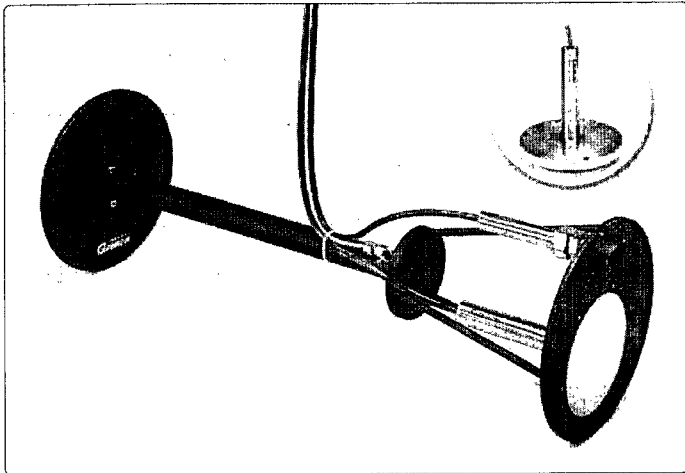
● Side and frontal views of the Model 4810 installed on existing structure.

Cells installed at the base of slabs and footings to measure bearing loads should always be positioned inside the concrete with the sensitive face pressed against the compacted fill. Cells placed in the fill below the concrete often become decoupled from the soil pressure due to the impossibility of adequately compacting the fill around the cell.



● Model 4810 installation in a spread footing.

### Model 4820 Jackout Pressure Cells

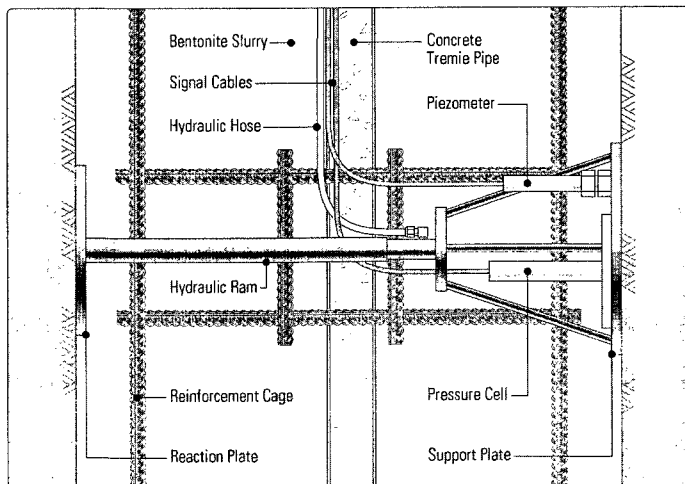


• Model 4820 shown in hydraulic ram assembly with piezometer and alone (inset).

The Jackout Pressure Cell is designed for installation in diaphragm walls (slurry walls) to monitor soil pressures on the walls as excavation proceeds. This allows the build-up of excessive pressures to be detected in time to take remedial measures.

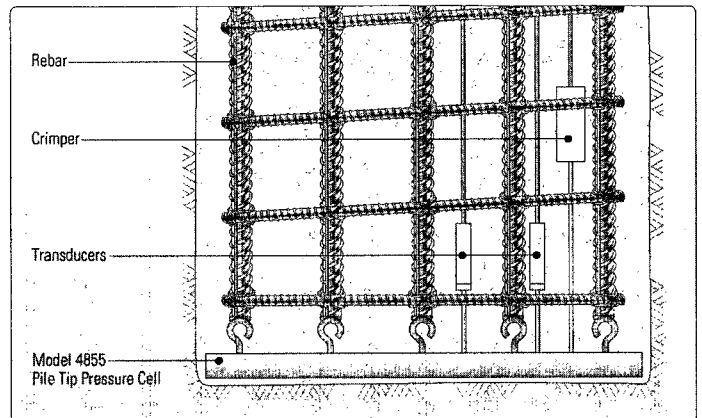
The Jackout Pressure Cell assembly consists of the cell mounted on a support plate, a reaction plate and a hydraulic ram. This assembly is attached, in its retracted position, to the reinforcement cage and is lowered into the slurry trench along

with the cage. When the cage is in position the hydraulic ram is extended by means of a hand pump situated at the top of the wall and connected to the ram by a hydraulic hose. Pressure is applied forcing the reaction plate and the cell against the walls of the trench. This pressure is maintained while the concrete is tremied into the trench and until the concrete cures. The cell may be supplemented by a piezometer attached to the support plate to measure pore water pressures.



• Jackout Pressure Cell assembly installed in diaphragm wall.

### Model 4855 Pile-Tip Pressure Cells

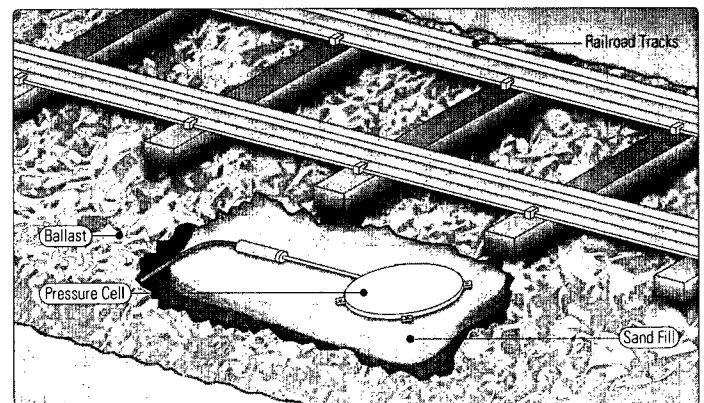


• Model 4855 Pile-Tip Pressure Cell installation

The Model 4855 Pile-Tip Load Cell is used to measure pile-tip loads in cast-in-place concrete piles (caissons). Like the Model 4810, the pile-tip pressure cell has a thick upper plate. The cell is manufactured to be close to the diameter of the pile and the back plate is supplied with hooks or sections of rebar to allow the cell to be connected to the bottom of

the reinforcement cage. Two vibrating wire pressure transducers are connected to the cell to provide some redundancy in the event that one transducer is damaged during installation. An added feature is a remote "crimping" mechanism to allow the cell to be inflated slightly so as to ensure good contact between the cell and the surrounding concrete.

### Model 3500 Series Earth Pressure Cells



• Model 3500 Earth Pressure Cell installed under railroad tracks.

The 3500 Series is similar in design to the 4800 Series but the vibrating wire transducer is replaced by a semi-conductor type transducer (to enable the measurement of dynamic pressures) which can have an output

of 2mV/V, 0-5VDC or 4-20mA. Typical applications are the measurement of traffic induced stresses on roadway sub grades, airport runways or under railroad tracks.

## Technical Specifications

	4800	4810	4820	4855	3500
Transducer Type	Vibrating Wire	Vibrating Wire	Vibrating Wire	Vibrating Wire	Semi-conductor
Output	2000-3000 Hz	2000-3000 Hz	2000-3000 Hz	2000-3000 Hz	2 mV/V, 0-5 VDC or 4-20 mA.
Standard Ranges <sup>1</sup>	0.35, 0.7, 1.7, 3.5, 5 MPa	0.35, 0.7, 1.7, 3.5, 5 MPa	0.35, 0.7, 1.7, 3.5, 5 MPa	3.5, 5, 7, 10.5 MPa	0-0.1, 0.2, 0.42, 0.7, 1.5, 3.5, 7 MPa
Resolution	±0.025% F.S.	±0.025% F.S.	±0.025% F.S.	±0.025% F.S.	Infinite
Accuracy <sup>2</sup>	±0.1% F.S.	±0.1% F.S.	±0.1% F.S.	±0.1% F.S.	±0.5% F.S.
Linearity	< 0.5% F.S.	< 0.5% F.S.	< 0.5% F.S.	< 0.5% F.S.	< 0.5% F.S.
Thermal Effect on Zero	< 0.05% F.S.	< 0.05% F.S.	< 0.05% F.S.	< 0.05% F.S.	< 0.05% F.S.
Typical Long-Term Drift	< 0.02% F.S./yr	< 0.02% F.S./yr	< 0.02% F.S./yr	< 0.02% F.S./yr	< ±0.02% F.S./yr
Standard Cell Dimensions <sup>3</sup> (HxD)	6 x 230 mm	12 x 230 mm	12 x 150 mm	25 x varies	12 x 230 mm
Transducer Dimensions (LxD)	150 x 25 mm	150 x 25 mm	150 x 25 mm	150 x 25 mm	150 x 32 mm
Excitation Voltage	2.5-12 v swept square wave	2.5-12 v swept square wave	2.5-12 v swept square wave	2.5-12 v swept square wave	10 v maximum
Material	304 Stainless Steel	304 Stainless Steel	304 Stainless Steel	304 Stainless Steel	304 Stainless Steel
Temperature Range <sup>1</sup>	-20°C to +80°C	-20°C to +80°C	-20°C to +80°C	-20°C to +80°C	-20°C to +80°C

**Note: PSI = kPa x 0.14503, or MPa x 145.03**

<sup>1</sup>Other ranges available on request.

<sup>2</sup>Calibrated accuracy of the pressure sensor.

<sup>3</sup>Other sizes available on request.



Geokon, Incorporated  
 48 Spencer Street  
 Lebanon, NH 03766  
 USA

222

☎ 1 • 603 • 448 • 1562  
 ☎ 1 • 603 • 448 • 3216  
 ✉ geokon@geokon.com  
 🌐 www.geokon.com

# THERMISTOR COMPONENTS

**T**hermistors from YSI provide highly accurate and stable temperature sensing for measurement, control, indication, and compensation. Tight interchangeability of our precision components allows precise measurement without calibration of circuitry to match individual components.

YSI Precision Thermistors are offered in six series that differ from each other by:

- the encapsulated material around the component,
- component leads,
- working temperature range, and
- interchangeability tolerances.

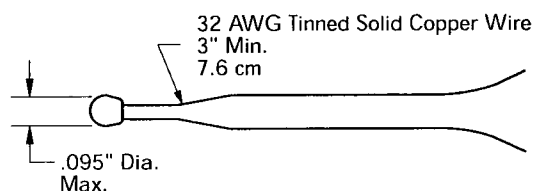
YSI thermistors are fabricated using proprietary processes to achieve highly accurate stable thermistors with each production lot. Comparing stability and accuracy specifications will highlight the advantages of the YSI process. When accuracy is important, there is only one choice - YSI.

## YSI 44000 Series Epoxy-Encapsulated for General Use

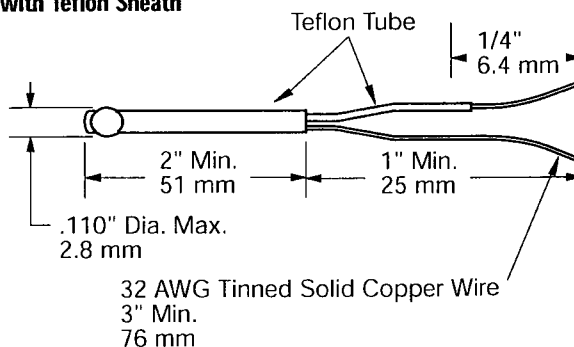
## YSI 44100 Series with Teflon Sheath for Harsh Environments

The YSI 44000 Series are epoxy encapsulated and designed for applications where cost, flexibility, and a wide range of resistance values are important. They are available in both  $\pm 0.2^{\circ}\text{C}$  and  $\pm 0.1^{\circ}\text{C}$  interchangeability tolerances. The YSI 44100 Series teflon-sheathed thermistors allow exposure to hostile environments such as conductive or corrosive liquids and particulate suspensions. 44100 Series is available with various resistances in  $\pm 0.2^{\circ}\text{C}$  tolerances.

### YSI 44000 Series Thermistors



### YSI 44100 Series Thermistors with Teflon Sheath



## Specifications

**Time Constant:** 1 sec. max for standard thermistors, 2.5 sec. max for Teflon-sheathed thermistors, when suspended by their leads in a well-stirred oil bath. In still air, 10 sec. max for standard thermistors, 25 sec. max for Teflon-sheathed thermistors.

**Dissipation Constant:** 8 mW/°C min when suspended by their leads in a well-stirred oil bath, or 1 mW/°C in still air.

**Stability:** YSI thermistors are chemically stable and not significantly affected by aging or exposure to strong nuclear radiation. The table below shows typical stability for a representative thermistor, the YSI 44005.

Operating Temperature	Typical Thermometric Drift	
	10 months	100 months
0°C	< 0.01°C	< 0.01°C
25°C	< 0.01°C	< 0.02°C
100°C	0.20°C	0.32°C
150°C	1.5°C	not recommended

**Resistance/Temperature Data:** A °C/°F resistance versus temperature table in 1°C increments is in the *YSI Precision™ Temperature Handbook*, or visit [www.YSI.com](http://www.YSI.com).

**Interchangeability Tolerance Data:** Tables in the *Handbook* show nominal resistance values, ohms per degree, and tolerance at select temperatures over the operating range.

**Temperature Probe Assemblies:** YSI 44000 Series Thermistors may be installed in many of the probes described in the Configure-to-Order Probe section of this catalog.

**Maximum Power:** 30 mW at 25°C to 1 mW at 125°C short-term.

	Ordering Part Numbers		Zero Power Resistance Ω at 25°C	Beta 0-50°C (K)	Ratio Ω 25/125°C	Maximum Working Temperature	Best Storage & Working Temperature	Mix	
	Standard	Teflon							
±0.2°C Interchangeability Tolerance 0 to 70°C	44001A	44101A	100	2854	11.49	100°C	-80+50°C	L	
	44002A	44102A	300	3118	15.15	100°C	-80+50°C	L	
	44003A	44103A	1000	3271	17.33	100°C	-80+50°C	L	
	44004	44104	2252	3891	29.26	150°C	-80+120°C	B	
	44005	44105	3000	3891	29.26	150°C	-80+120°C	B	
	44007	44107	5000	3891	29.26	150°C	-80+120°C	B	
	44017	44117	6000	3891	29.26	150°C	-80+120°C	B	
	44016	44116	10K	3891	29.26	150°C	-80+120°C	B	
	44006	44106	10K	3574	23.51	150°C	-80+120°C	H	
	44008	44108	30K	3810	29.15	150°C	-80+120°C	H	
	44011	44111	100K	3988	34.82	150°C	-80+120°C	H	
	44014	44114	300K	4276	46.02	150°C	-80+120°C	H	
	44015	44115	1 meg	4582	61.96	150°C	-80+120°C	H	
	±0.1°C Interchangeability Tolerance 0 to 70°	44035	-	1000	3271	17.33	100°C	-80+50°C	L
		44033	-	2252	3891	29.26	150°C	-80+75°C	B
44030		-	3000	3891	29.26	150°C	-80+75°C	B	
44034		-	5000	3891	29.26	150°C	-80+75°C	B	
44037		-	6K	3891	29.26	150°C	-80+75°C	B	
44036		-	10K	3891	29.26	150°C	-80+75°C	B	
44031		-	10K	3574	23.51	150°C	-80+75°C	H	
44032		-	30K	3810	29.15	150°C	-80+75°C	H	

## Temperature Tip

### What is Meant by Interchangeability?

The term interchangeability refers to how accurately thermistors track a nominal resistance curve. In the case of a ±0.2°C part, through all portions of the interchangeable range, the part is within ±0.2°C of the nominal value for that part. This term is sometimes confused with accuracy. Keep in mind the ±0.2°C figure only refers to the nominal curve; absolute accuracy for thermistor at a measured temperature is significantly better. Refer to the *YSI Precision™ Temperature Handbook* or visit [www.YSI.com](http://www.YSI.com) for more information.

### How to Order

Please order from your YSI representative or YSI Customer Service.

Call 937 427-1231 ext. 770



# *i Site-HS*

## Remote Instrumentation Monitoring System for Structural Health Monitoring

the latest technology for collecting data  
from field sensors at high speed

>>>> *get rid of wires*

> *collect data from remote locations*

>>>> *reduce errors*

>>>> *lower costs*

§ **remote  
acquisition of  
instrumentation  
data at high  
speed**

The *i Site-HS* system is designed for high speed monitoring applications where the user needs access to data from remote instrumentation quickly and inexpensively. The system consists of standalone dataloggers which take and store readings at programmed intervals up to 1,000 readings per second per channel. Units are networked with Ethernet connections. By connecting the units through a switch to a G3 cell modem, data can be streamed to a remote location at up to maximum speed of the modem. Alternately units may be connected to an onsite computer with WiFi modules attached to each data logger. Software operating on a networked workstation can receive data in a streaming mode and save to files. The only limit to the number of dataloggers placed into the network is communications bandwidth of the network to download the data. Any channel on any datalogger can be remotely configured using the included software.

§ **works with most  
sensors using DC  
excitation**

The *i Site-HS* system can be programmed to run multiple data logging sessions simultaneously. A common use of this option is to run one session to log readings of each sensor every hour over a long time period; then run a second session to take readings at a high sampling rate when a trigger is set. High speed data logging can be controlled by (1) reading on any sensor exceeding a preset threshold value, an external trigger that sets one of the digital inputs high, or a preset start time.

§ **8 analog inputs  
per logger**

The datalogger is housed in a NEMA-4 plastic enclosure that provides protection against moisture. One version provides push pin connectors with through-box gland cable connectors to allow direct connection of sensor cables. The other version provides Amphenol bayonet connectors on the exterior of the enclosure for plug type connection of sensors to the data logger.

§ **expandable to  
unlimited cells  
per remote  
network**

The *i Site* system is compatible with any sensor with dc voltage output of up to  $\pm 2.5$  volts, including strain gages. Each datalogger can excite and read up to eight sensors. The unit provides sensor excitation that is adjustable by software between 5 and 10 VDC for each channel. An option provides built-in, three-staged lightning and surge protection on each sensor. All components, including options, are preassembled inside the weather resistant NEMA 4 metal enclosure. Installation is simple and quick. Adjust the excitation level by software to that required by a particular sensor and connect the sensor. Install the unit. Set the reading interval and initiate data logging.

§ **easy installation**

§ **gets rid of wires  
and saves money**

The *i Site-HS* removes the need for wires connecting sensors to a central data logging unit. This greatly lowers the materials and installation costs for most field monitoring applications. The *i Site-HS* is useful in many field monitoring applications that use DC based sensors and require high speed data logging. Some of these include monitoring structural loads and strains, effects of impact loads, effects of extreme weather events, vibrations and blast monitoring.

See [www.geocomp.com](http://www.geocomp.com) or  
[www.iSiteCentral.com](http://www.iSiteCentral.com) for  
more information about this  
product.

GEOCOMP Corporation  
1145 Massachusetts Ave.  
Boxborough, MA 01719

TEL 978-635-0012  
FAX 978-635-0266  
email: [isite@geocomp.com](mailto:isite@geocomp.com)

# i Site-HS Remote Data Acquisition System Specifications

## INPUTS

### NUMBER OF CHANNELS

8 differential, individually configured.

### ANALOG INPUTS

ACCURACY:  $\pm 0.002\%$  of FSR (-40E to 85EC)

### RANGE AND RESOLUTION

Software selected by channel

Input Range (mV) Resolution ( $\mu$ V)

$\pm 2500$	0.15
$\pm 1250$	0.075
$\pm 625$	0.037
$\pm 313$	0.019
$\pm 156$	0.009
$\pm 78$	0.005
$\pm 39$	0.002
$\pm 20$	0.001

### SAMPLE RATES FOR RESOLUTION

16 bits at 1,000 Hz

18 bits at 150 Hz

### SAMPLING FREQUENCY

Programmable from 25 to 1,000 Hz in high speed mode. User programmable from 1 per day to 25 Hz in normal sampling mode.

### INPUT POLARITY

user programmable unipolar or bipolar

### A/D OUTPUT NOISE

3mV at 2 gain and 150 Hz sampling

6mV at 2 gain and 1,000 Hz sampling

0.2mV at 128 gain and 150 Hz sampling

0.6mV at 128 gain and 1,000 Hz sampling

### NOISE FREE RESOLUTION

17 bits at 2 gain and 150 Hz sampling

16 bits at 2 gain and 1,000 Hz sampling

15 bits at 128 gain and 150 Hz sampling

14 bits at 128 gain and 1,000 Hz sampling

### COMMON MODE REJECTION

1.2 to 4.05 volts

### DC COMMON MODE REJECTION

120 dB

### INPUT CURRENT

0.5 nA for gain $\geq$ 1

### INPUT RESISTANCE

2.5 Gohms typical

### SENSOR EXCITATION

Programmable per channel 5-10 VDC, 100 mA maximum

## DIGITAL INPUT/OUTPUT

4 lines programmable for input or output

## CPU AND INTERFACE

PROCESSOR: ARM 9

## PROGRAM STORAGE

512 Kbytes

## DATA STORAGE

4 Mbytes FLASH with zero power backup with circular FIFO storage

## ALARMS

User programmable high and low on each input channel

## PERIPHERAL INTERFACE

Ethernet using 100 Mbit TCP/IP protocol

## CLOCK ACCURACY

$\pm 1$  minute per month

## OPERATING TEMPERATURE

-25E to +60EC

## BATTERY BACKUP

CR1225 lithium battery for clock 220 with mAh for up to 2 months reserve

## TYPICAL CURRENT DRAIN

70 mA

## EXTERNAL POWER SOURCE

12 to 18 VDC or 9 to 12 VAC

## SENSOR CONNECTORS

MIL-C-26482 12-10 size circular bayonet lock connector, or Molex push pin header

## ENCLOSURE

NEMA 4 plastic with lock cover

SIZE: 13.1 x 11.3 x 7.3 inches

333 x 287 x 185 mm

5 lb (3.2 kgm)

## LIGHTENING AND SURGE

### PROTECTION (optional)

1<sup>st</sup> stage: tripolar plasma surge arrestors

2<sup>nd</sup> stage: SiDactor™ medium voltage

surge arrestors

3<sup>rd</sup> stage: SiDactor™ low voltage surge arrestors

## REMOTE ACCESS

TCP/IP via wired Ethernet

Optional WiFi using IP access point

Optional IP cell phone

## WARRANTY

Three years against defects in materials and workmanship. Damage from abuse, misuse or direct lightning strike excluded.

Specifications subject to change without prior written notice. Visit [www.Geocomp.com](http://www.Geocomp.com) for most up-to-date information. Customized units can be built to order in many but not all cases.

# iSite Remote monitoring systems: real-time Web access for your critical data needs

*iSite is designed for monitoring applications where the user needs Web-accessible data from remote instrumentation reliably, easily and cost-effectively. A "plug-and-work" system compatible with virtually any sensor with DC excitation, including digital, analog, strain gage or vibrating-wire – iSite is flexible and easy to install.*

The iSite system consists of stand-alone loggers that take and store sensor data on demand or at programmed intervals. Loggers are networked wirelessly through our proprietary Remote Area Network (RAN). Any sensor can be reached from any location within the network. The RAN can be accessed via an RS232 serial port, or through a landline, cell-phone or satellite connection, providing a seamless gateway to iSiteCentral.

Authorized users can log-on to iSiteCentral anywhere, anytime to access their critical data using a standard Web browser. Our automated data-reduction system turns raw data into knowledge you can use, with output in graph, table, or spreadsheet form. The iSite alarm option provides immediate notification of potential issues by mobile phone, e-mail, or pager. All data are safely stored and backed up on redundant and robust iSiteCentral servers.

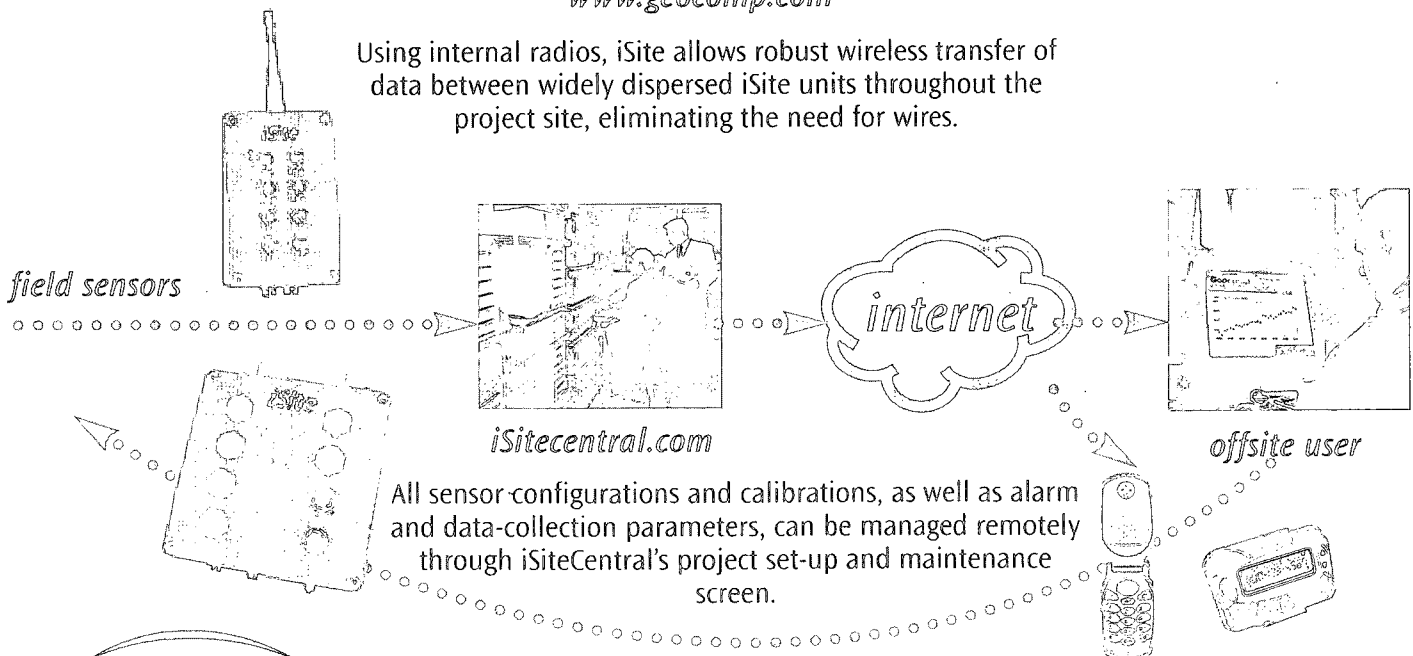
iSite removes the need for wires connecting sensors to a central data-logging unit. This greatly lowers the materials and installation costs for most field-monitoring applications. iSiteCentral's real-time Web access also eliminates the need to send employees to remote sites for data collection or to change instrument-reporting parameters.

## OEM Customers

iSite and iSiteCentral can be private-labeled for manufacturers of a wide range of structural and environmental sensors. This enables you to offer your customers the latest in logger technology and real-time Web access to critical data captured by your sensors, without requiring you to invest in new technology or data-storage centers.

[www.geocomp.com](http://www.geocomp.com)

Using internal radios, iSite allows robust wireless transfer of data between widely dispersed iSite units throughout the project site, eliminating the need for wires.



All sensor-configurations and calibrations, as well as alarm and data-collection parameters, can be managed remotely through iSiteCentral's project set-up and maintenance screen.

Geocomp  
1145 Massachusetts Avenue  
Boxborough, MA 01719 USA  
978 635 0012 Tel  
978 635 0266 Fax  
www.geocomp.com

Geocomp  
products

*Site specifications at a glance. Contact Geocomp or visit our Web site for complete product specifications.*

#### INPUTS

NUMBER OF CHANNELS: Up to 96 differential, individually configured.

#### ANALOG INPUTS

SAMPLE AND STORE: 1 per 5 seconds

SAMPLING FREQUENCY: user programmable from 3.75 to 15 Hz  
INPUT GAIN: user programmable for values of 1, 2, 4, 8, 16, 32 and 64

SENSOR EXCITATION: 5-10 Vdc programmable for each channel; 100 mA maximum

#### FREQUENCY INPUTS

SAMPLE RATE: 16 kHz

MAXIMUM FREQUENCY: 8 kHz

MINIMUM FREQUENCY: 400 Hz

#### GPU AND INTERFACE

PROCESSOR: WINBOND W77LE58

PROGRAM STORAGE: 32 Kbytes

DATA STORAGE: 512-Kbytes FLASH with zero power backup aa and circular

FIFO storage (4 Mbytes optional)

ALARMS: User programmable high and low on each input channel

PERIPHERAL INTERFACE: RS232 using 38,000-baud ASCII protocol with one start bit, one stop bit, eight data bits, no parity.

OPERATING TEMP: -25° to +80°C

MAIN INTERNAL BATTERY: 3.6 Vdc 7000 mAh NiMH rechargeable

TYPICAL CURRENT DRAIN: 50 mA continuous

EXTERNAL CHARGING POWER SOURCE: 7.5 to 20 Vdc

OPTIONAL CHARGERS: AC/DC adaptor, 12 volt battery, or solar panel

#### SENSOR CONNECTORS

Hirose SR30 miniature, MIL-C-26482 12-10 S circular bayonet lock connector or Phoenix contact connector

#### ENCLOSURE SIZE:

7.8 x 7.8 x 4.7 inches

195 x 195 x 120 mm

7.1 lbs (3.2 kgm)

or

4.7 x 3.1 x 2.4 inches

120 x 78 x 60 mm

1.7 lbs (.8 kgm)

#### LIGHTNING AND SURGE PROTECTION (optional)

1st stage: tripolar plasma surge arrestors

2nd stage: SiDactor™ medium voltage surge arrestors

3rd stage: SiDactor™ low voltage surge arrestors

#### RADIO TRANSCIVER (optional)

FREQUENCY: 916 MHz ISM band

916 MHz spread spectrum

2.4 GHz spread spectrum

INTERFERENCE: Collision detection, automatic retry with a error checking

ANTENNA: 3 dB gain tamper proof

#### REMOTE ACCESS COMMUNICATIONS (optional)

-CDMA cell module

-GSM tri-band world-wide cell module

-Land-line modem module

## About Geocomp

Geocomp Products – provides and supports remote-monitoring systems that enable real-time, Web-based access to critical data from structural- and environmental-monitoring instruments at sites worldwide. We also supply automated lab-testing systems to government, industrial, and university labs

Geocomp Consulting – provides comprehensive services to identify, manage, and mitigate underground risk to clients across the United States and around the globe

Geotesting Express – GTX, our sister company, performs a complete range of mechanical- and physical-properties tests on all materials used in underground construction. GTX specializes in lab- and field-testing of soil, rock, geosynthetics, and other geo-materials

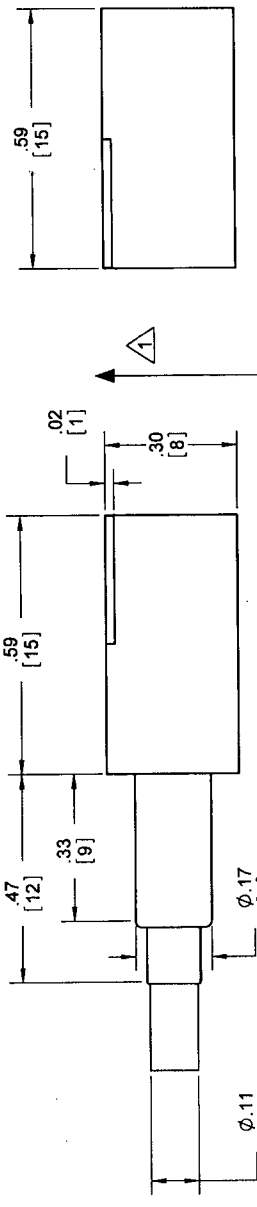
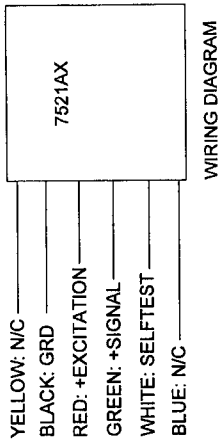
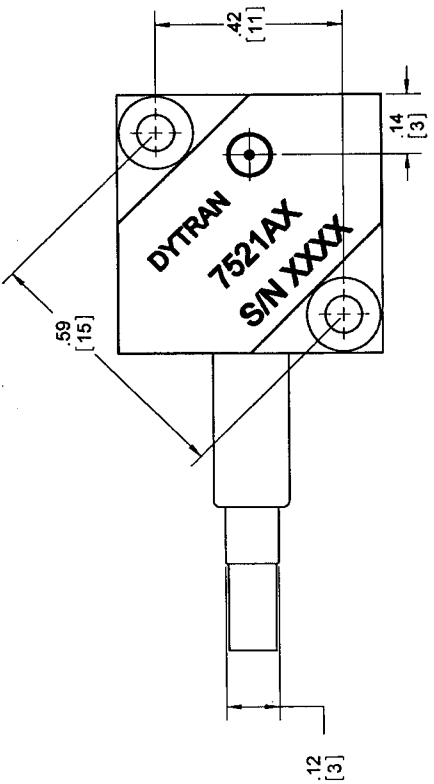
127-7521A <sup>REV</sup> 1 <sup>REV</sup> C

**PROPRIETARY AND CONFIDENTIAL**

THE INFORMATION CONTAINED IN THIS DRAWING IS THE SOLE PROPERTY OF DYTRAN INSTRUMENTS INC. ANY REPRODUCTION OR TRANSMISSION OF THIS DRAWING WITHOUT THE WRITTEN PERMISSION OF DYTRAN INSTRUMENTS INC IS PROHIBITED.

**REVISIONS**

REV.	ECN	DESCRIPTION	BY/DATE	CHK	APPR
A	5112	INITIAL RELEASE	03/07/08	CES	PML
B	5263	REVISED POLARITY MARKING	JS 06/05/08 DV	RA	DV
C	5547	SEE ECN	01/05/09	AMS	<i>DV</i>



7521A1	550mV/g
7521A2	280mV/g
7521A3	93mV/g
7521A4	55mV/g
7521A5	36mV/g
7521A6	18mV/g
7521A7	8mV/g

DRILL HOLE SIZE	TOLERANCE
0135 THRU .175	+ .004 / - .001
.190 THRU .250	+ .005 / - .001
.250 THRU .500	+ .006 / - .001
.500 THRU .750	+ .007 / - .001
.750 THRU 1.000	+ .007 / - .001
1.000 THRU 2.000	+ .007 / - .001
2.000 THRU 3.000	+ .007 / - .001
3.000 THRU 4.000	+ .007 / - .001
4.000 THRU 5.000	+ .007 / - .001
5.000 THRU 6.000	+ .007 / - .001
6.000 THRU 8.000	+ .007 / - .001
8.000 THRU 10.000	+ .007 / - .001
10.000 THRU 12.000	+ .007 / - .001
12.000 THRU 14.000	+ .007 / - .001
14.000 THRU 16.000	+ .007 / - .001
16.000 THRU 18.000	+ .007 / - .001
18.000 THRU 20.000	+ .007 / - .001
20.000 THRU 24.000	+ .007 / - .001
24.000 THRU 28.000	+ .007 / - .001
28.000 THRU 32.000	+ .007 / - .001
32.000 THRU 36.000	+ .007 / - .001
36.000 THRU 40.000	+ .007 / - .001
40.000 THRU 48.000	+ .007 / - .001
48.000 THRU 56.000	+ .007 / - .001
56.000 THRU 64.000	+ .007 / - .001
64.000 THRU 72.000	+ .007 / - .001
72.000 THRU 80.000	+ .007 / - .001
80.000 THRU 96.000	+ .007 / - .001
96.000 THRU 112.000	+ .007 / - .001
112.000 THRU 128.000	+ .007 / - .001
128.000 THRU 144.000	+ .007 / - .001
144.000 THRU 160.000	+ .007 / - .001
160.000 THRU 192.000	+ .007 / - .001
192.000 THRU 224.000	+ .007 / - .001
224.000 THRU 256.000	+ .007 / - .001
256.000 THRU 288.000	+ .007 / - .001
288.000 THRU 320.000	+ .007 / - .001
320.000 THRU 384.000	+ .007 / - .001
384.000 THRU 448.000	+ .007 / - .001
448.000 THRU 512.000	+ .007 / - .001
512.000 THRU 576.000	+ .007 / - .001
576.000 THRU 640.000	+ .007 / - .001
640.000 THRU 704.000	+ .007 / - .001
704.000 THRU 768.000	+ .007 / - .001
768.000 THRU 832.000	+ .007 / - .001
832.000 THRU 896.000	+ .007 / - .001
896.000 THRU 960.000	+ .007 / - .001
960.000 THRU 1024.000	+ .007 / - .001
1024.000 THRU 1088.000	+ .007 / - .001
1088.000 THRU 1152.000	+ .007 / - .001
1152.000 THRU 1216.000	+ .007 / - .001
1216.000 THRU 1280.000	+ .007 / - .001
1280.000 THRU 1344.000	+ .007 / - .001
1344.000 THRU 1408.000	+ .007 / - .001
1408.000 THRU 1472.000	+ .007 / - .001
1472.000 THRU 1536.000	+ .007 / - .001
1536.000 THRU 1600.000	+ .007 / - .001
1600.000 THRU 1664.000	+ .007 / - .001
1664.000 THRU 1728.000	+ .007 / - .001
1728.000 THRU 1792.000	+ .007 / - .001
1792.000 THRU 1856.000	+ .007 / - .001
1856.000 THRU 1920.000	+ .007 / - .001
1920.000 THRU 1984.000	+ .007 / - .001
1984.000 THRU 2048.000	+ .007 / - .001
2048.000 THRU 2112.000	+ .007 / - .001
2112.000 THRU 2176.000	+ .007 / - .001
2176.000 THRU 2240.000	+ .007 / - .001
2240.000 THRU 2304.000	+ .007 / - .001
2304.000 THRU 2368.000	+ .007 / - .001
2368.000 THRU 2432.000	+ .007 / - .001
2432.000 THRU 2496.000	+ .007 / - .001
2496.000 THRU 2560.000	+ .007 / - .001
2560.000 THRU 2624.000	+ .007 / - .001
2624.000 THRU 2688.000	+ .007 / - .001
2688.000 THRU 2752.000	+ .007 / - .001
2752.000 THRU 2816.000	+ .007 / - .001
2816.000 THRU 2880.000	+ .007 / - .001
2880.000 THRU 2944.000	+ .007 / - .001
2944.000 THRU 3008.000	+ .007 / - .001
3008.000 THRU 3072.000	+ .007 / - .001
3072.000 THRU 3136.000	+ .007 / - .001
3136.000 THRU 3200.000	+ .007 / - .001
3200.000 THRU 3264.000	+ .007 / - .001
3264.000 THRU 3328.000	+ .007 / - .001
3328.000 THRU 3392.000	+ .007 / - .001
3392.000 THRU 3456.000	+ .007 / - .001
3456.000 THRU 3520.000	+ .007 / - .001
3520.000 THRU 3584.000	+ .007 / - .001
3584.000 THRU 3648.000	+ .007 / - .001
3648.000 THRU 3712.000	+ .007 / - .001
3712.000 THRU 3776.000	+ .007 / - .001
3776.000 THRU 3840.000	+ .007 / - .001
3840.000 THRU 3904.000	+ .007 / - .001
3904.000 THRU 3968.000	+ .007 / - .001
3968.000 THRU 4032.000	+ .007 / - .001
4032.000 THRU 4096.000	+ .007 / - .001
4096.000 THRU 4160.000	+ .007 / - .001
4160.000 THRU 4224.000	+ .007 / - .001
4224.000 THRU 4288.000	+ .007 / - .001
4288.000 THRU 4352.000	+ .007 / - .001
4352.000 THRU 4416.000	+ .007 / - .001
4416.000 THRU 4480.000	+ .007 / - .001
4480.000 THRU 4544.000	+ .007 / - .001
4544.000 THRU 4608.000	+ .007 / - .001
4608.000 THRU 4672.000	+ .007 / - .001
4672.000 THRU 4736.000	+ .007 / - .001
4736.000 THRU 4800.000	+ .007 / - .001
4800.000 THRU 4864.000	+ .007 / - .001
4864.000 THRU 4928.000	+ .007 / - .001
4928.000 THRU 4992.000	+ .007 / - .001
4992.000 THRU 5056.000	+ .007 / - .001
5056.000 THRU 5120.000	+ .007 / - .001
5120.000 THRU 5184.000	+ .007 / - .001
5184.000 THRU 5248.000	+ .007 / - .001
5248.000 THRU 5312.000	+ .007 / - .001
5312.000 THRU 5376.000	+ .007 / - .001
5376.000 THRU 5440.000	+ .007 / - .001
5440.000 THRU 5504.000	+ .007 / - .001
5504.000 THRU 5568.000	+ .007 / - .001
5568.000 THRU 5632.000	+ .007 / - .001
5632.000 THRU 5696.000	+ .007 / - .001
5696.000 THRU 5760.000	+ .007 / - .001
5760.000 THRU 5824.000	+ .007 / - .001
5824.000 THRU 5888.000	+ .007 / - .001
5888.000 THRU 5952.000	+ .007 / - .001
5952.000 THRU 6016.000	+ .007 / - .001
6016.000 THRU 6080.000	+ .007 / - .001
6080.000 THRU 6144.000	+ .007 / - .001
6144.000 THRU 6208.000	+ .007 / - .001
6208.000 THRU 6272.000	+ .007 / - .001
6272.000 THRU 6336.000	+ .007 / - .001
6336.000 THRU 6400.000	+ .007 / - .001
6400.000 THRU 6464.000	+ .007 / - .001
6464.000 THRU 6528.000	+ .007 / - .001
6528.000 THRU 6592.000	+ .007 / - .001
6592.000 THRU 6656.000	+ .007 / - .001
6656.000 THRU 6720.000	+ .007 / - .001
6720.000 THRU 6784.000	+ .007 / - .001
6784.000 THRU 6848.000	+ .007 / - .001
6848.000 THRU 6912.000	+ .007 / - .001
6912.000 THRU 6976.000	+ .007 / - .001
6976.000 THRU 7040.000	+ .007 / - .001
7040.000 THRU 7104.000	+ .007 / - .001
7104.000 THRU 7168.000	+ .007 / - .001
7168.000 THRU 7232.000	+ .007 / - .001
7232.000 THRU 7296.000	+ .007 / - .001
7296.000 THRU 7360.000	+ .007 / - .001
7360.000 THRU 7424.000	+ .007 / - .001
7424.000 THRU 7488.000	+ .007 / - .001
7488.000 THRU 7552.000	+ .007 / - .001
7552.000 THRU 7616.000	+ .007 / - .001
7616.000 THRU 7680.000	+ .007 / - .001
7680.000 THRU 7744.000	+ .007 / - .001
7744.000 THRU 7808.000	+ .007 / - .001
7808.000 THRU 7872.000	+ .007 / - .001
7872.000 THRU 7936.000	+ .007 / - .001
7936.000 THRU 8000.000	+ .007 / - .001
8000.000 THRU 8064.000	+ .007 / - .001
8064.000 THRU 8128.000	+ .007 / - .001
8128.000 THRU 8192.000	+ .007 / - .001
8192.000 THRU 8256.000	+ .007 / - .001
8256.000 THRU 8320.000	+ .007 / - .001
8320.000 THRU 8384.000	+ .007 / - .001
8384.000 THRU 8448.000	+ .007 / - .001
8448.000 THRU 8512.000	+ .007 / - .001
8512.000 THRU 8576.000	+ .007 / - .001
8576.000 THRU 8640.000	+ .007 / - .001
8640.000 THRU 8704.000	+ .007 / - .001
8704.000 THRU 8768.000	+ .007 / - .001
8768.000 THRU 8832.000	+ .007 / - .001
8832.000 THRU 8896.000	+ .007 / - .001
8896.000 THRU 8960.000	+ .007 / - .001
8960.000 THRU 9024.000	+ .007 / - .001
9024.000 THRU 9088.000	+ .007 / - .001
9088.000 THRU 9152.000	+ .007 / - .001
9152.000 THRU 9216.000	+ .007 / - .001
9216.000 THRU 9280.000	+ .007 / - .001
9280.000 THRU 9344.000	+ .007 / - .001
9344.000 THRU 9408.000	+ .007 / - .001
9408.000 THRU 9472.000	+ .007 / - .001
9472.000 THRU 9536.000	+ .007 / - .001
9536.000 THRU 9600.000	+ .007 / - .001
9600.000 THRU 9664.000	+ .007 / - .001
9664.000 THRU 9728.000	+ .007 / - .001
9728.000 THRU 9792.000	+ .007 / - .001
9792.000 THRU 9856.000	+ .007 / - .001
9856.000 THRU 9920.000	+ .007 / - .001
9920.000 THRU 9984.000	+ .007 / - .001
9984.000 THRU 10048.000	+ .007 / - .001
10048.000 THRU 10112.000	+ .007 / - .001
10112.000 THRU 10176.000	+ .007 / - .001
10176.000 THRU 10240.000	+ .007 / - .001
10240.000 THRU 10304.000	+ .007 / - .001
10304.000 THRU 10368.000	+ .007 / - .001
10368.000 THRU 10432.000	+ .007 / - .001
10432.000 THRU 10496.000	+ .007 / - .001
10496.000 THRU 10560.000	+ .007 / - .001
10560.000 THRU 10624.000	+ .007 / - .001
10624.000 THRU 10688.000	+ .007 / - .001
10688.000 THRU 10752.000	+ .007 / - .001
10752.000 THRU 10816.000	+ .007 / - .001
10816.000 THRU 10880.000	+ .007 / - .001
10880.000 THRU 10944.000	+ .007 / - .001
10944.000 THRU 11008.000	+ .007 / - .001
11008.000 THRU 11072.000	+ .007 / - .001
11072.000 THRU 11136.000	+ .007 / - .001
11136.000 THRU 11200.000	+ .007 / - .001
11200.000 THRU 11264.000	+ .007 / - .001
11264.000 THRU 11328.000	+ .007 / - .001
11328.000 THRU 11392.000	+ .007 / - .001
11392.000 THRU 11456.000	+ .007 / - .001
11456.000 THRU 11520.000	+ .007 / - .001
11520.000 THRU 11584.000	+ .007 / - .001
11584.000 THRU 11648.000	+ .007 / - .001
11648.000 THRU 11712.000	+ .007 / - .001
11712.000 THRU 11776.000	+ .007 / - .001
11776.000 THRU 11840.000	+ .007 / - .001
11840.000 THRU 11904.000	+ .007 / - .001
11904.000 THRU 11968.000	+ .007 / - .001
11968.000 THRU 12032.000	+ .007 / - .001
12032.000 THRU 12096.000	+ .007 / - .001
12096.000 THRU 12160.000	+ .007 / - .001
12160.000 THRU 12224.000	+ .007 / - .001
12224.000 THRU 12288.000	+ .007 / - .001
12288.000 THRU 12352.000	+ .007 / - .001
12352.000 THRU 12416.000	+ .007 / - .001
12416.000 THRU 12480.000	+ .007 / - .001
12480.000 THRU 12544.000	+ .007 / - .001
12544.000 THRU 12608.000	+ .007 / - .001
12608.000 THRU 12672.000	+ .007 / - .001
12672.000 THRU 12736.000	+ .007 / - .001
12736.000 THRU 12800.000	+ .007 / - .001
12800.000 THRU 12864.000	+ .007 / - .001
12864.000 THRU 12928.000	+ .007 / - .001
12928.000 THRU 12992.000	+ .007 / - .001
12992.000 THRU 13056.000	+ .007 / - .001
13056.000 THRU 13120.000	+ .007 / - .001
13120.000 THRU 13184.000	+ .007 / - .001
13184.000 THRU 13248.000	+ .007 / - .001
13248.000 THRU 13312.000	+ .007 / - .001
13312.000 THRU 13376.000	+ .007 / - .001
13376.000 THRU 13440.000	+ .007 / - .001
13440.000 THRU 13504.000	+ .007 / - .001
13504.000 THRU 13568.000	+ .007 / - .001
13568.000 THRU 13632.000	+ .007 / - .001
13632.000 THRU 13696.000	+ .007 / - .001
13696.000 THRU 13760.000	+ .007 / - .001
13760.000 THRU 13824.000	+ .007 / - .001
13824.000 THRU 13888.000	+ .007 / - .001
13888.000 THRU 13952.000	+ .007 / - .001
13952.000 THRU 14016.000	+ .007 / - .001
14016.000 THRU 14080.000	+ .007 / - .001
14080.000 THRU 14144.000	+ .007 / - .001
14144.000 THRU 14208.000	+ .007 / - .001
14208.000 THRU 14272.000	+ .007 / - .001
14272.000 THRU 14336.000	+ .007 / - .001



**SPECIFICATIONS, SERIES 7521A ACCELEROMETER**

**PERFORMANCE BY MODEL NUMBER**

	<u>7521A1</u>	<u>7521A2</u>	<u>7521A3</u>	<u>7521A4</u>	<u>7521A5</u>	<u>7521A6</u>	<u>7521A7</u>	<b>UNITS</b>
Input Range	±2	±5	±15	±33	±50	±100	±225	g
Output, bias, ±10%	2.5	2.5	2.5	2.5	2.5	2.5	2.5	V
Output range	±1.1	±1.4	±1.4	±1.8	±1.8	±1.8	±1.8	V
Bandwidth	0-1500	0-1500	0-1500	0-400	0-400	0-400	0-400	Hz
Sensitivity	550	280	93	55	36	18	8	mV/g
Output Noise (typical)	3	3	5	25	30	40	55	mGrms
Output Impedance	3500	3500	3500	500	500	500	500	Ω

**PERFORMANCE FOR ALL MODEL NUMBERS**

	<b>MIN</b>	<b>NOM</b>	<b>MAX</b>	<b>UNITS</b>
Maximum Mechanical Shock			4000	g peak
Resonance Frequency		5000		Hz
Transverse Sensitivity			2	%
Operating Temperature	-55		+257	°F
Compensated Temperature Range (CTR)	-20		+158	°F
Thermal Zero			0.0009	% FS/°F
Thermal Sensitivity Drift			0.0006	% FS/°F
Storage Temperature	-55		+302	°F
Non-Linearity			0.3	%
Excitation, regulated		4.8-5.2		VDC
Current consumption, nom		2		mA

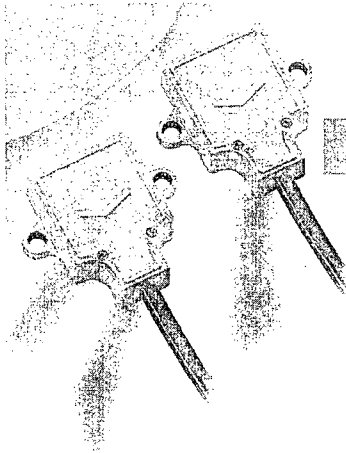
**PHYSICAL PARAMETERS FOR ALL MODEL NUMBERS**

Case Material		anodized aluminum		
Cable Length		79		inch
Mounting Provision		two M2 screws (provided)		
	<b>MIN</b>	<b>NOM</b>	<b>MAX</b>	<b>UNITS</b>
Case Length		0.59		inch
Case Width		0.59		inch
Case Height		0.30		inch
Mounting Hole Spacing		0.59		inch
Mass			3.7	grams

**NOTES:**

**SUPPLIED ACCESSORIES:**

(2) Mounting Screws (Model 6722), M2 x 12 flathead



# SCA121T Series

## Stand Alone Inclinometer

Dual Axis Analog Output

### FEATURES

- Silicon 3D MEMS sensor
- 0,1° accuracy
- Resolution < 0,001°
- Operating temperature range -40...+85 °C
- Long term stability < 0,02°
- Shock resistance >20 000 g
- Sensing element -3 dB @ 18 Hz
- Main dimensions: 30x30x13 mm size, single or dual axis
- Voltage output
- RoHS compatible

### BENEFITS

- Excellent long term stability
- Sensing element controlled frequency response
- Outstanding shock durability
- Harsh environment robustness

### APPLICATIONS

- Platform tilt measurement
- Equipment and instrument condition monitoring
- Inclination based position measurement
- Rotational orientation measurement

For customised product please contact VTI Technologies

Parameter	Condition	Min.	Typ	Max.	Units	
Supply voltage	Unregulated or regulated	7	16	35	V	Applies to: -D03, -D07
	ratimetric	4,75	5	5,25	V	Applies to: -D05
Current consumption			5		mA	
Output load	Resistive	10			kΩ	
	Capacitive			20	nF	

Parameter	Condition	SCA121T-D03	SCA121T-D07	SCA121T-D05	Units
Measuring range <sup>1</sup>		±90	±30	±90	°
Supply voltage		7...35	7...35	5...0,25	V
Measuring axis	(see "Directions")	X-Y	X-Y	X-Y	
Offset @ 0° <sup>2</sup>	Output at 0°	2,5	2,5	2,5	V
Offset zero point error <sup>3</sup>	Max. deviation	1	1	1	°
Offset temperature error	0...70 °C	-0,2	-0,2	+0,2	°
	-25...85 °C	-0,6	-0,6	-0,6	°
Sensitivity		2	4	2	mV/°
		35	70	35	mV/(°@offset pos.)
Sensitivity temperature error <sup>6</sup>	0...70 °C	-0,8...0,3	-0,8...0,3	-0,8...0,3	%
	-25...85 °C	-1,5...0,5	-1,5...0,5	-1,5...0,5	%
Nonlinearity	Sinus output	N/A	0,1	N/A	°
Frequency response -3 dB <sup>4</sup>		18	18	18	Hz
Cross-axis sensitivity <sup>4</sup>		3	3	3	%

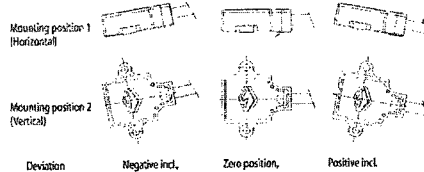
Typical values unless otherwise specified.

- Note 1 The measuring range is limited by the sensitivity and offset.  
 Note 2 Offset specified as Output @ 0°.  
 Note 3 The frequency response is determined by the sensing element's internal gas damping. The output has true DC (0 Hz) response.

- Note 4 The cross-axis sensitivity determines how much inclination, perpendicular to the measuring axis, couples to the output.  
 Note 5 For optimum zero point accuracy, mounting angle of the part can be adjusted.

### MEASURING DIRECTIONS

#### X-axis



#### Y-axis

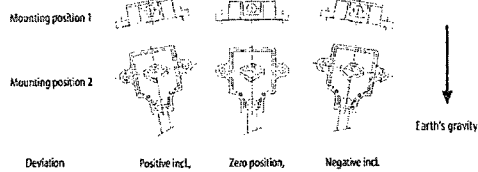


Figure 1. Positions

#### Notes:

- It is important that the part is parallel to the mounting plane, and that the output equals the zero value when sensor is in zero position.
- Zero position: Please note the picture above which provides information on how the output of the accelerometer behaves in different circumstances when assembled. Please also note that you can rotate the part around the measuring plane for optimum mounting location.



**ELECTRICAL CONNECTION**

SCA121T series

Wire color	Name	Function
Blue	GND	Ground
Red	V <sub>cc</sub>	Power supply
Yellow	Out X	X-axis output
Green	Out Y	Y-axis output
White		Not connected

**MECHANICAL SPECIFICATION MOUNTING**

Cable length: -D03, -D07 30 cm  
 -D05 110 cm  
 Total weight: Approx. 60 grams  
 Protection class: IP66  
 Housing: Zinc casting with passivation

The sensor module is to be mounted on a flat and smooth surface with 2 screws, dimension M4. Mounting torque 5 ±1 Nm.

**SENSOR DIMENSIONS**

Dimensions in mm.

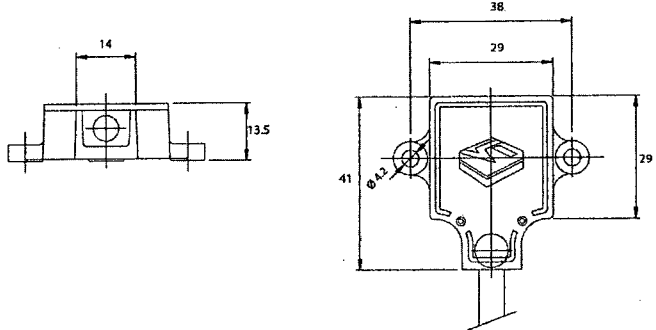


Figure 2.

**VOLTAGE TO ANGLE CONVERSION**

$$\text{Inclination angle} = \arcsin \left( \frac{V_{out} - \text{Offset}}{\text{Sensitivity}} \right)$$

where:  
 V<sub>out</sub> = analog output [V]  
 Offset = 2.5 V, output at 0° inclination position  
 Sensitivity = sensitivity of device [V/g]

